DEGRADATION MECHANISMS IN ALUMINUM MATRIX COMPOSITES ALUMINA/ALUMINUM AND BORON/ALUMINUM

By

George C. Olsen

N82-10121

N82-10121 #

DEGRADATION MECHANISMS IN ALUMINUM MATRIX COMPOSITES - ALUMINA/ALUMINUM

AND BORON/ALUMINUM

By

George C. Olsen

A thesis submitted to the Graduate Faculty of
North Carolina State University at Raleigh
in partial fulfillment of the
requirements for the Degree of
Doctor of Philosophy

DEPARTMENT OF MECHANICAL AND AEROSPACE ENGINEERING

RALEIGH

1 9 8 1

APPROVED BY:

<table>
<tr><td>Fred R. DeJarnette</td><td>_____</td></tr>
<tr><td>_____</td><td>_____
Chairman of Advisory Committee</td></tr>
<tr><td>Joe A. Marlin</td><td></td></tr>
</table>

ABSTRACT

OLSEN, GEORGE C.: Degradation Mechanisms in Aluminum Matrix Composites –

Alumina/Aluminum and Boron/Aluminum (Under the direction of DR. J. A.

BAILEY)

Aluminum matrix composites reinforced with continuous high-strength

fibers have been developed for special applications. They are intended

for use at temperatures up to 590 K. However, fiber–matrix interactions

during fabrication and elevated temperature use are often detrimental to

composite properties. This experimental investigation was conducted to

determine the effects of fabrication and long-term thermal exposure (up

to 10 000 hours at 590 K) on two types of aluminum matrix composites.

One type, an alumina/aluminum composite, was made of continuous

αAl_2O_3 fibers in a matrix of commercially pure aluminum alloyed with 2.8%

lithium.   The mechanical properties of the material, the effect of iso-

thermal exposure, cyclic thermal exposure, and fatigue are presented.

Two degradation mechanisms are identified. One was caused by formation

of a nonstoichiometric alumina during fabrication, the other by a loss of

lithium to a surface reaction during long-term thermal exposure.

The other type composite, boron/aluminum, made of boron fibers in an

aluminum matrix, was investigated using five different aluminum alloys

for the matrices. The mechanical properties of each material and the

effect of isothermal and cyclic thermal exposure are presented. The

effects of each alloy constituent on the degradation mechanisms are discussed. Several reactions between alloy constituents and boron fibers were more detrimental to the composite properties than aluminum reactions with the boron fibers. One reaction was beneficial to fiber strength.

BIOGRAPHY

George Carl Olsen was born ████████████████████████

He attended Boston public schools through the third grade. In 1948, his

family moved to Princess Anne County, Virginia, where he continued his

elementary and secondary education, graduating from Princess Anne High

School in 1957. Between 1957 and 1968 (part-time 1963-1968), he worked

for a local firm of architects and engineers, beginning as a draftsman

and advancing to project engineer. He enrolled in Old Dominion College

School of Engineering in September 1963 and received a Bachelor of

Science Degree in Engineering in June 1967. He continued in graduate

school at Old Dominion with the aid of a fellowship.

In June 1968, the author accepted a position as a research engineer

with the National Aeronautics and Space Administration's Langley Research

Center in Hampton, Virginia. During his first year with NASA, he

completed the requirements for a Master of Science in Engineering degree

which he received from Old Dominion College in June 1969. Under the

auspices of the NASA Graduate Training Program, Mr. Olsen enrolled in the

North Carolina State University Department of Mechanical and Aerospace

Engineering Doctor of Philosophy Program. He studied in residence at the

University from September 1969 through August 1970.

The author has had a variety of technical assignments as an NASA

researcher. They include development of thermal protection system

technology for reentry vehicles, aerothermodynamic analysis in high-speed

flow fields, and development of metal-matrix composites for structural aerospace applications. He has published a number of technical papers in these areas. His present assignment is in his original field, aerothermodynamic analysis. He is a registered professional engineer in The Commonwealth of Virginia.

The author is married to the former Carol Ann ▇▇▇▇▇ They have two sons, Jeff and Eric.

ACKNOWLEDGEMENTS

TABLE OF CONTENTS

GENERAL INTRODUCTION

Technology advances in the design of aerospace structures, jet engines, industrial machines, etc. often require materials with combinations of properties not found in a single metal alloy. Applications often require the low mass of an aluminum be combined with the high strength and stiffness of a carbon steel, the elevated temperature capability of a titanium, and the dimensional stability of a ceramic. In addition there may be requirements for corrosion resistance, impact resistance, fracture toughness, or a multiplicity of other properties. Material specifications like these are responsible for the development of metal-matrix composite technology: a technology that attempts to merge two or more materials with different assets and liabilities into a single material with the best attributes of the components.

Aluminum is often used as the matrix material in composites because it is lightweight, readily available, has many of the required assets, and aluminum technology is highly developed. Continuous fibers are the most common method of reinforcing an aluminum matrix. Some of the fibers that have been used are boron, alumina, silicon carbide, and graphite. Fabrication techniques for aluminum matrix composites depends on the reinforcing being used but include diffusion bonding, liquid-metal infiltration, flame spraying, vapor deposition, etc.

Both the matrix material and the reinforcing fibers have their own extensive sets of physical, thermal, and chemical characteristics. The

properties of a composite material are not only dependent on the properties of each component but also the interaction of those properties and the properties of additional phases that may form between the components. As a result, composites are extremely complex materials. Their development has often been by trial-and-error considering only bulk effects. This approach has left many observed anomalies unanswered.

The purpose of the investigations reported herein was to characterize the materials, determine the effects of long-term thermal exposure, and determine alloy constituent effects on degradation. With these data, it may be possible to improve elevated temperature performance.

The first paper deals with an alumina fiber reinforced aluminum matrix. The matrix is a commercially pure aluminum with a small amount of lithium added to promote wetting during fabrication. Degradation mechanisms active during fabrication and thermal exposure are discussed.

The second paper deals with boron fiber reinforced aluminum matrices. Five aluminum alloys are used for matrices. The effect of each alloying constituent on the degradation mechanisms is discussed and suggestions for improving boron/aluminum composites are made.

EFFECTS OF TEMPERATURE, THERMAL EXPOSURE AND FATIGUE

ON AN ALUMINA/ALUMINUM COMPOSITE[1]

George C. Olsen

DECEMBER 1980

SUMMARY

The effects of thermal exposure and mechanical fatigue on the properties of a composite material of aluminum matrix unidirectionally reinforced with polycrystalline alumina (αAl_2O_3) fibers were experimentally evaluated. Some specimens were isothermally exposed for up to 10,000 hours at 590 K while others were thermally cycled between 200 K and 590 K for 6000 cycles. As-fabricated specimens and thermally exposed specimens were exposed to 10^6 tension-tension fatigue cycles. Strengths and elastic moduli of the as-fabricated material and the effects of thermal and fatigue exposure on them were determined by mechanically testing the specimens. The effects of fabrication, thermal exposure, and mechanical fatigue on the microstructure of the material were evaluated with metallurgical techniques such as scanning electron microscopy, optical microscopy, and X-ray diffraction.

Tests showed that fiber strength was severely degraded by the fabrication process, probably because of the formation of vacancies and accompanying stress fields in the fiber near the surface during a surface reduction of alumina to a nonstoichiometric form. However, isothermal exposure at 590 K, thermal cycling, and fatigue cycling all restored the fiber's original strength by allowing the vacancies to be annihilated. Comparison of specific properties of the as-fabricated material with several other aerospace materials over the temperature range from 295 K to 590 K shows that it is an attractive candidate for select applications. Long duration isothermal exposure did not cause

1

matrix-fiber reactions but did weaken the matrix by overaging and the diffusional loss of lithium to a surface reaction forming lithium carbonate. Thermal cycling caused some damage to the material by initiating cracks in the matrix which in turn induced some fiber failures. Tension-tension fatigue cycling between one-tenth and two-thirds of the ultimate tensile strength caused no apparent damage to the as-fabricated material, but in fact, strengthened it to the rule-of-mixtures value. Fatigue cycling after thermal exposure did have a cumulative damage effect on the material.

INTRODUCTION

Alumina is a well characterized ceramic material (ref. 1) suitable for a broad range of applications. Reinforcement for metal matrix composites is one such application. Single-crystal whiskers, rods and filaments of alumina have been used to reinforce aluminum, silver, copper, and nickel matrices (refs. 2, 3 and 4). However, limited availability and high cost of these forms of alumina have inhibited its widespread use in composite materials.

A high-volume low-cost process has been developed for making polycrystalline alumina (αAl_2O_3) fibers which are commercially available (ref. 5). Although this fiber does not have the high tensile strength of its single-crystal predecessors, it is chemically and thermally stable, and has a high modulus of elasticity and moderate strength. These are attractive attributes for composite material fabrication and appli-

cations. The matrix materials being considered for use with these poly-
crystalline alumina fibers include aluminum, magnesium, lead, resins,
glass, and ceramics. This study addresses the alumina/aluminum compos-
ite system.

The alumina/aluminum composite system was consolidated with a liquid-
metal infiltration technique. Aluminum by itself does not wet alumina;
therefore, a small amount of lithium was added to the aluminum melt as a
wetting agent. Because lithium has a lower surface-free-energy than
aluminum, it concentrates at free surfaces of the melt and interfaces
between the matrix melt and fibers during fabrication. The actual
wetting mode has not been determined, but considering the reactivity of
lithium and its aggressive attack on alumina (ref. 1), wetting by
formation of an intermetallic compound is the likely mechanism.
Previous investigations of chemically extracted fibers have identified
small amounts of lithium-aluminum oxide ($LiAlO_2$) on the fibers by X-ray
diffraction (ref. 5) and of lithium spinel ($LiAl_5O_8$) by electron
diffraction (ref. 6). Lithium spinel has also been identified by X-ray
diffraction of over-reacted fibers (ref. 7). Lithium may also form
second phase Al_3Li particles in the aluminum matrix as reported in
quenched lithium-aluminum alloys (refs. 8, 9, and 10).

This study of alumina/aluminum composite material had several
purposes. One was to determine selected mechanical properties of the
as-fabricated composite between room temperature and 590 K and compare
them with properties of other well characterized aerospace materials.

3

Another purpose was to determine the effect of continuous long-term isothermal exposure and thermal cycling on the composite material. The final purpose was to determine the effect of mechanical fatigue on the composite material.

MATERIALS AND EXPOSURE CONDITIONS

Materials and Test Specimens

The composite material is an aluminum alloy matrix unidirectionally reinforced with 52 volume percent of alumina fiber. The continuous fibers are 99+ percent pure polycrystalline αAl_2O_3 with a diameter of 19.5 μm (mean of 25 measurements). In their virgin state, they are white and have an ultimate strength of 1346 MPa (mean of 10 tests) and a reported elastic modulus of 379 GPa (ref. 5). The matrix material is 1100 aluminum alloy with 2.8 weight percent of lithium added to the melt to promote fiber wetting. In the annealed condition, lithium adds little to the 90 MPa strength of the aluminum but increases its modulus from 69 GPa to 76.5 GPa (ref. 11). Unidirectionally reinforced plates of the composite material were consolidated by the material supplier using a liquid metal infiltration process. A mold was filled with aligned fibers held in place by a fugitive binder. A vacuum was drawn on the mold and held throughout the infiltration process. The mold was heated to burn off the fugitive binder and then submerged in a melt of the matrix material. After the mold reached thermal equilibrium with the melt, a seal was punctured to allow the melt to infiltrate the mold

4

and fibers. When fully infiltrated after approximately 5 minutes, the mold was removed from the melt and quenched with a water spray. The mold was then cut away leaving a composite plate approximately 150 mm x 200 mm x 25 mm. More detailed descriptions of the fiber and fabrication process are available in reference 5.

Test specimens, in the configurations listed in Table I, were cut from the composite plates with a diamond cut-off wheel and finished with diamond surface grinding. Scanning electron microscopy of the machined edges revealed no fiber damage as a result of the machining. Prior to mechanical testing at room temperature, aluminum gripping tabs and strain gages were bonded with epoxy to the tension and compression specimens. Two gages were mounted back to back on the centerline to measure longitudinal strain, and a third gage was mounted to measure transverse strain. Tabs and strain gages on specimens to be tested at elevated temperature were bonded with high temperature ceramic base adhesives which required curing at 530 K for 5 hours. Sets of three replicate specimens were prepared for each test and exposure condition.

Thermal Exposures

Continuous isothermal exposures.- Continuous isothermal exposures were conducted in an air circulating electric oven. Sets of specimens were exposed at 590 K for 2500, 5000, and 10 000 hours. After removal from the oven, the specimens were allowed to cool in ambient air.

5

<u>Cyclic thermal exposures.-</u> Cyclic exposures were conducted in a dual chamber apparatus. Specimens, mounted on a mechanically driven sliding tray, were alternately inserted in an air-circulating, electrically heated hot chamber (590 K) and a liquid nitrogen-cooled cold chamber (200 K). A full cycle was 10 minutes long with exposure of 7.3 minutes in the hot chamber and 2.7 minutes in the cold chamber required to obtain thermal equilibrium. A schematic drawing of the apparatus and a typical specimen temperature profile for one cycle are shown in figure 1. The specimens were exposed to this environment for 6000 cycles.

Fatigue Conditioning

Three sets of longitudinal tensile specimens were mechanically fatigue conditioned: one set as-fabricated, one after 2500 hours at 590 K, and a third after 6000 thermal cycles. Fatigue conditioning was conducted at room temperature in a hydraulic testing machine. The testing machine, operated in a load control mode, loaded the specimens in a tension-tension sinusoidal cycle. Maximum load for the cycle was 11 kN (approximately 2/3 ultimate load for as-fabricated specimens) and the minimum load was 1.1 kN (1/10 the cycle maximum load). Specimens were conditioned for 10^6 cycles at 100 Hz with no significant specimen heating noted.

TEST PROCEDURES

Mechanical Property Tests

Composite specimens were tested in tension and compression. Test standards, method for determining shear modulus (ref. 12), properties reported and cross-head speeds for these tests are shown in table II. (Symbols appearing in the tables and figures are defined in the appendix.) All tests were performed in air at atmospheric pressure in a 44.5 kN, mechanically driven test machine equipped with an environmental chamber for elevated temperature tensile tests. Wedge grips were used for tensile tests, and an IITRI wedge grip fixture (described in ref. 13) was used for compression tests. Elevated temperature compression specimens were heated with a clam shell electric resistance heater around the specimen gage length. Load cell and strain gage outputs for tension and compression tests were recorded and reduced on a digital computer system.

Individual fiber breaking loads were determined experimentally for virgin fibers and for fibers chemically removed from their composite matrix with a heated NaOH solution. Ten fibers from each group were tested on a bench-mounted fiber tensile tester. The motor driven tester was equipped with a load cell and linearly variable displacement transducer. The load cell and displacement transducer outputs were recorded on an X-Y plotter. Fibers were centered in the 25 mm test section and attached with a thermoplastic adhesive.

Metallurgical Analysis

Metallurgical analysis of the composite specimens included examination of fracture surfaces with scanning electron microscopy (SEM) and examination of polished and etched (Keller's reagent) cross-sections with optical microscopy. X-ray diffraction analysis was used to determine crystalline structure. Diffraction patterns were made using a copper $K\alpha$ incident X-ray beam, a diffracted beam monochromater, a diffractometer and a goniometer. Polished specimens were attached to an oscillating holder to reduce effects of preferred crystalline orientation. Additional analysis of fibers chemically removed from the composite matrix included thermogravimetric analysis, scanning differential calorimeter analysis with gaseous reaction product analysis, and X-ray diffraction of powdered samples.

RESULTS AND DISCUSSION

Ultimate stresses and elastic modulii determined from each $\alpha Al_2O_3/Al$ composite specimen tested are shown in tables III and IV. For each set of room temperature data in these tables, the standard deviation as a percentage of the mean value did not exceed 7 percent. The standard deviation for the elevated temperature tensile test data was as high as 18 percent, and for the compression data, as high as 36 percent. High variability in elevated-temperature compression test data is the result of limited test data and alignment perturbation by thermal expansion. All compression testing is alignment sensitive, but when elevated tem-

peratures soften the matrix and reduce its side support of the fibers the sensitivity is magnified. Reduction of the variability would require more data and better elevated temperature alignment control and would probably increase the mean values of compression strength.

As-Fabricated Material

Room-temperature properties.- Mean values of the as-fabricated material properties at room temperature (295 K) are shown in table V. The longitudinal tensile strength is 26 percent lower than would be expected from a rule-of-mixtures (ROM) calculation using the virgin fiber and matrix properties. Comparison of the strengths and moduli of the $\alpha Al_2O_3/Al$ composite with those of a well characterized B/Al composite (50 volume percent of 0.14 mm diameter boron fibers in a 6061 aluminum matrix, ref. 14) shows its longitudinal tensile strength to be 37 percent lower than the B/Al. The longitudinal elastic modulus and the shear modulus of the two materials are the same. Properties of the $\alpha Al_2O_3/Al$ composite that exceed those of B/Al include transverse tensile strength, 40 percent higher; transverse elastic modulus, 16 percent higher, and compressive strength, 76 percent higher. Compression loading of the $\alpha Al_2O_3/Al$ composite specimens takes advantage of the inherently high compressive strength of the ceramic fibers; the composite's longitudinal compressive strength is approximately five times higher than its longitudinal tensile strength.

Fractographs from typical as-fabricated longitudinal and transverse tensile specimens are shown in figure 2. Longitudinal specimens failed in a noncumulative mode (ref. 15) characterized by flat surfaces with no fiber pullout or shear steps. The noncumulative failure mode indicates a well-bonded composites with high interfacial shear strength. Transverse specimens failed by dimpled rupture of the matrix material with no indication of interface failure or fiber splitting.

X-ray diffraction patterns from the as-fabricated composite material were complex but provided correlation with every indexed peak for αAl_2O_3 (ASTM card no. 10-173) and aluminum (ASTM card no. 4-0787). One peak was unidentified. This peak could have originated from the 110 plane of a superlattice phase, Al_3Li, in the matrix. This phase is not easily identified by standard X-ray diffraction techniques but has been observed (refs. 8, 9 and 10) in quenched aluminum/lithium alloys. Reportedly, Guinier-Preston zones of Al_3Li nucleate and grow into small spherical particles in a matter of days at room temperature. No evidence of $LiAlO_2$ or $LiAl_5O_8$ was found in the composite material X-ray data. If the formation of either or both of these compounds is the wetting mechanism, the fabrication technique was successful in limiting their growth to regions so thin as to be undetectable by standard X-ray diffraction techniques.

An optical photomicrograph of a typical polished cross section from an as-fabricated specimen is shown in figure 3. No indication of

matrix-fiber interaction is apparent in these cross sections. The variations in fiber diameter and spacing are typical for this material.

Fiber properties. - Fibers chemically removed from the composite matrix were dark gray. X-ray diffraction patterns from powdered samples of virgin fibers and chemically removed fibers correlated with every indexed peak for αAl_2O_3 (ASTM card no. 10-173) with an intensity greater than 5 percent. No other peaks were present in the patterns. The only difference was a half-maximum peak broadening of approximately 15 percent in the patterns from the chemically removed fibers compared with the patterns from the virgin fibers.

Thermograviometric analysis (TGA) of the gray fiber in air at atmospheric pressure between room temperature and 900 K did not show any measurable weight change. However, the fiber sample changed back to its original white color during the test. Differential scanning calorimeter analysis (DSCA), including gaseous product analysis for temperatures up to 900 K, did not show any change in heat capacity or any gaseous products from the gray fiber. Again, the fiber returned to its original white color during the test. These data are inconclusive because they fail to indicate that the observed changes in fiber color are due to the formation and/or evaporation of a separate reaction product. However, color changes from white to gray have been observed previously (refs. 16, 17, 18, and 19) and were attributed to the formation of a nonstoichiometric alumina with a composition of approximately $Al_2O_{2.96}$. Reheating the gray nonstoichiometric alumina to 773 K in the presence of

11

oxygen reportedly reoxidizes the alumina and restores its original white color as observed in the fiber TGA and DSCA tests. The formation of a nonstoichiometric alumina in the fibers is accompanied by an increase in vacancy density, which broadens the X-ray diffraction peaks as observed.

Individual fiber tensile tests for virgin fibers and fibers chemically removed from as-fabricated specimens show a 45 percent loss of fiber strength during the fabrication process. The reduced fiber strength correlates with the lower than expected longitudinal tensile strength of the as-fabricated composite material. Fibers lose strength during fabrication probably because of a high density of quenched-in vacancies in the fiber near the fiber surface caused by the reduction of alumina to a nonstoichiometric form. These vacancies increase the stress fields in the fibers and reduce the fiber strength.

Effect of elevated test temperature.- As-fabricated $\alpha Al_2O_3/Al$ composite specimens were mechanically tested at room temperature (295 K), 500 K, and 590 K. Results of the tests, the mean values normalized by dividing by the room-temperature mean values, are shown in figure 4. The fiber-dominated properties - ultimate longitudinal tensile strength and longitudinal elastic modulus - are nearly constant over the temperature range. Matrix dominated properties - ultimate transverse tensile strength, transverse elastic modulus, ultimate longitudinal compression strength, and shear modulus - degraded with increasing temperature. The shaded area above the mean compression strength curve is bounded above by the maximum compression test data obtained. If the

elevated-temperature compression test variability previously discussed were eliminated, the material mean compression strength would probably lie in the neighborhood of the upper limit.

Several key properties of the $\alpha Al_2O_3/Al$ composite were selected for comparison with other materials on a specific basis, i.e. the material property divided by the material density, for applications that are weight critical. The comparison materials include two aerospace alloys (ref. 20), Al 7075-T6 and Ti-6Al-4V (annealed), and three composite materials (ref. 14), 50 volume percent boron fibers in a 6061 aluminum matrix (B/Al), 61 volume percent graphite fibers in an epoxy resin matrix (Gr/Ep), and 63 volume percent graphite fibers in a polyimide resin matrix (Gr/PI). Because the fiber volume contents of these composites would not give a direct comparison, their properties and densities were scaled to an equivalent 52 volume percent fiber content. The resulting scale factors for the specific properties were 1.04 for B/Al, 0.88 for Gr/Ep, and 0.84 for Gr/PI. Longitudinal properties were multiplied by the scale factors and transverse properties were divided by them. In addition, the maximum rated temperatures for the Gr/Ep and Gr/PI composites are 450 K and 533 K, respectively. The specific properties of these materials as a function of test temperature are shown in figure 5. Specific stiffness (fig. 5(a)) of the $\alpha Al_2O_3/Al$ composite is several times higher than the alloys but slightly lower than the other composites. Specific transverse tensile strength (fig. 5(b)) of $\alpha Al_2O_3/Al$ is similar to B/Al, about twice the value of the resin matrix composites, but much less than the alloys. Specific longitudinal ten-

sile strength (fig. 5(c)) of $\alpha Al_2O_3/Al$ is similar to the titanium but much less than the other composite materials. Specific longitudinal compression strength (fig. 5(d)) of $\alpha Al_2O_3/Al$ is in the same range as the other composites and much higher than the alloys. As in the previous figure, the shaded area represents the probable increase in compression strength if testing variability is eliminated. These comparisons suggest that $\alpha Al_2O_3/Al$ composite could be an attractive candidate for selected applications, ones for which specific stiffness, transverse tensile and/or compression strength are critical, especially if material cost is a significant factor. Furthermore, if weight is not a limiting factor, the $\alpha Al_2O_3/Al$ is more attractive because on an absolute basis, its stiffness, transverse tensile strength and compression strength exceed the other composite materials considered.

Thermal Exposure Effects

Continuous isothermal exposure. - Typical stress-strain curves for longitudinal and transverse tensile tests on $\alpha Al_2O_3/Al$ composite specimens continuously exposed at 590 K for 2500, 5000, and 10 000 hours and tested at room temperature are shown in figure 6. Exposure for 2500 hours increased the longitudinal tensile strength by 14 percent but additional exposure for 5000 hours reduced it 18 percent (to 6 percent below the as-fabricated strength). Further exposure, to 10 000 hours, did not cause additional degradation of the longitudinal tensile strength. Transverse tensile strength was degraded 39, 58, and 60 percent by the 2500-, 5000-, and 10 000-hour exposures, respectively.

14

Transverse strain-to-failure decreased in a similar manner. After 2500-hour exposure, compression strength decreased 17 percent and shear modulus increased 6 percent.

Isothermal exposure at 590 K in an air circulating oven produced a tenacious dark gray reaction layer on the surface of the specimens. After 2500 hours, the reaction layer was thin; but after 5000 and 10 000 hours, the reaction layers were thick enough to scrape off powder samples. X-ray diffraction patterns made from these powder samples correspond to lithium carbonate (Li_2CO_3 ASTM card no. 22-1141). Formation of lithium carbonate on the surface requires diffusion of lithium from the bulk material for reaction with carbon dioxide and oxygen in the air. During fabrication some of the lithium in the matrix melt concentrates at the fiber-matrix interfaces, because it has lower surface free energy, and wets the fibers. Therefore, it is reasonable to assume that much, if not all, of the lithium diffusing to the surface comes from the area near the interface. The counterflux of vacancies from the surface therefore produces a concentration of microvoids near the interfaces.

Fracture surfaces of longitudinal tensile specimens became macroscopically rougher with increased thermal exposure. Microscopically, the fractographs (fig. 7) show some increase in surface roughness with respect to the planes of fiber fracture surfaces compared with the as-fabricated fracture surface (fig. 2). In addition, elevated tear ridges in the matrix and increased necking of matrix away from the fibers indicate that matrix ductility increased with increasing exposure time.

Rougher fracture surfaces are an indication of degradation of the mechanism of load transfer between the matrix and the fibers. Transverse tensile fractographs (fig. 8) show similar effects. With increased thermal exposure, the transverse failures progressively occur at the fiber-matrix interface, in contrast with as-fabricated specimen failure in the matrix (fig. 2). The formation of dimples near the fiber surfaces (note especially the 10 000-hour specimen) indicate the coalescence of microvoids formed near the interface. Again, the elevated tear ridges and large dimples indicate increased matrix ductility, similar to that seen when precipitation-hardened aluminum alloys are overaged.

Fibers chemically removed from the composite matrix were individually tensile tested. Mean values and standard deviations of the breaking loads from 10 tests at each condition are shown in figure 9. These data show that fiber strength lost during fabrication is nearly restored to its virgin strength by isothermal exposure. Apparently thermal exposure enhances the movement and annihilation of the vacancies formed during fabrication.

These data indicate that mechanical property degradation due to long duration isothermal exposure at 590 K is a result of an interfacial diffusion phenomena and not interfacial chemical reaction. Even when the material was exposed at extreme time-temperature conditions for aluminum alloys, 500 hours at 730 K, no interface reaction was observed (ref. 21) although strengths were severely degraded.

<u>Cyclic thermal exposure</u>.- Effects of 6000 thermal cycles between 200 K and 590 K on typical longitudinal and transverse tensile stress-strain curves of the composite material are shown in figure 10. Thermal cycling increased the longitudinal strength and elastic modulus of the material by 10 and 5 percent, respectively, and reduced the transverse tensile strength by 64 percent. After thermal cycling, there was no elastic region in the transverse stress-strain curves so no transverse modulus could be determined. Thermal cycling decreased compression strength and shear modulus, both matrix dominated properties by 31 and 48 percent, respectively (Table IV).

Longitudinal and transverse tensile fractographs of the thermally cycled specimens are shown in figure 11. The longitudinal surface (fig. 11(a)) was rough and had matrix shear steps but very little bare fiber was exposed. Matrix material was still adhering to the fiber indicating that the interface was stronger than the matrix. The transverse fracture surface (fig. 11(b)) shows tear ridges between fibers and a dense population of small fragments of the matrix attached to the fibers. These fragments appear to be the result of accumulated crack damage in the matrix incurred during thermal cycling. The angularity of the fragments suggest brittle failure probably occurring at the low temperature as a result of stresses induced by the differential in thermal expansion between the matrix and fiber.

Fibers chemically removed from a thermally cycled specimen and individually tensile tested showed the same strength restoration seen in the

17

isothermally exposed specimens. These data indicate that thermal cycling causes matrix cracking which severely degrades transverse properties. During longitudinal mechanical loading, the matrix cracks induce stress concentrations in the fibers causing them to fail prematurely and partially offset the fiber strength restoration.

Fatigue Cycling Effects

Longitudinal tensile test results from composite specimens that had been exposed to 10^6 fatigue cycles are shown in figure 12. Fatigue cycling increased the strength of the as-fabricated material (fig. 12(a)) by 30 percent and the elastic modulus by 12 percent; these properties attained the ROM values. Fatigue cycling of specimens which had been isothermally exposed for 2500 hours at 590 K (fig. 12(b)) returned the strength to the as-fabricated value, but the increase in stiffness was retained. Fatigue cycling (fig. 12(c)) after thermal cycling reduced the composite strength to 16 percent below the as-fabricated strength.

Breaking loads for individual fibers chemically removed from fatigue cycled specimens are shown in figure 13 and compared with fibers from unfatigued specimens. Fiber strength reduced in fabrication is restored by fatigue cycling as noted previously for the thermally exposed specimens. These results indicate that stress levels encountered during the fatigue cycling enhanced movement and annihilation of the quenched-in vacancies. Strength of fibers from thermally exposed and fatigue cycled

18

specimens was approximately 10 percent less than the strength of fibers from specimens that were thermally exposed only. This is a small difference in a quantity with large variability but may indicate a detrimental cumulative effect of thermal exposure and fatigue cycling on fiber strength.

Fractographs of the fatigue cycled specimens are shown in figure 14. Comparison of as-fabricated specimen failure surfaces with fatigue (fig. 14(a)) and without fatigue (fig. 2) shows an apparent work hardening of the matrix material. There is less ductile necking of the matrix and flatter more brittle failure of the fibers. The overall failure surface is flatter and there is no apparent fatigue-induced damage. These same observations are true when comparing specimens exposed for 2500 hours at 590 K with fatigue (fig. 14(b)) and without fatigue (fig. 7(a)) and specimens thermally cycled with fatigue (fig. 14(c)) and without fatigue (fig. 11(a)). The effect of fatigue cycling on the specimens is more readily seen in the polished and etched longitudinal cross sections shown in figure 15. As-fabricated specimens with and without fatigue (fig. 15(a)) are identical in appearance and show no indication of fatigue induced damage. Comparison of specimens exposed for 2500 hours at 590 K with and without fatigue (fig. 15(b)) does show fatigue-induced damage. The specimen with fatigue has cracking in the matrix and fibers not present prior to fatigue cycling. The thermally cycled specimen without fatigue (fig. 15(c)) has extensive cracking in the matrix and fibers induced by the thermal expansion mismatch, but the

19

addition of fatigue cycling causes increased damage and more fiber cracking.

These data indicate that the fatigue conditions imposed on the as-fabricated specimens had no detrimental effects on the composite but in fact restored the fiber properties and strengthened the composite. However, the combination of thermal exposure and fatigue cycling did adversely affect the composite properties by cracking both the matrix and the fibers. Although transverse tensile properties of the fatigue cycled specimens were not measured, they would certainly be further degraded by fatigue-induced matrix damage.

SUMMARY OF RESULTS

Mechanical properties of as-fabricated $\alpha Al_2O_3/Al$ composite material were measured and the effects of elevated test temperature, continous long duration thermal exposure, thermal cycling, and fatigue cycling were determined. Failure mechanisms and degradation mechanisms active in the material were investigated. The major findings were:

1. The fabrication process severely degraded fiber strength, apparently by quenching in vacancies and accompanying stress fields introduced during the formation of a nonstoichiometric form of alumina. Each of the thermal exposure conditions and the fatigue cycle conditioning used in the study enhanced annihilation of the vacancies which relaxed the stress fields and restored the fiber strength.

2. Mechanical property tests conducted at temperatures up to 590 K did not show any significant temperature dependance of the fiber-dominated properties but matrix-dominated properties were temperature dependant in the typical manner of aluminum. Comparing specific properties between 295 K and 590 K of the $\alpha Al_2O_3/Al$ composite with the specific properties of several aerospace alloys and composite materials show that it is an attractive candidate for select applications.

3. Long duration isothermal exposure (up to 10 000 hours at 590 K) did not cause any measurable fiber-matrix interaction or fiber damage. It did, however, increase ductility in the matrix material and weaken the interface bond by the loss of lithium to a surface reaction forming lithium carbonate.

4. Thermal cycling caused matrix cracking as a result of the differential in thermal expansion between the fibers and matrix. Matrix cracks severely reduced transverse strength and induced stress-concentrations in the fibers during longitudinal loading which caused premature fiber failure.

5. Fatigue cycling (10^6 tension-tension cycles to two-thirds ultimate) of longitudinal tensile specimens did not cause any damage to the as-fabricated specimens but in fact increased their residual strength to the rule-of-mixtures value by restoring the fiber strength. Fatigue cycling of isothermally exposed specimens caused cracking in the matrix and fatigue cycling of thermally cycled specimens compounded matrix

cracking. Matrix cracks induced stress concentrations in the fibers
during mechanical loading and caused premature fiber failure.

Langley Research Center
National Aeronautics and Space Administration
Hampton, VA 23665

December 2, 1980

22

APPENDIX

SYMBOLS

$\bar{E}_1$ mean longitudinal elastic modulus, GPa

$\bar{E}_2$ mean transverse elastic modulus, GPa

$\bar{G}_{12}$ mean shear modulus, GPa

$\bar{\nu}_{12}$ mean Poisson's ratio for transverse strain resulting from longitudinal stress

$\bar{\rho}$ mean density. $kg \cdot m^{-3}$

$\bar{\sigma}_{1t}$ mean ultimate longitudinal tensile strength, MPa

$\bar{\sigma}_{1c}$ mean ultimate longitudinal compression strength, MPa

$\bar{\sigma}_{tt}$ mean ultimate transverse tensile strength, MPa

REFERENCES

1. Gitzen, Walter H.: Alumina as a Ceramic Material. American Ceramic Society, 1970.

2. Tressler, Richard E.: Interfaces in Oxide Reinforced Metals. Interfaces in Metal Matrix Composites, Arthur G. Metcalfe, ed., Academic Press, Inc., 1974, pp. 285-328.

3. Mehan, R. L.; and Noone, M.J.: Nickel Alloys Reinforced With αAl_2O_3 Filaments. Metallic Matrix Composites, Kenneth G. Kreider, ed., Academic Press, Inc., 1974, pp. 159-227.

4. Lynch, C. T.; and Kershaw, J. P.: Metal Matrix Composites. Chemical Rubber Co., c. 1972.

5. Champion, A. R.; Krueger, W. H.; Hartman, H. S.; and Dhingra, A. K.: Fiber FP Reinforced Metal Matrix Composites. DuPont paper presented at Second Interantional Conference on Composite Materials (Toronto, Canada), Apr. 16-20, 1978.

6. Prewo, K. M.: Fabrication and Evaluation of Low Cost Alumina Fiber Reinforced Metal Matrices R77-912245-3 (contract N00014-76-C0035), United Technol. Res. Center, May 1977. (Available from DTIC as AD A040953)

7. Kim, W. H.; Koczak, M.J.; and Lawley, A.: Effects of Isothermal and Cyclic Exposures on Interface Structure and Mechanical Properties of FP αAl_2O_3/Aluminum Composites. Paper presented at Symposium on New Developments and Application in Composites. 1978, TMS-AIME Fall Meeting (St. Louis, Missouri), Oct. 1978.

8. Yoshi-yama, Tsuyoshi, Hasebe, Katsuhiko; and Mannami, Michi-Liko: Al_3 Li Superlattice in Al-4.5 Wt. % Li Alloy. J. Phys. Soc. Japan, vol. 25, 1968, p. 908.

9. Ceresara, S., Giarda, A.; and Sanchez, A.: Annealing of Vacancies and Ageing in Al-Li Alloys. Phil. Mag., vol. 35, no. 1, Jan. 1977, pp. 97-110.

10. Ceresara, S., Cocco, G.; Fagherazzi, G.; and Schiffini, L.: Determination of the δ'Coherent Solvus in the Al-Li System by Small-Angle X-Ray Scattering. Phil. Mag., vol. 35, no. 2, Feb. 1977, pp. 373-378.

11. Mondolfo, L. F.: Aluminum Alloys: Structure and Properties. Butterworth Inc., 1976.

12. Greszczuk, L. B.: Shear-Modulus Determination of Isotropic and Composite Materials. Composite Materials: Testing and Design, Spec. Tech. Publ. No. 460, American Soc. Testing Mater., c. 1969, pp. 140-149.

13. Clark, Ronald K., and Lisagor, W. Barry: Effects of Method of
    Loading and Specimen Configration on Compressive Strength of
    ite/Epoxy Composite Materials. NASA TM 81796, April 1980.

14. Advanced Composites Design Guide. Volume IV. Materials. Third
    ed. Air Force Materails Lab., U.S. Air Force, Jan. 1973.
    (Available form DTIIC as AD-916 682L.)

15. Herring, Harvey W.: Fundamental Mechanisms of Tensile
    Fracture in Aluminum Sheet Unidirectional Reinforced With
    Boron Filament. NASA TR-383, April 1972.

16. Teichner, S., Juillet, F.; and Apghiropoulos, B.: Sur une Nouvelle
    Forme d'Alumine Coloree aet Non Stoechiometrique. Bull. Soc.
    Chim., 1959, pp. 1491-1495.

17. Juillet, Francoise; Prettre, Marcel; and Teichner, Stanislas:
    Evoluation Texturale de L'alumine Coloree Non Stoechiometrique.
    Compt. Rend. Acad. Sci., t. 249, no. 15, Oct. 12, 1959, pp.
    1356-1358.

18. Arghiropoulos, Basile; Elaston, Jean; Juillet, Francois; and
    Teichner, Stanislas: Sur une Nouvelle Methode de Preparation de
    L'alumine Coloree Non Stoechiometrique. Compt. Rend. Acad. Sci.,
    t. 249, no. 23, Dec. 9, 1959, pp. 2549-2551.

19. Arghiropoulos, Basile; Juillet, Francois; Prettre, Marcel; and Teichner, Stanislas: Evolution Structurale et Proprietes Electriques de L'alumine Coloree Non Stoechiometrique. Compt. Rend. Acad. Sci., t. 249, no. 19, Nov. 9, 19549, pp. 1895-1897.

20. Mechanical Properties Data Center, Battelle Columbus Lab.: Aerospace Structural Metals Handbook - 1980 Publication. (Formlery AFML-TR-68-115.)

21. Olsen, George C.: Thermal Exposure Effects on the Mechani cal Properties of a Polycrystalline Alumina Fiber/Aluminum Matrix Composite. The Enigma of the Eighties: Environment, Economics, Energy, Volume 24 of National SAMPE Symposium and Exhibition, Soc. ADvance. Mater. and Process Eng., c. 1979, pp. 1069-1080.

TABLE I.- CONFIGURATIONS OF UNIDIRECTIONAL $\alpha Al_2O_3/Al$ COMPOSITE

TEST SPECIMENS

Test	Fiber orientation	Specimen dimensions, mm			
		Length	Width	Thickness	Gage length
Tension	0°	150	12.7	2.6	50.8
	45°	150	12.7	2.6	50.8
	90°	100	25.4	2.6	25.4
Compression	0°	150	6.4	2.6	12.7

TABLE II.- MECHANICAL PROPERTY TESTS

Test	Fiber orientation	Standard or reference	Properties reported	Cross-head speed, mm/sec
Tension	0°	ASTM D-3552	$\bar{E}_1$, $\bar{\sigma}_{1t}$, $\bar{\nu}_{12}$,	0.0085
	45°	ASTM D-3552 and Ref. 12	$\bar{G}_{12}$	.0085
	90°	ASTM D-3552	$\bar{E}_2$, $\bar{\sigma}_{tt}$	.0085
Compression	0°	[a]ASTM D-3410	$\bar{\sigma}_{1c}$	0.0004

[a]Standard for resin matrix composites.

28

TABLE III.- $\alpha Al_2O_3/Al$ COMPOSITE LONGITUDINAL AND TRANSVERSE TENSILE TEST RESULTS

Specimen history	Test temperature, K	Longitudinal		Transverse	
		Ultimate stress, MPa	Elastic modulus, GPa	Ultimate stress, MPa	Elastic modulus, GPa
As fabricated	295	537 543 575	213 207 209	188 187 184	171 150 159
	500	541 455 654	219 224 (a)	118 118 110	123 119 108
	590	548 510 493	221 229 220	74 72 73	110 130 106
2500 hr at 590 K	295	637 658 601	230 228 226	119 114 106	130 130 141
5000 hr at 590 K	295	547 510 505	216 229 210	80 77 80	108 104 (a)
10 000 hr at 590 K	295	528 513 515	227 226 223	70 70	(a) 106
6000 cycles between 200 K and 590 K	295	557 630 637	219 226 219	69 60 70	(b)
10^6 fatigue cycles	295	704 744 697	234 233 236		
2500 hr at 590 K and 10^6 fatigue cycles	295	509 563 508	(a) 234 (a)		
6000 cycles between 200 K and 590 K and 10^6 fatigue cycles	295	454 469	206 202		

[a]Strain gages failed.
[b]Insufficient elastic zone.

TABLE IV.- $\alpha Al_2O_3/Al$ COMPOSITE COMPRESSION AND SHEAR

MODULUS TEST RESULTS

| Specimen history | Test temperature, K | Compression | | Shear modulus, GPa |
		Ultimate stress, MPa	Elastic modulus, GPa	
As fabricated	295	2781	216	58.6
		2465	209	56.5
		2636	215	58.3
	500	1932	202	64.0
		1470	194	54.7
		1159	190	54.2
	590	1625	207	50.8
		962	202	45.4
				51.4
2500 hr at 590 K	295	2152	228	62.1
		2276	226	61.0
		2122	231	61.2
6000 cycles between 200 K and 590 K	295	1831	219	30.6
		1812	219	28.0
		1767	235	31.1

TABLE V.- MECHANICAL PROPERTIES OF AS-FABRICATED $\alpha Al_2O_3/Al$ COMPOSITE

Longitudinal tensile strength, $\bar{\sigma}_{1t}$, MPa 522
Longitudinal elastic modulus, $\bar{E}_1$, GPa 210
Transverse tensile strength, $\bar{\sigma}_{tt}$, MPa 186
Transverse elastic modulus, $\bar{E}_2$, GPa 160
Longitudinal compressive strength, $\bar{\sigma}_{1c}$, MPa 2627
Shear modulus, $\bar{G}_{12}$, GPa 58
Poisson's ratio, $\bar{\nu}_{12}$ 0.27
Density, $\bar{\rho}$, kg-m^{-3} 3203
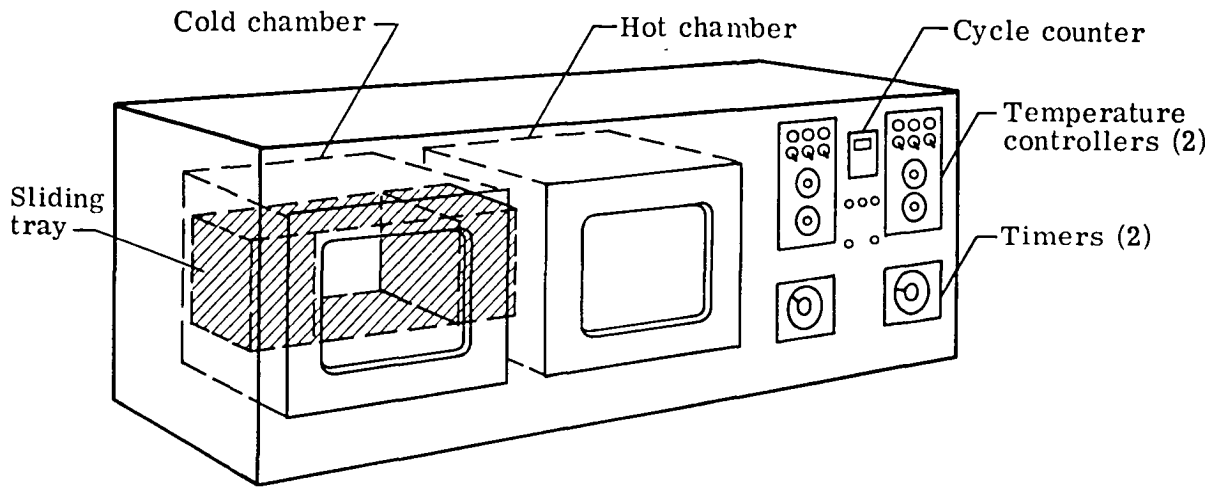
30

(a) Thermal cycling apparatus.
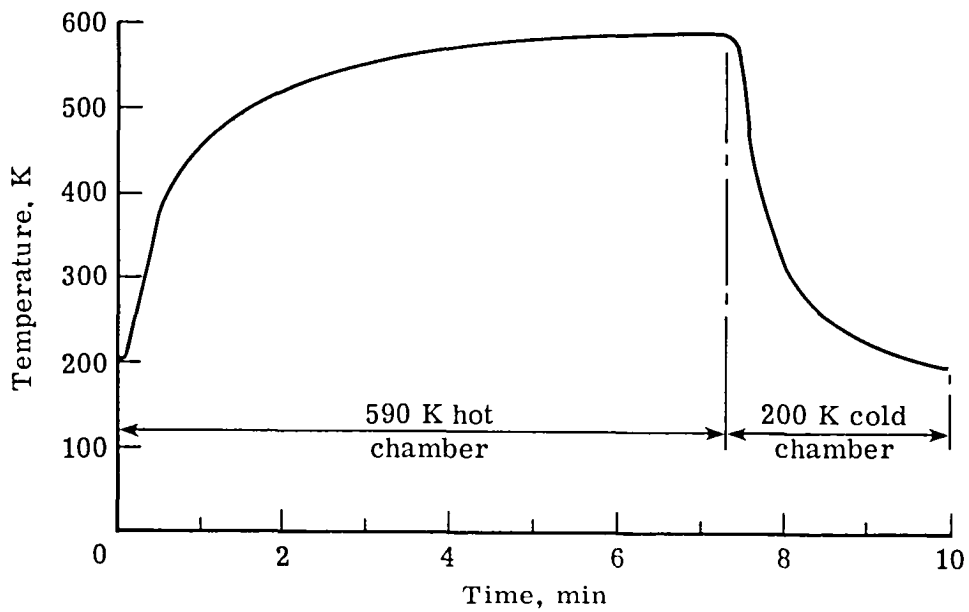
(b) Typical specimen temperature history for one cycle.

Figure 1.- Cyclic thermal exposure.

31
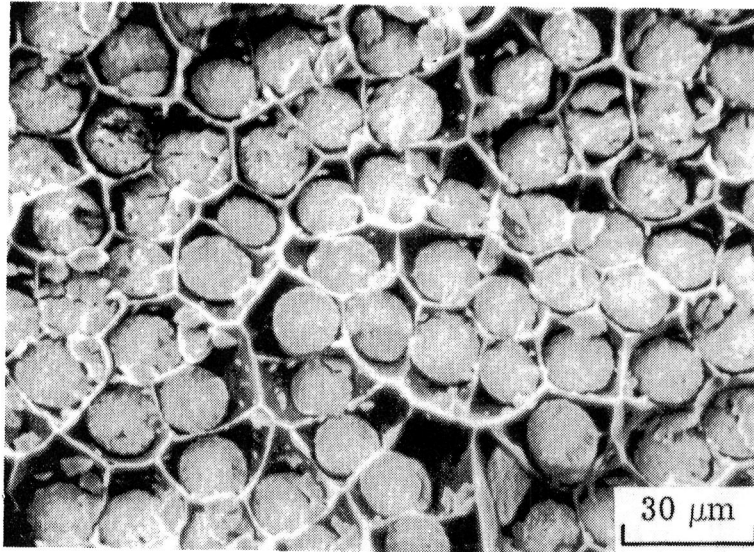
(a) Longitudinal.
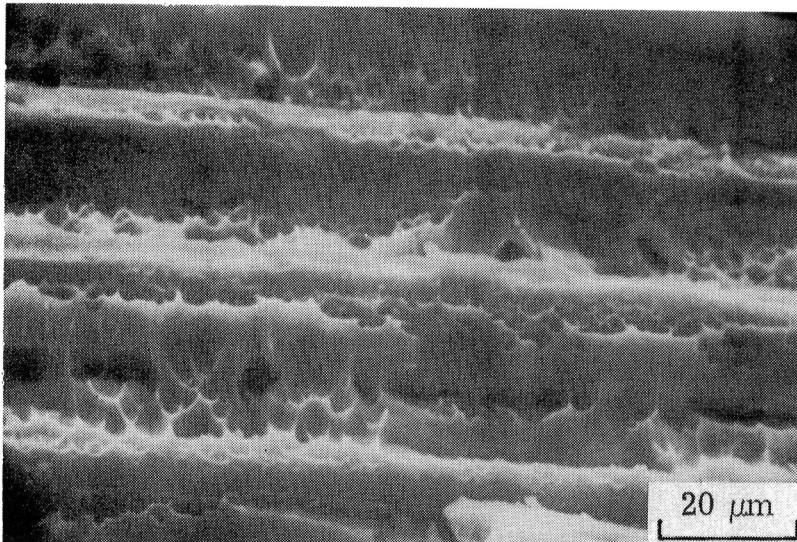
(b) Transverse.

L-80-220

Figure 2.- Typical fracture surfaces of as-fabricated $\alpha Al_2O_3/Al$ composite specimens.
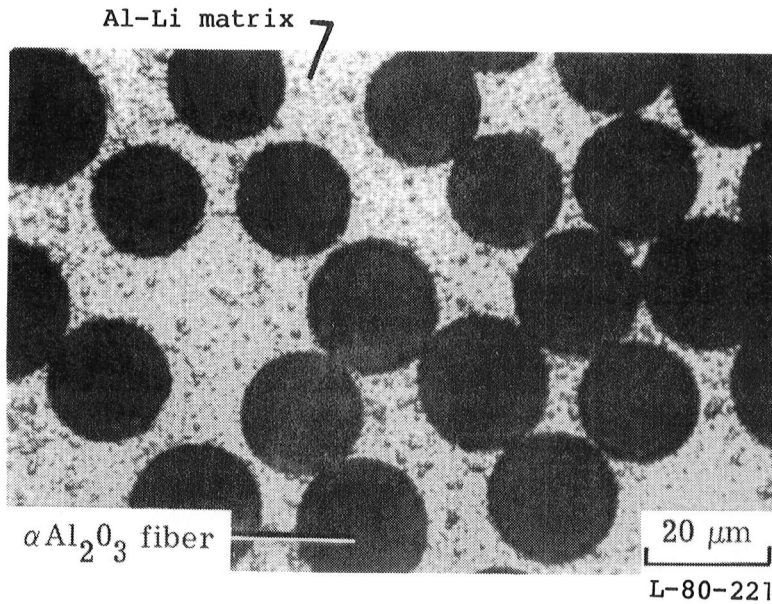
Figure 3.-Typical cross section of as-fabricated $\alpha Al_2O_3/Al$ composite specimens.
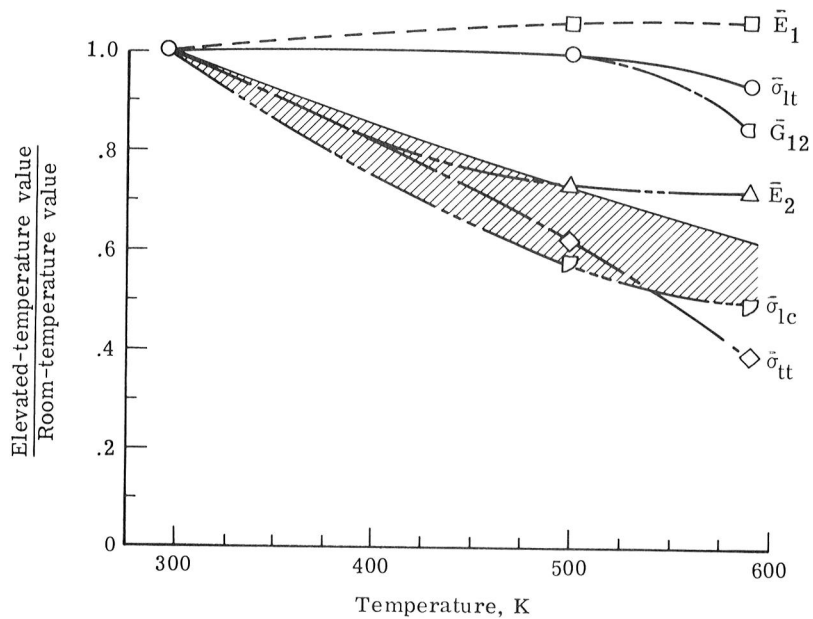
Figure 4.- Effect of elevated test temperature on as-fabricated $\alpha Al_2O_3/Al$ composite material, normalized by room-temperature properties.
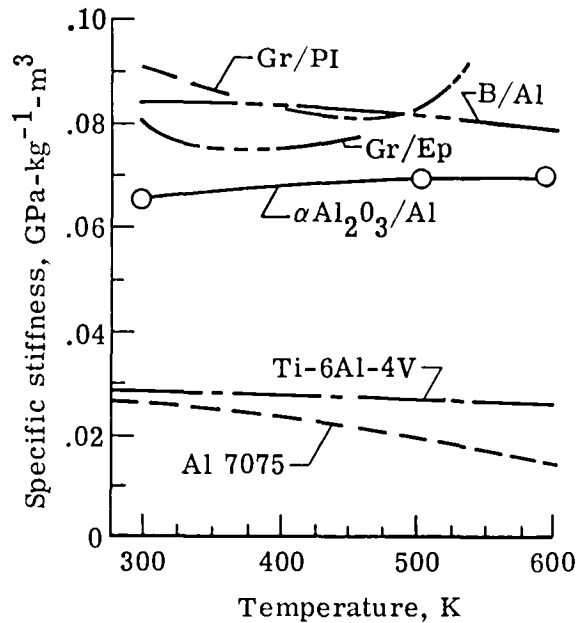
(a) Specific stiffness.
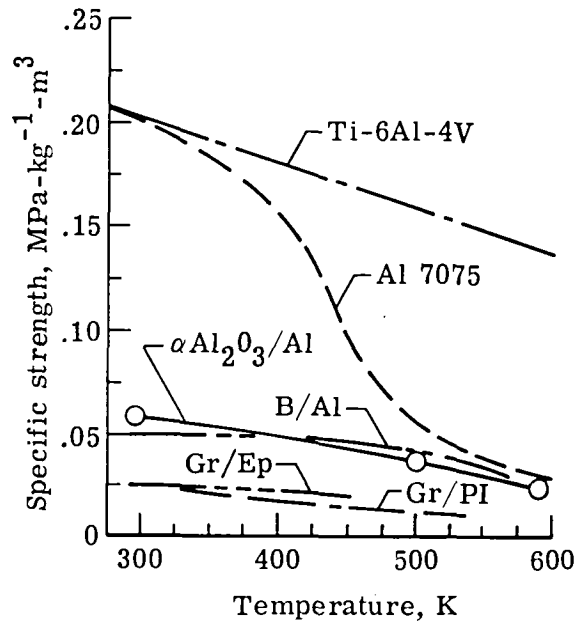
(b) Specific transverse tensile strength.
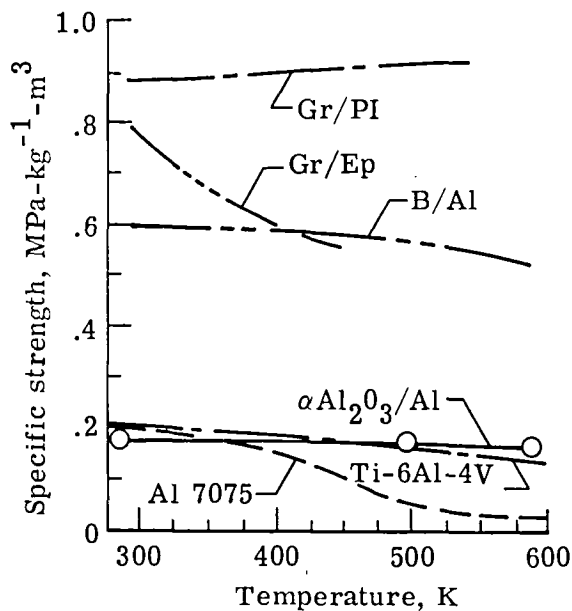
(c) Specific longitudinal tensile strength.
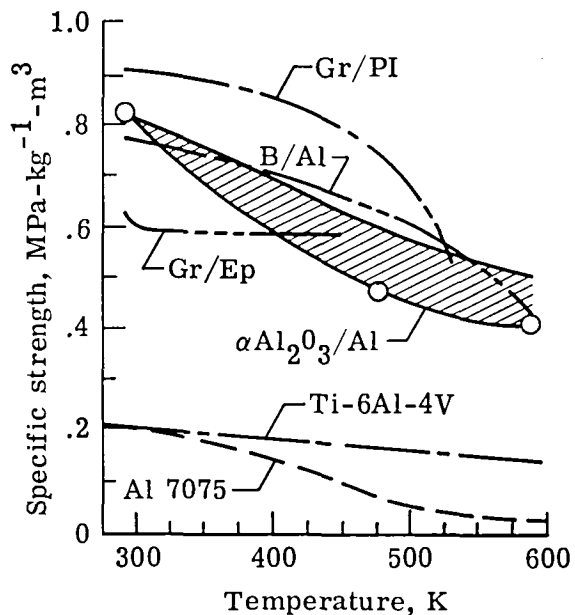
(d) Specific longitudinal compression strength.

Figure 5.- Specific properties versus test temperature of $\alpha Al_2O_3/Al$ composite compared with Al 7075, Ti-6Al-4V, B/Al, Gr/Ep, and Gr/PI.
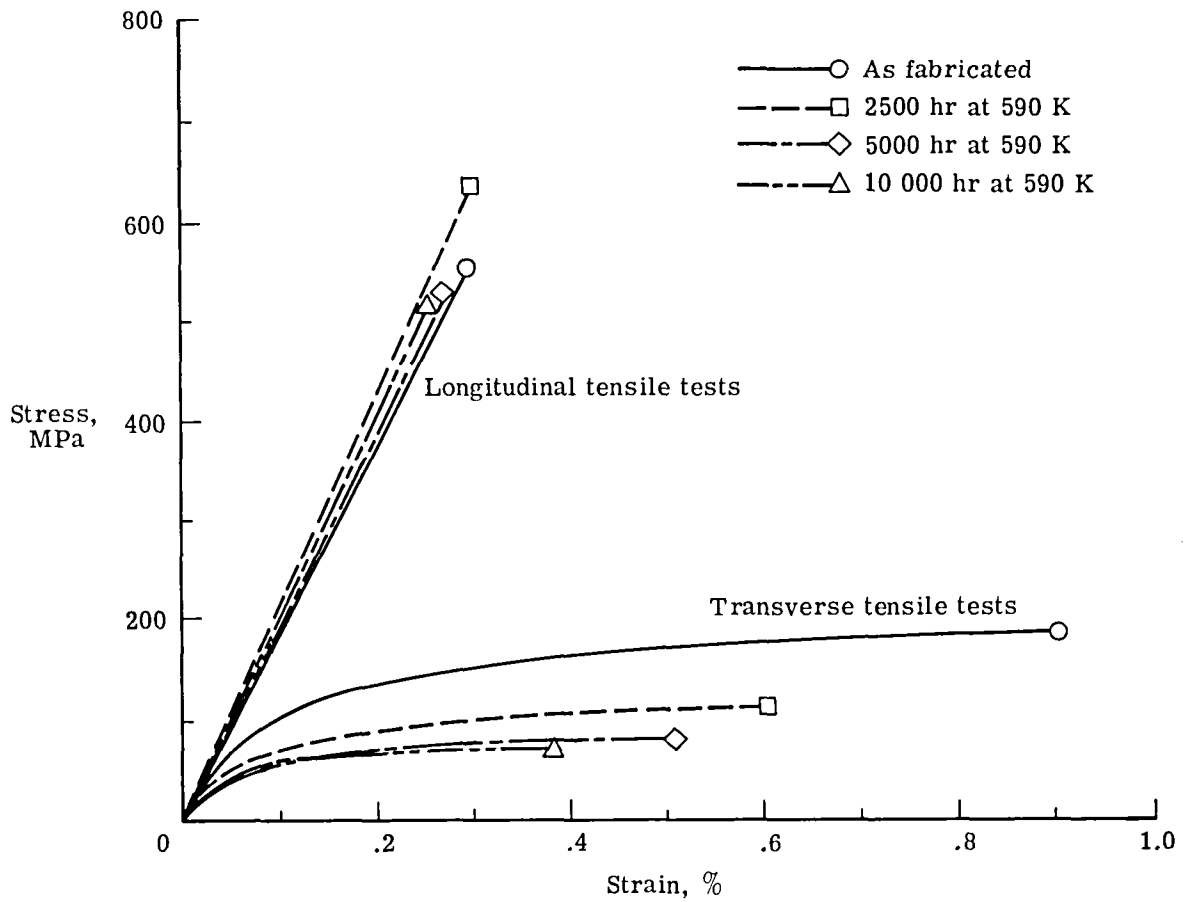
Figure 6.- Typical room-temperature longitudinal and transverse stress-strain curves for $\alpha Al_2O_3/Al$ composite material exposed at 590 K.
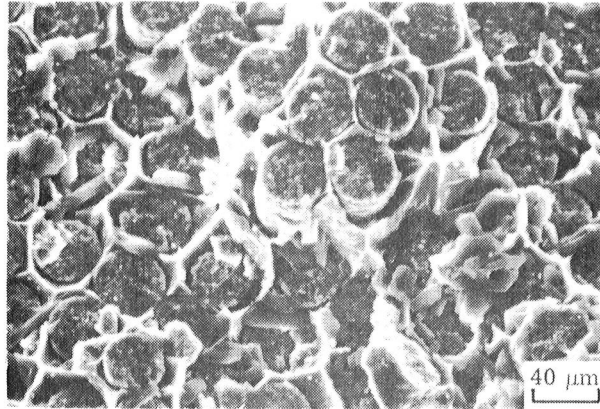
(a) 2500 hours.
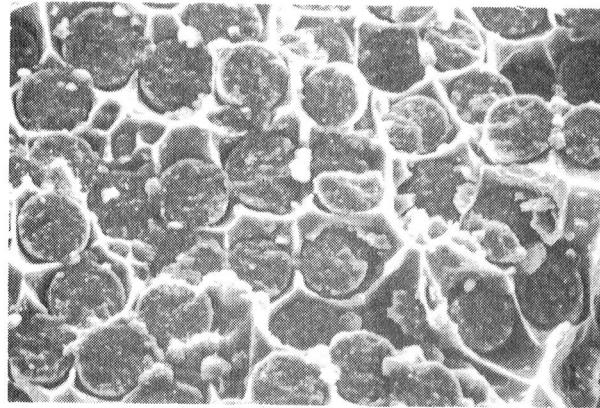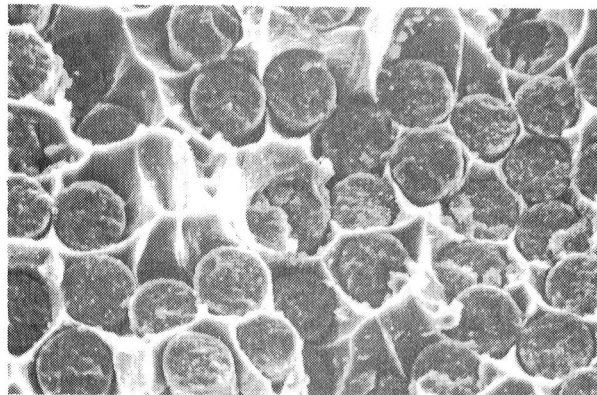
(b) 5000 hours.

(c) 10 000 hours.

L-80-222

Figure 7.- Typical longitudinal tensile fracture surfaces of $\alpha Al_2O_3/Al$ composite specimens thermally exposed at 590 K.
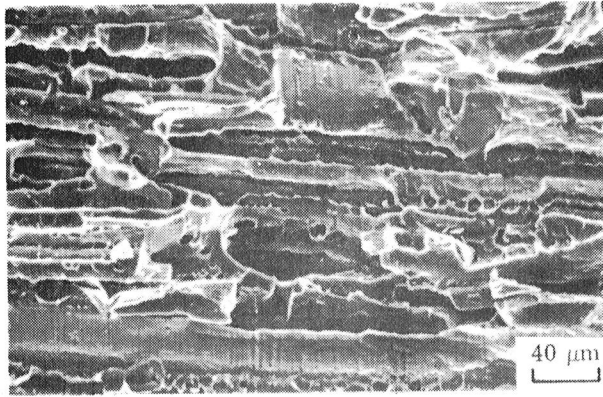
(a) 2500 hours.
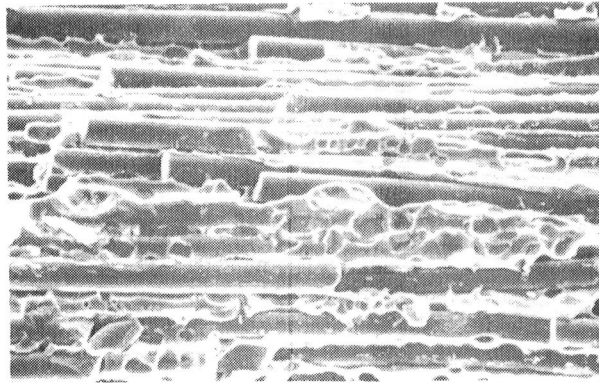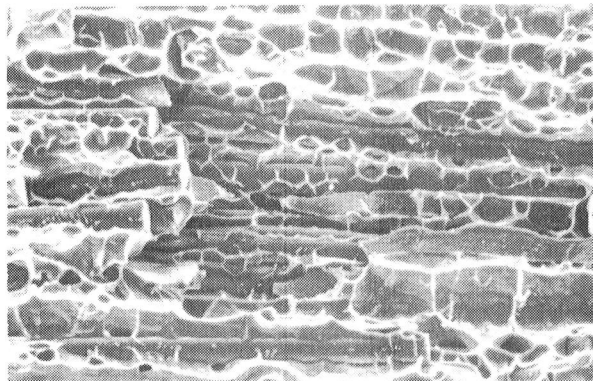
(b) 5000 hours.

(c) 10 000 hours.

L-80-223

Figure 8.- Typical transverse tensile fracture surfaces of $\alpha Al_2O_3/Al$ composite specimens thermally exposed at 590 K.
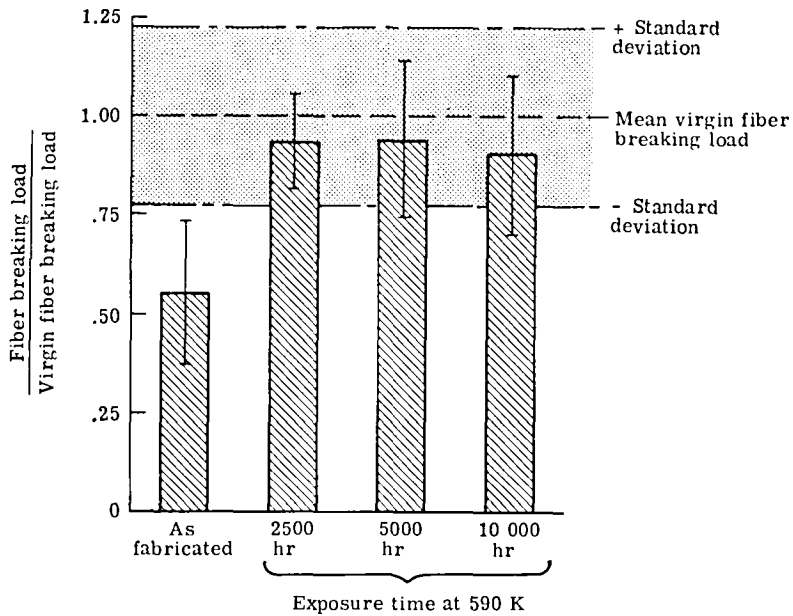
Figure 9.- αAl_2O_3 fiber breaking loads after removal from composite specimens thermally exposed at 590 K.
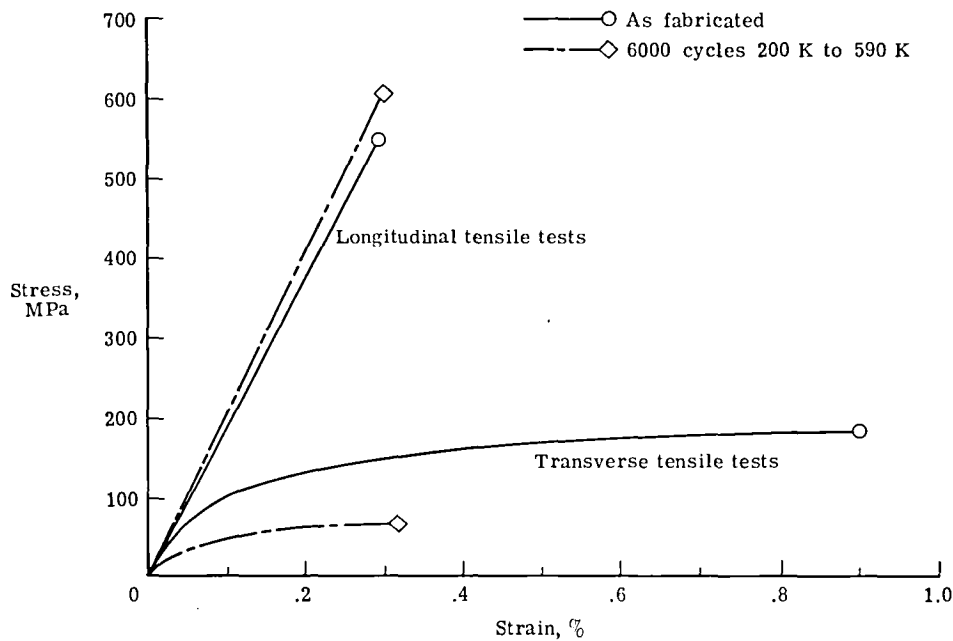
Figure 10.- Typical room-temperature longitudinal and transverse stress-strain curves for $\alpha Al_2O_3/Al$ composite material after 6000 thermal cycles between 200 K and 590 K.
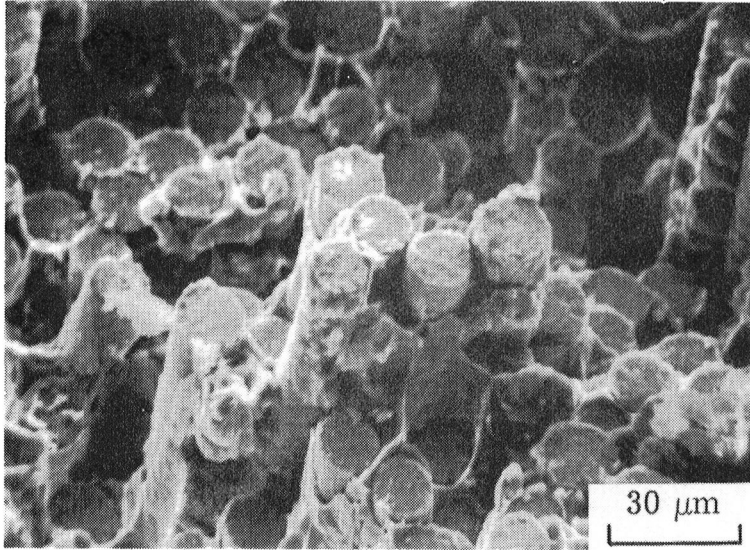
(a) Longitudinal.
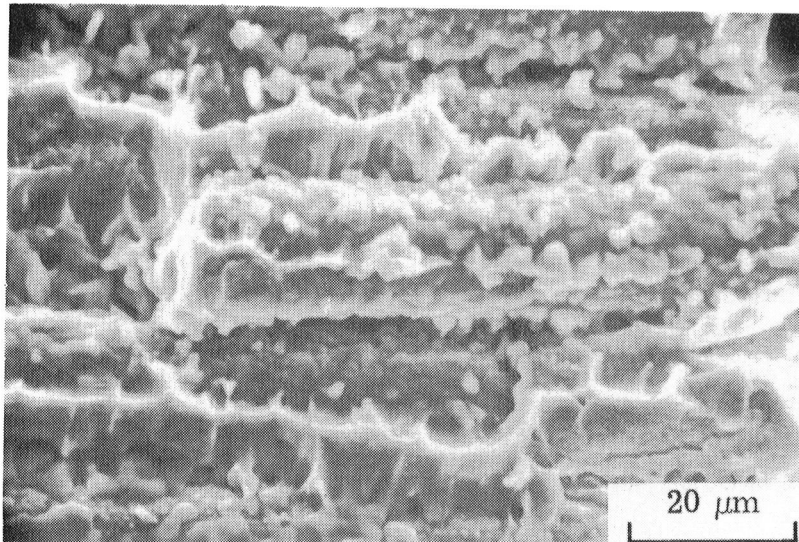
(b) Transverse.

L-80-224

Figure 11.- Typical fracture surfaces of $\alpha Al_2O_3/Al$ composite specimens after 6000 thermal cycles between 200 K and 590 K.
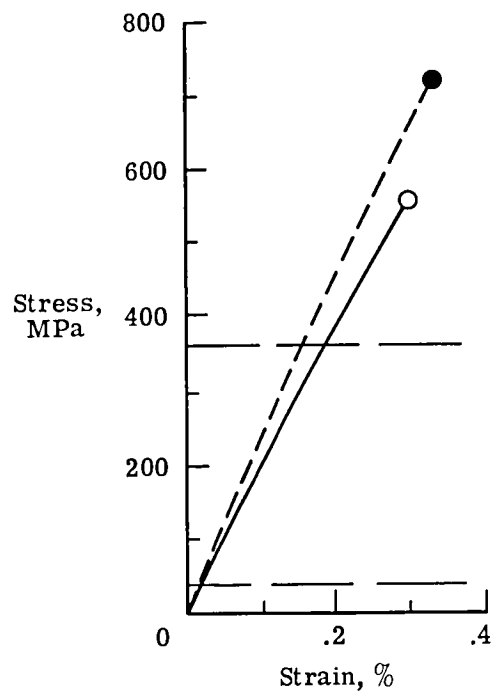
Figure 12.- Typical room-temperature longitudinal stress-strain curves for
$\alpha Al_2O_3/Al$ composite material after 10^6 fatigue cycles.
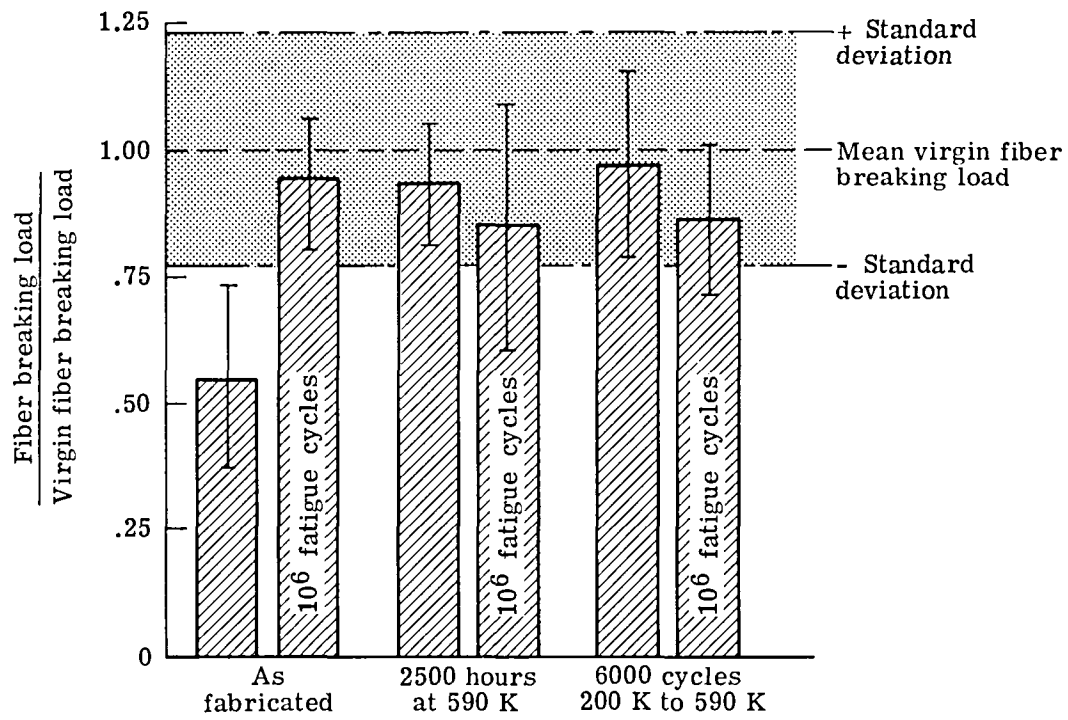
Figure 13.- αAl_2O_3 fiber breaking loads after removal from composite specimens exposed to 10^6 fatigue cycles.
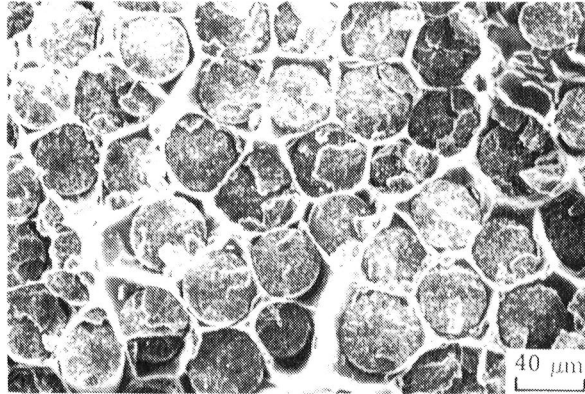
(a) As fabricated.
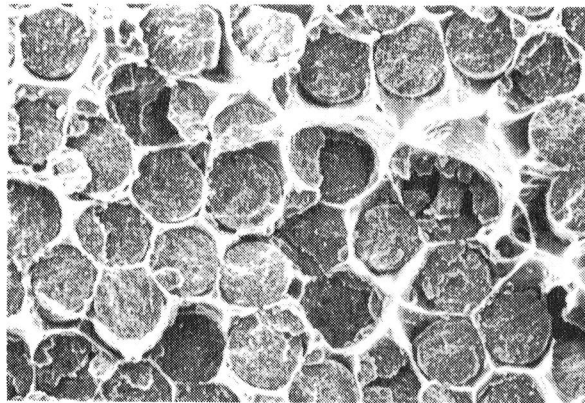
(b) 2500 hours at 590 K.
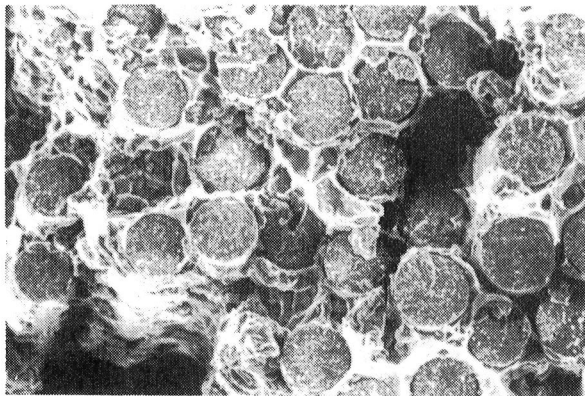
(c) 6000 thermal cycles between
200 K and 590 K.

L-80-225

Figure 14.- Typical longitudinal tensile fracture surfaces of $\alpha Al_2O_3/Al$ composite specimens after 10^6 fatigue cycles.
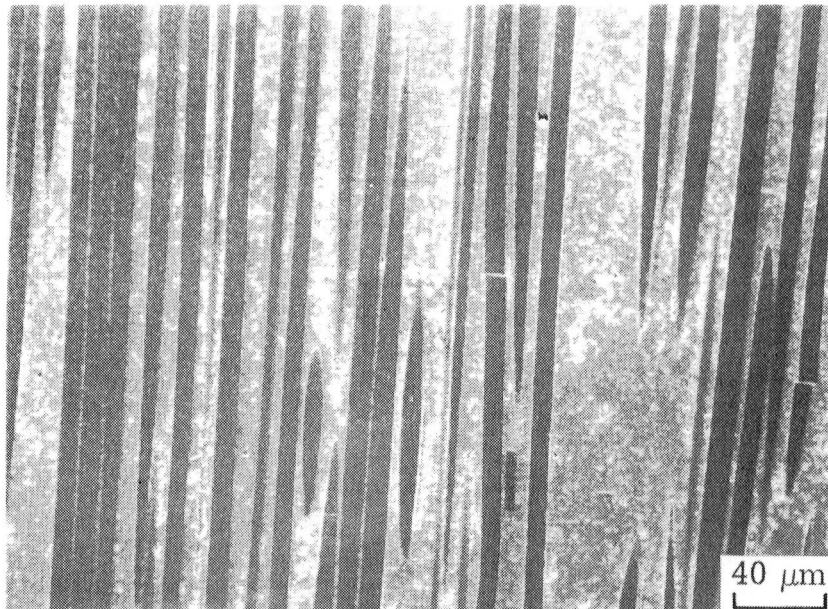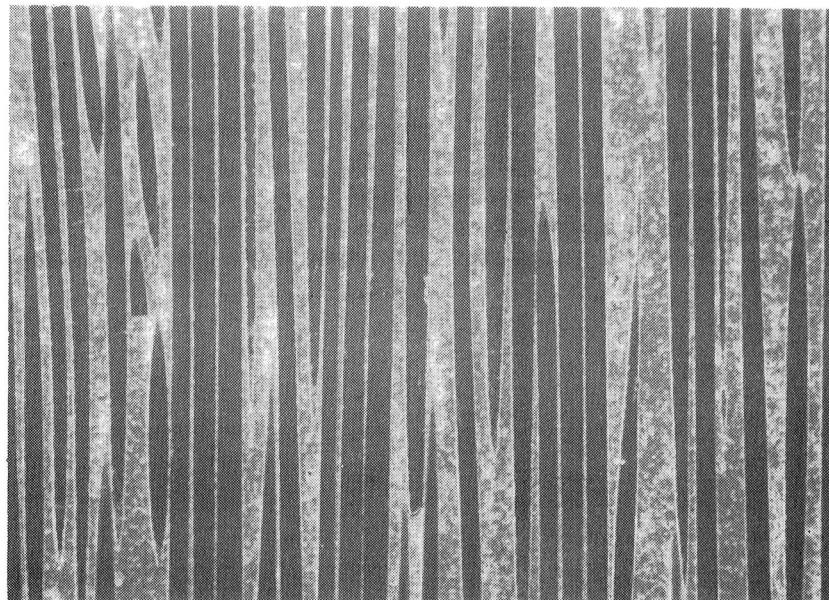
Without fatigue

With fatigue

L-80-226

(a) As fabricated.

Figure 15.- Typical transverse cross sections of polished and etched $\alpha Al_2O_3/Al$ composite specimens before and after exposure to 10^6 fatigue cycles.

43
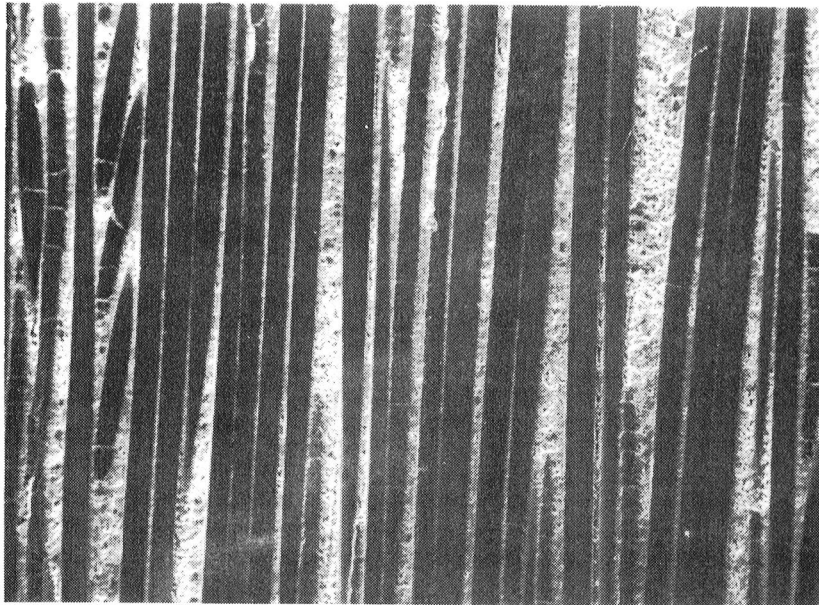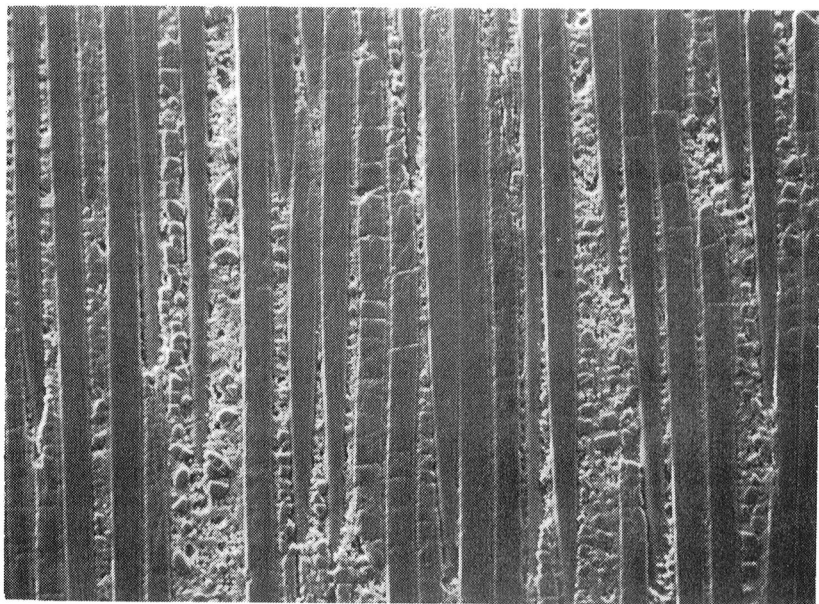
Without fatigue

With fatigue

L-80-227

(b) 2500 hours at 590 K.

Figure 15.- Continued.
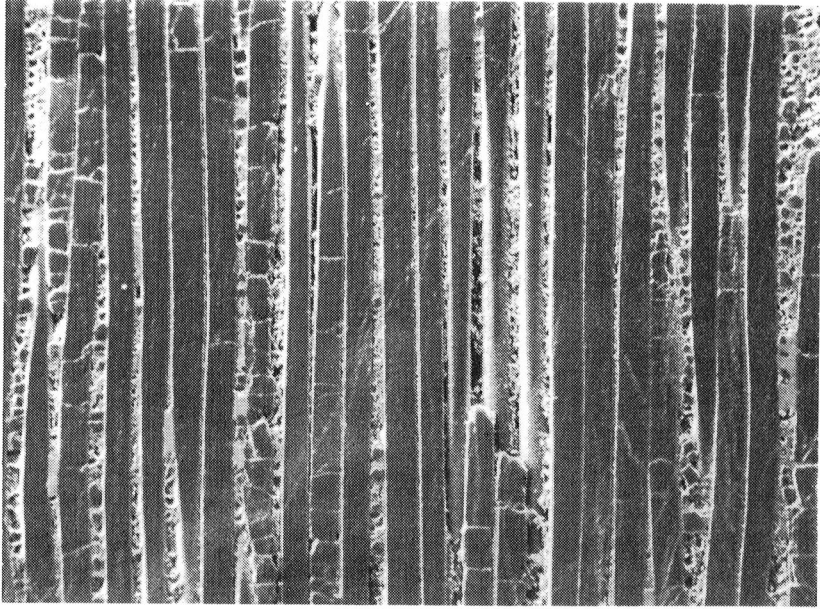
Without fatigue
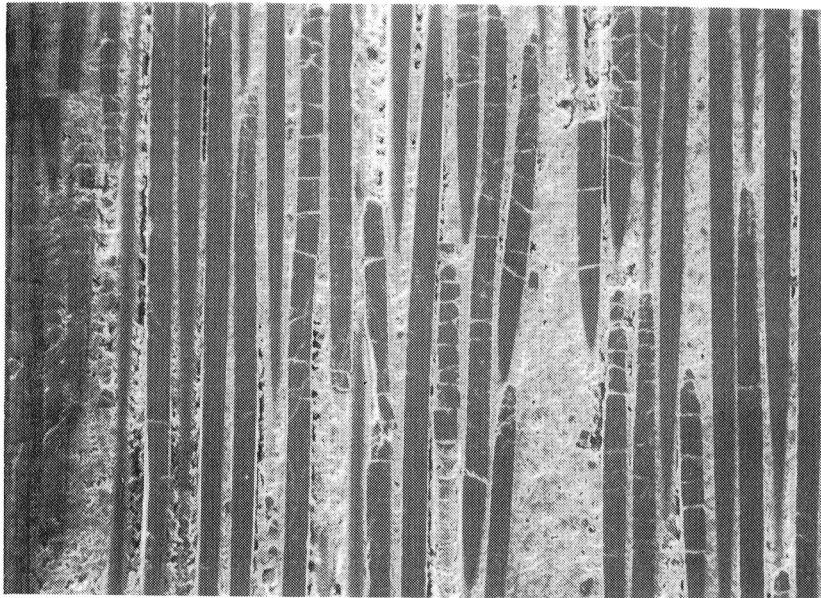
With fatigue

L-80-228

(c) 6000 thermal cycles between 200 K and 590 K.

Figure 15.- Concluded.

FIVE BORON/ALUMINUM COMPOSITES: LONG-TERM THERMAL

DEGRADATION AND ALLOYING CONSTITUENT EFFECTS[1]

George C. Olsen

SEPTEMBER 1981

SUMMARY

The effects of thermal exposures on the properties of five boron-aluminum composite systems were experimentally investigated. Composite specimens were fabricated with 49 volume percent boron fibers (203 μm diameter) in aluminum alloy matrices 1100 Al, 2024 Al, 3003 Al, 5052 Al, and 6061 Al. In addition specimens of matrix alloy only were identically fabricated. The specimens were tested as-fabricated and after thermal exposures of up to 10 000 hours at 500 K and 590 K, up to 500 hours at 730 K, and up to 2000 thermal cycles between 200 K and 590 K. Composite longitudinal and transverse tensile strengths, longitudinal compression strength, and in-plane shear strength were determined in each condition by mechanical testing. None of the systems was severely degraded by the long-term exposure at 590 K. The best performing system was B/2024 Al with no transverse tensile strength degradation due to interaction and less than 10 percent longitudinal tensile strength degradation due to interaction.

The effects of the matrix alloying constituents on the degradation mechanisms of each of these systems were experimentally investigated. Composite specimens and individual fibers were metallurgically analyzed using a scanning electron microscope and an electron microprobe to determine failure characteristics, chemical element distribution, and reaction layer morphology. Alloying constituents were found to effect the degradation mechanisms as follows: iron causes low temperature degradation

1

unless manganese is present as a stabilizer; magnesium, iron, and manganese increase degradation; and copper strengthens fibers.

INTRODUCTION

Technological advances in the aerospace industry continuously demand stronger, stiffer, lighter weight structural materials capable of long service life at elevated temperatures. Often these demands cannot be efficiently met by metal alloys. As one alternative, boron/aluminum composite technology began to develop 25 years ago. Improvements in the technology have included the evolution of 203 μm diameter boron fibers with less core-flaw sensitivity (ref. 1)and improved diffusion bonding techniques (ref. 2). Currently boron/aluminum composites have strength-to-weight and stiffness-to-weight ratios three times higher than aluminum and titanium alloys.

Initially, the accepted temperature for long term use of boron/aluminum composites was 590 K (refs. 3 and 4). This limitation was imposed by the aluminum matrix properties and considered to be below the point of serious interaction problems (ref. 4). Most thermal degradation studies were therefore confined to temperatures typical of fabrication and secondary processing operations. However, a more recent study of Boron/ 6061 aluminum degradation at exposure temperatures of 450 K, 560 K, and 700 K for up to 10 000 hours reported severe strength degradation and recommended a maximum use temperature of 450 K (ref. 5).

Fiber-matrix bonding and composite property degradation have been attributed to an aluminum-boron reaction forming AlB_2 (ref. 6). Other constituents of aluminum alloys were said to be less reactive with boron than aluminum and were not considered significant contributors to composite degradation (ref. 2). As a result, aluminum matrix alloys have been selected on the basis of bonding characteristics, fracture toughness, creep forming capability, strength, and corrosion resistance (ref. 2) without concern about the effect of their alloying constituents. However, recent work on Boron/6061 aluminum composites (refs. 7 and 8) suggests magnesium, an alloying constituent in the matrix, is an active reactant with the fiber. If magnesium significantly contributes to thermal degradation of boron/aluminum composites, it could account for the extremely different degradation rates for composites with different alloys reported in the literature (refs. 9 and 10). In addition, this theory raises questions about the effect of other alloy constituents on composite degradation.

This investigation had two purposes. One was to determine the effects of long term thermal exposure and cyclic thermal exposure on the mechanical properties of boron/aluminum composites. The other was to determine the effects of the aluminum alloy constituents on the degradation mechanisms in boron/aluminum composites. To accomplish these purposes boron/aluminum composites made from five commercially available aluminum alloy foils were studied. The composites were exposed for up to 10 000 hours at 500 K and 590 K to study behavior in the anticipated use range and for up to 500 hours at 730 K to study behavior at an over temp-

erature condition. Composites were thermally cycled for up to 2000 cycles between 200 K and 590 K to study effects of rapid temperature reversals.

Mechanical property tests including longitudinal and transverse tensile tests, longitudinal compression tests, and in-plane shear tests were conducted on the composite specimens. Composite specimens and individual fibers were metallurgically analyzed using a scanning electron microscope and an electron microprobe to determine failure characteristics, chemical element distributions, and reaction layer morphology.

MATERIALS AND EXPOSURE CONDITIONS

Materials and Test Specimens

Boron-aluminum composites made from five different aluminum alloys were investigated. The alloys, in the form of 115 µm thick foils, were 1100 Al (a commercially pure aluminum), 2024 Al (a heat-treatable aluminum-copper-magnesium alloy), 3003 Al (an aluminum-manganese alloy), 5052 Al (an aluminum-magnesium alloy), and 6061 Al (a heat-treatable aluminum-magnesium-silicon alloy). The nominal composition, tensile strength in the original temper condition, and tensile strength in the fully annealed condition of each of these alloys are listed in Table I (ref. 11). The 203 µm diameter boron fibers are amorphous boron vapor

4

deposited on a 12 μm diameter tungsten wire substrate. In the virgin state the fiber strength was 3.78 GPa (the mean of 25 measurements) and the elastic modulus was 400 GPa (vendor supplied data).

Composite panels, 500 mm by 300 mm by 2 mm thick, were fabricated with the component materials. Alternate layers of aluminum foil and boron fibers were laid-up to form eight-ply laminates with 49 volume-percent-fibers (except for B/3003 Al which had 47 volume-percent fibers). Separate panels were fabricated with fibers oriented either unidirectionally or at ±45 degrees. These panels were consolidated by a hot press diffusion bonding process. The bonding parameters for each alloy system are listed in Table II. The alloys with more aluminum content have more coherent oxide layers which offer more resistance to diffusion. As a result, these alloys require higher processing temperatures and longer processing times to produce well-bonded composites. In addition to the composite panels, panels of the aluminum alloys were fabricated in exactly the same manner as the composite panels except no boron reinforcing fibers were used.

Test specimens, in the configurations listed in Table III, were cut from the panels with diamond cut-off wheels. Sets of three replicate specimens for each test and exposure condition were prepared. Each specimen was cleaned, inspected, and systematically numbered and measured. After thermal exposure, to be described later, strain gages were bonded to the specimens. An epoxy adhesive was used for specimens to be tested at room temperature and a ceramic base adhesive was used for specimens to

5

be tested at elevated temperature. Four gages were bonded to each specimen, two back-to-back on the centerline to measure longitudinal strain and two back-to-back on the centerline to measure transverse strain. In addition, compression specimens were equipped with epoxy bonded aluminum gripping tabs for room temperature testing and ceramic bonded titanium tabs for elevated temperature testing.

Thermal Exposures

Continuous isothermal exposures.- Continuous isothermal exposures were conducted in air-circulating electric ovens. Exposure temperatures were 500 K, 590 K, and 730 K. At 500 K specimens were exposed for 5000 and 10 000 hours. At 590 K specimens were exposed for 2500, 5000, 7500, and 10 000 hours. At 730 K specimens were exposed for 100, 300, and 500 hours. After removal from the ovens, specimens were allowed to cool in ambient air.

Cyclic thermal exposures.- Cyclic exposures were conducted in a dual chamber apparatus. Specimens, mounted on a mechanically driven sliding tray, were alternately inserted in an air-circulating, electrically heated 590 K hot chamber and a liquid-nitrogen-cooled 200 K cold chamber. A full cycle was 29 minutes long with exposures of 21 minutes in the hot chamber and eight minutes in the cold chamber required to approach the test temperatures. A schematic drawing of the apparatus and a typical specimen temperature profile for one cycle are shown in figure 1. Sets of specimens were exposed to 500 and 2000 cycles.

TEST PROCEDURES

Mechanical Property Tests

Longitudinal and transverse tensile tests were performed on all five of the composite materials. Longitudinal compression and in-plane shear tests were performed on the B/1100 Al, B/3003 Al, and B/6061 Al composite systems. Tensile tests were performed on the alloy specimens (specimens with no boron reinforcement). The test standards followed, the properties determined, and load rate used for each of the tests are shown in Table IV. Room temperature tests were conducted in a 245 kN hydraulic test frame equipped with hydraulic grips. The hydraulic grips were used for tension and shear tests. Minimum gripping pressure was applied and acetate inserts protected the specimen surfaces from damage by the grips. An IITRI wedge grip fixture (fixture description in ref. 12) was used for compression tests. Elevated temperature tests were conducted in a 490 kN hydraulic test frame equipped with an electrically heated environmental test chamber. Longitudinal tensile specimens were tested with mechanical clevis grips and transverse tensile and shear specimens were tested with wedge grips. Elevated temperature compression tests also used the IITRI compression fixture. All load and strain data were processed through an on-line data acquisition system programmed to record, reduce and plot the data.

Fibers were chemically removed from their aluminum matrix with a heated NaOH solution (ASTM Standard D 3553-76). Individual fiber break-

ing stresses were determined experimentally using the fiber bend test fixture shown schematically in figure 2. Fibers approximately 100 mm long were bent around the successively smaller mandrels of the test fixture until they failed. The mandrel on which the fiber failed corresponds to a stress range determined by the equation for elastic bending stresses in a beam, $\sigma_{max} = E_f (r_f/R_m)$ (ref. 13), where σ_{max} is the maximum stress, E_f is the fiber elastic modulus, r_f is the fiber radius, and R_m is the mandrel radius. A minimum of 40 fibers were tested from each specimen. Strength distributions were determined for fibers removed from as-fabricated specimens that were not mechanically tested and compared with the range and mean of the virgin fiber strength distribution (vendor supplied data). In addition, residual fiber strength distributions were determined for all systems after mechanical testing of the composite. These fiber populations are biased by composite mechanical testing (i.e. weaker fibers are removed) but still show changes in upper bound strengths and variations in mean fiber strength and distribution.

Metallurgical Analysis

Representative specimens of each composite system in the as-fabricated condition, after 10 000 hours at 500 K, 10 000 hours at 590 K, 500 hours at 730 K, and 2000 thermal cycles were metallurgically examined. Longitudinal and transverse tensile fracture surfaces of the composites were examined with a scanning electron microscope (SEM) to determine fracture modes. Polished and etched (Keller's reagent) cross-sections

from longitudinal tensile specimens were analyzed with an electron micro-probe to qualitatively determine chemical element distribution. Resolution of the microprobe is approximately 5μm so that reaction layers thinner than 5 μm could not be investigated.

Fibers were chemically removed from the composite matrix (by digesting the aluminum in a heated NaOH solution) for further examination. Reaction layer morphology was examined by first etching one end of the fibers with Murakami's reagent to remove the reaction layer. Then the interfaces between the etched and unetched regions of the fibers were examined with an SEM and the chemical elements in the reaction layer determined with an energy dispersion analysis of X-rays (EDAX). Boron, a certain constituent of the reaction layer, cannot be detected by energy dispersion techniques (elements with atomic numbers less than 11 are transparent to X-rays, boron's atomic number is 5).

Reaction layers on chemically removed fibers were analyzed for crystalline structure using X-ray diffraction techniques. Fibers were laid up side-by-side to form a sample for analysis. Other fibers were ground and sieved to produce a powder sample higher in reaction product concentration. Some of the powder sample was further concentrated by chemically leaching away the boron fiber particles with Murakami's reagent. X-ray diffraction patterns were made from these samples using a copper Kα incident X-ray beam, a diffracted beam monochromator, a diffractometer, and a goniometer.

RESULTS AND DISCUSSION

Results of all mechanical property tests are shown in Tables V

through X. Typical stress-strain curves for each condition are shown in

Appendices A through E. Trends in these data are illustrated in the fol-

lowing sections of the report by graphic plots. These plots were pre-

pared in the following manner: mean values of the data were plotted and

fitted with straight line segments for the well behaved data (alloy ten-

sile data and the composite transverse tensile and in-plane shear data

especially). Data that exhibited large scatter or deviated significantly

from a straight line (composite longitudinal tensile and compression

data, principally) were fitted with a first or second order polynomial in

a least squares regression analysis. Data points whose standardized

residuals were more than two standard deviations from zero were dropped

as out-lying points and the mean value calculation and regression analy-

sis repeated for the remaining points. Those data dropped as out-lying

points are identified in the tables by an asterisk.

As-Fabricated Material

Fabrication effects on matrix strength.- The effect of the diffusion

bonding process on the matrix material strength can be seen by comparing

the strength of the diffusion-bonded matrix - only specimens (Table X)

with the tempered and annealed strengths of the alloys (Table I). Fabri-

cation temperatures and times (Table II) required to produce well bonded

composite materials were sufficient to fully anneal the non-heat-treat-

10

able strain-hardened 1100 Al and 3003 Al alloys. The remaining strain-hardened alloy, 5052 Al, consolidated at a slightly lower temperature and shorter time, approached the annealed condition (approximately 81 percent annealed). The heat-treatable alloys, 2024 Al, and 6061 Al, were partially annealed (approximately 31 percent) during fabrication.

Fabrication effects on fiber strength.- Fiber strength distributions for fibers chemically removed from specimens after fabrication without performing mechanical property tests are shown in figure 3. Before fabrication, the virgin fiber mean strength was 3.78 GPa normally distributed over the range of 3.26 GPa to 4.14 GPa as indicated in the figure. After exposure to the fabrication process, fiber strength distributions ranged from similar to the virgin fibers to radically altered. Fibers from the 1100 Al system (fig. 3 (a)) showed only minor degradation. Fibers from the 2024 Al system (fig. 3 (b)) had a slightly higher mean value but the lower limit of strength was lower and the upper limit was significantly higher. This broadened range suggests that at least two mechanisms were functioning, one which weakened the fibers and another which strengthened them. Fibers from the 3003 Al system (fig. 3(c)) suffered a uniform degradation in strength of 15 to 20 percent as a result of the fabrication process. Fibers from the 5052 Al system (fig. 3(d)) were radically altered, their mean strength was lower, their upper limit was higher and their lower limit was significantly lower. Again, as with the fibers from the 2024 Al system, dual mechanisms are suggested but in this alloy the degradation mechanism was more active and the strengthening mechanism was less active. The mean strength of fibers from the

6061 Al system (fig. 3(e)) increased approximately 10 percent without any significant change in the lower limit but a significant increase in the upper limit. This upward shift suggests that a strengthening mechanism was active.

Reaction layers on individual fibers were enhanced by partial etching. These fibers were studied in an SEM and the elemental composition of the reaction layers determined by EDAX (recall that boron, a certain constituent of the reaction layer cannot be detected by EDAX). SEM photomicrographs of the fiber reaction layers are shown in figure 4. Fibers from the 1100 Al system (fig. 4(a)) have a dendritic reaction layer composed of aluminum with a trace of silicon. Interspersed light colored particles are iron rich. Fibers from the 2024 Al system (fig. 4(b)) have a reaction layer composed of approximately one part aluminum and 0.2 parts magnesium with traces of silicon and copper. Interspersed light colored particles are 1.4 parts magnesium to one part aluminum. Fibers from the 3003 Al system (fig. 4(c)) have a reaction layer of dark spherical particles composed of aluminum and manganese with a trace of silicon and light spherical particles rich in iron. Fibers from the 5052 Al system (fig. 4(d)) have a thick reaction layer of approximately 1.7 parts magnesium to one part aluminum with traces of silicon, chromium, iron, and copper. Interspersed light particles are iron rich. Fibers from the 6061 Al system (fig. 4(e)) have a thick reaction layer with equal aluminum and magnesium content and traces of silicon, chromium, iron, and copper.

Polished cross-sections of as-fabricated specimens were scanned with
an electron microprobe to determine elemental gradients. Traces across
reaction zones did not indicate any increased elemental concentrations at
the reaction zones. Gradients of boron and aluminum concentrations at
the interfaces did not have plateaus indicating the reaction zone. The
lack of these plateaus only indicates the reaction zone was smaller than
the resolution of the microprobe ($5 \mu m$).

Comparing these observed effects of fabrication on the fiber strength
distributions with the alloying constituents shown in Table I, several
hypotheses can be proposed. First, only minor degradation in fiber
strength occured during fabrication as a result of reaction with commer-
cially pure aluminum. Second, manganese as the only alloying element in
3003 Al contributed to a uniform degradation of fiber strength. Third,
magnesium, usually present in the form of Mg_5Al_8 or in solid solution in
the 2024 Al and 5052 Al alloys, caused the fiber strength degradation and
lower limit reduction noted in those systems. The order of increasing
magnesium content of these alloys corresponds to the order of increased
strength degradation observed. Isolation of the lower strength fibers,
especially in the 5052 Al system, suggests the degradation was not uni-
form but a localized phenomena probably dependent on particle contact
with the fiber. Magnesium is also an alloying constituent in 6061 Al,
but there it is bound in Mg_2Si particles and not available for further
reaction. Finally, increased mean fiber strength and upper limit of the
fiber strength distributions were noted in the 2024 Al, 5052 Al and
6061 Al alloy systems. These are copper bearing alloys with copper pre-

13

sent in the form of $CuAl_2$ or in solid solution. The order of increasing copper content of these alloys corresponds to the order of increased strength observed, suggesting that copper contributes to a fiber strengthening mechanism.

Room temperature composite properties.- Typical room temperature as-fabricated stress-strain curves for each composite and test type are shown in figure 5. The first stage longitudinal elastic moduli (when both fiber and matrix are elastic) and the second stage elastic moduli (when the matrix is plastic and contributes little to the composite strength) correspond to the rule-of-mixture (ROM) prediction for moduli. Longitudinal tensile strengths, however, do not agree with ROM calculations based on mean fiber strength. Transverse tensile strengths (fig. 5(b)) were similar to the matrix alloys but with much lower strains to failure because of fiber restriction. Strain hardening steps typical of strain hardenable aluminum alloys are present in the plastic region of the B/5052 Al transverse tensile curve and the B/6061 Al system transverse tensile and in-plane shear curves (fig. 5(d)). This phenomena, as well as early fiber failures may have contributed to the perturbations seen in the latter stages of some of the longitudinal tensile curves. The B/6061 Al composite, a well characterized composite system, will be used as a basis of comparison for the other systems. Mean values of room-temperature as-fabricated mechanical properties for each composite system as well as its percentage difference (in parentheses) compared to B/6061 Al are listed in Table XI. The longitudinal tensile strength of the B/1100 Al system is only 11% less than the B/6061 Al system although

14

the matrix dominated transverse tensile strength, longitudinal compression strength and in-plane shear strength are 63%, 37%, and 33% less, respectively. The longitudinal tensile strength of the B/2024 Al system is only 7% less than the B/6061 Al system and its transverse tensile strength is 27% greater. The B/3003 Al system longitudinal tensile strength, transverse tensile strength, longitudinal compression strength, and in-plane shear strength are 27, 53, 29, and 32 percent less than the B/6061 Al system, respectively. The longitudinal tensile strength of the B/5052 Al system in 29 percent less than the B/6061 Al system but its transverse tensile strength is only 2 percent less.

Longitudinal tensile fracture surfaces of all five systems were macroscopically irregular with matrix shear steps typically causing 5 mm variations in the failure planes. However, no fiber pullout is evident in the microscopic fractographs, figure 6. The B/1100 Al system fracture surface (fig. 6(a)) has high necking tear ridges typical of the commercially-pure highly-ductile alloy. The B/3003 Al (fig. 6(c),) B/5052 Al (fig. 6(d)) and the B/6061 Al (fig. 6(e)) systems show less ductility and ultimate matrix failure by the dimpled rupture mode. The B/2024 Al system (fig. 6(b)) shows little ductility and a strong dimpled rupture mode resulting from its higher alloy content. All these fractographs show some evidence of incomplete matrix-matrix bonding.

Transverse tensile fracture surfaces, for all but the B/6061 Al system, were macroscopically flat for the most part but with some tendancy toward a 45° failure plane indicating a mixed failure mode that was pri-

15

marily tensile but with some local shear failure. The B/6061 Al systems failed on 45° planes indicating a matrix shear mode failure. Additional fracture surface details are shown in the microscopic fractographs, figure 7. The B/1100 Al system (fig. 7(a)) failed in tension through the matrix. Some bare fiber appears in the fracture surface, probably as a result of incomplete bonding. The B/2024 Al system (fig. 7(b)) failed entirely at the fiber/matrix interface. The B/3003 Al (Fig. 7(c)) and the B/5052 Al (fig. 7(d)) systems failed in mixed modes of matrix and interface tension failures. The B/6061 Al system (fig. 4(e)) failed in the matrix with elongated dimples indicating a shear failure.

Residual fiber strength distributions (fibers removed from composite specimens after tensile testing) are shown in figure 8. The residual distributions are approximately the same as those obtained from untested specimens (fig. 3) except the lower bounds have been modified by the failure of low strength fibers during composite tensile testing. Fiber stresses at the composite failure strain are indicated for each system and show that composite failure occurs when only a few percent of fibers have failed.

Effect of elevated test temperature.- As-fabricated specimens from each composite system were mechanically tested at room temperature (295 K), 500 K and 590 K. Typical stress-strain curves for each test condition and composite system are shown in Appendix A. The effect of test temperature on the mean ultimate strengths of the composite systems are shown in figure 9. The matrix alloys alone (fig. 9(a)), though varying

16

from 70 MPa to 368 MPa at 295 K, tend toward the same strength as test temperature increases with the variation at 590 K only 20 MPa to 66 MPa. The composite transverse tensile strengths (fig. 9(b)) behaved in the same manner as the alloys. Fiber dominated longitudinal tensile strengths (fig. 9(c)) of the B/1100 Al, B/2024 Al, B/3003 Al, and B 6061 Al systems had only small losses in strength with increasing test temperature, whereas the B/5052 Al system had an anomalous increase in strength at 590 K. This increase probably resulted from improved diffusion bonding which occurs during the two hours required to bring the specimen and equipment to thermal equilibrium at 590 K. Longitudinal compression strengths (fig. 9(d)) for the B/1100 Al, B/3003 Al and B/6061 Al systems at 590 K were 70 to 80 percent less than their room temperature strengths. In-plane shear strengths for the same materials were only slightly decreased by the elevated temperatures (fig. 9(e)). These data show that matrix dominated strength properties of the composite system tended to converge as test temperature increased, but in general the order of highest to lowest strength was maintained throughout the temperature range.

Effects of Isothermal Exposures

Exposure at 500 K.- The effects of isothermal exposure for up to 10 000 hours at 500 K on the tensile strengths of the matrix alloys and the longitudinal and transverse tensile strengths of the composites are shown in figure 10. In addition, typical stress-strain curves for each composite material and each test type are shown in Appendix B. Matrix

17

tensile strengths (fig. 10(a)) of the non-heat-treatable alloys indicate 1100 Al and 3003 Al were not affected by the 500 K exposure and 5052 Al reached its fully annealed condition early in the exposure period and remained constant thereafter. The heat-treatable alloys, 2024 Al and 6061 Al, approached their fully annealed strengths during the exposure period. Composite transverse tensile strengths (fig. 10(b)) behaved in the same manner as the matrix alloys alone and their strength losses may be attributed entirely to matrix annealing. Composite longitudinal tensile strengths (fig. 10(c)) show losses of 22 percent for the B/1100 Al system, 17 percent for the B/6061 Al system and 10 percent for the B/2024 Al and B/3003 Al system. Most of the losses occur in the first 5000 hours of exposure. The B/5052 Al system longitudinal tensile strength was not degraded by the 500 K exposure.

Residual fiber strength distributions for fibers removed from specimens after 10 000 hours exposure at 500 K and tensile testing are shown in figure 11. Fiber stress at the composite failure strain is indicated for each system. Comparison of these residual strengths with the as-fabricated residual strengths (fig. 8) shows uniform degradation of approximately 5 percent in the upper bound and mean strength of fibers from the B/1100 Al system and a 10 percent reduction in fiber stress at failure. Mean strength of fibers from the B/2024 Al system was degraded but the upper bound of the strength distribution and fiber stress at failure were unchanged. The mean and upper bound of B/3003 Al system fiber strength were unchanged but the fiber stress at failure was degraded approximately six percent. The upper bound of fiber strength

from the B/5052 Al system was degraded but there were only small losses in mean strength and stress at failure. Mean fiber strength of the B/6061 Al system was degraded approximately 10 percent and stress at failure was degraded 18 percent.

Longitudinal tensile fracture surfaces were macroscopically and microscopically similar to the as-fabricated specimens. Transverse tensile fracture surfaces for the B/1100 Al, B/3003 Al and B/5052 Al systems were macroscopically irregular indicating mixed mode failures as in the as-fabricated composites. The B/2024 Al and B/6061 Al systems failed on 45 degree planes indicating a matrix shear mode failure. Additional fracture surface details are shown in the microscopic fractographs, figure 12. The B/1100 Al system (fig. 12(a)) failure occured more at the interface than in the matrix as in the as-fabricated case (fig. 7(a)). The B/2024 Al system (fig. 12(b)) failed entirely by matrix shear, a change from the interface failure seen in the as-fabricated specimens. The remaining system failures were similar to the as-fabricated system failures.

Exposure at 590 K.- The effects of isothermal exposure for up to 10 000 hours at 590 K on the matrix alloys tensile strength and the composite system strengths are shown in figure 13. In addition, typical stress-strain curves for each composite material and each test type are shown in Appendix C. The effect of 590 K thermal exposure on the matrix alloy strength (fig. 13(a)) was similar to the effect of 500 K exposure except the 2024 Al, 5052 Al and 6061 Al alloys reached their fully

annealed condition during the first 2500 hours of exposure and remained constant thereafter. Composite transverse tensile strength degradations (fig. 13(b)) were again similar to the matrix materials and may be attributed entirely to matrix annealing. The longitudinal tensile strengths of all the composite systems were degraded by the long term 590 K exposure (fig. 13(c)), with most of the losses occurring in the first 2500 hours of exposure. Strength losses over the 10 000 hour exposure for the B/1100 Al, B/2024 Al, B/3003 Al, B/5052 Al, and B/6061 Al systems were 10, 14, 10, 8, and 14 percent, respectively.

Longitudinal compression strengths (fig. 13(d)) of the 1100 Al, 3003 Al and 6061 Al systems degraded in an approximately linear manner over the 10 000 hour exposure with a maximum loss of 38 percent. In-plane shear strengths (fig. 13(e)) of the B/1100 Al and B/3003 Al system were unaffected by the 590 K exposure. The B/6061 Al system lost 22 percent of its in-plane strength in the first 2500 hours period, probably the result of annealing, but then increased linearly over the remaining 7500 hours for a net increase in strength of 8 percent.

Longitudinal tensile specimen fracture surfaces for the 590 K exposure specimens were similar both macroscopically and microscopically to the as-fabricated specimens. Transverse tensile fracture surfaces of specimens exposed for 10 000 hours at 590 K, figure 14, are unchanged from the as-fabricated specimens except for the B/2024 Al system (fig. 14(b)) which failed in matrix shear. The transition of the failure mode

from interfacial to matrix shear occurred in the initial 2500 hour exposure period as a result of matrix annealing.

Residual fiber strength distributions for fibers removed from specimens after 10 000 hours exposure at 590 K and tensile testing are shown in figure 15. Comparing these distributions with the residual distributions from as-fabricated specimens (fig. 8), the mean strength and stress at composite failure strain of fibers from the B/1100 Al system were degraded approximately 5 percent. Fiber stress at composite failure strain of fibers from the B/2024 Al system was degraded approximately 7 percent by the exposure even though the mean strength apparently increased. Mean strength of fibers from the B/3003 Al system was degraded approximately 15 percent but the stress at composite failure strain was degraded only 8 percent. Stress at composite failure strain of fibers from the B/6061 Al system was not degraded by the exposure but the mean strength dropped approximately 7 percent.

Reaction layers on individual fibers are shown in figure 16. Thermal exposure has increased the thickness and density of the reaction layer in the B/1100 Al system (fig. 16(a)) but the EDAX results indicate the make-up, aluminum with a trace of silicon and iron rich particles, is the same as the as-fabricated specimens. Fibers from the 2024 Al system (fig. 16(b)) have irregular reaction layers with large light colored areas that have an acicular growth pattern. The reaction layer is composed of one part aluminum and 1.32 parts magnesium with traces of silicon, iron and copper. Light colored areas are one part aluminum and 0.8 parts magne-

sium. Fibers from the 3003 Al system (fig. 16(c)) have a reaction layer of large spherical particles. EDAX shows the reaction layer is largely manganese and aluminum with traces of silicon and iron. Darker particles are richer in aluminum than the lighter particles. Fibers from the 5052 Al system (fig. 16(d)) have a thick acicular reaction layer composed of one part aluminum and 0.8 parts magnesium with traces of silicon, chromium and iron. Fibers from the 6061 Al system (fig. 16(e) have a moderately thick reaction layer with light colored nodes and an acicular growth pattern. The reaction layer is composed of one part aluminum, 0.4 parts magnesium, and 0.1 part silicon and traces of chromium, iron, and copper. The light colored nodes have a similar composition but with less aluminum.

The effect of exposure temperature on the longitudinal tensile strength of the composite systems exposed 10 000 hours, shown in figure 17, is divided into two groups. The first group of systems (B/2024 Al, B/3003 Al and B/5052 Al) degrade in a linear manner with increasing exposure temperature (12, 12 and 6 percent, respectively). The second group (B/1100 Al and B/6061 Al), however, degraded approximately 22 percent at 500 K but only 9 percent at 590 K. These data indicate that there is a low temperature degradation mechanism active at 500 K but not at 590 K and that there is some temperature between 295 K and 590 K that produces a maximum degradation. This phenomena may be the result of a low temperature boron reaction with the metastable phase $FeAl_6$ in the matrix (iron is present as an impurity). The metastable phase is stabilized by manganese (ref 14) which is present as an alloying

constituent in the 2024 Al, 3003 Al, and 5052 Al alloys but not in the
1100 Al and 6061 Al alloys (Table I). Also shown in figure 17 are data
from reference 2 for 10 000 hour exposures of a B/6061 Al composite at
297 K, 450 K, 561 K, and 700 K. The composite was a 6-ply unidirectional
configuration with 49 volume percent of 142 µm diameter boron fibers.
Strength degradation in this system was more severe than for the
B/6061 Al system with 203 µm diameter fibers considered in this study.
Much of the difference can be attributed to the smaller diameter fiber
which has less strength initially, more surface area per unit volume for
reaction, and is more sensitive to stress concentrations both at the
surface and in the core.

The maximum mechanical property degradations of each system caused by
up to 10 000 hours exposure at 500 K or 590 K are summarized in Table
XII. Transverse tensile strength degradations were caused entirely by
matrix annealing. The systems ranked according to their minimum room
temperature transverse tensile strengths are:

<div align="center">

B/2024 Al - 178 MPa

B/5052 Al - 150 MPa

B/6061 Al - 133 MPa

B/3003 Al -   77 MPa

B/1100 Al -   62 MPa

</div>

Longitudinal tensile strength degradations for the B/2024 Al, B/3003 Al,
and B/5052 Al systems were 10 percent or less (disregarding matrix

annealing). The systems ranked according to their minimum room temperature longitudinal tensile strengths are:

$$B/6061 \text{ Al} - 1349 \text{ MPa}$$
$$B/2024 \text{ Al} - 1343 \text{ MPa}$$
$$B/1100 \text{ Al} - 1130 \text{ MPa}$$
$$B/5052 \text{ Al} - 1089 \text{ MPa}$$
$$B/3003 \text{ Al} - 1044 \text{ MPa}$$

Longitudinal compression strengths of the three systems tested were degraded 38 percent by 10 000 hours exposure at 590 K. However, they are still 25 to 60 percent higher than the longitudinal tensile strengths. The systems ranked according to their minimum room temperature longitudinal compression strengths are:

$$B/6061 \text{ Al} - 2190 \text{ MPa}$$
$$B/3003 \text{ Al} - 1574 \text{ MPa}$$
$$B/1100 \text{ Al} - 1399 \text{ MPa}$$

In-plane shear strengths of these systems were degraded 12 percent or less (disregarding matrix annealing). The systems ranked according to their minimum room temperature in-plane shear strengths are:

$$B/6061 \text{ Al} - 157 \text{ MPa}$$
$$B/3003 \text{ Al} - 123 \text{ MPa}$$
$$B/1100 \text{ Al} - 76 \text{ MPa}$$

Design applications utilizing B/Al composites in elevated temperature environments must be based on their fully annealed strengths and/or their minimum thermally degraded strength and/or their elevated temperature strength. Ranking the five B/Al systems tested in this investigation for long term use at temperatures up to 590 K gives the following order of performance:

B/2024 Al - High strengths

Low degradation

B/5052 Al - Moderate strengths

Low degradation

B/6061 Al - High strengths

Moderate degradation at 500 K

B/3003 Al - Low strengths

Low degradation

B/1100 Al - Low strengths

High degradation at 500 K

Exposure at 730 K.- The effects of isothermal exposure for up to 500 hours at 730 K on the matrix alloys tensile strength and the composite systems strength are shown in figure 18. In addition, typical stress-strain curves for each composite material and each test type are shown in Appendix D. Tensile strengths of the non-heat-treatable alloys (fig. 18(a)) behaved in the same manner as noted in the lower temperature exposures, 1100 Al and 3003 Al were unaffected by the exposure and 5052 Al reached the fully annealed condition early in the exposure and

25

then remained constant. The tensile strengths of the heat-treatable alloys 2024 Al and 6061 Al exposed at 730 K did not behave in the same manner as observed at 500 K and 590 K. The strength of the 2024 Al alloy was not degraded at all by the 730 K exposure. Strength degradation for the 6061 Al alloy at 730 K was one-third less than at the lower temperatures. Less strength loss occurred at the higher temperature because at 730 K these materials are in their solution heat treating regime. In this regime, the solubility limits for their strengthening phases are increased and less percipitation occurs.

Transverse tensile strengths of the composite systems (fig. 18(b)) again behaved in a manner similar to the non-reinforced matrix material except that the B/2024 Al system strength degraded linearly with exposure time. After 500 hours exposure at 730 K the transverse tensile strengths of the B/2024 Al, B/5052 Al, and B/6061 Al systems were degraded 12, 16, and 11 percent, respectively.

Composite longitudinal tensile strength degradations were more severe for the 730 K exposure (fig. 18(c)) than for the lower temperature exposures. The B/1100 Al, B/2024 Al, B/3003 Al, B/5052 Al, and B/6061 Al system strengths were degraded by 37, 42, 32, 37, and 45 percent, respectively. The B/1100 Al and B/6061 Al systems degraded in a linear manner with exposure time. The other systems degraded in a non-linear manner with the rate of degradation decreasing with increasing exposure time. The B/3003 Al and B/5052 Al systems reached their minimum strength after 300 hours and remained constant through 500 hours. Because longitudinal

tensile strength, a key property of these materials, was severely degraded, these materials are not suitable for long-life applications at 730 K.

Longitudinal compression strengths of the composite systems exposed at 730 K (fig. 18(d)) varied in a non-linear manner with exposure time initially decreasing then increasing. During the initial exposure periods the B/1100 Al, B/3003 Al, and B/6061 Al system strengths degraded 13, 2, and 18 percent, respectively. During the later period the strength recovered 4, 13, and 12 percent, respectively. Compression strength relies on matrix support of the fiber to prevent buckling. One possible cause of the observed strength recovery is that the reaction zone formed at 730 K provides improved fiber support.

In-plane shear strength of the B/1100 Al, B/3003 Al, and B/6061 Al systems degraded linearly 25, 25, and 40 percent, respectively, during the 500 hour exposure.

Longitudinal tensile fracture surfaces of the specimens exposed 500 hours at 730 K were macroscopically flat and did not have the irregular shear steps noted on the as-fabricated specimens. Microscopically, however, the 730 K specimens and the as-fabricated specimens were similar. Transverse tensile fracture surfaces of specimens exposed 500 hours at 730 K are shown in figure 19. The B/1100 Al and B/3003 Al fracture surfaces (figs. 19(a) and 19(c), respectively) are not significantly different from the as-fabricated specimens (figs. 7(a) and 7(c)). The

B/2024 Al specimen (fig. 19(b)), however, has several unique features. It failed primarily at the interface of the reaction layer and the matrix, leaving the heavy reaction layer attached to the fiber. At discrete sites along the fiber the failure surface penetrated the reaction layer and extended into the fiber, removing a chip of fiber. The chipped sites are visible on the fiber in the center of the fractograph and the chips that were removed from a fiber on the opposing fracture surface are visible in the adjacent valley. In addition, several fibers failed by splitting their entire length (left side of fractograph). The B/5052 Al (fig. 19(d)) also failed at the interface leaving a heavy reaction layer on the fiber and it also shows evidence of fiber chipping. The B/6061 Al system (fig. 19(e)) failed in matrix shear as it did in the as-fabricated condition, but, areas near the fiber show evidence of a thick fragmented reaction layer.

Fiber strength distributions from specimens exposed for 500 hours at 730 K are shown in figure 20. Strength degradation of fibers from all matrix alloy systems was severe. The mean strength of fibers from 1100 Al, 3003 Al, and 6061 Al matrices were degraded approximately 35 percent (to 2.4 GPa) and the fibers from the 2024 Al and 5052 Al matrices were degraded approximately 50 percent (to 2.0 GPa) as a result of the exposure. The greater degradation of the latter two systems was probably the result of magnesium in the matrix as cited in the discussion on fabrication effects.

Reaction layers on individual fibers taken from the composite specimens exposed 500 hours at 730 K are shown in figure 21. Fibers from the 1100 Al matrix (fig. 21(a)) have thin compact reaction layers that are dark with light colored fringes and particles. EDAX results again show the dark areas are aluminum with a trace of silicon and the light areas are iron rich particles. Fibers from the 2024 Al matrix (fig. 21(b)) have a thick, fluffy, light colored reaction layer. EDAX results indicate the composition is approximately one part aluminum and 1.6 parts magnesium with traces of silicon, iron, manganese, and copper. Electron microprobe traces across interfaces of a polished cross-section of a B/2024 Al specimen indicate magnesium concentration in the reaction layer is ten times higher than in the matrix. Thickness of the reaction layer, determined by measuring the magnesium peak width at half the maximum peak height, is approximately 5 μm. Fibers from the 3003 Al matrix (fig. 21(c)) have a thin gray reaction layer covered by small light colored spherical particles. EDAX results show the reaction products contain aluminum and iron with traces of manganese and silicon. Fibers from the 5052 Al matrix (fig. 21(d)) have a thick, fluffy, light colored reaction layer with small white spherical particles imbedded. EDAX results show the fluffy area is one part aluminum and 1.6 parts magnesium with traces of silicon, chromium, and manganese and the white particles are again iron rich. Fibers from the 6061 Al matrix (fig. 21(e)) have a two layer reaction zone. The inner layer is the same in appearance and elemental content as the as-fabricated specimens. The outer layer is a thick, fluffy, light colored reaction product with some small white particles imbedded. EDAX results of the outer layer show it is one part aluminum

and 1.6 parts magnesium with a trace of iron, chromium, silicon, and copper.

Attempts to use X-ray diffraction techniques to identify the phases present in the reaction layers seen here (and the thinner ones presented in earlier sections) were unsuccessful. Specimens used in the attempts included beds of fibers, powder samples made by grinding and sieving fibers to increase the volume percent of reaction products, and powder samples leached with Murakami's reagent to remove boron and further concentrate the reaction products. In each case, the patterns generated contained only two indistinct peaks (broad and weak) typical of amorphous boron (ref. 15). This suggests that the compounds formed have no long-range crystallinity agreeing with doubts that true crystalline borides form below 773 K (ref. 16).

Effects of Thermal Cycling

The effects of thermal cycling between 200 K and 590 K for up to 2000 cycles on the matrix alloys tensile strength and the composite systems strengths are shown in figure 22. In addition, typical stress-strain curves for each composite material and each test type are shown in Appendix E. The effects of thermal cycling on the matrix alloy tensile strengths (fig. 22(a)) are the same as noted for the 500 K and 590 K isothermal exposures i.e. the 1100 Al and 3003 Al alloys, annealed during fabrication, were unaffected and the 2024 Al, 5052 Al and 6061 Al alloys, partially annealed during fabrication, reached their fully annealed con-

dition within the first 500 cycles and then remained constant. Transverse tensile strengths of the B/1100 Al and B/3003 Al composite systems (fig. 22(b)) were unaffected by thermal cycling, but, transverse tensile strengths of the B/2024 Al, B/5052 Al and B/6061 Al systems were degraded 38, 54 and 33 percent, respectively, as a result of 2000 thermal cycles. These losses are 21, 30 and 5 percent, respectively, more than the losses incurred as a result of isothermal exposure at 590 K. Longitudinal tensile strengths of the B/1100 Al and B/2024 Al (fig. 22(c)) degraded linearly with number-of-cycles for total losses of 23 and 16 percent, respectively, after 2000 cycles. The B/3003 Al, B/5052 Al, and B/6061 Al systems lost less than 5 percent of their longitudinal tensile strength as a result of 2000 thermal cycles. Longitudinal compression strengths of the B/1100 Al, B/3003 Al, and B/6061 Al systems (fig. 22(d)) degraded linearly with number-of-cycles for total losses of 22, 26, and 39 percent, respectively, after 2000 cycles. In-plane shear strengths of these systems (fig. 22(e)) were unaffected by thermal cycling.

Longitudinal tensile fracture surfaces of the thermally cycled specimens were macroscopically and microscopically similar to the as-fabricated specimens. Transverse tensile fracture specimens were macroscopically similar to the as-fabricated specimens, but, microscopic fractographs, figure 23, show higher densities of large dimples and voids in the interfacial regions and spheroidized matrix material attached to the fibers. These phenomena occur as a result of thermal cycling because of the high shear stresses induced by the large differences in thermal expansion between the fiber and matrix (4:1) (ref. 17). Initially these

31

stresses produce plastic deformation and nucleate dislocations in the matrix material. Further cycling condenses the dislocations into voids. The stronger the matrix material is the higher its stress field will be and the more dislocations it will generate. This phenomena produced the larger transverse tensile strength degradations observed for the thermally cycled B/2024 Al, B/5052 Al, and B/60612 Al systems in comparison with the degradation caused by long-term thermal exposure.

Fiber strength distributions from thermally cycled specimens, figure 24, compared with the as-fabricated fiber strength distributions, figure 8, show there was no degradation as a result of the exposure.

Ranking the five B/Al systems tested in this investigation for use in a cyclic thermal environment gives the following order:

B/6061 Al

B/2024 Al

B/3003 Al

B/5052 Al

B/1100 Al

Constituent Effects

The reactions occurring within the B/Al composite systems are functions of the constituents, concentrations, temperatures, and time. Identification of these reactions is complicated by their short-range

structures, low concentrations and by boron transparency to X-rays. As a result, direct identification of the reaction products using the available equipment and techniques was not possible. However, the foregoing metallurgical analyses, elemental identifications, and mechanical property data together with data gleaned from the literature provides a basis from which the effects of the various elemental constituents can be deduced.

Boron.- The amorphous boron fibers retain the same basic icosohedral (12 atom) cluster structure found in crystalline borons. The icosohedral clusters, however, are randomly oriented in the amorphous form (ref. 18). In the crystalline form long-range order leaves large inter-icoso-hedral spaces. These spaces host the metal atoms in boron-rich metal borides (ref. 19). Random orientation leaves even larger inter-icoso-hedral spaces and higher energy sites to accept metal atoms.

Boron fibers are the primary source of strength in the composites. Failure of the fiber dominated longitudinal tensile specimens occurred catastrophically without evidence of an accumulation of fiber failures (i.e. no change in elastic modulus near failure). The failures occurred when the fibers were loaded near the lower bound of their strength dis-tribution ranges and were not a function of reaction layer thickness (for exposure up to 590 K). This behavior corresponds to the critical energy release rate theory of B/Al composites (ref. 20) where the critical rate is exceeded as soon as fibers in the main body of the distribution range begin to fail. Because the lower bound of fiber strength governs

the composite failure, localized reactions between the fiber and matrix
that cause stress concentrations and reduce the lower bound of fiber
strength are more detrimental to ultimate composite strength than are
uniform reactions which lower the entire strength distribution.

Aluminum.- Aluminum/boron reactions are inevitable in the B/Al com-
posite system. However, at temperatures up to 590 K, the slow uniform
non-crystalline reaction causes little degradation even after 10 000
hours. At the composite fabrication temperature (770 tpo 840 K), the
reactions occur more rapidly but short exposure times minimize the
effects. Long-term exposure at 730 K caused severe degradation and
clearly is beyond the useful temperature range of B/Al composites. Alum-
inum forms the boron rich borides AlB_2, AlB_4 and AlB_{12} with a wide range
of stoichiometry (ref. 19). The diboride phase, the one usually
expected, has a hexagonal crystalline form dominated by the metal struc-
ture. However, at the reaction temperatures in this study, the boron
atoms probably take up random interstitial sites in the face-centered-
cubic aluminum structure resulting in a distorted structure. This, com-
pounded by a wide range of stoichiometery and the ability of the other
diboride-forming constituent metals to enter into isostructural diborides
with aluminum, prevent the phase from forming any long range structure.
The higher borides, if they are formed, have structures dominated by the
icosohedral cluster structure of boron with the metal atoms taking
positions in the relatively large inter-cluster spaces. Their formation
would require diffusion of aluminum into the boron and would probably be

restricted to the surface or near-surface of the boron fiber and would assume the amorphous boron structure.

Iron.- Iron is not an alloying constituent in any of the alloys tested but it is present as an impurity (<1 percent) in all commercial alloys. Iron rich particles were found in the fiber reaction layers and probably formed where iron bearing particles in the matrix were next to the fibers. These highly localized reaction sites cause stress concentrations that are detrimental to fiber strength. Two binary phases can form in the B-Fe system, FeB and Fe_2B (ref. 19). Both phases have structures determined by the metal lattice. In addition, there are two metal-rich ternary phases that can form in the Al-B-Fe system, B_3Fe_3Al and B_2Fe_2Al (ref. 14).

Alloy systems not containing manganese, 1100 Al and 6061 Al, were degraded more at the lower exposure temperature (500 K) than at 590 K. Apparently, manganese, a known iron stabilizer which combines with the metastable $FeAl_6$ phase to form (FeMn) Al_6 (ref. 14), protects the fibers from iron attack at lower temperatures. Since removal of iron from aluminum alloys would be impractical, the addition of a small amount of manganese to the matrix alloy offers some control of the deleterious iron effect at lower temperatures.

Silicon.- Silicon is an alloying constituent in the 6061 Al system (0.06%) but it is present in all commercial aluminum alloys as an impurity. Silicon was a minor constituent in all of the reaction layers. It

was uniformly distributed in the reaction products except in the B/6061 Al system where it was bound in Mg_2Si and reduced the detrimental magnesium reaction effect found in other systems. Boron and silicon do not form binary compounds below 1073 K but 0.81 atomic percent of silicon is soluble in boron at room temperature (ref. 21).

Copper.- Copper appears as an alloying constituent in three of the alloys tested, 2024 Al (4.5%), 5052 Al (0.1%), and 6061 Al (0.3%). Fiber reaction products from these systems contained only small amounts of copper uniformly distributed. However, the as fabricated fiber strength distributions from these systems showed upper strength limits increased in proportion to their copper content. Copper forms only CuB_{22} or higher boride phases with boron (the exact stoichiometry is a matter of contention in the literature). These phases would again be dominated by the boron structure and would have to form by diffusion of copper into the boron fiber where it would take up either an interstitial position or substitute for a boron atom (ref. 22). Copper strengthening of boron by this type of mechanism has been reported for crystalline boron at temperatures above 1200 K (refs. 23 and 24). A similar phenomena may occur in amorphous boron at the temperatures encountered in this study. Penetration into the fiber would probably be minimal but the strengthening would occur at the fiber surface and help negate the effect of the inherent surface flaws.

Magnesium.- Magnesium is an alloy constituent in three of the alloys tested, 2024 Al (1.5%), 5052 Al (2.5%), and 6061 Al (1.0%). Fiber reac-

tion products from all these systems contained magnesium and in some instances it appeared as the predominant constituent. It appeared in the uniform reaction products as well as in concentrated particles. In the case of the 500 hour exposure at 730 K, the magnesium in the B/2024 Al composite diffused to the fiber surface and was uniformly concentrated there. Magnesium in the uniform reaction products probably comes from solid solution in the matrix and probably substitutes for aluminum to form $(MgAl)B_2$ (refs. 7 and 8). Particles with high concentrations of magnesium are probably from magnesium bearing particles in the matrix reacting with the fiber. Magnesium particles formed in the B/6061 Al system also contained silicon (from Mg_2Si phase).

Manganese.- Manganese appears as a minor alloying constituent in the 2024 Al (0.6%) and 5052 Al (0.1%) systems and as the only alloying constituent in the 3003 Al (1.2%) system. Although a small amount of manganese is apparently desirable to stabilize iron at low temperatures, an excess caused increased fiber degradation (by comparison of 1100 Al and 3003 Al system fiber strength) during fabrication. Together manganese and boron form six binary borides (Mn_4B, Mn_2B, MnB, Mn_3B_4, MnB_2, and MnB_4 (ref. 19)) and with aluminum they form two ternary borides (Mn_2AlB_2 and Mn_5AlB_{11} (ref. 25)). There was no indication in this investigation which of these phases formed under the various exposure conditions.

Improving Boron/Aluminum Composites for Elevated Temperature Use

One of the purposes of this investigation was to determine the active degradation mechanisms in five B/Al composite systems with the supposition that the information could aid in formulating an improved matrix alloy for elevated temperature use. In this context, an "improved matrix alloy" is one which minimizes the strength losses due to fiber-matrix reactions during fabrication and subsequent long term use at elevated temperature. Specific applications may require additional considerations such as corrosion resistance, impact resistance, fatigue strength, etc. to define an improved matrix alloy. Also in this context, "elevated temperature use" is used for environments up to 590 K. This limit is set because test results showed moderate degradation of fiber strength at 590 K but severe degradation at 730 K. Further investigation at intermediate temperatures may prove the 590 K limit to be conservative.

Aluminum alloys begin to anneal at temperatures as low as 370 K (ref. 11). Therefore, when considering them for extended use at temperatures up to 590 K, only the fully annealed properties can be considered. In fact, it may be advantageous to anneal the aluminum foil prior to composite fabrication to assure maximum formability and improve bonding.

Boron fibers are a brittle material sensitive to surface flaws which cause stress concentrations. They inherently contain many surface flaws which cause them to have a wide range of tensile strengths. The composite longitudinal tensile failures observed in this investigation all

38

occur near the lower bound of the fiber strength distributions. This indicates that, for these large 203 μm diameter fibers at least, the critical energy release criteria for composite failure is exceeded almost as soon as the first fibers fail. Therefore, any reaction which tends to introduce more flaws or worsen those already present, even though not significantly reducing the mean strength of the fibers as a whole, can significantly reduce composite strength.

By induction, from the discussion of alloying constituent effects in the previous section, several general conclusions about fiber-matrix interactions and composite strength degradation can be drawn.

1. Localized reactions between matrix phases and the fiber which form metal-rich borides introduce new surface flaws or worsen existing ones. These reactions are the most detrimental to composite strength.

2. Uniform reactions of aluminum and boron produce boron-rich borides which cause nominal fiber degradation.

3. Uniform reactions forming very-boron-rich borides (i.e. CuB_{22}) may actually help to heal existing fiber surface flaws and strengthen them.

More specifically, considering the alloying constituents included in this investigation, an aluminum copper alloy with a small amount of manganese

to aid in stabilizing iron impurities should reduce composite strength degradation in use environments up to 590 K.

There are three existing aluminum-copper alloys, none of which exactly conforms to the suggested composition. They are aluminum alloys 2011, 2025 and 2219 (ref. 11). Aluminum 2011 contains 5.5 percent copper but no manganese, it also contains 0.5 percent lead and 0.5 percent bismuth. Lead is reportedly insoluble in boron and forms no phases with it (ref. 21) and no confirmed bismuth phases appear in the literature (ref. 16). Aluminum 2025 contains 4.5 percent copper and 0.8 percent manganese but it also contains 0.8 percent silicon. However, the results of this study indicate that the effects of small concentrations of silicon are probably not significant in composite strength degradation. Aluminum 2219 contains 6.3 percent copper and 0.3 percent manganese, it also contains 0.15 percent zirconium and 0.1 percent vanadium. Both zirconium and vanadium form metal-rich borides (ref. 19) and are probably undesirable as alloying constituents.

The results also suggest another method for improving composite strength. If, as postulated, the formation of very boron-rich borides such as CuB_{22} does "heal" existing fiber flaws, then, the vapor deposition of a small amount of copper on the surface of the fiber could improve its strength. This operation could be added as a final step to the vapor deposition process for fabricating the fibers.

CONCLUSIONS

Boron-aluminum composites were investigated to determine the effects of long-term thermal exposure on the composite mechanical properties and the effects of the matrix alloying constituents on the degradation mechanisms. Five aluminum alloys, 1100 Al, 2024 Al, 3003 Al, 5052 Al, and 6061 Al, were used as matrix materials. Eight-ply composite panels of each matrix material reinforced with 49 volume percent boron fibers were fabricated by diffusion bonding. The 203 μm diameter boron fibers were oriented unidirectionally or at ±45 degrees. The composites were investigated in the as-fabricated condition, after iosthermal exposures of up to 10 000 hours at 500 K, up to 10 000 hours at 590 K, up to 500 hours at 730 K, and after thermal cycling exposure of up to 2000 cycles between 200 K and 590 K. Mechanical properties, including longitudinal, transverse, and ±45 degrees tensile, and longitudinal compression were measured in each condition. Fibers, chemically removed from the matrices, were individually bend tested to determine their strength distributions. Composite specimens and individual fibers were metallurgically analyzed using a scanning electron microscope and an electron microprobe to determine failure characteristics, chemical element distributions, and reaction layer morphology.

The results of the investigation show that:

1. The five B/Al composite systems studied had good mechanical strength retention after long-term exposures of up to 10 000 hours at 500 K and 590 K. Specific findings were as follows:

   a. Transverse tensile strengths of all the composite systems were unaffected by the exposures (except for matrix annealing).

   b. Longitudinal tensile strengths of the B/2024 Al, B/3003 Al, and B/6061 Al systems were degraded by 10 percent or less by the exposures.

   c. Longitudinal tensile strengths of the B/1100 Al and B/6061 Al systems were degraded more (22 and 13 percent, respectively) by exposure at 500 K than at 590 K.

   d. Longitudinal compression strength of the systems tested were degraded by 38 percent. However, their compression strengths were still 25 to 60 percent higher than their tensile strengths.

   e. The order of best performance of the composite systems based on initial strength, strength at temperature and amount of degradation is:

B/2024 Al

B/5052 Al

B/6061 Al

B/3003 Al

B/1100 Al

2. Thermal cycling the composite materials for 2000 cycles between 200 K and 590 K caused more transverse tensile strength degradation in the stronger matrix alloys than long-term thermal exposure.

3. Matrix alloying constituents do affect the degradation mechanisms of B/Al composites. Therefore, by tailoring the matrix alloy, property degradation caused by long-term thermal exposure could be reduced. Some of the specific observations were:

a. Low temperature degradation caused by iron impurities can be reduced by selecting a matrix alloy containing a small amount of iron stabilizing manganese.

b. Boron aluminum composite property degradation is increased when magnesium, iron and/or manganese are available to participate in the reaction.

c. The presence of copper in the matrix alloy increases fiber strength.

APPENDICES

The mechanical property data for all the B/Al composite tests conducted in this investigation are listed in Tables V through IX in the text. The following Appendices (A through E) present stress-strain curves typical of each material at each test condition presented in those tables. The test conditions for materials in each appendix are as follows:

Appendix A.- As-fabricated specimens tested at 195 K, 500 K, and 590 K.

Appendix B.- Specimens exposed up to 10 000 hours at 500 K and tested at room temperature.

Appendix C.- Specimens exposed up to 10 000 hours at 590 K and tested at room temperature.

Appendix D.- Specimens exposed up to 500 hours at 730 K and tested at room temperature.

Appendix E.- Specimens thermally cycled up to 2000 cycles between 200 K and 590 K and tested at room temperature.
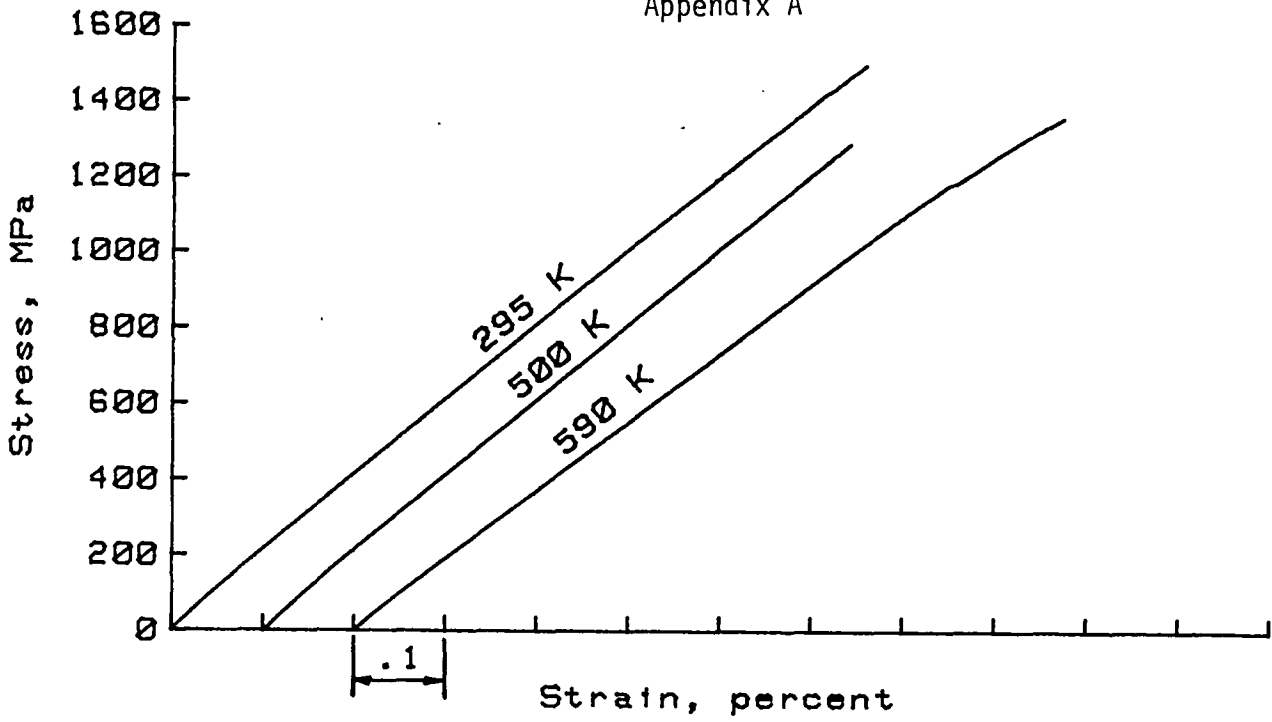
(a) Longitudinal tensile
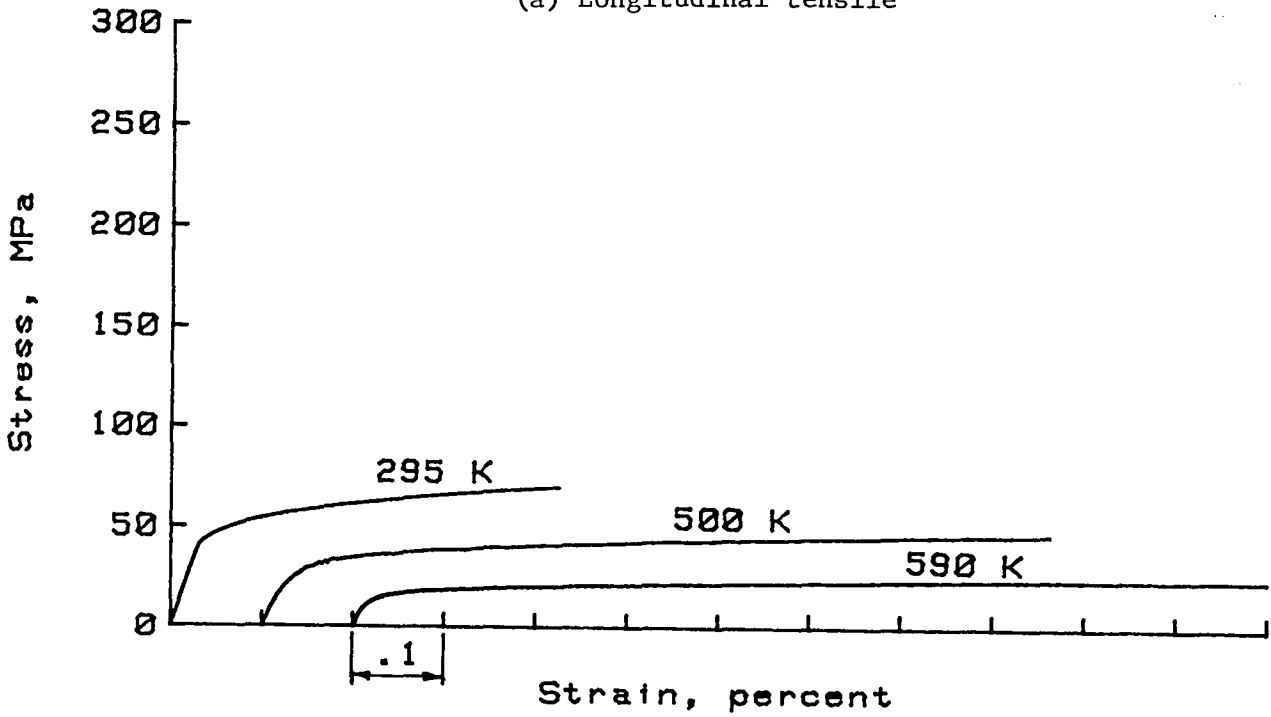
(b) Transverse tensile

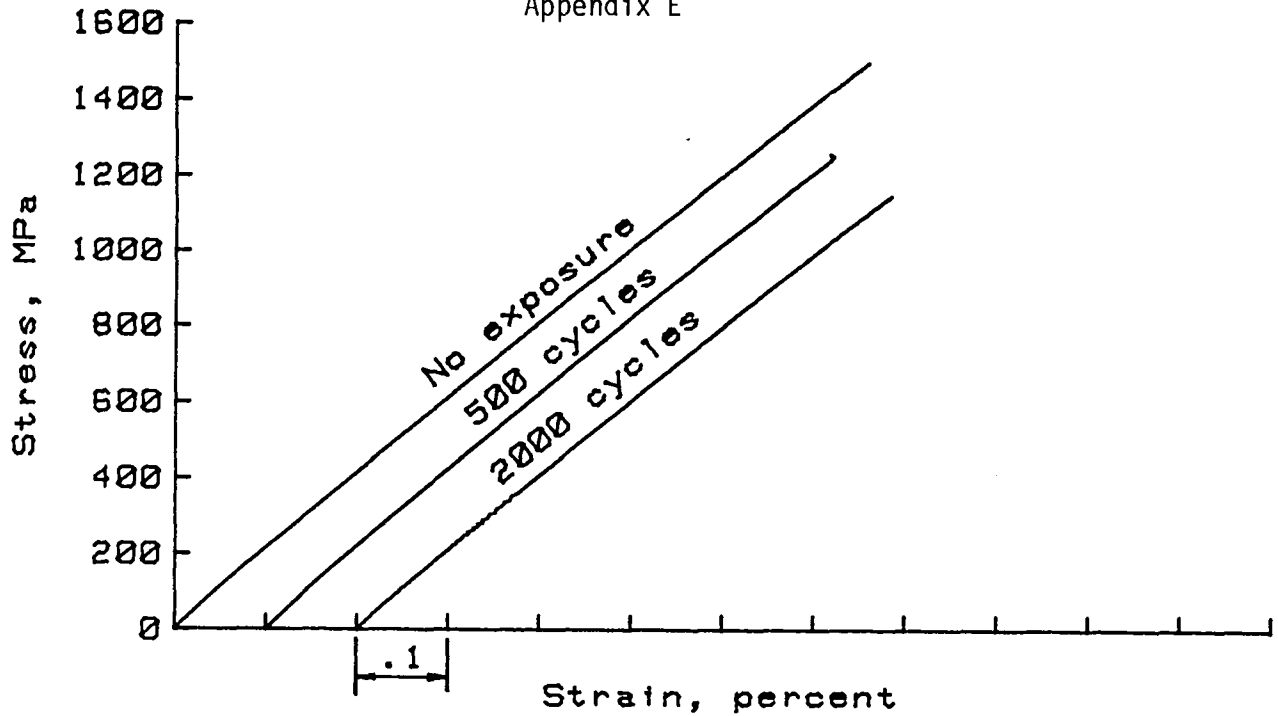Figure A-1.- Typical elevated test temperature stress-strain curves for B/1100 Al composite.
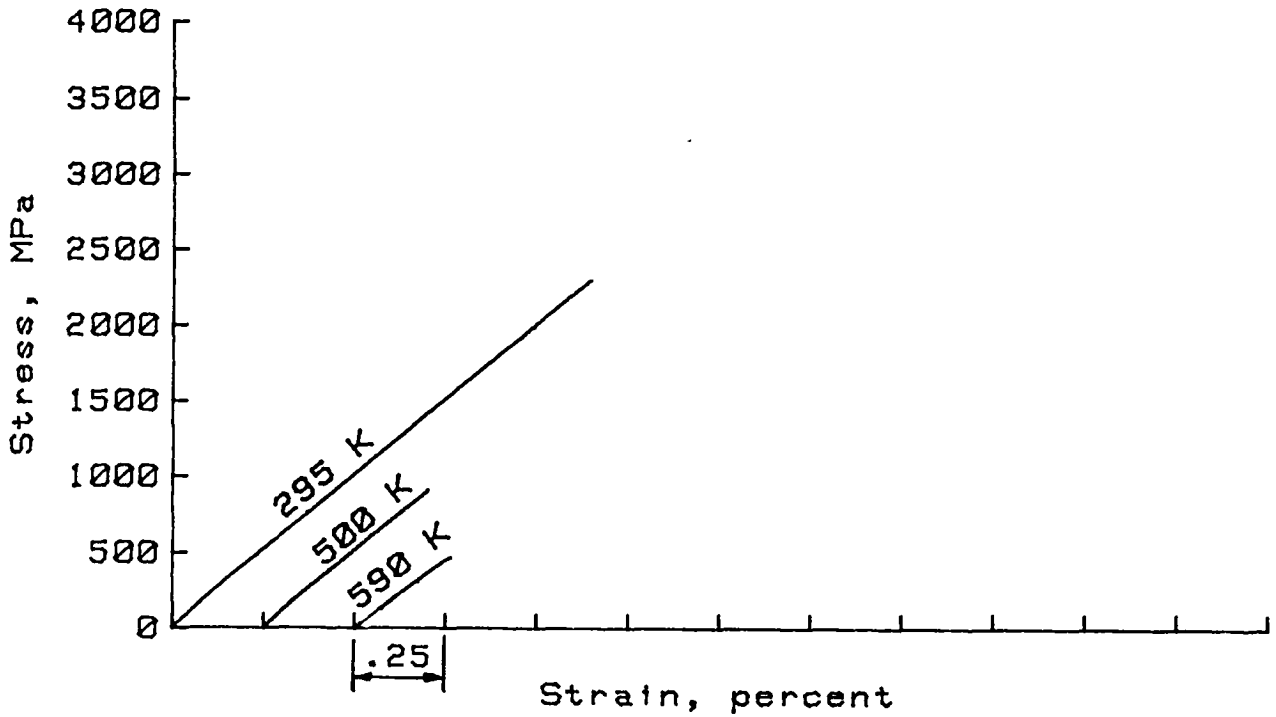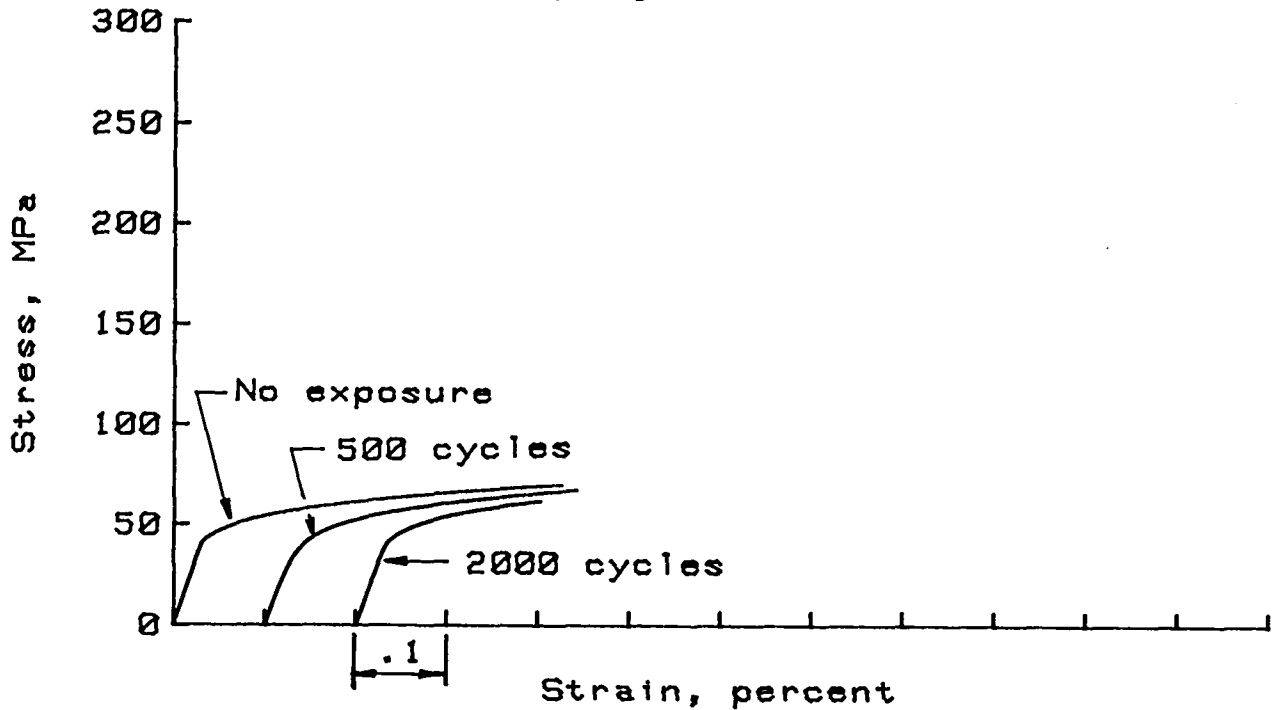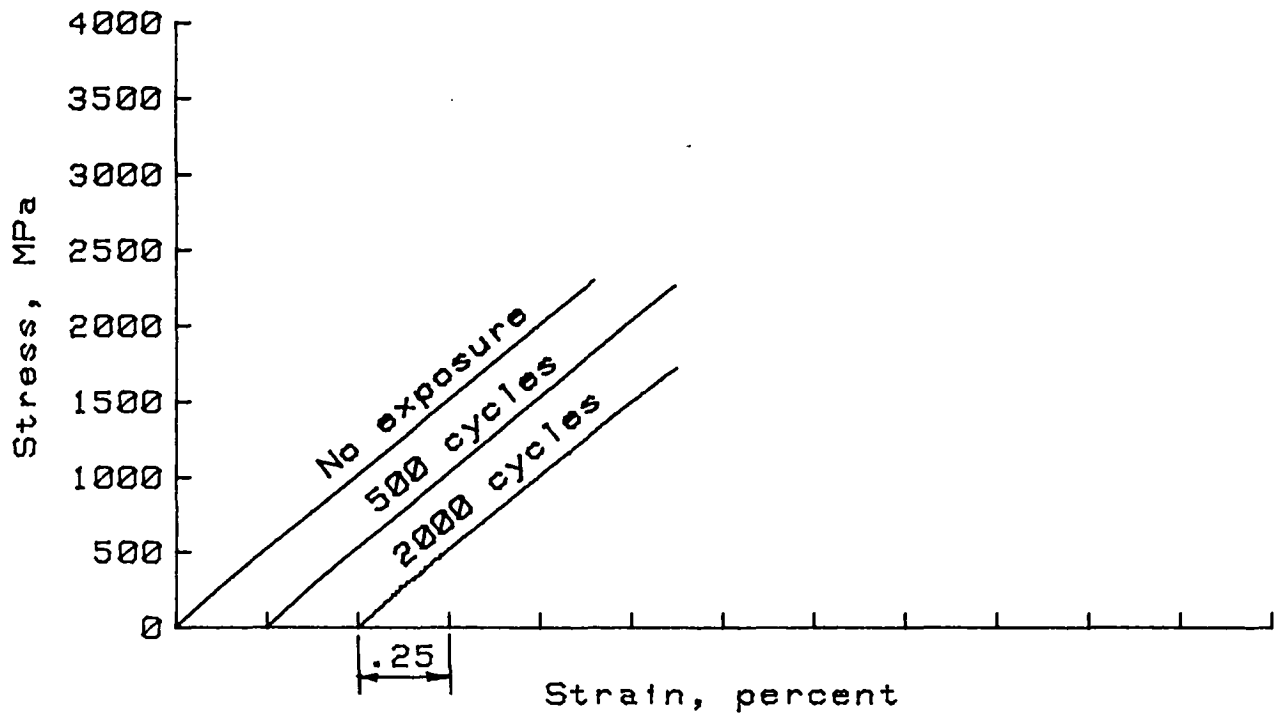
(c) Longitudinal compression
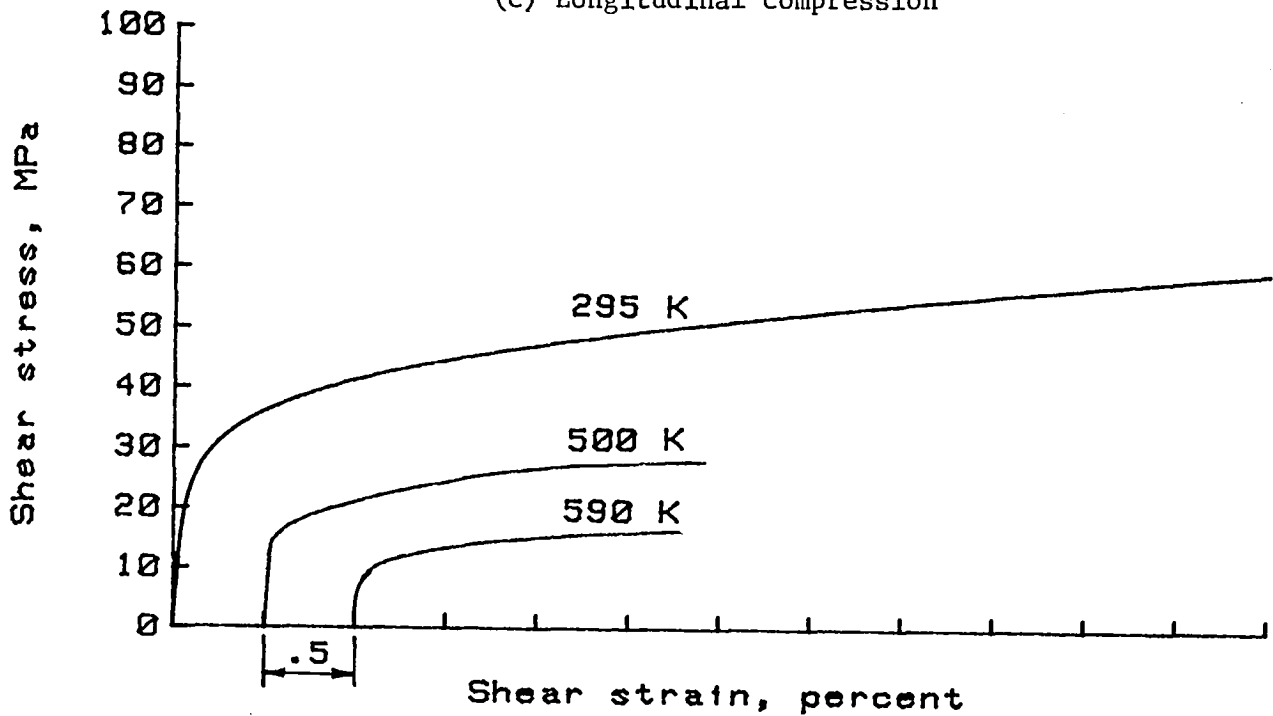
(d) In-plane shear

Figure A-1.- Concluded.
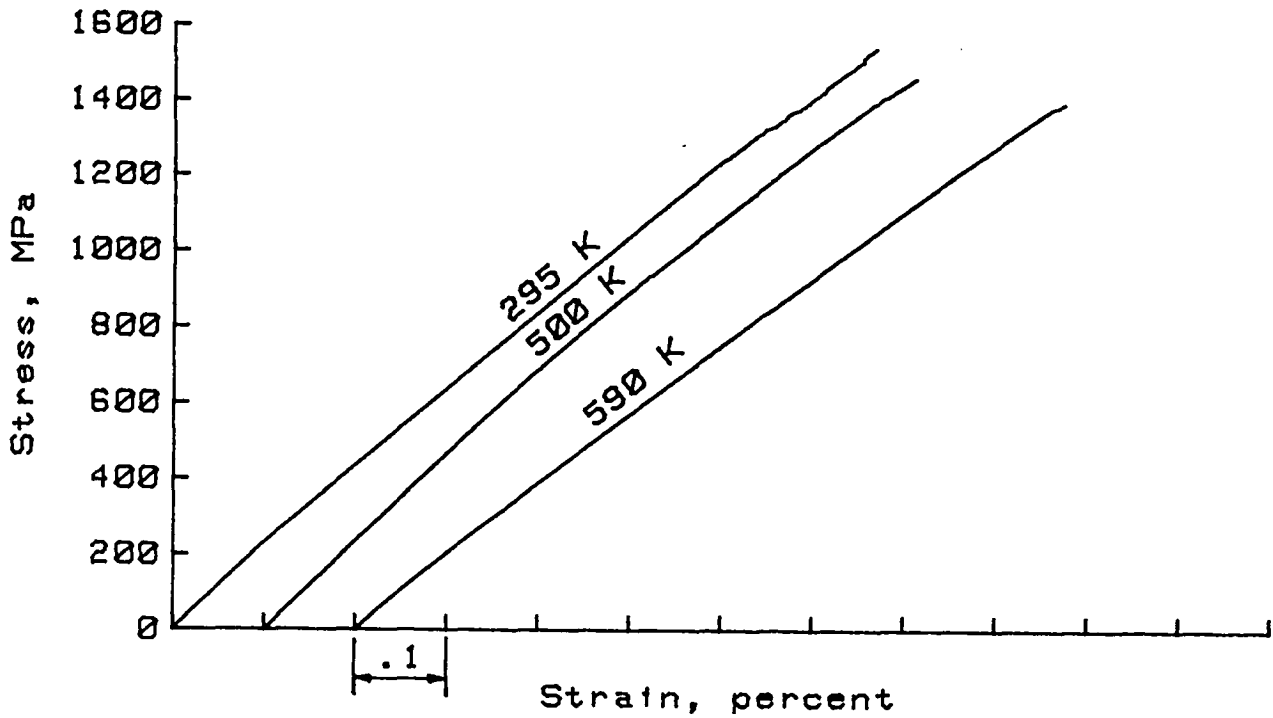
(a) Longitudinal tensile
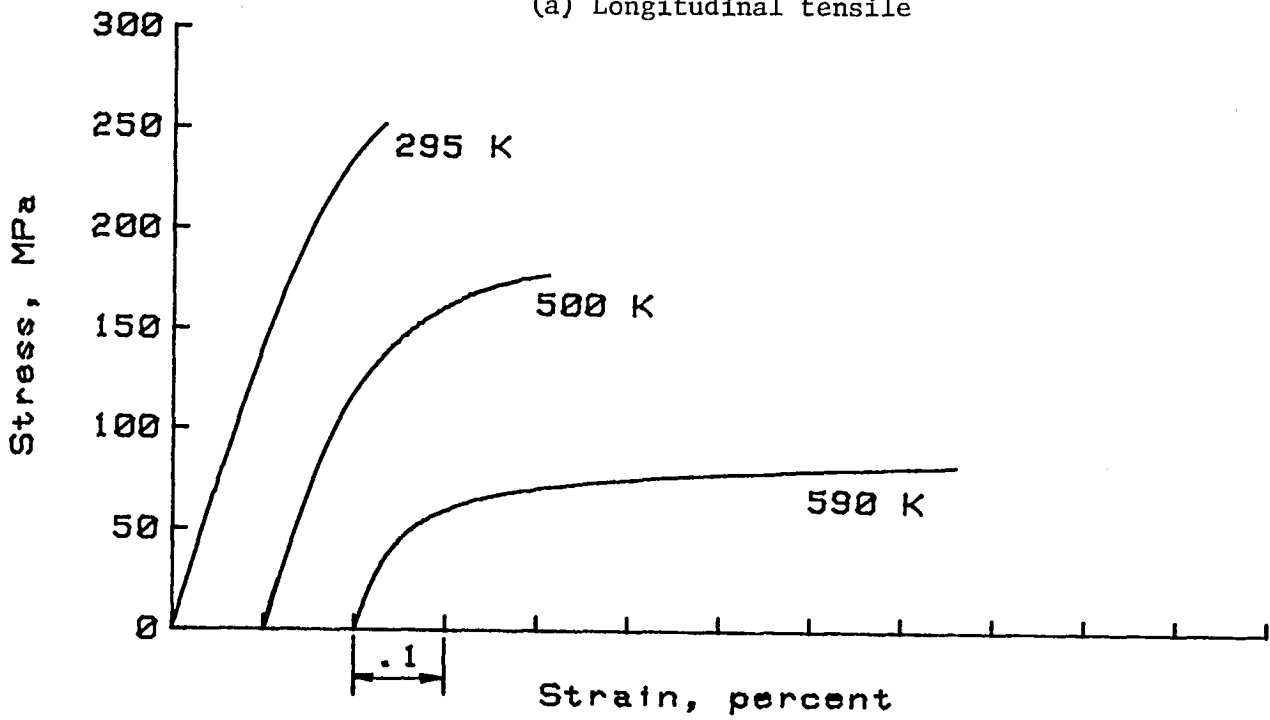
(b) Transverse tensile

Figure A-2.- Typical elevated test temperature stress-strain curves for B/2024 Al composite.

47
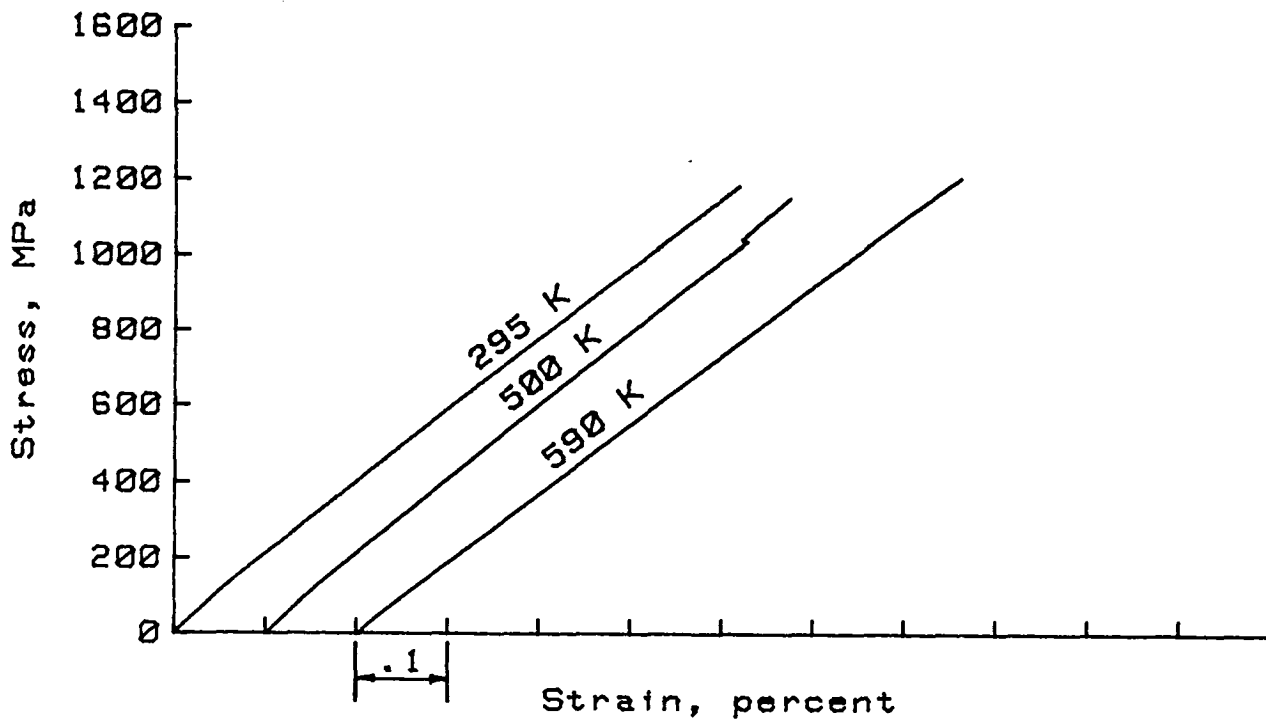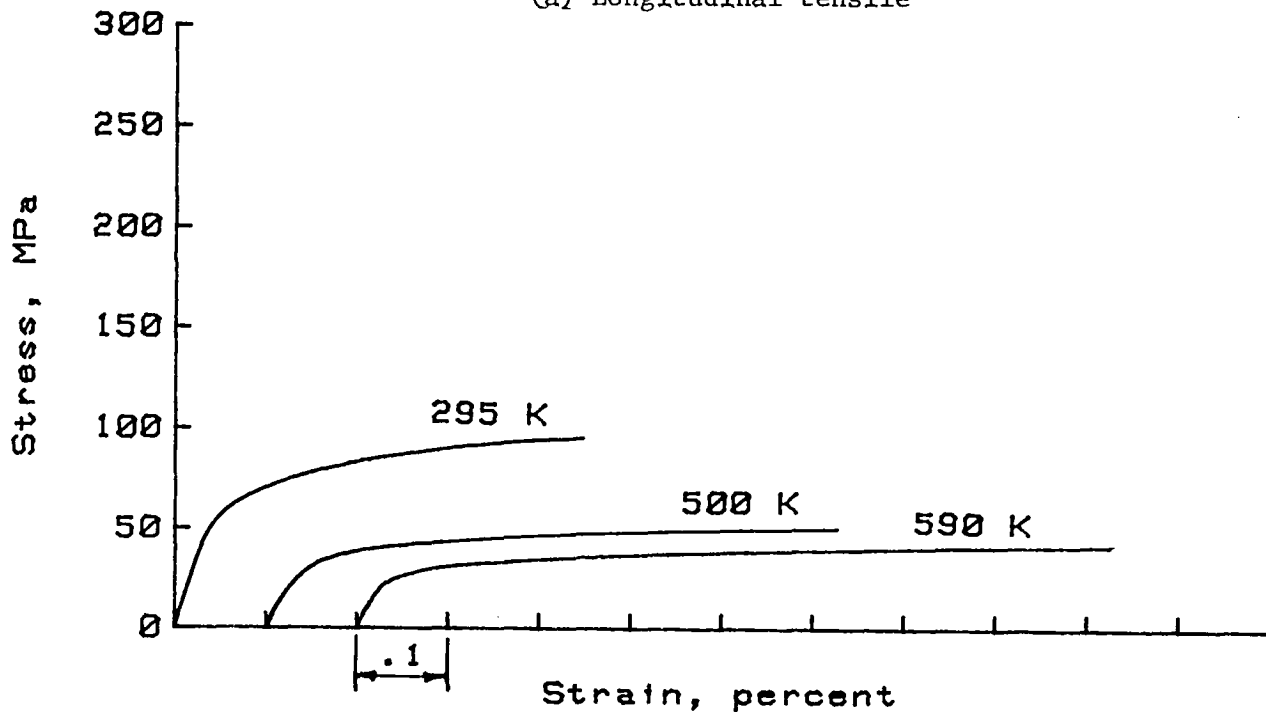
Figure A-3.— Typical elevated test temperature stress-strain curves for B/3003 Al composite.
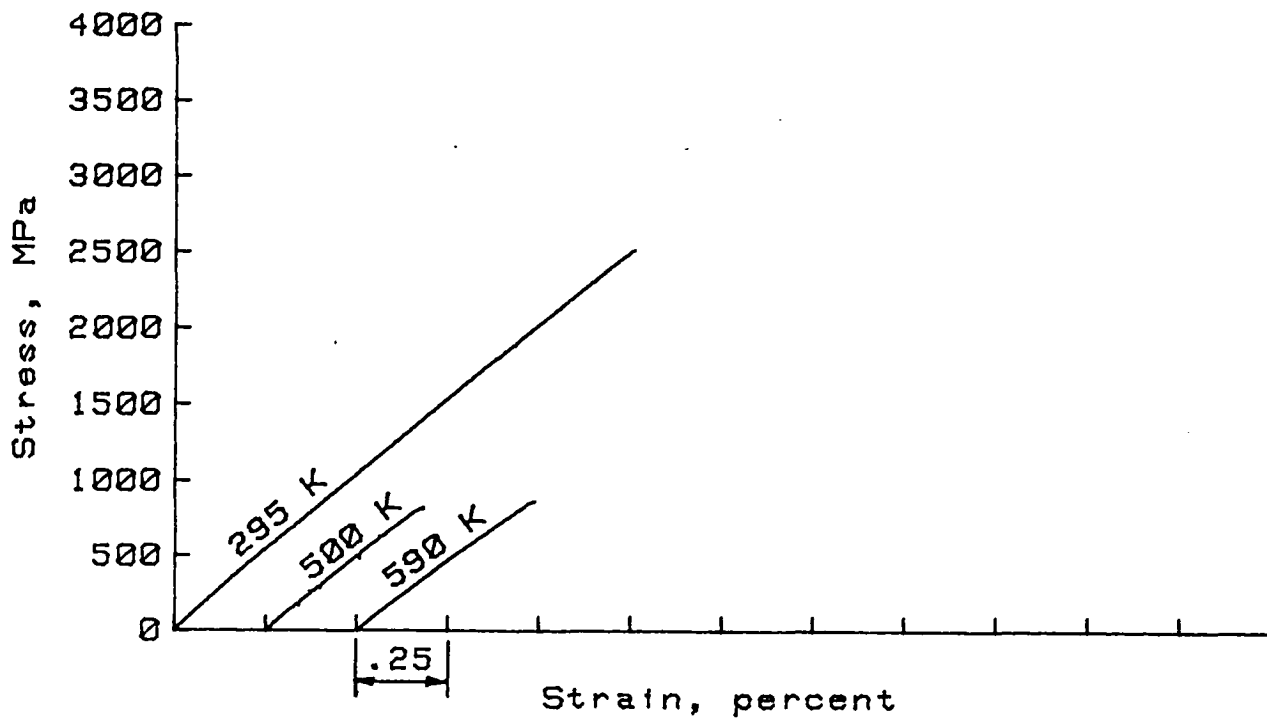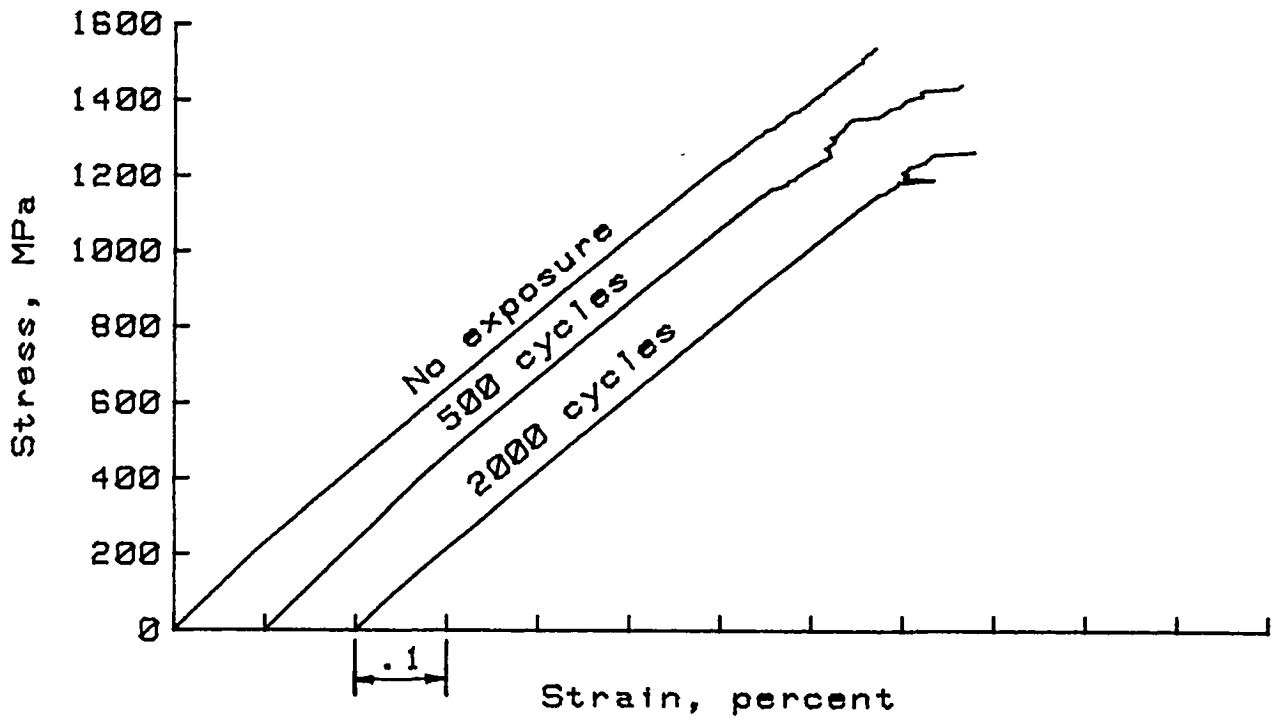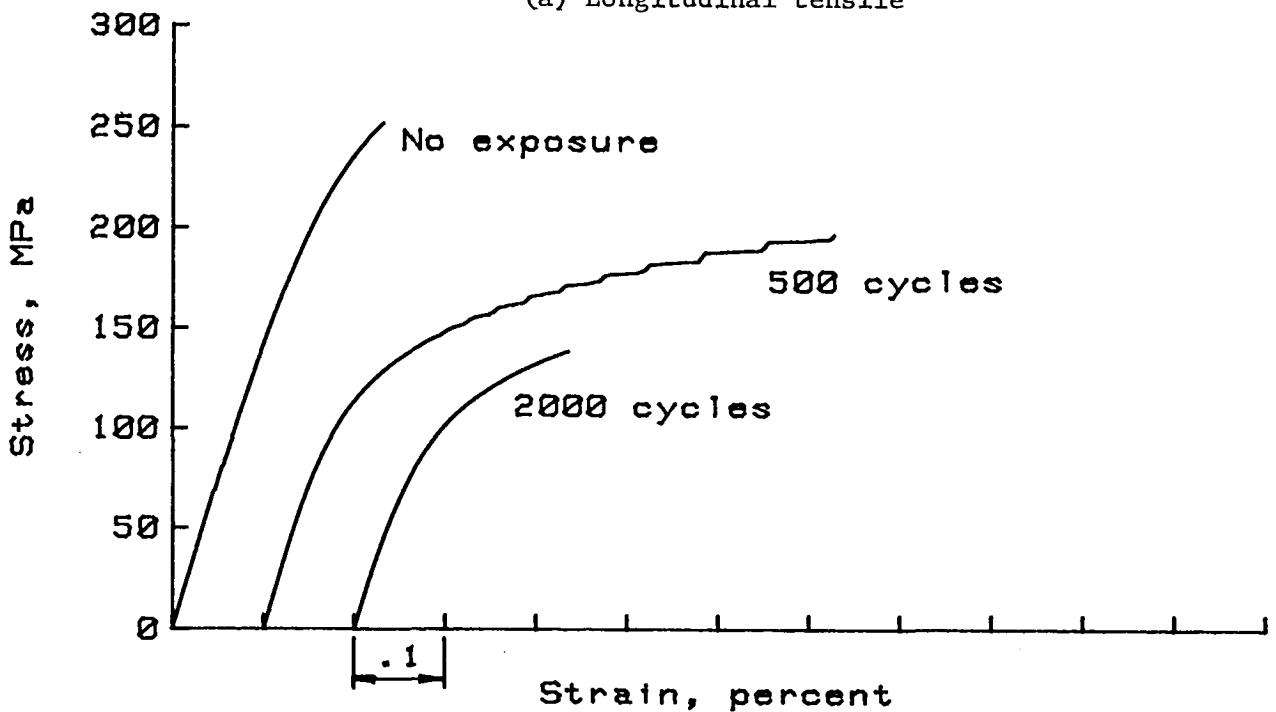
(c) Longitudinal compression
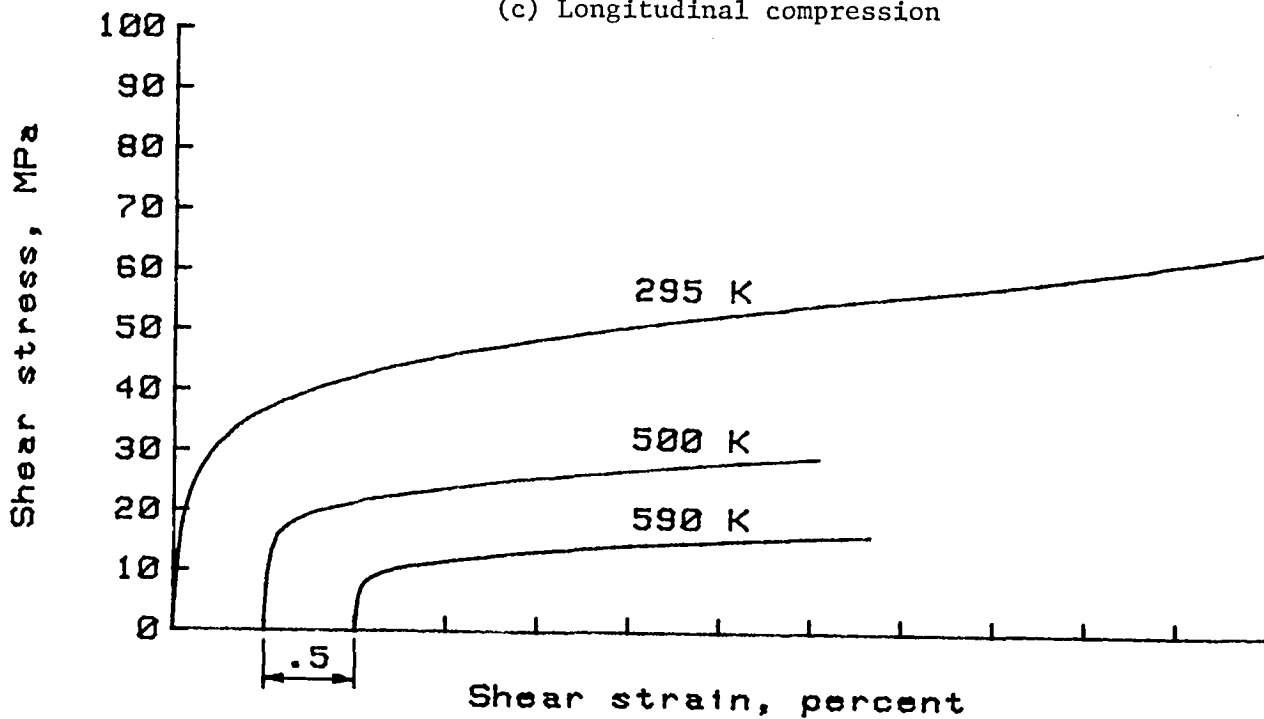
(d) In-plane shear

Figure A-3.- Concluded.
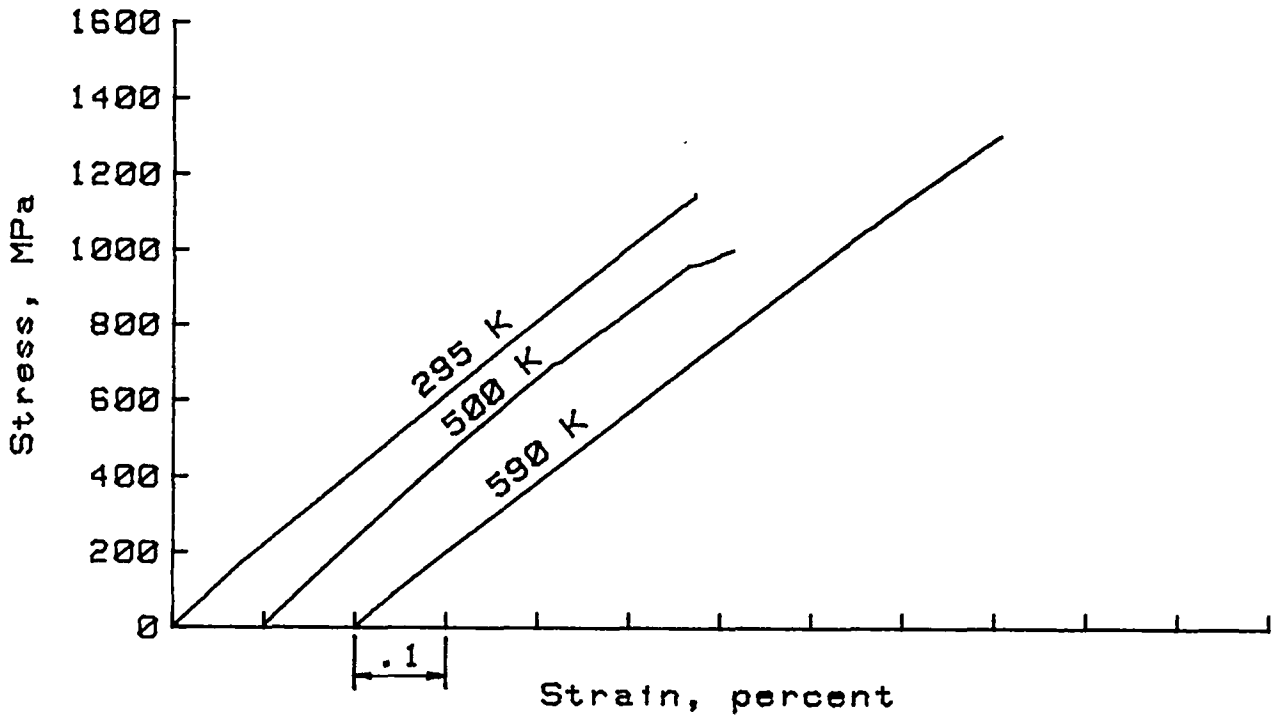
(a) Longitudinal tensile
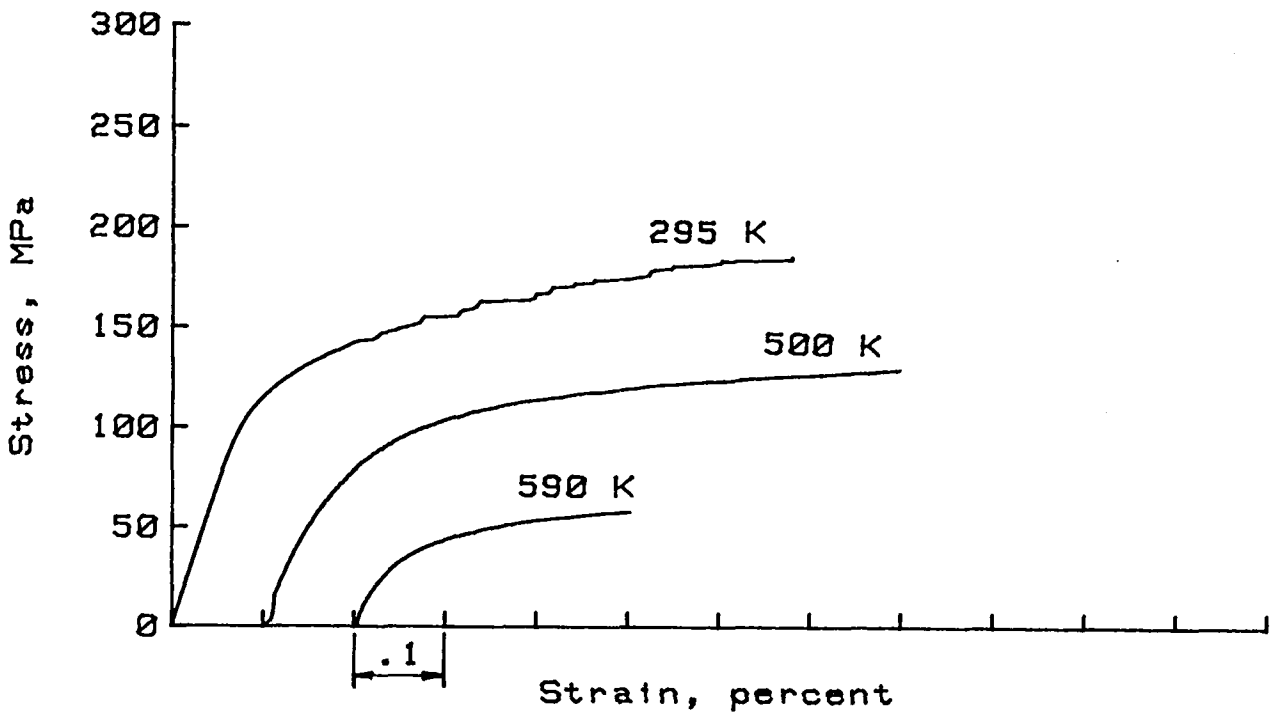
(b) Transverse tensile

Figure A-4.- Typical elevated test temperature stress-strain curves for B/5052 Al composite.

50
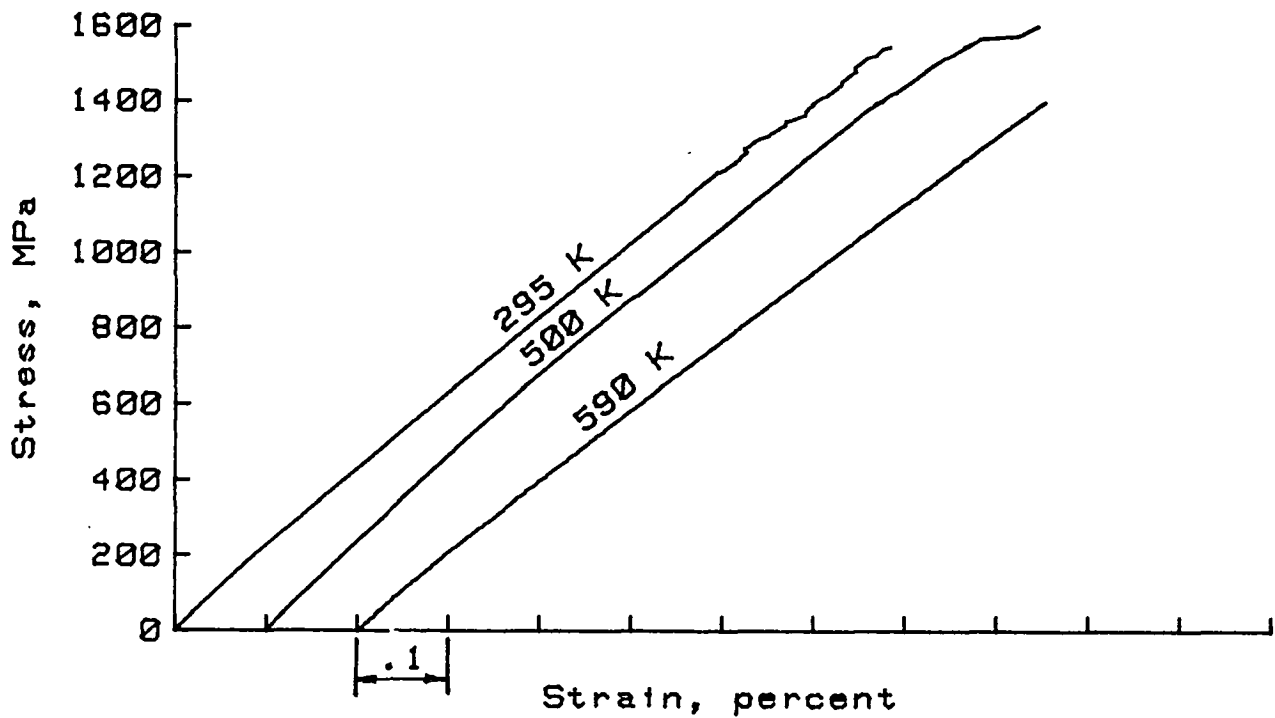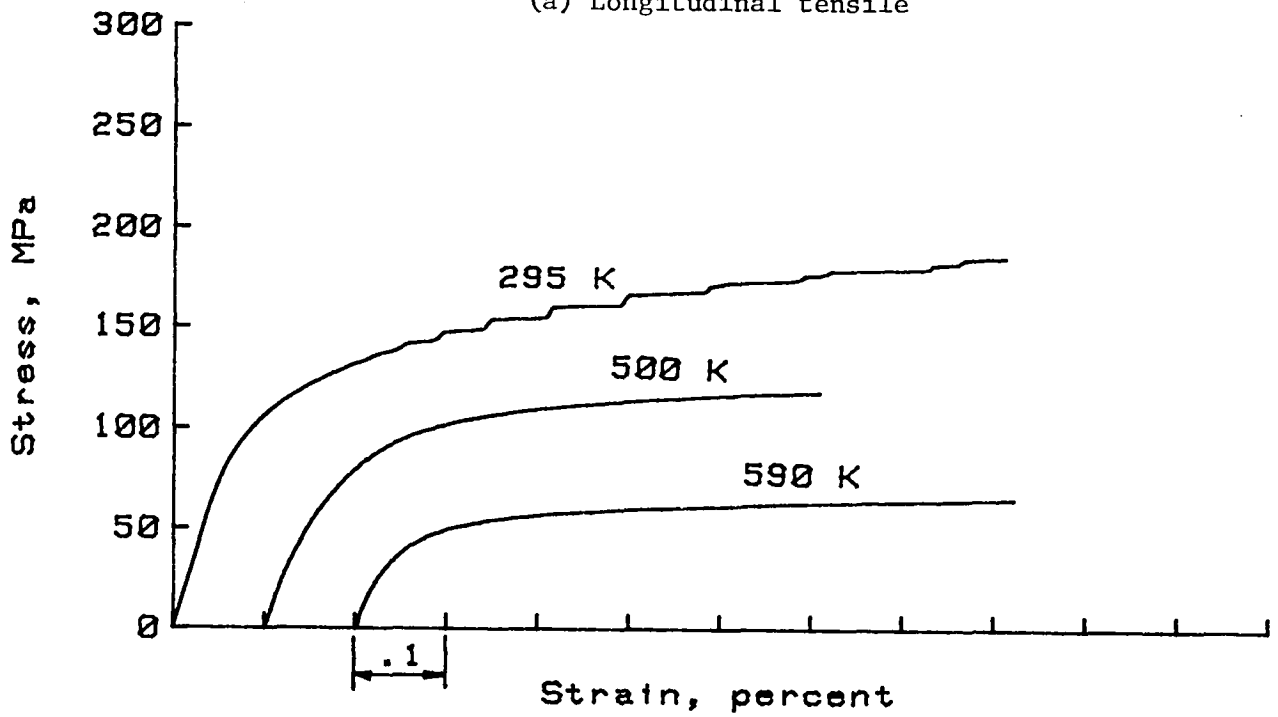
Figure A-5.– Typical elevated test temperature streee-strain curves for B/6061 Al composite.
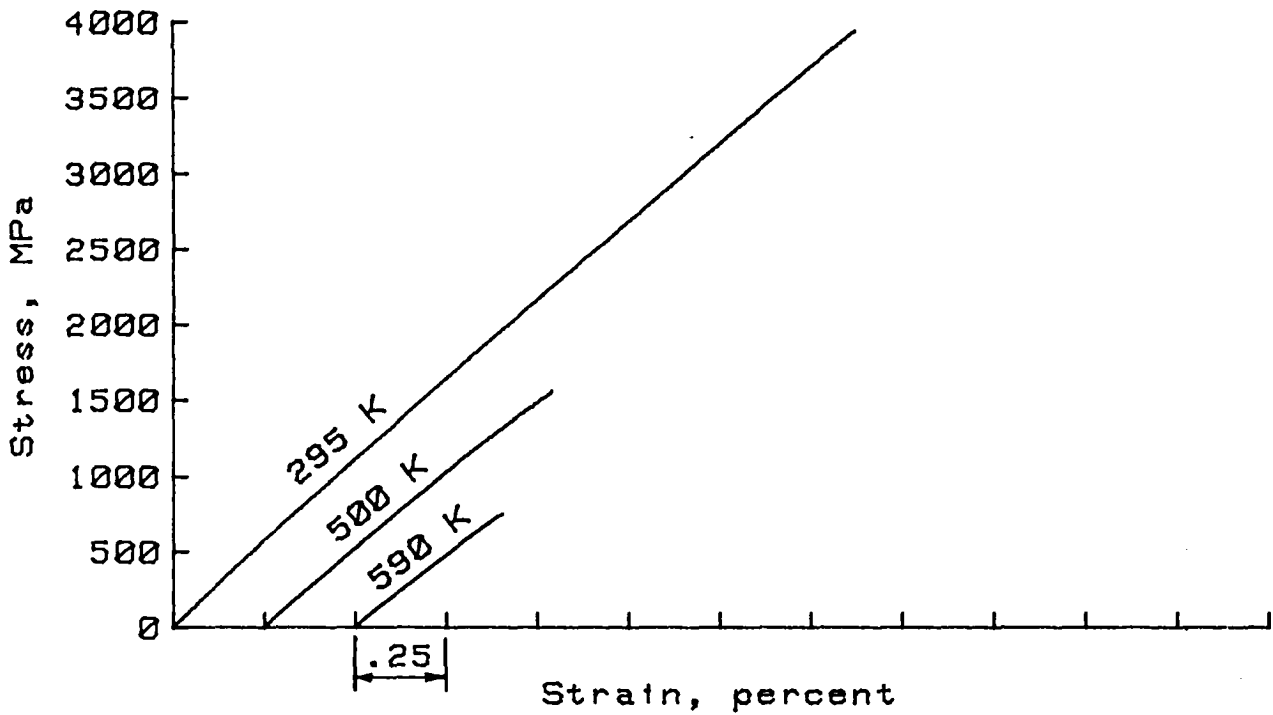
(c) Longitudinal compression
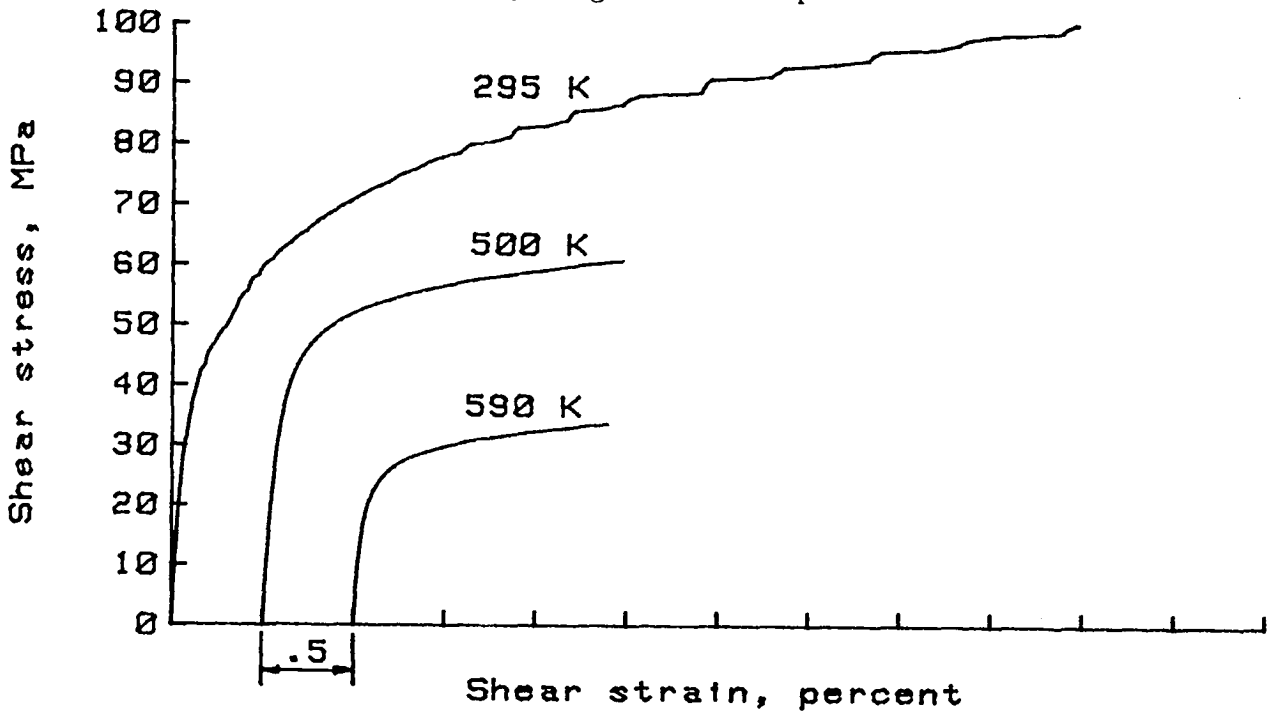
(d) In-plane shear

Figure A-5.- Concluded.
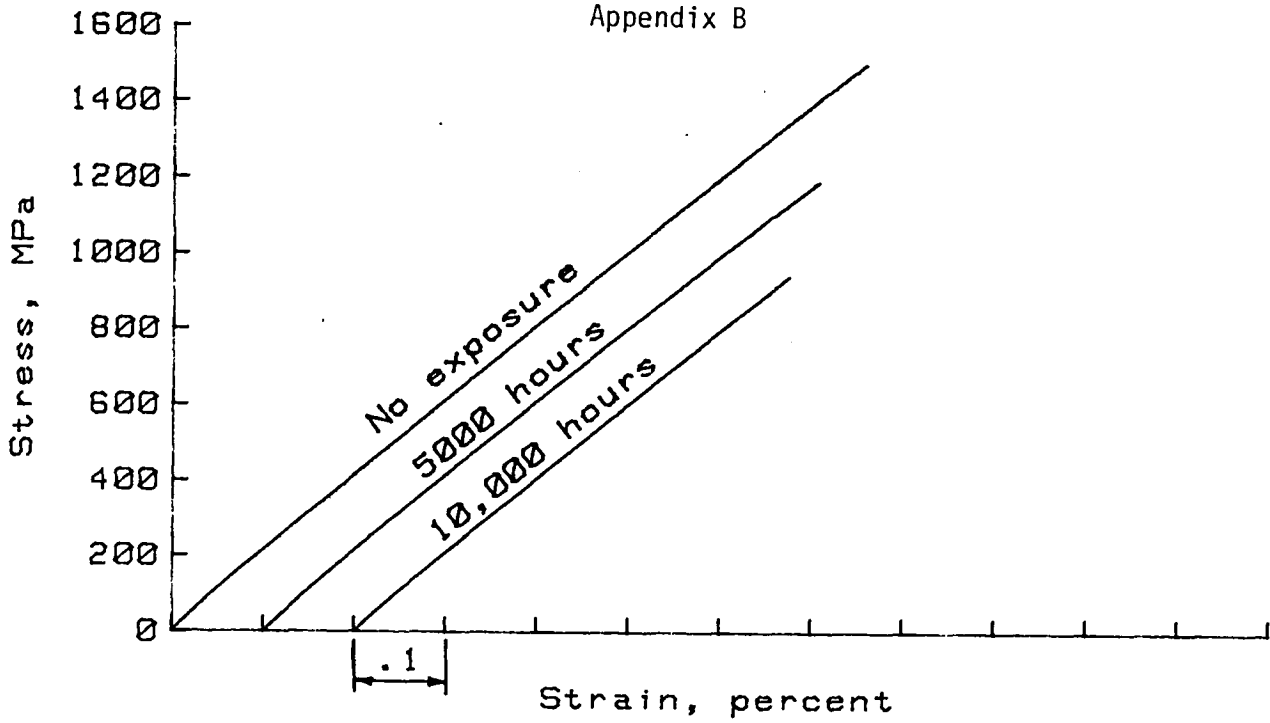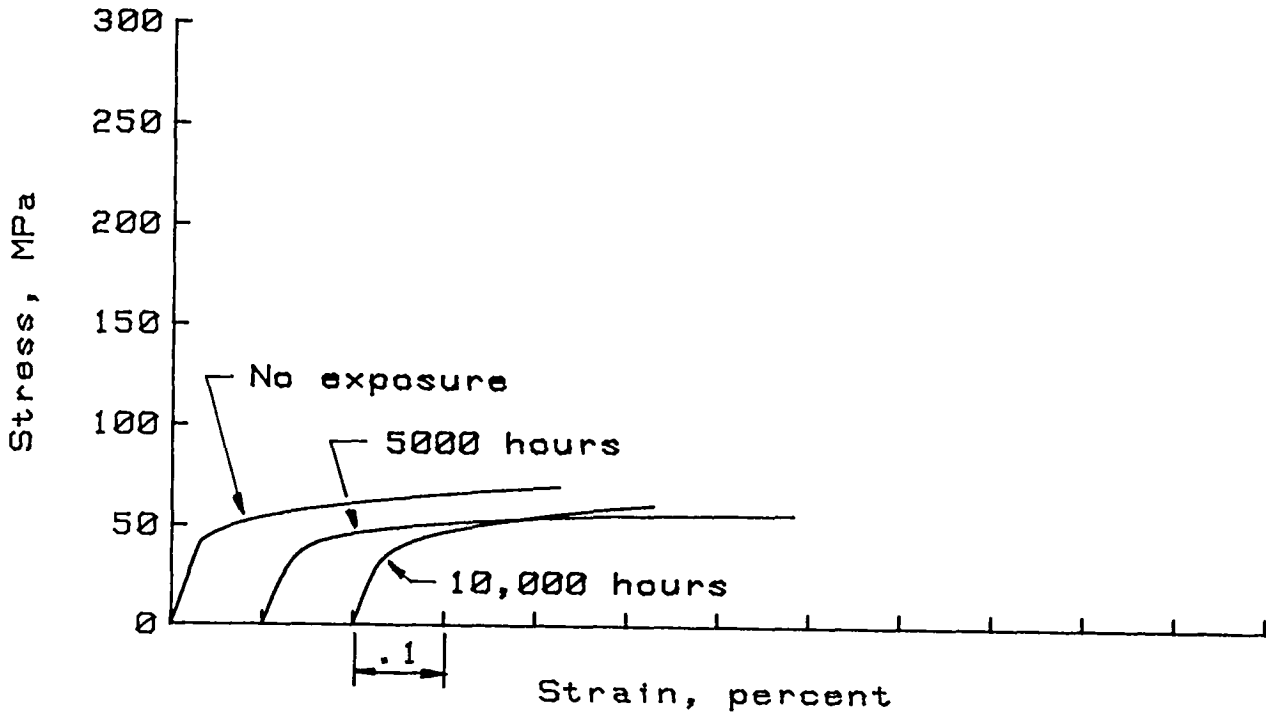
Figure B-1.– Typical room temperature stress-strain curves for B/1100 Al composite material exposed at 500 K.
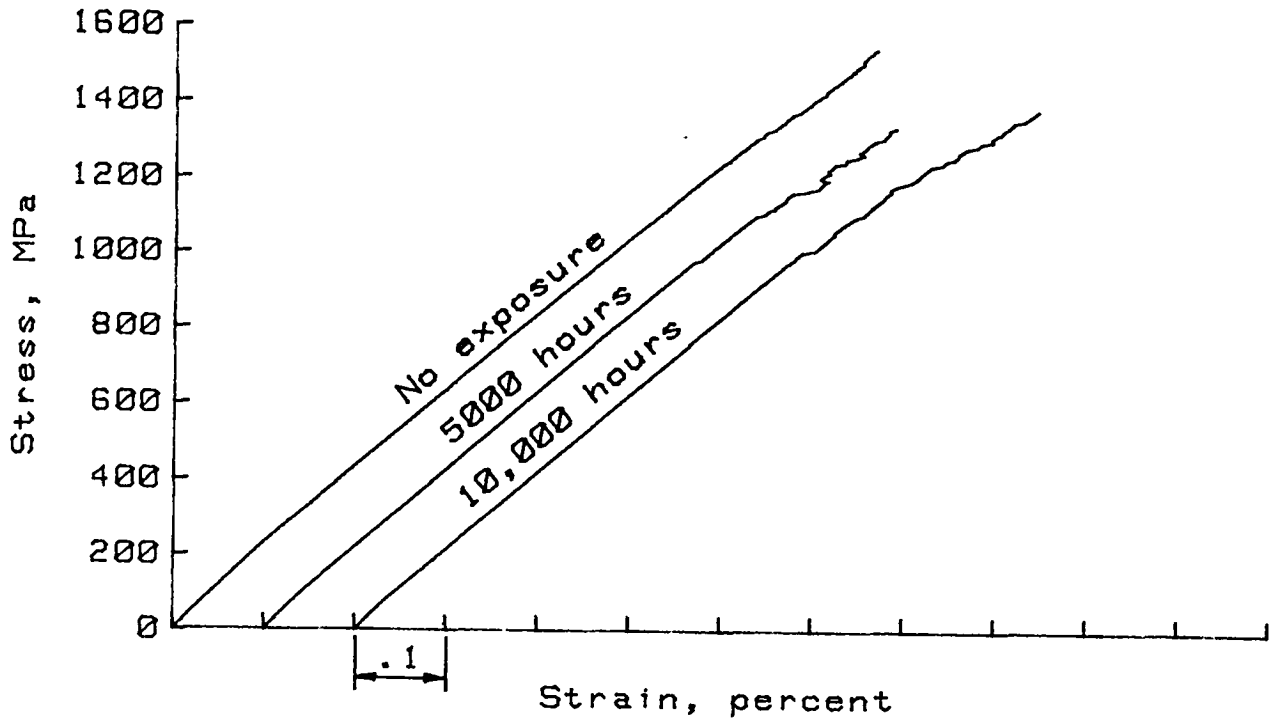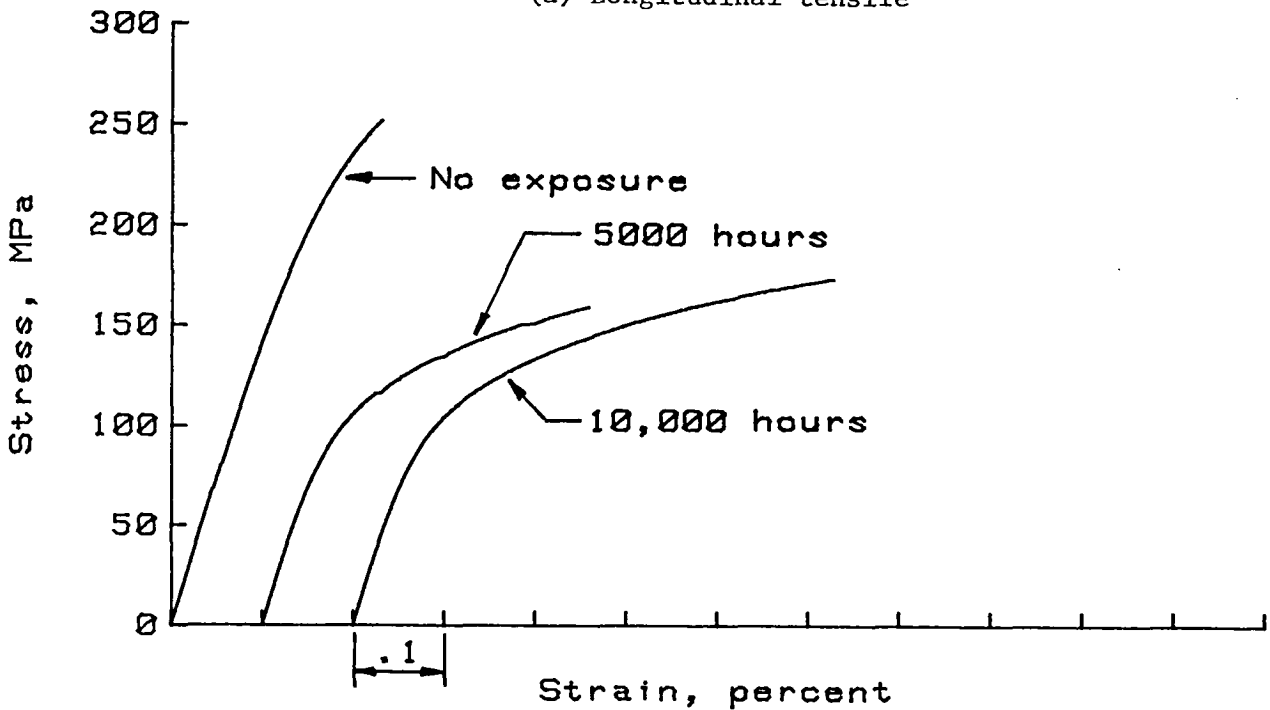
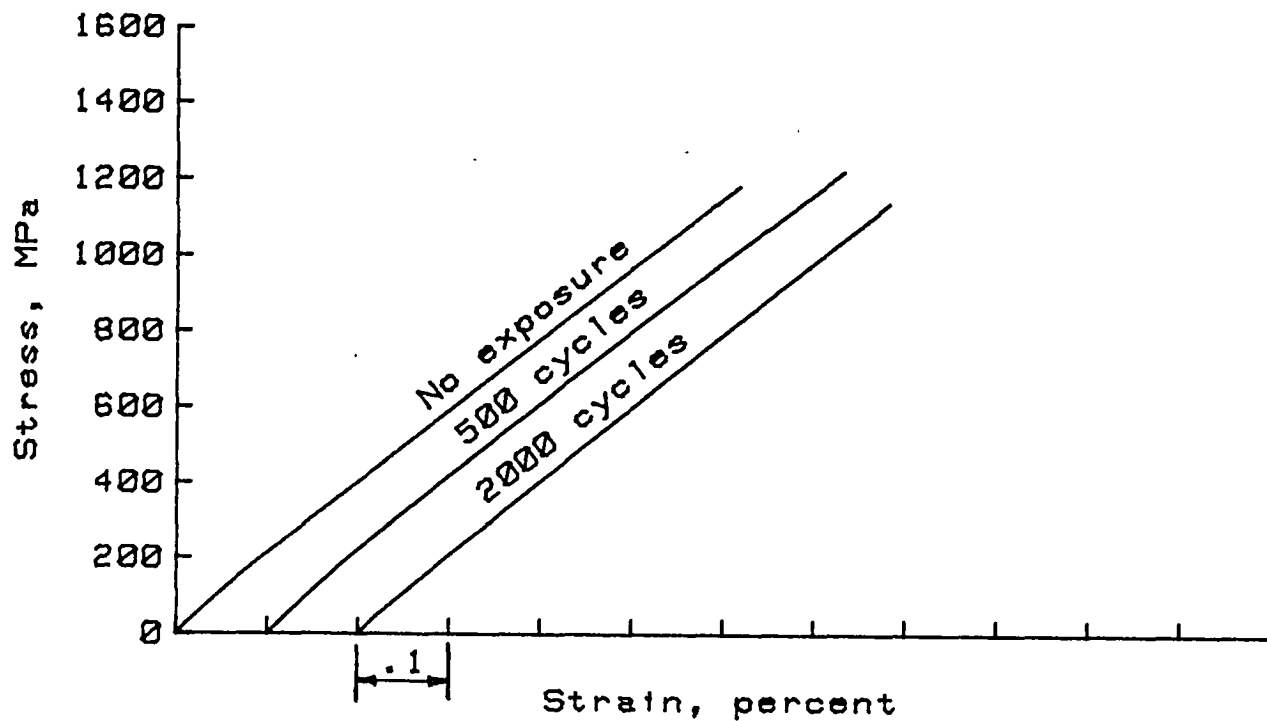Figure B-2.- Typical room temperature stress-strain curves for B/2024 Al composite material exposed at 500 K.
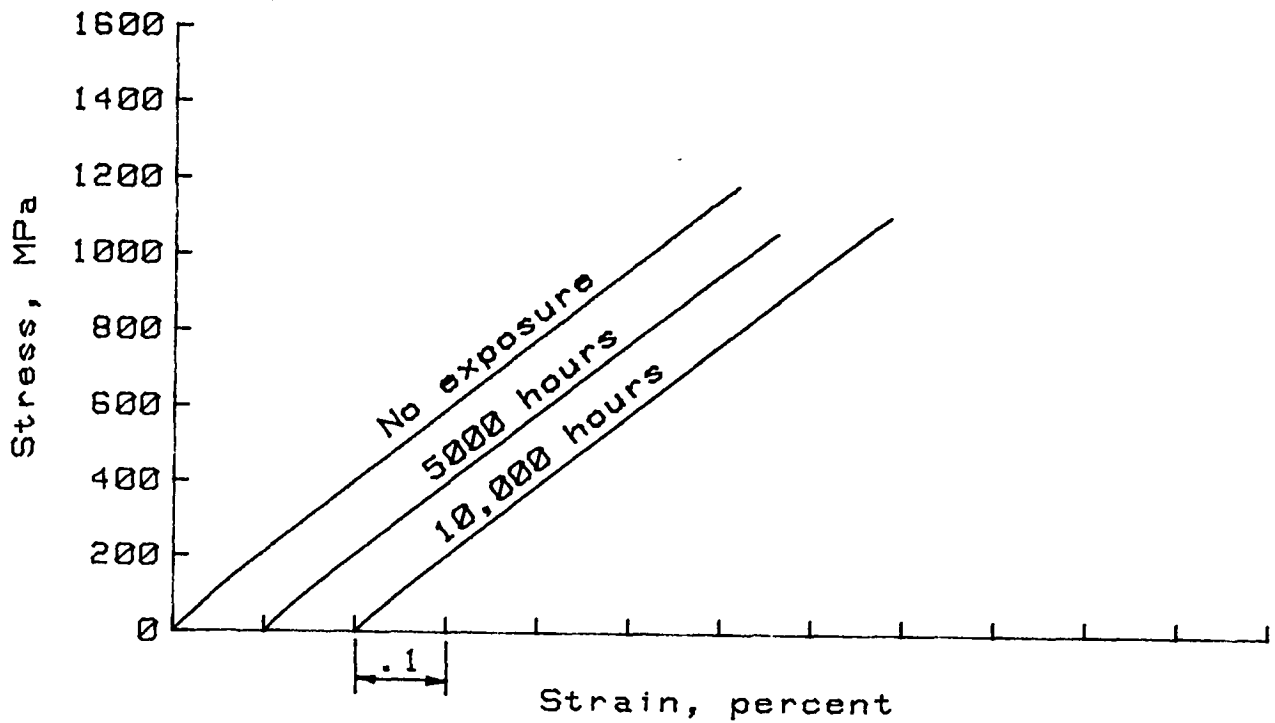
(a) Longitudinal tensile
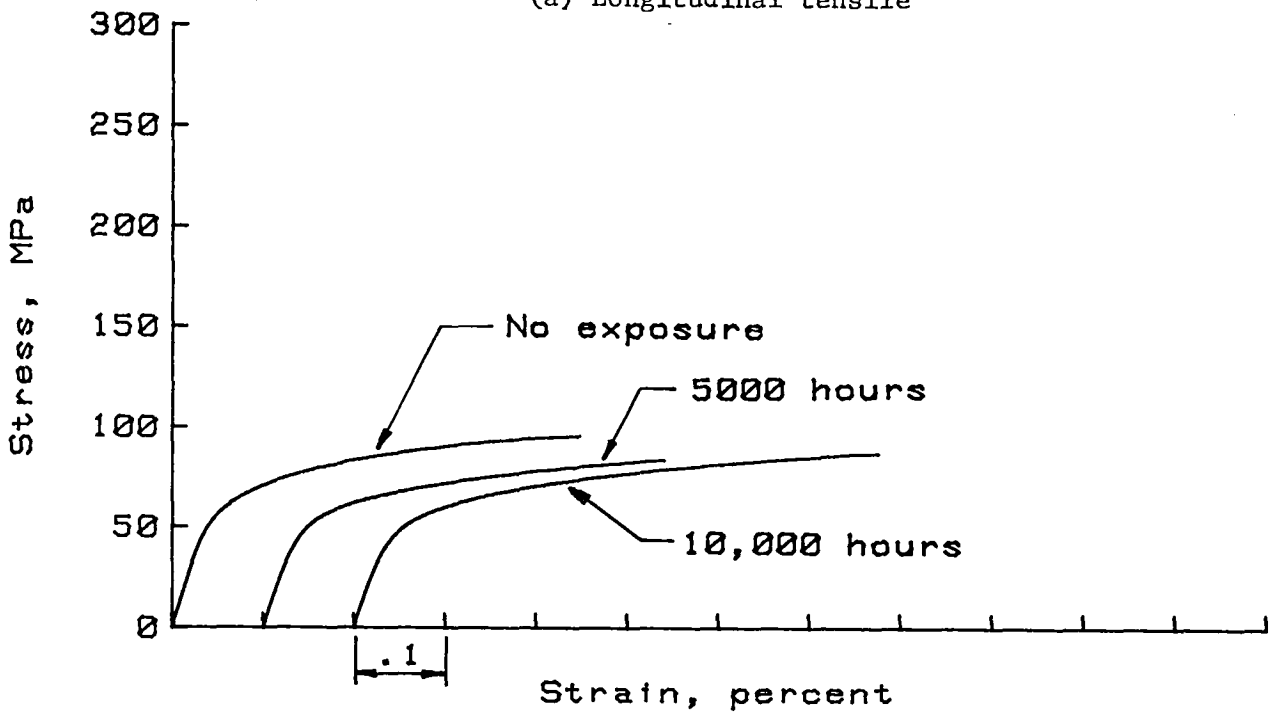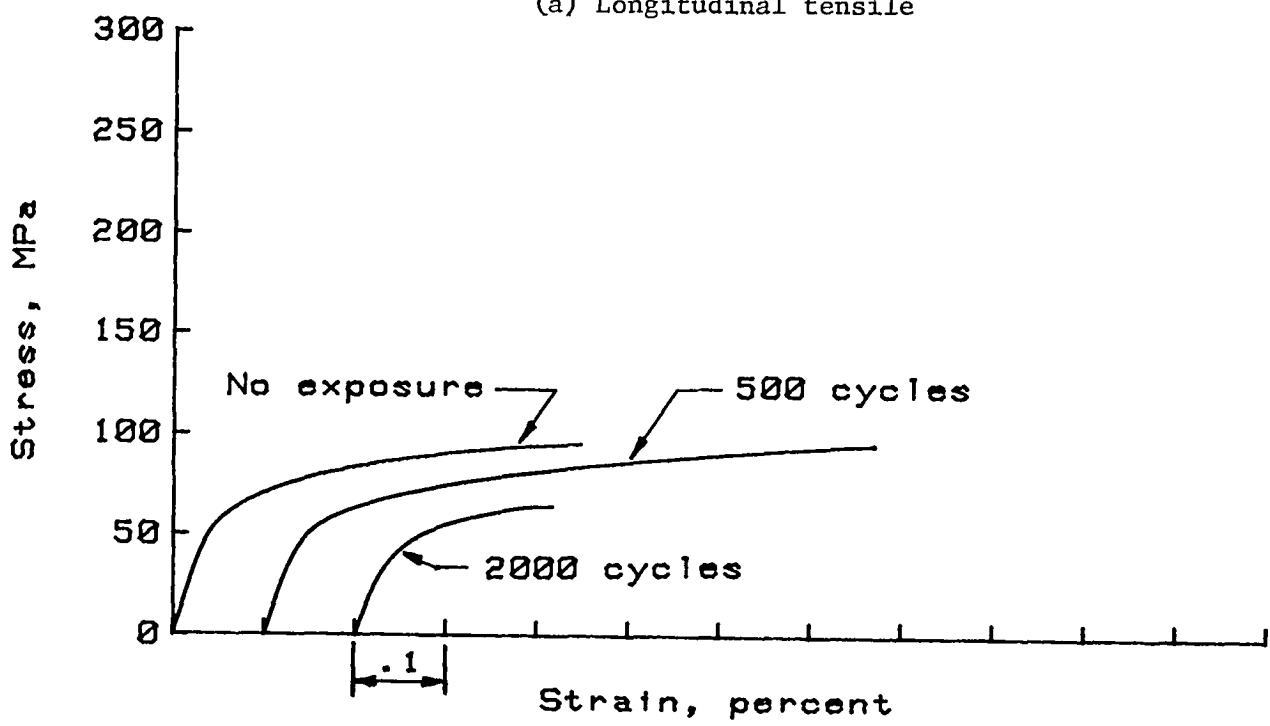
(b) Transverse tensile

Figure B-3.- Typical room temperature stress-strain curves for B/3003 Al composite material exposed at 500 K.

Figure B-4.- Typical room temperature stress-strain curves for B/5052 Al composite material exposed at 500 K.
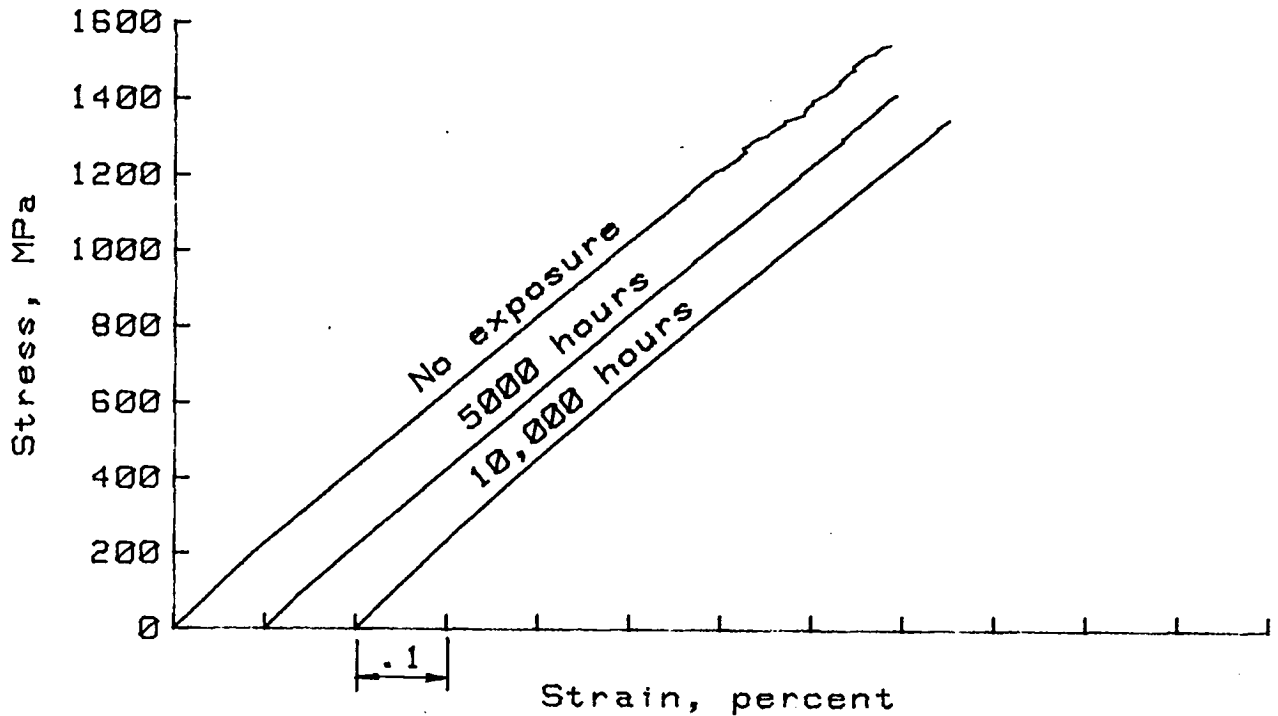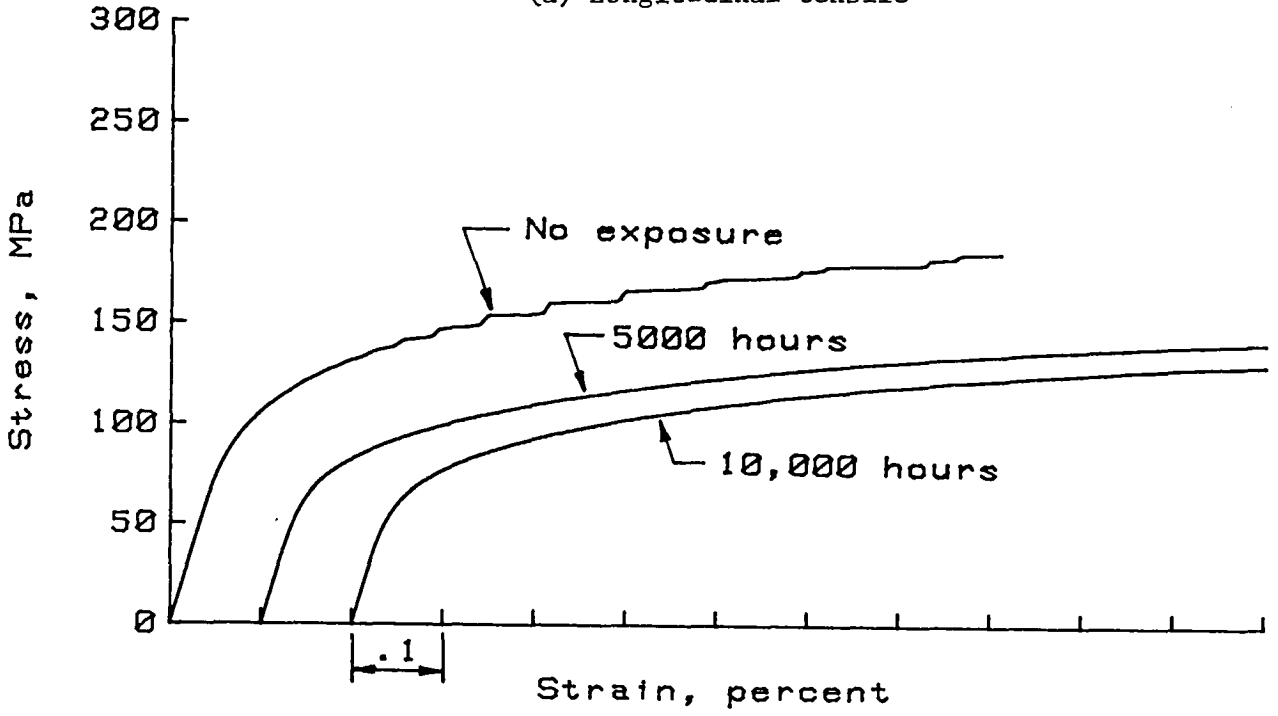
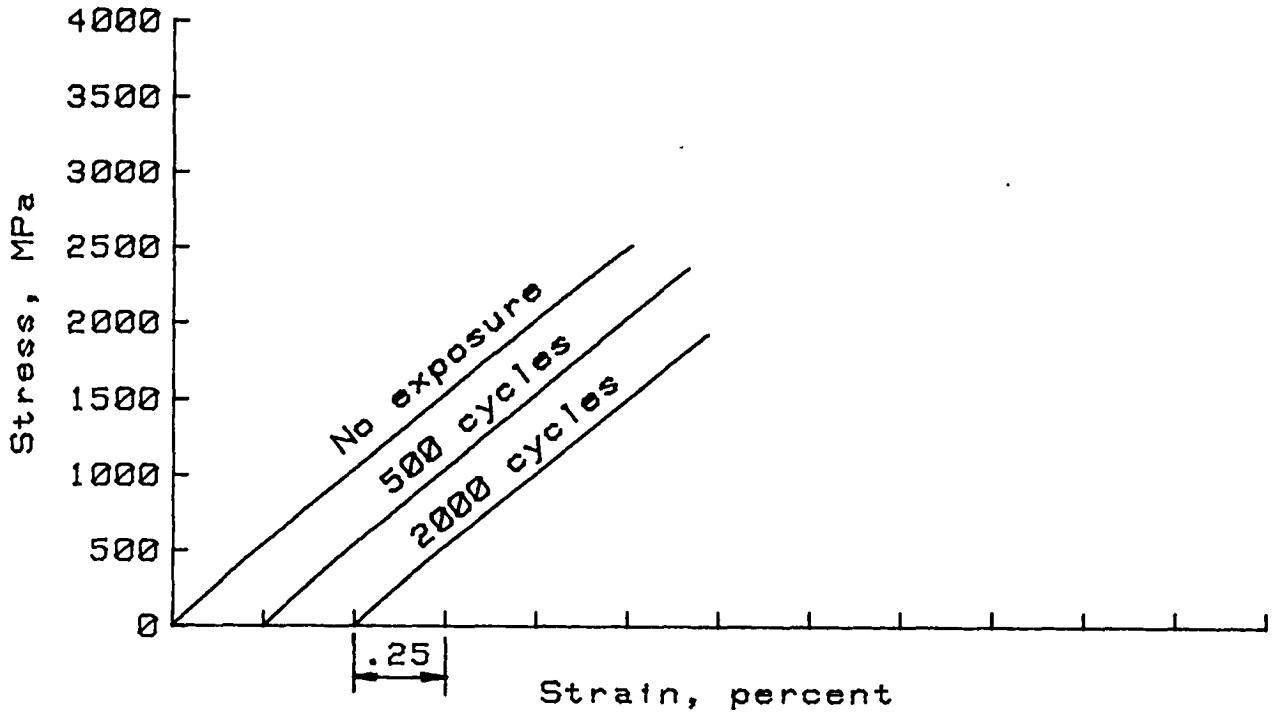Figure B-5.- Typical room temperature stress-strain curves for B/6061 Al composite material exposed at 500 K.
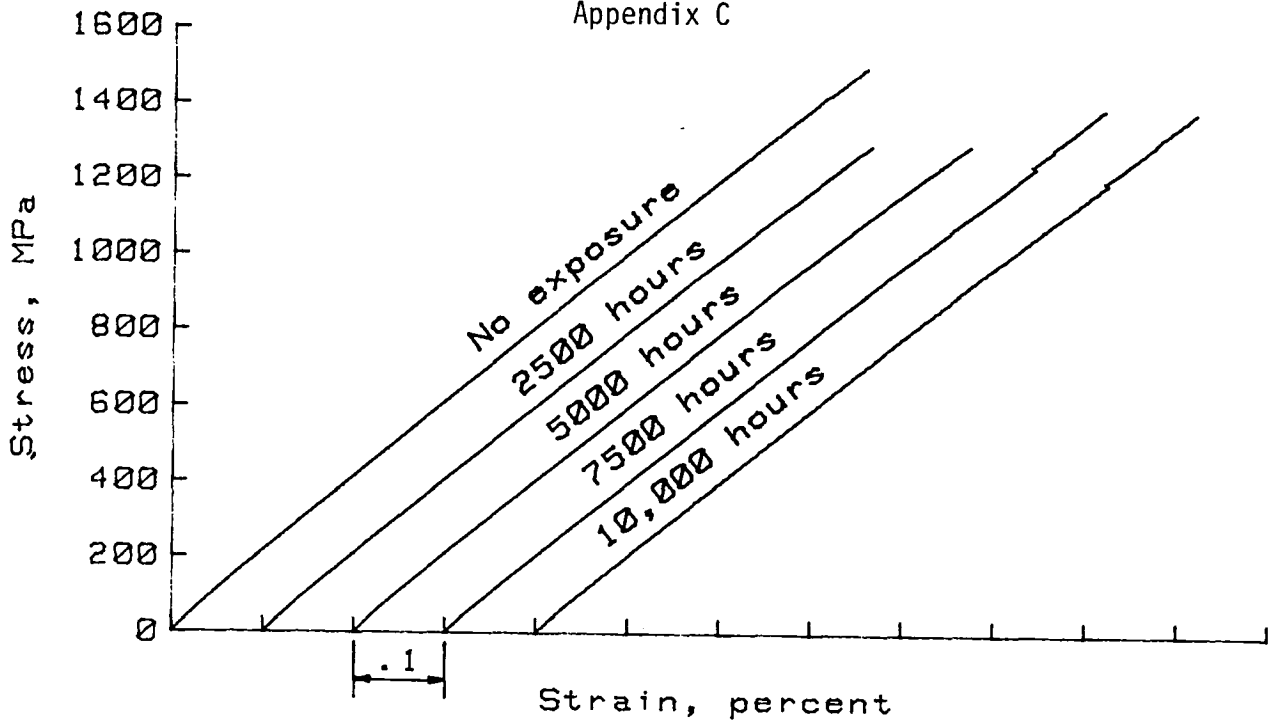
(a) Longitudinal tensile
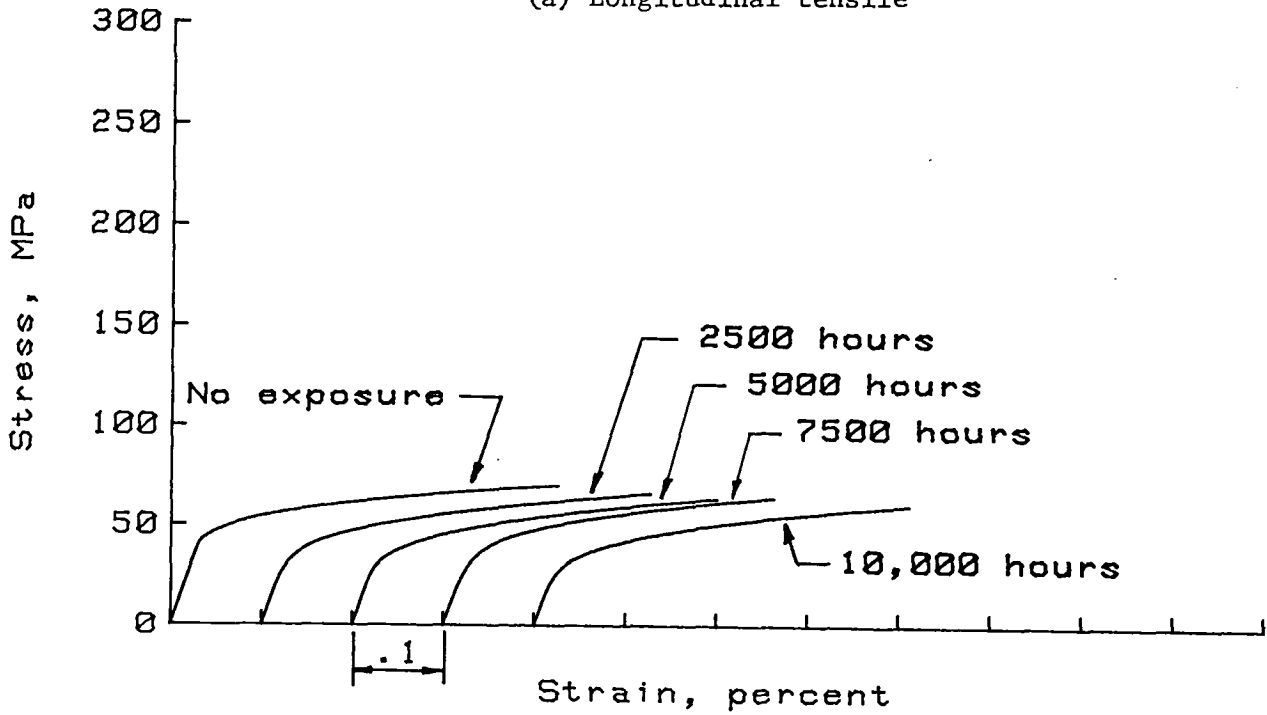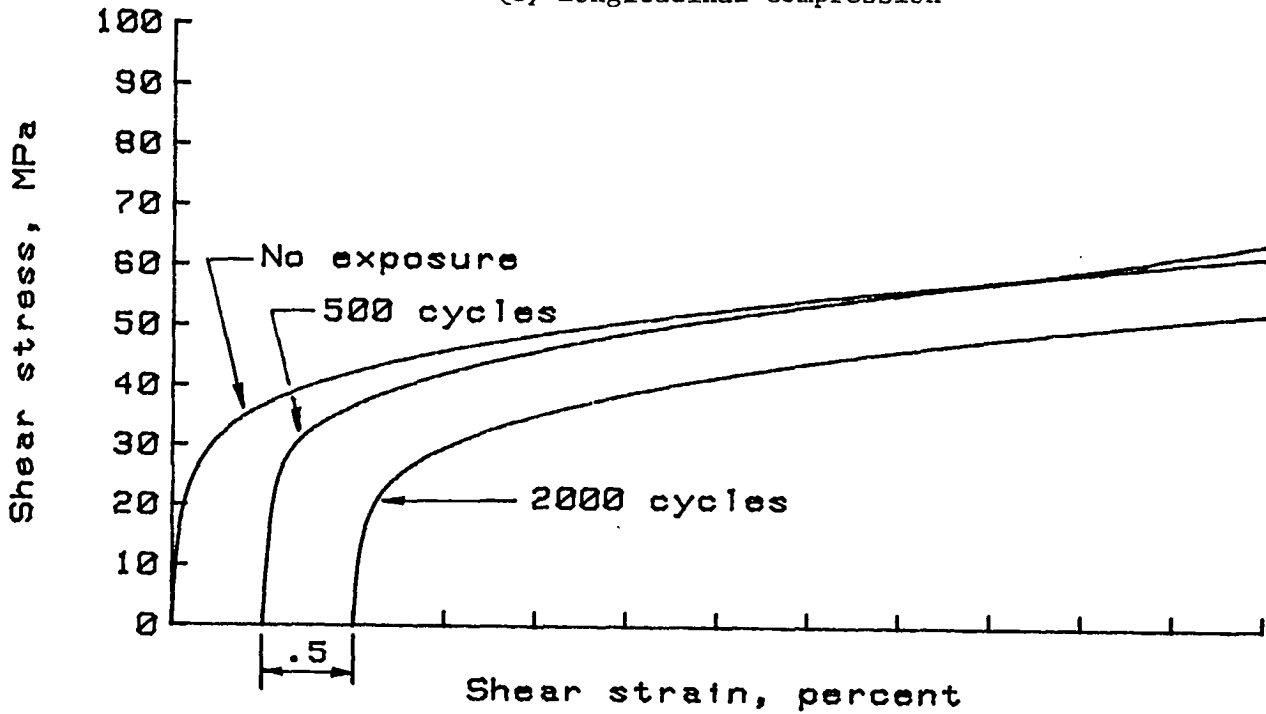
(b) Transverse tensile

Figure C-1.- Typical room temperature stress-strain curves for B/1100 Al composite material exposed at 590 K.
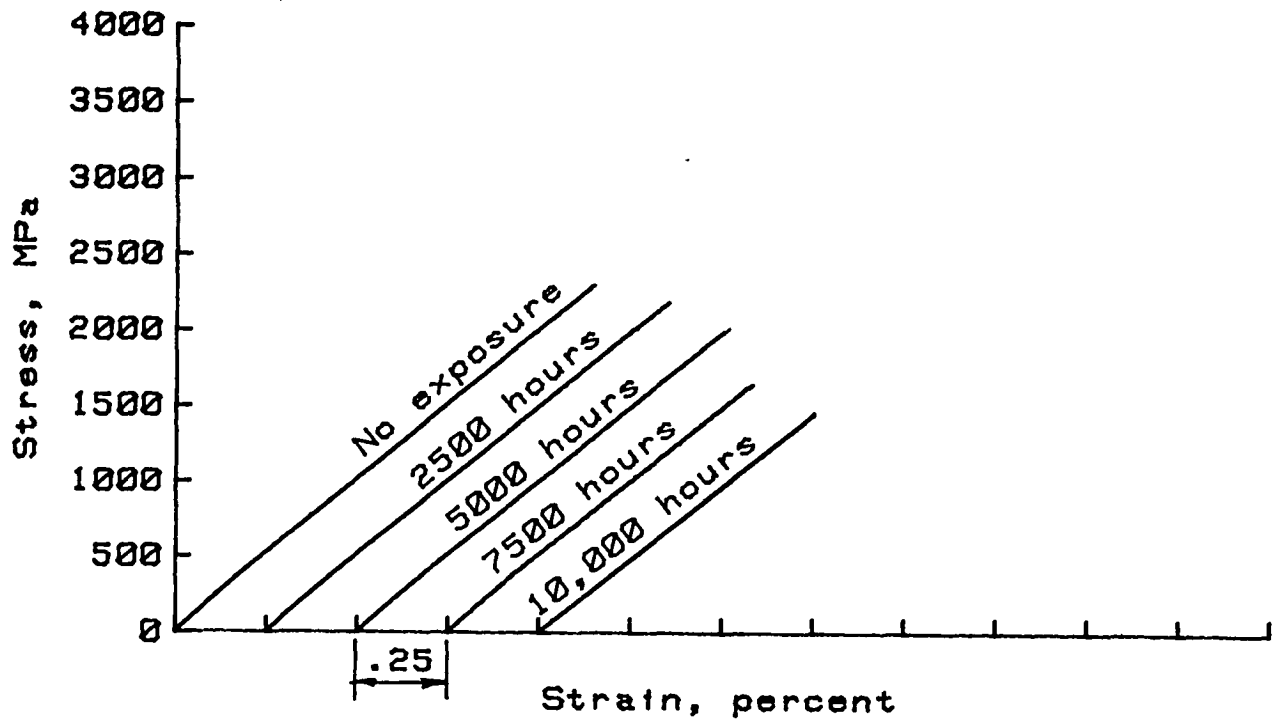
(c) Longitudinal compression
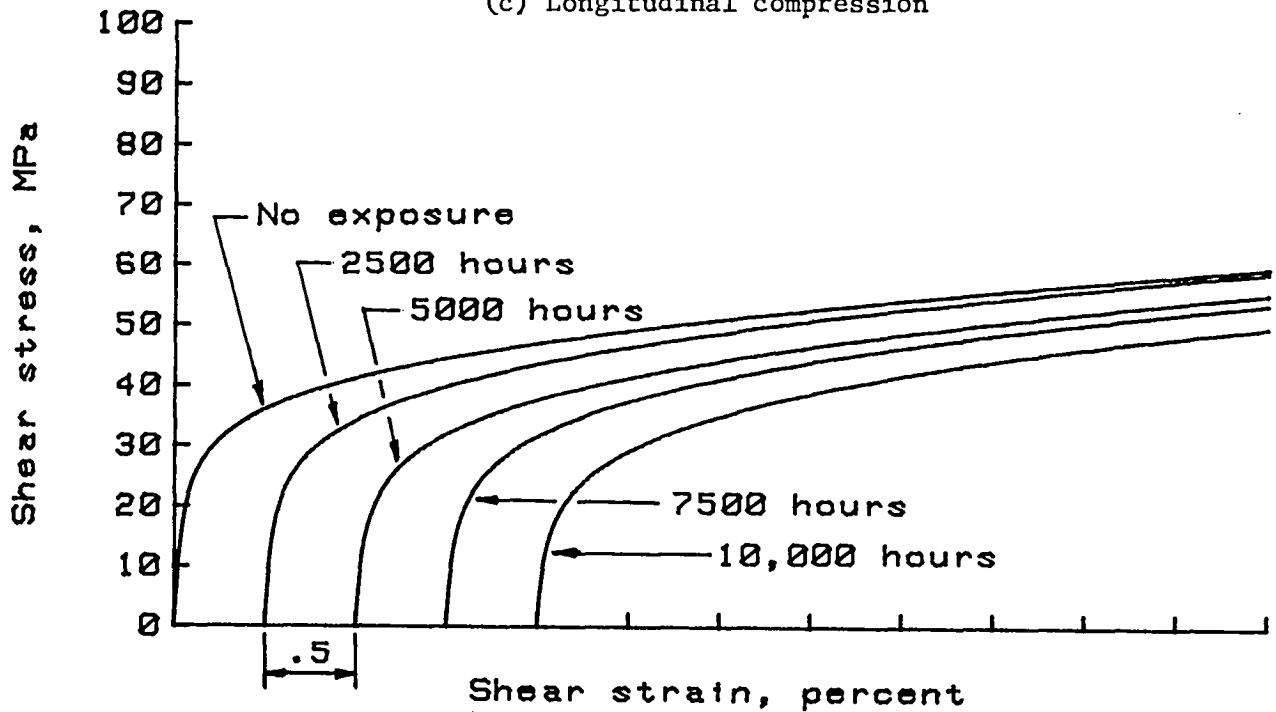
(d) In-plane shear

Figure C-1.- Concluded.
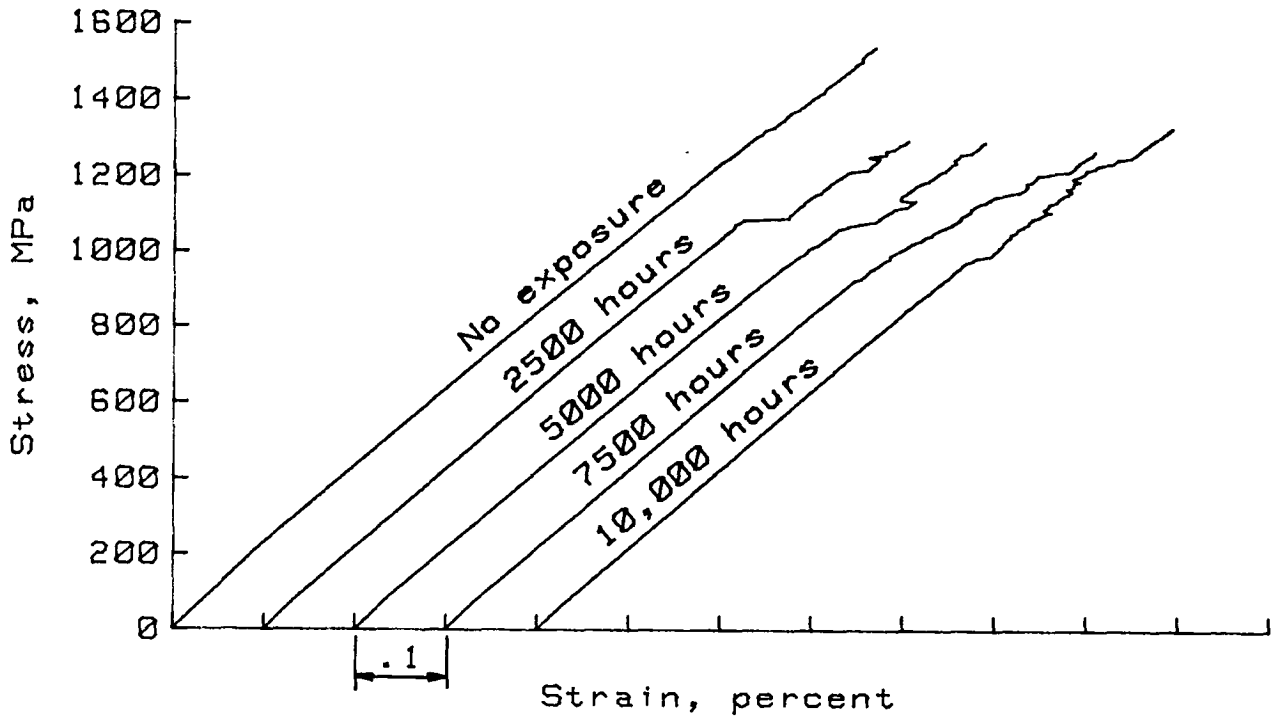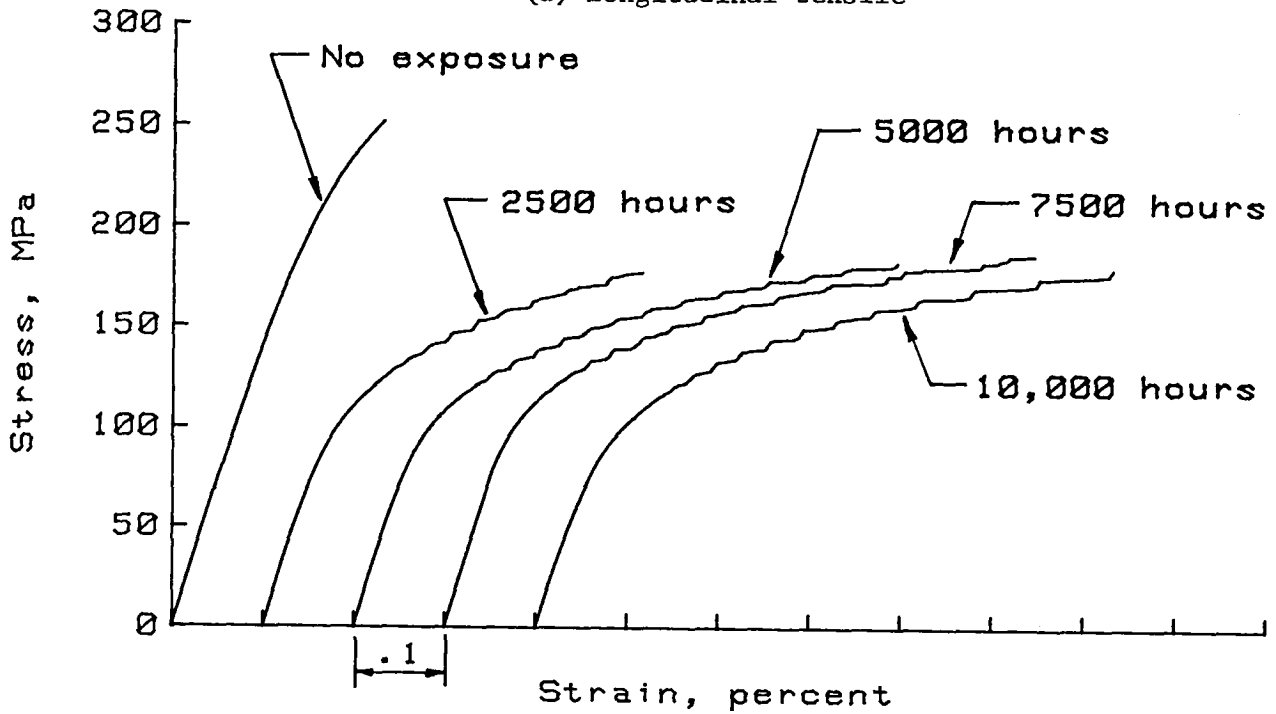
Figure C-2.— Typical room temperature stress-strain curves for B/2024 Al composite material exposed at 590 K.
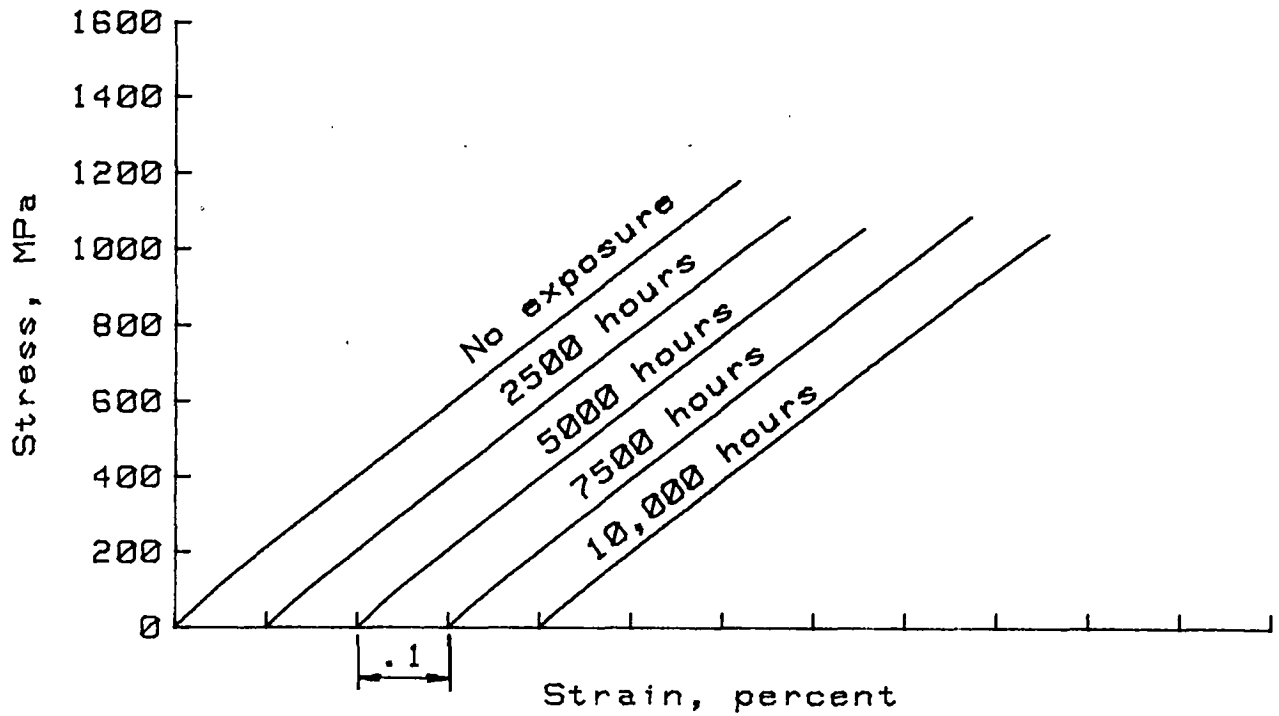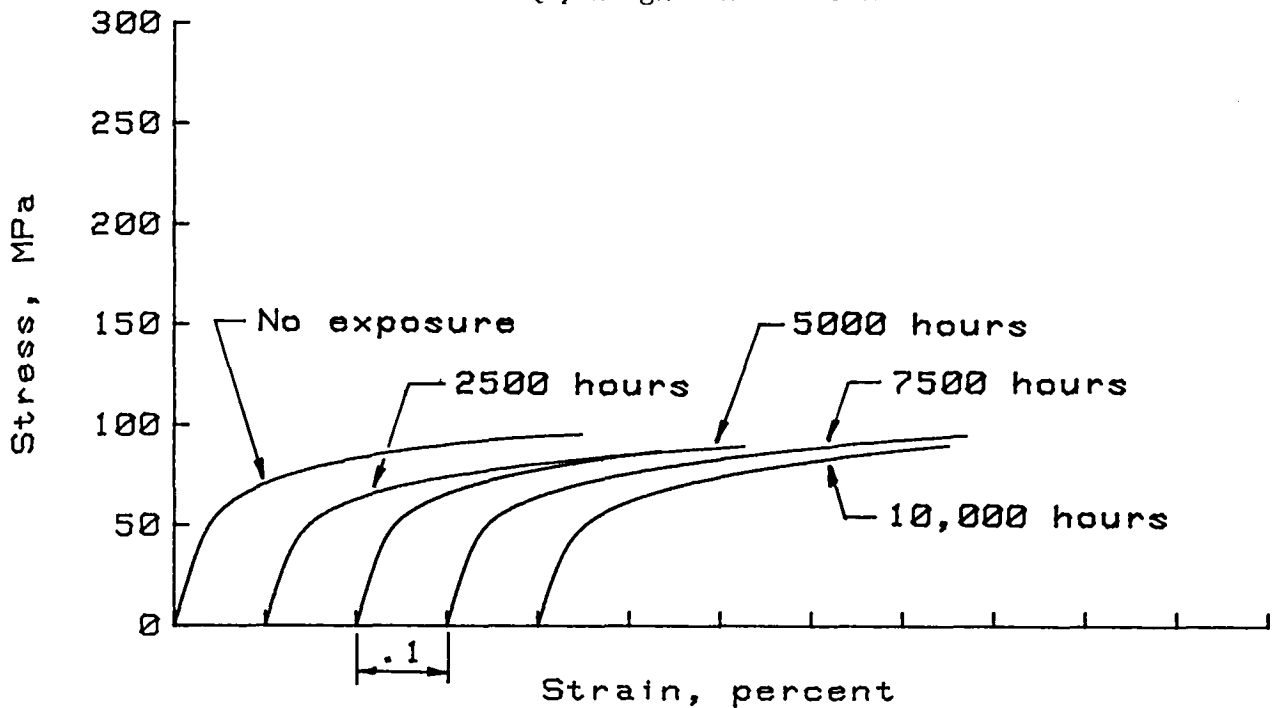
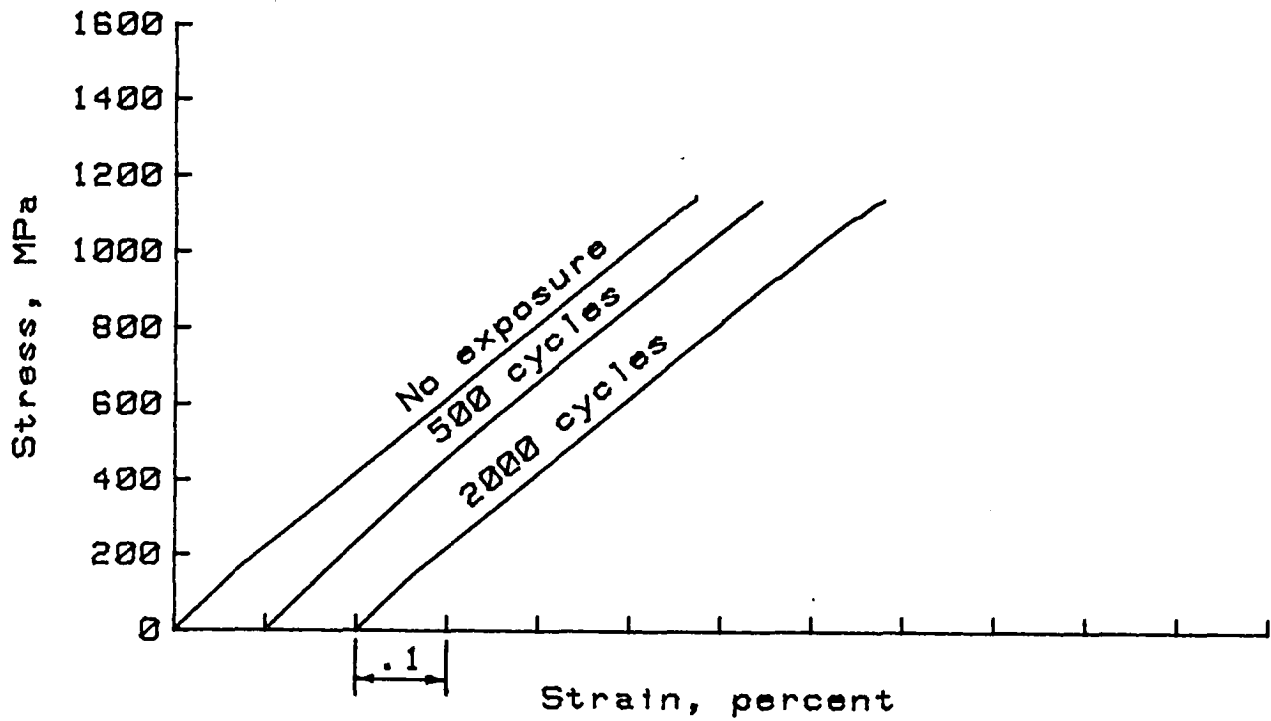Figure C-3.- Typical room temperature stress-strain curves for B/3003 Al composite material exposed at 590 K.
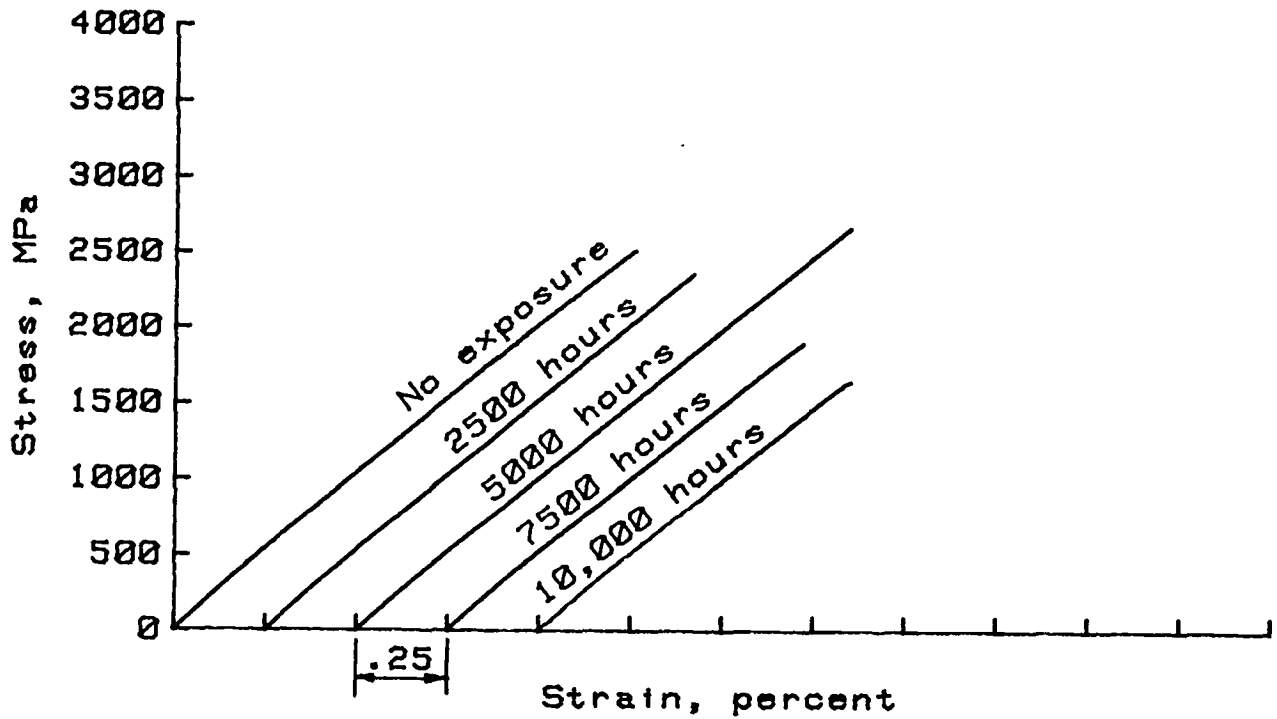
(c) Longitudinal compression
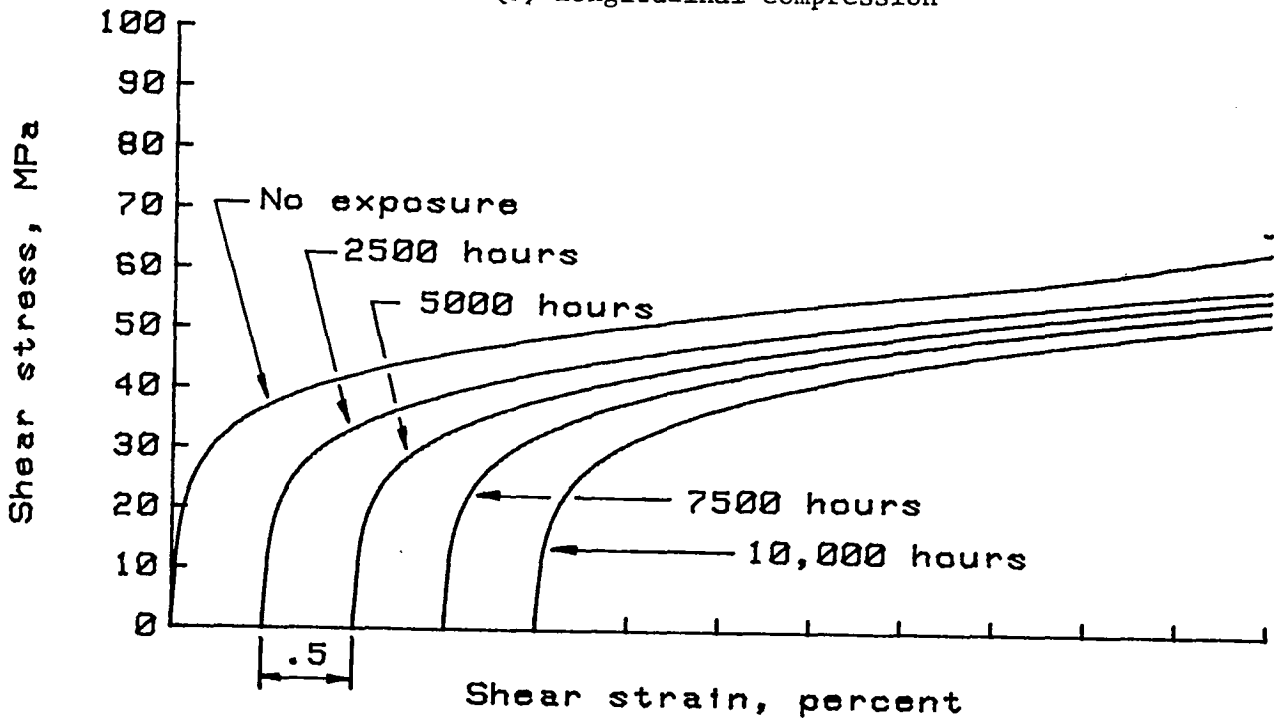
(d) In-plane shear

Figure C-3.- Concluded.
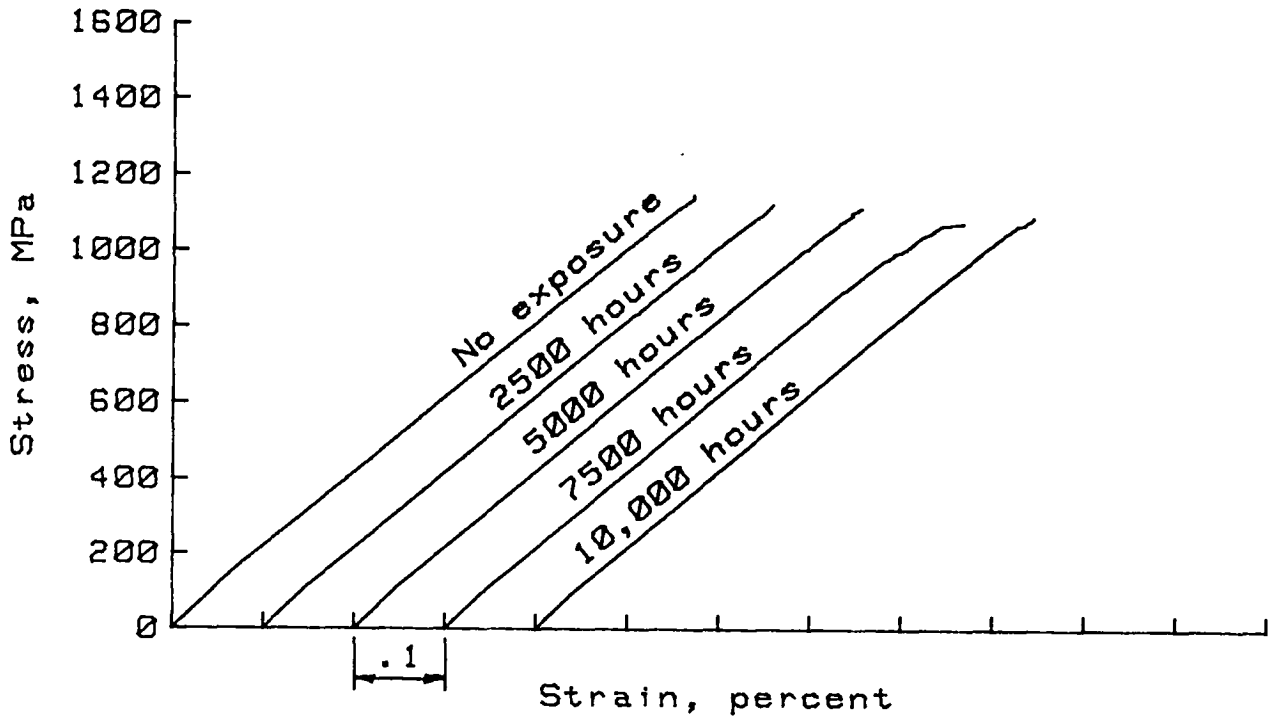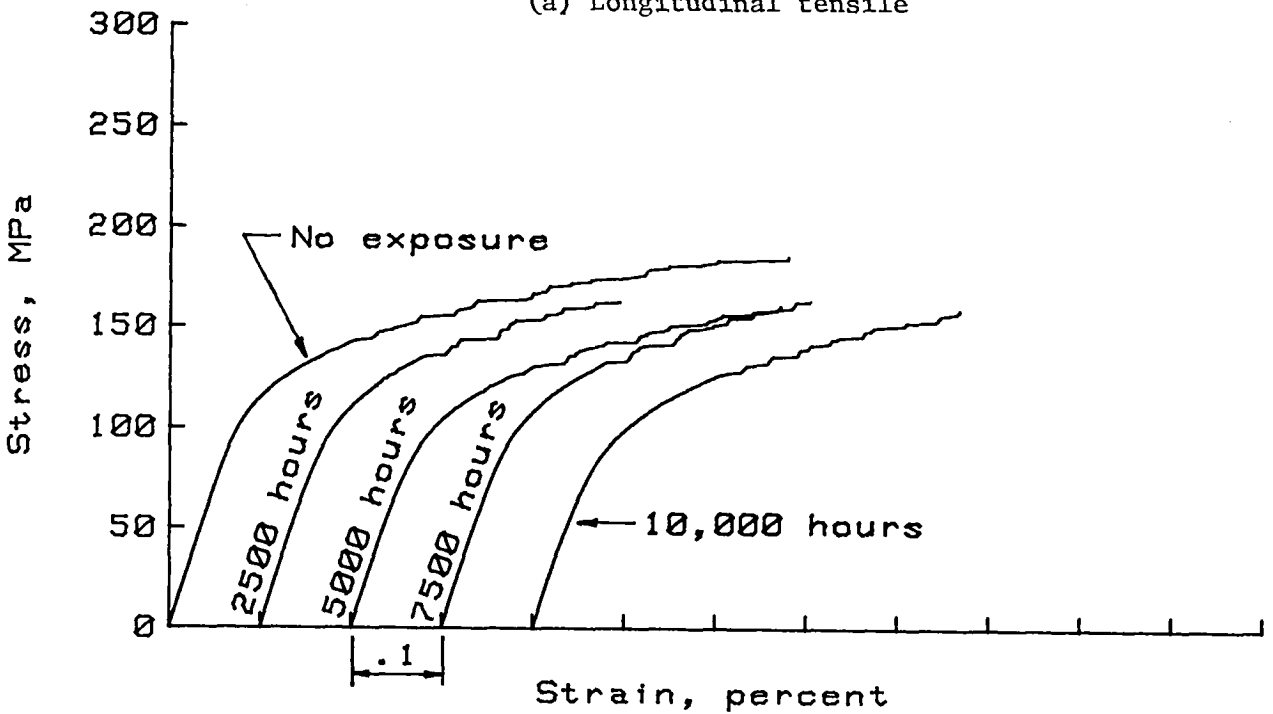
Figure C-4.— Typical room temperature stress-strain curves for B/5052 Al composite material exposed at 590 K.
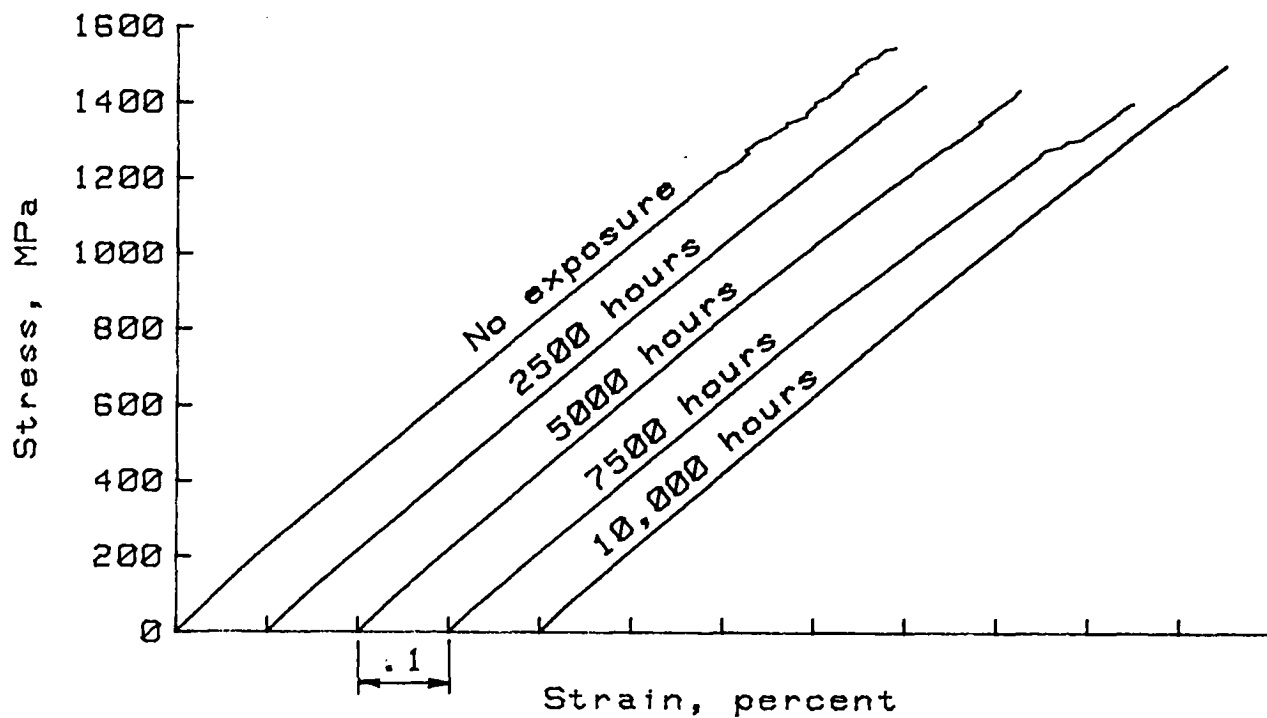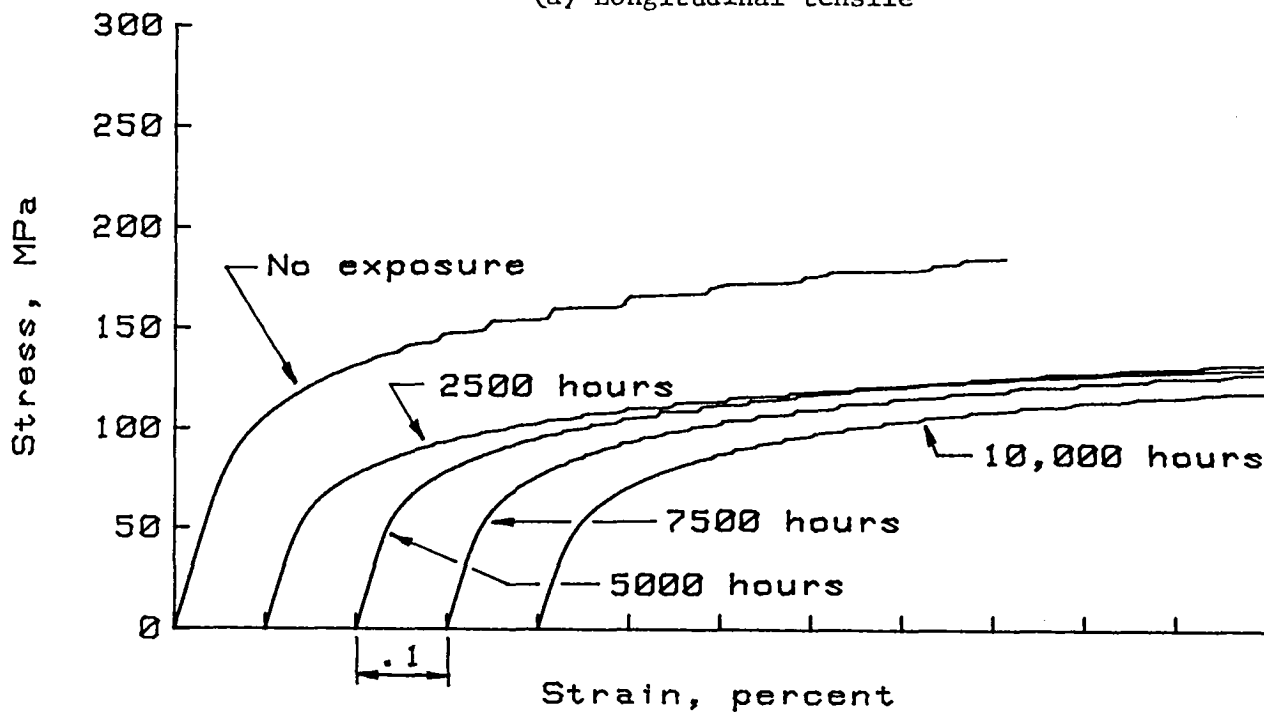
Figure C-5.— Typical room temperature stress-strain curves for B/6061 Al composite material exposed at 590 K.
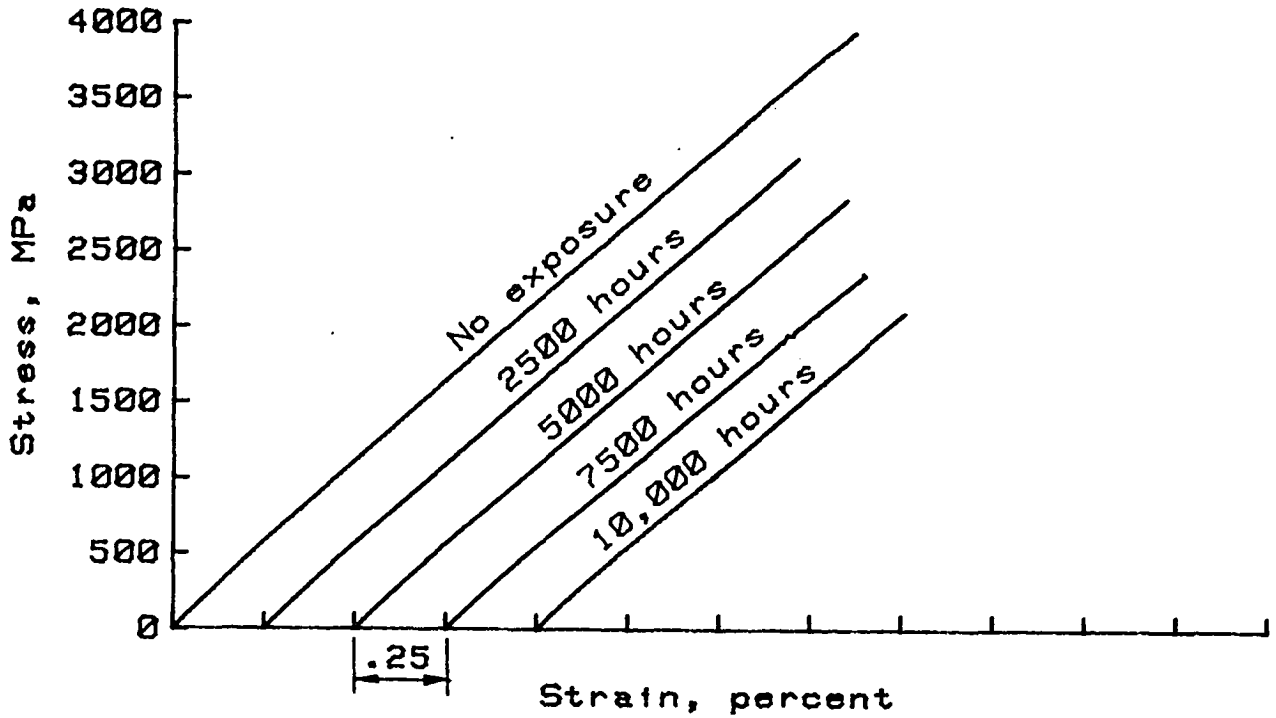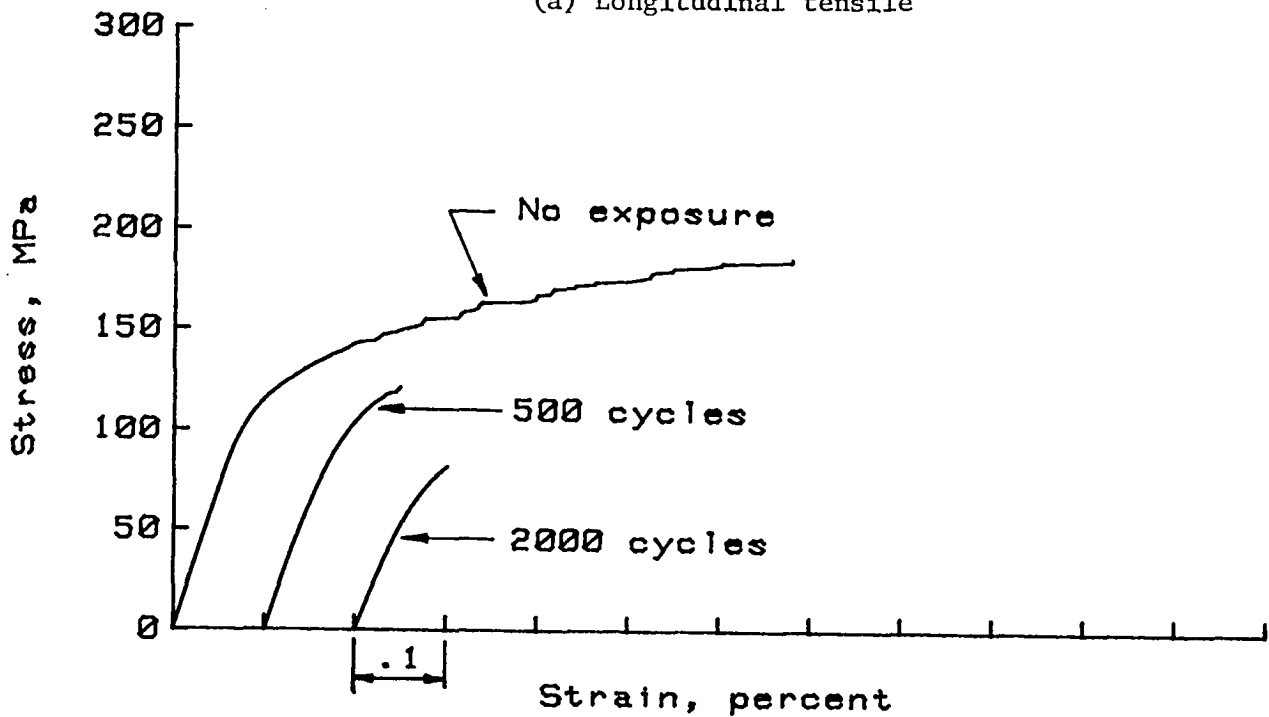
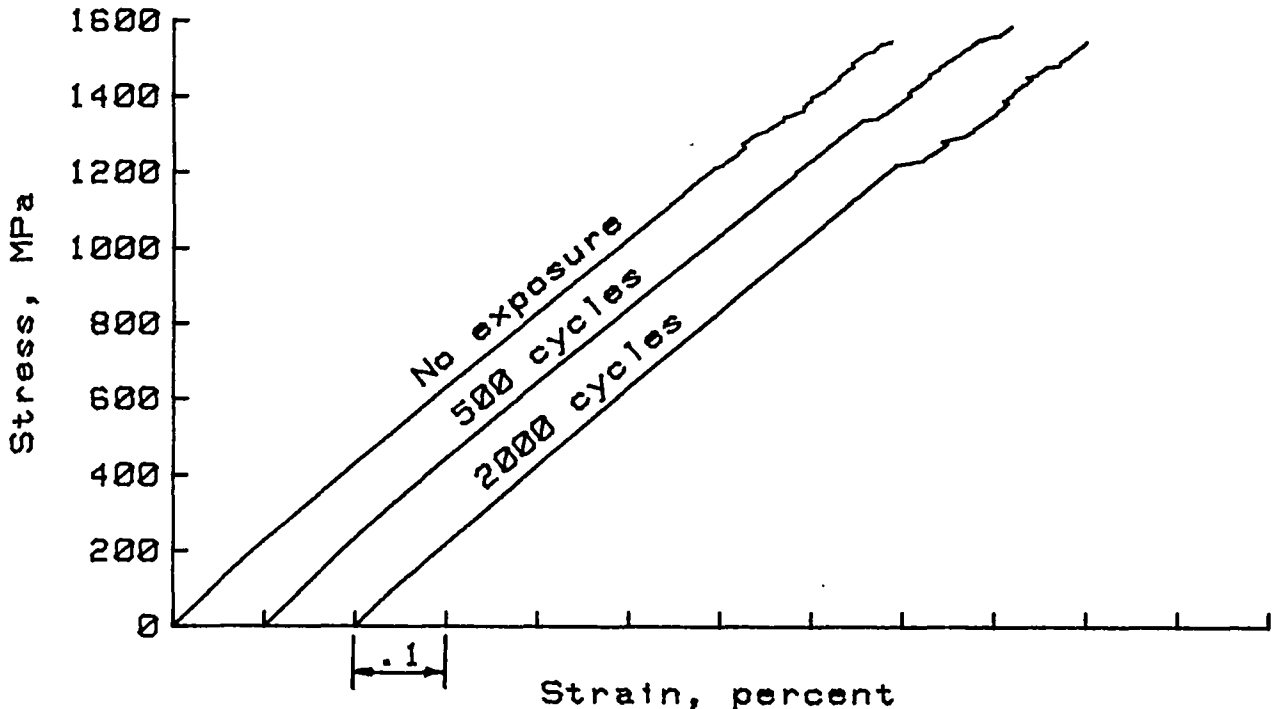(c) Longitudinal compression
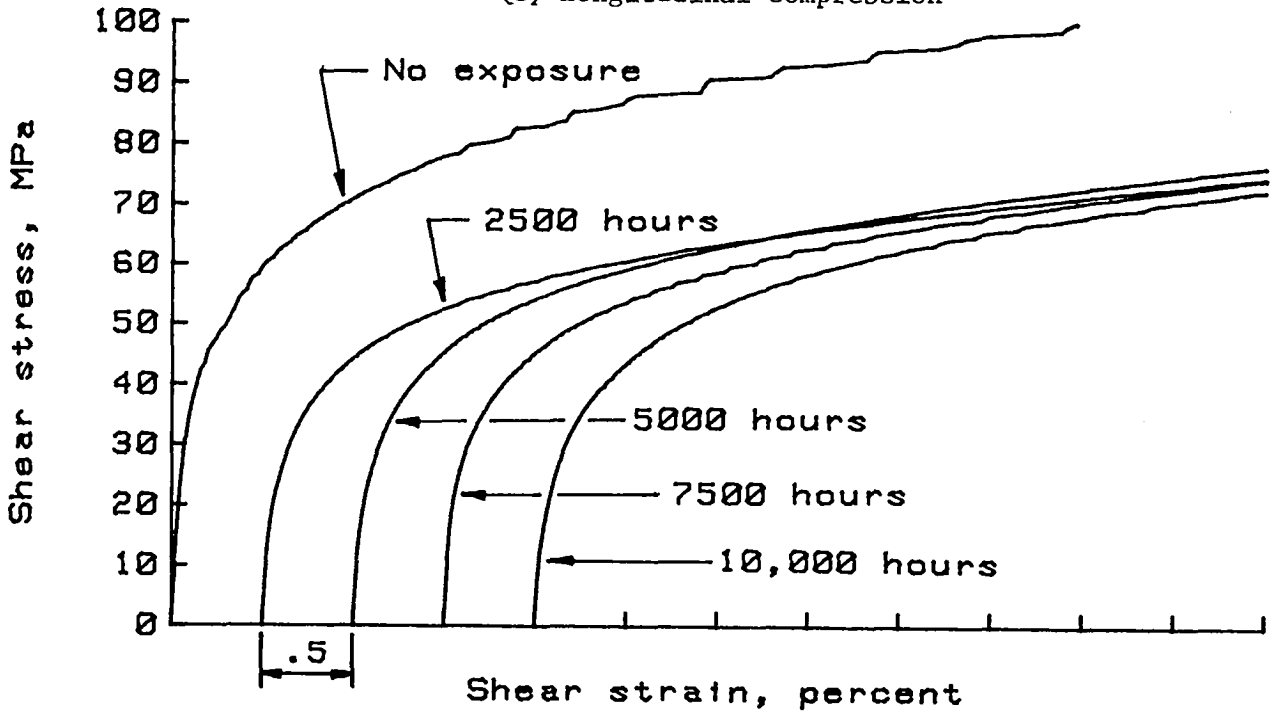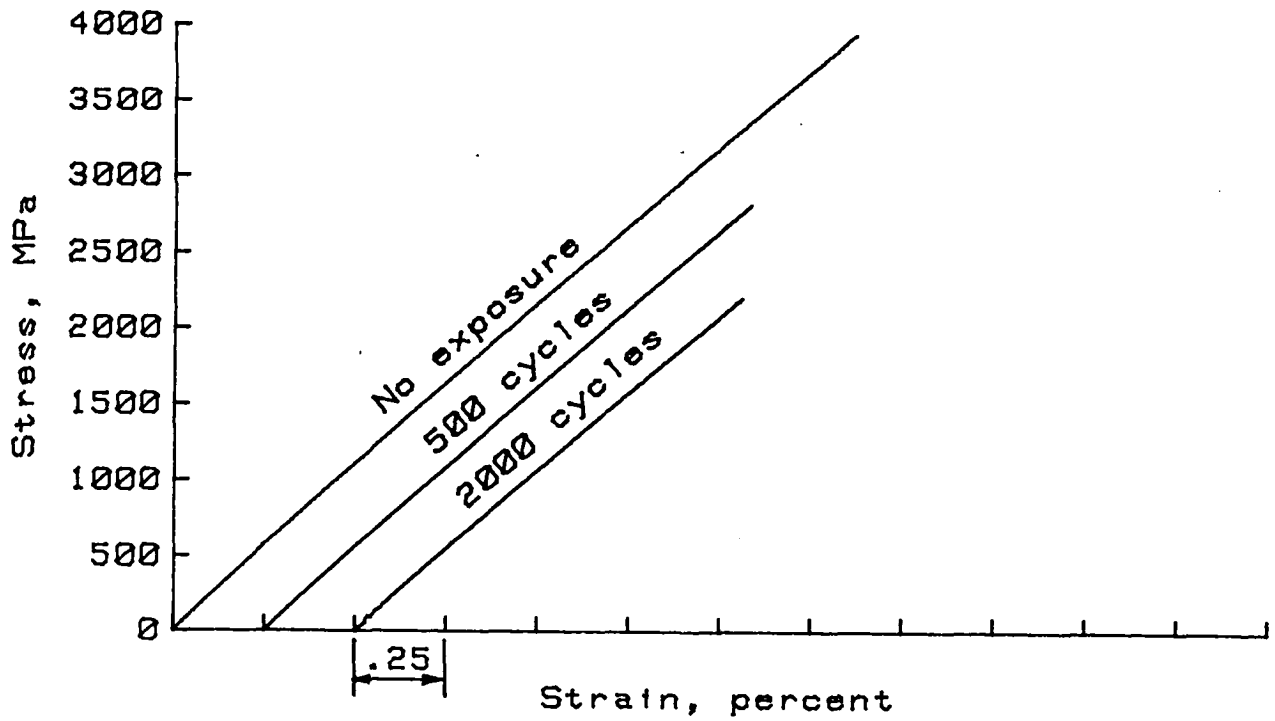
(d) In-plane shear

Figure C-5.- Concluded.

(a) Longitudinal tensile
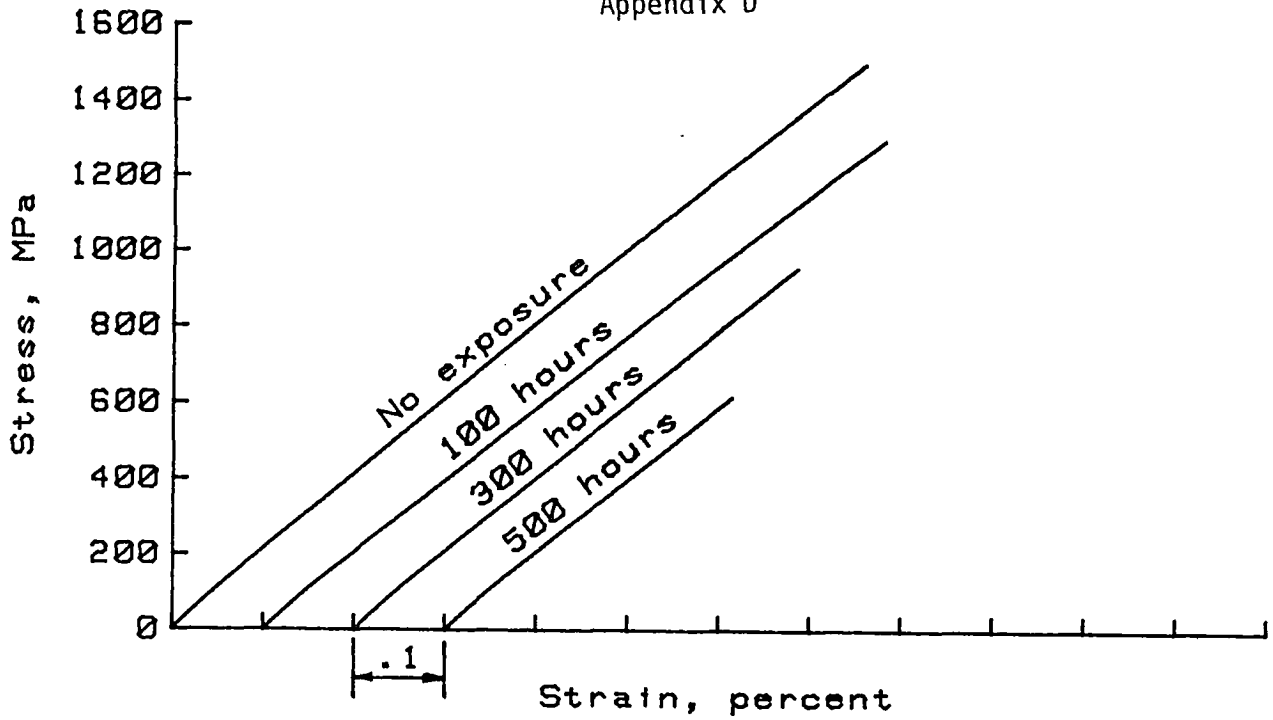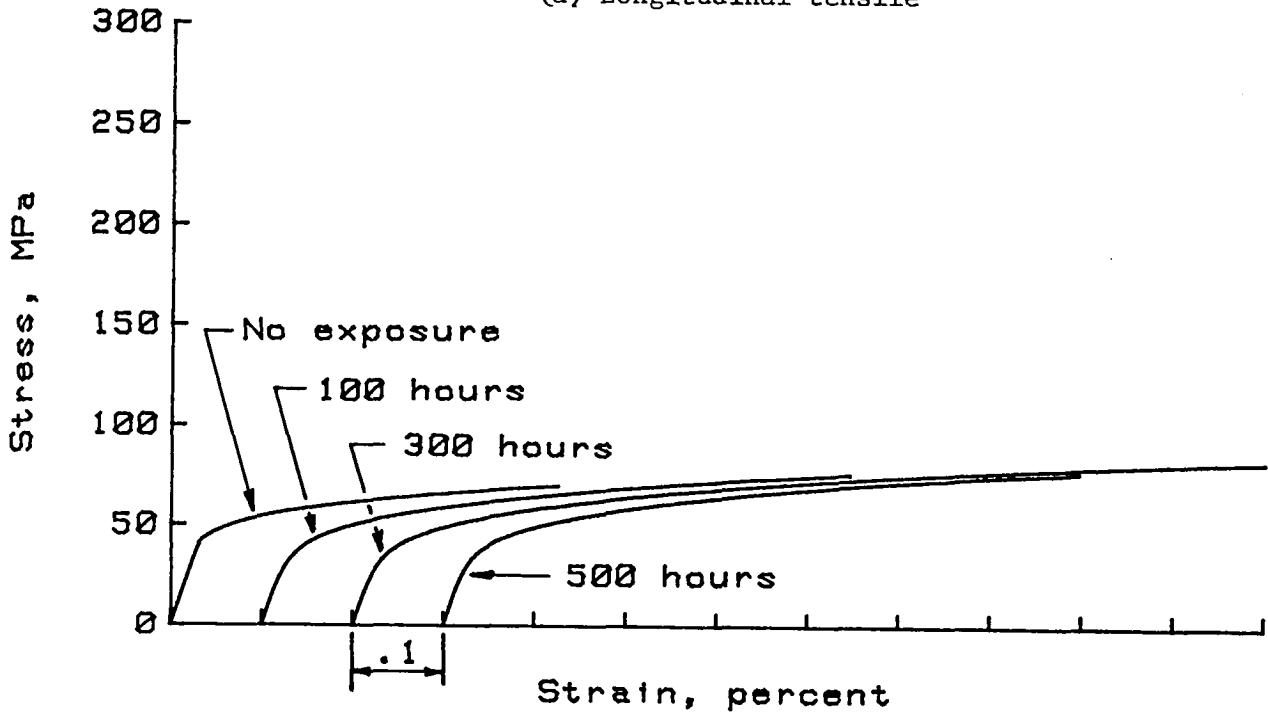
(b) Transverse tensile

Figure D-1.— Typical room temperature stress-strain curves for B/1100 Al composite material exposed at 730 K.
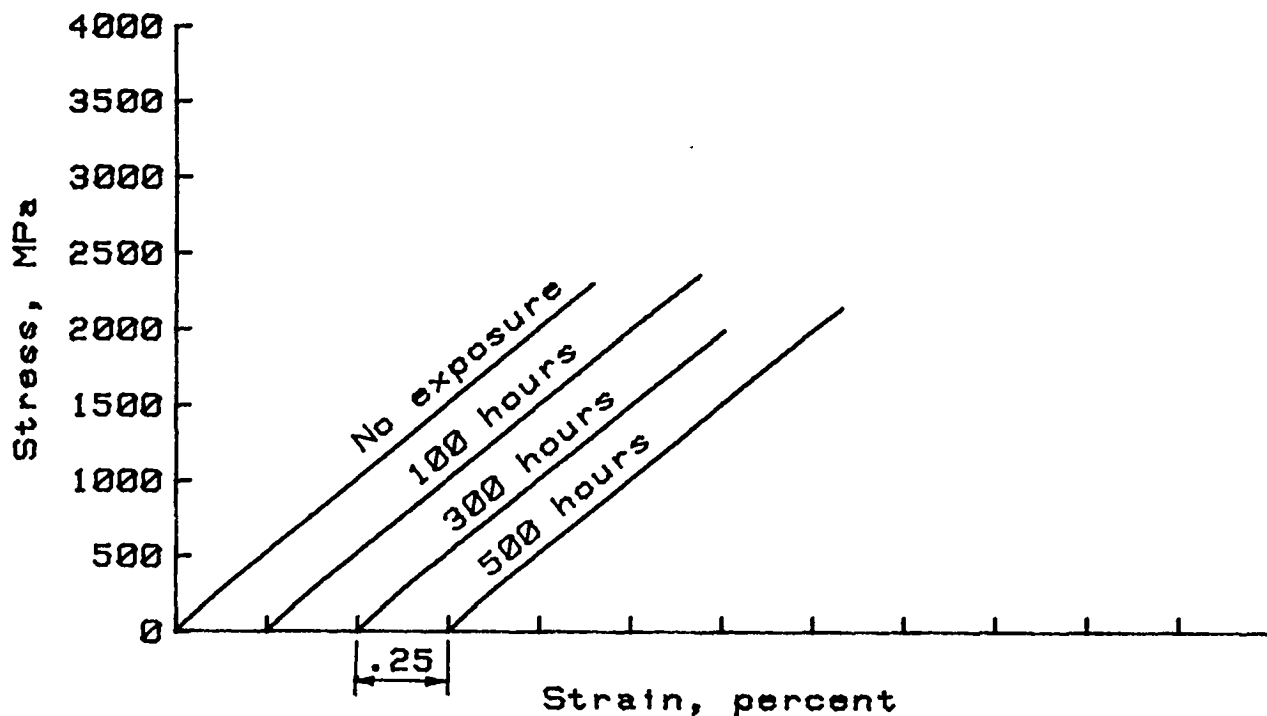
(c) Longitudinal compression
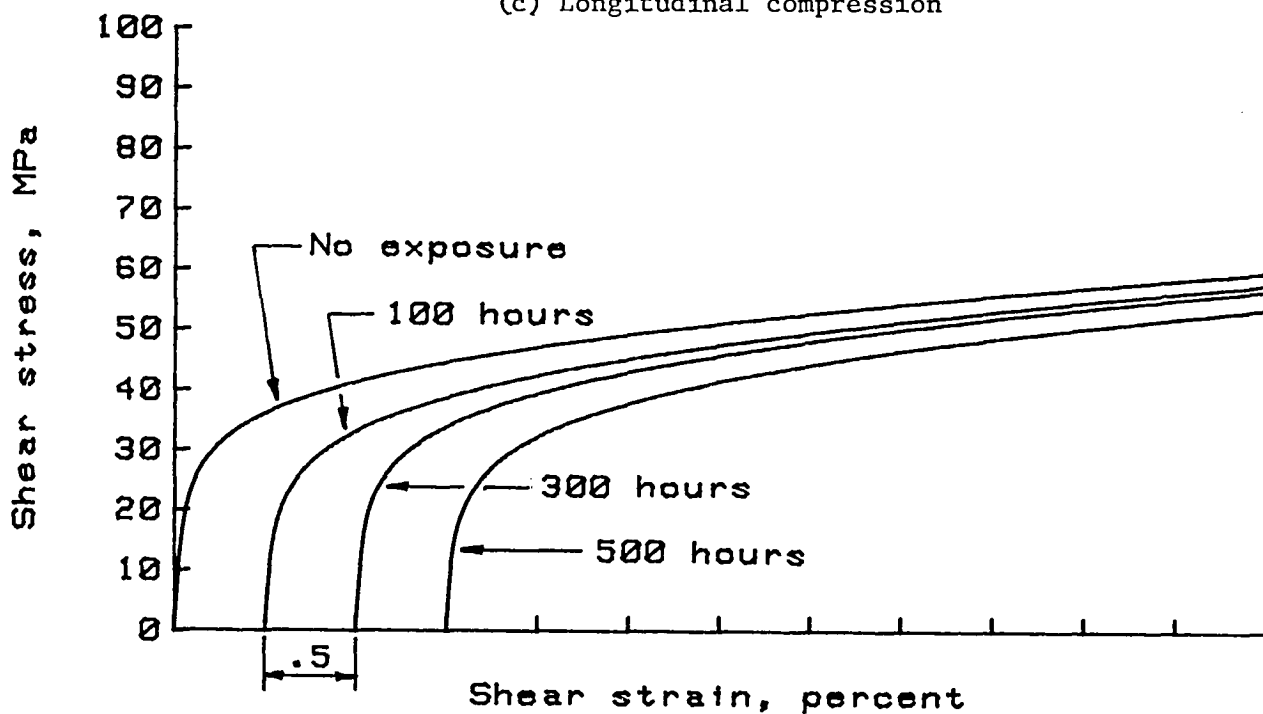
(d) In-plane shear

Figure D-1.- Concluded.
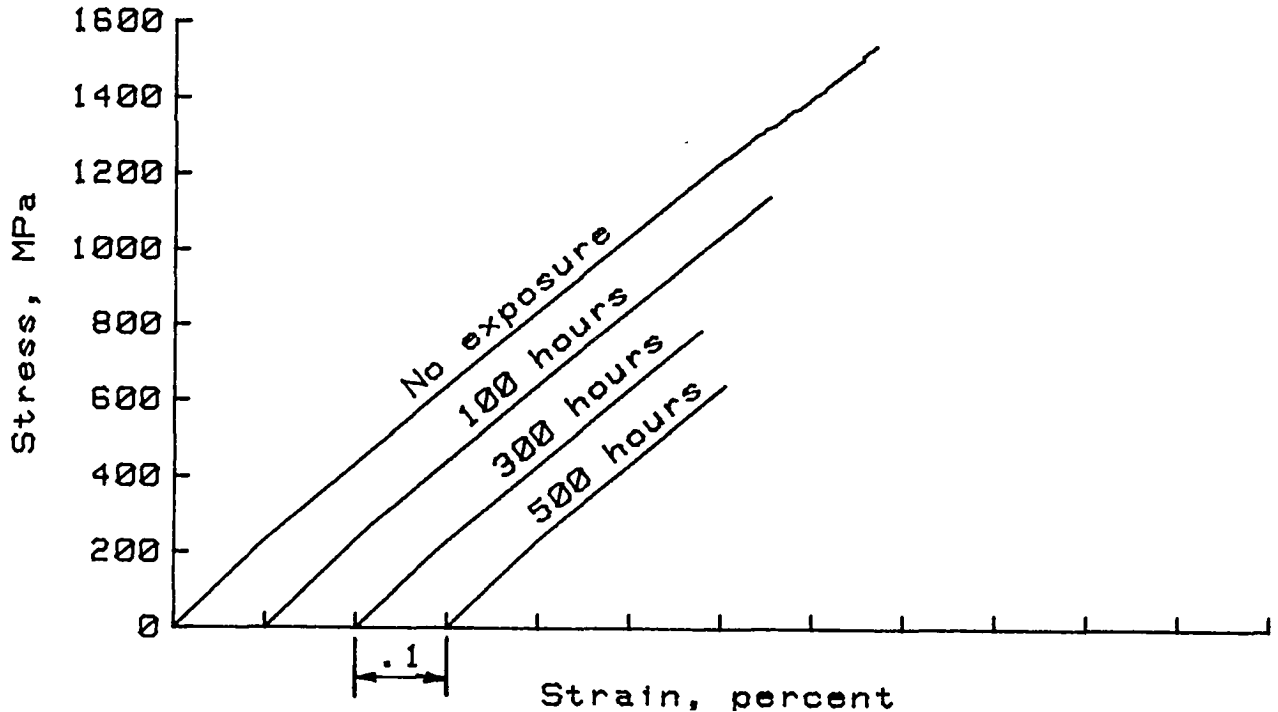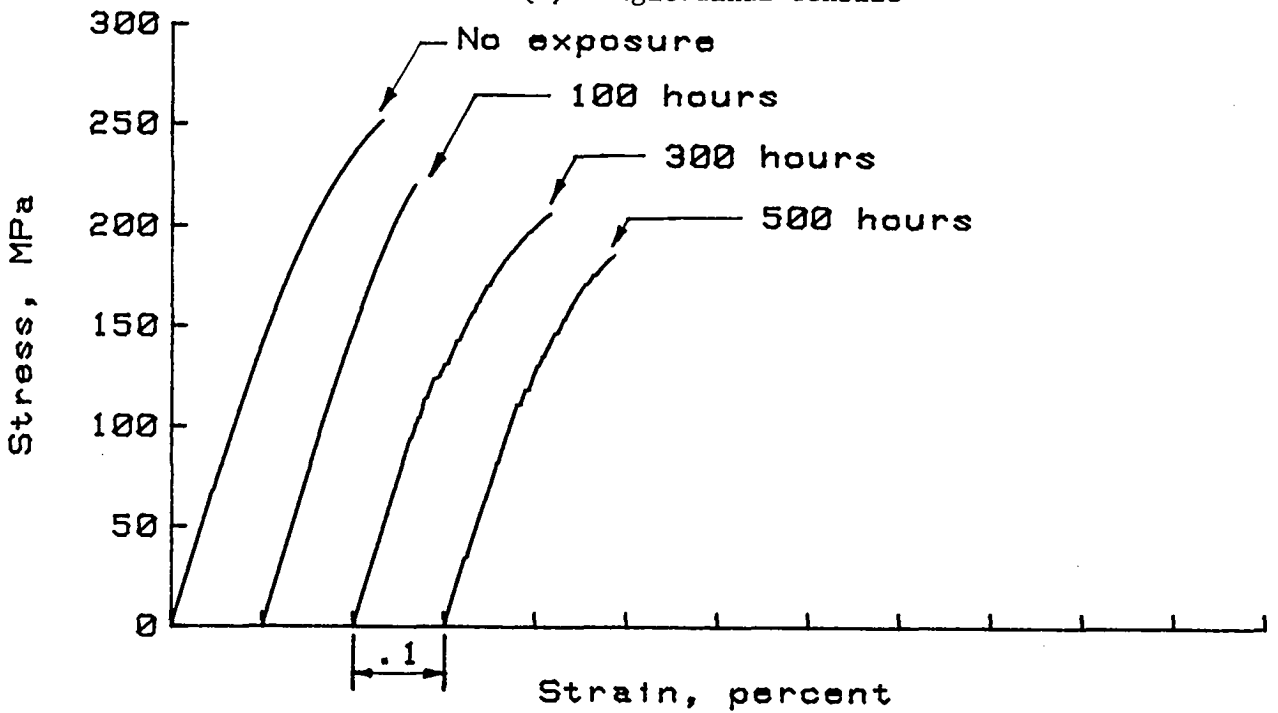
Figure D-2.- Typical room temperature stress-strain curves for B/2024 Al composite material exposed at 730 K.
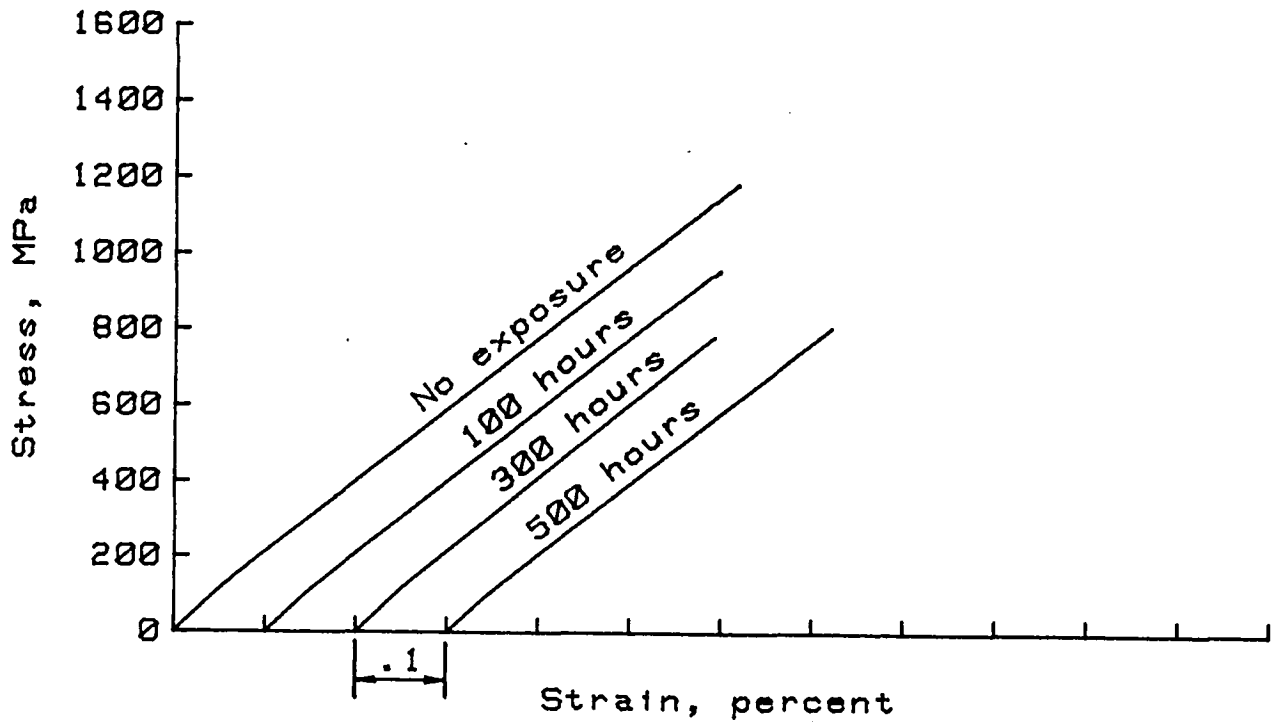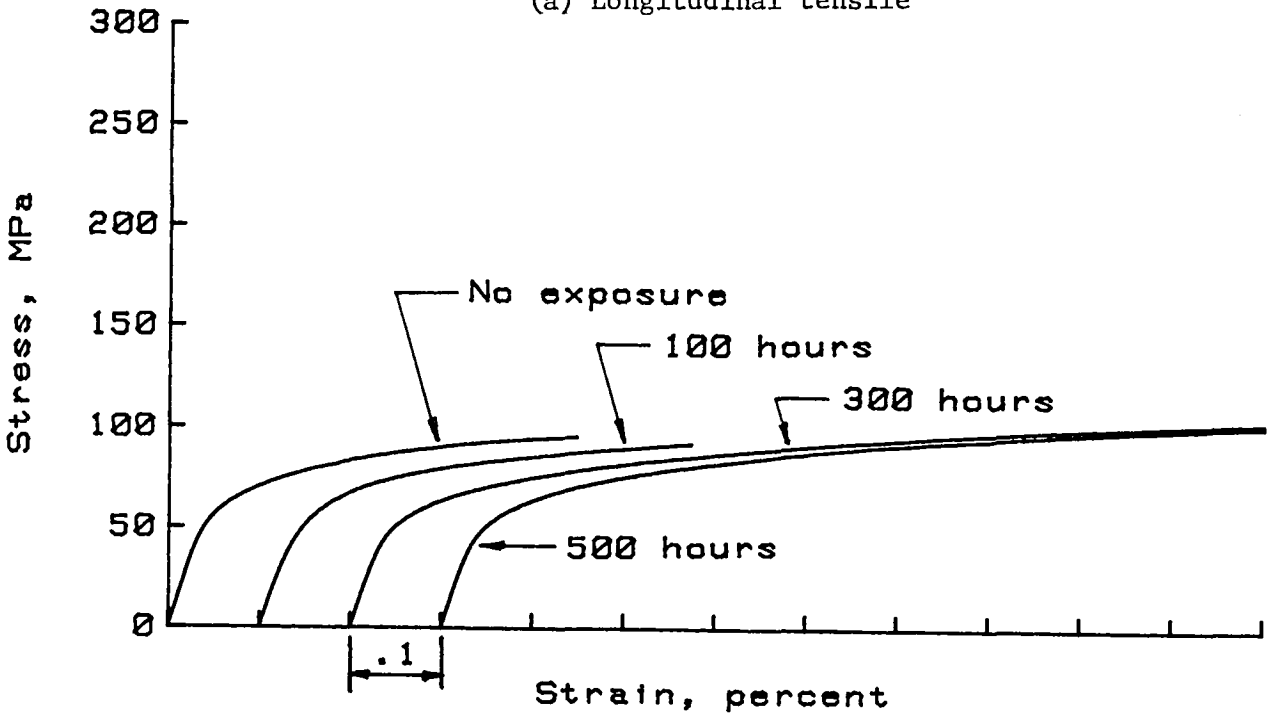
Figure D-3.- Typical room temperature stress-strain curves for B/3003 Al composite material exposed at 730 K.
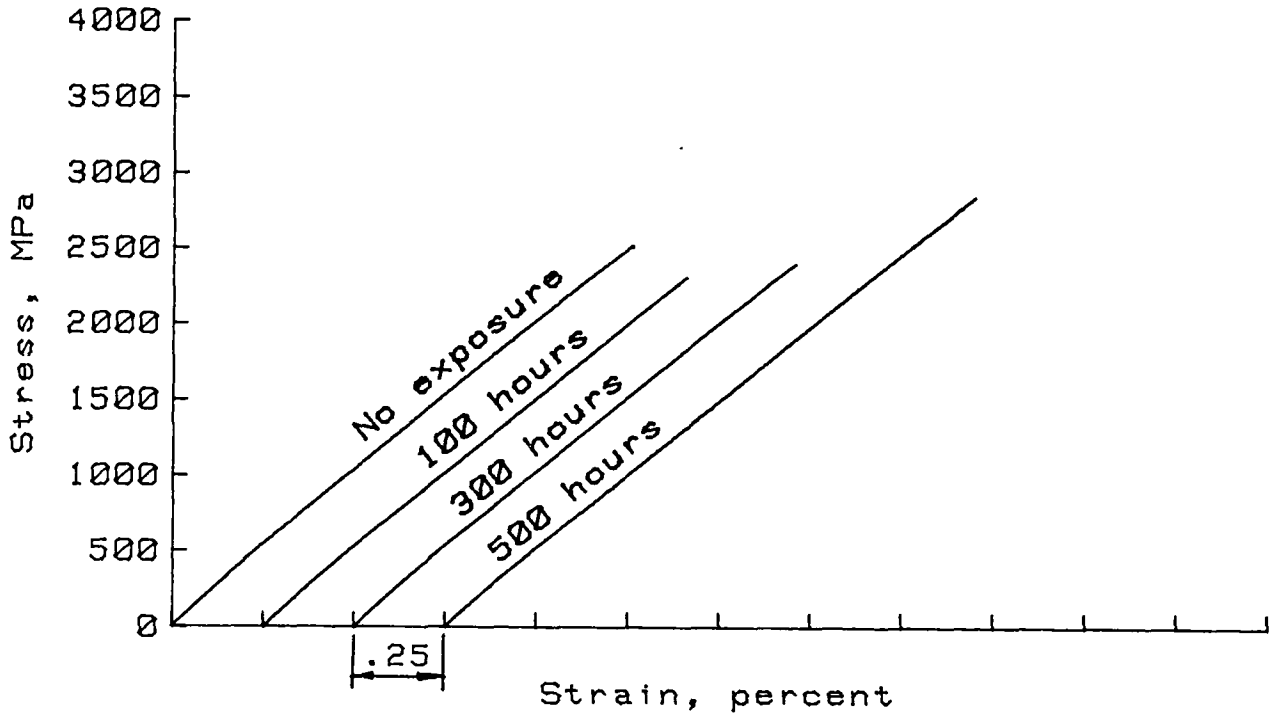
(c) Longitudinal compression
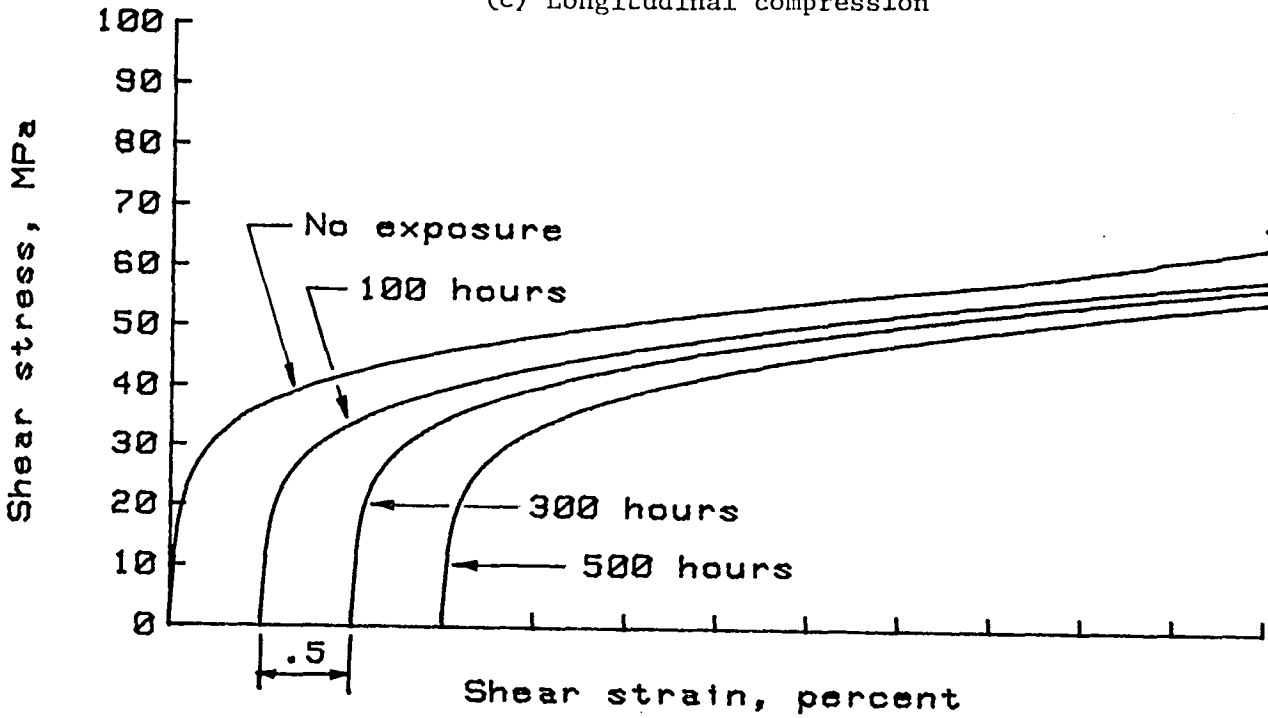
(d) In-plane shear

Figure D-3.- Concluded.

70
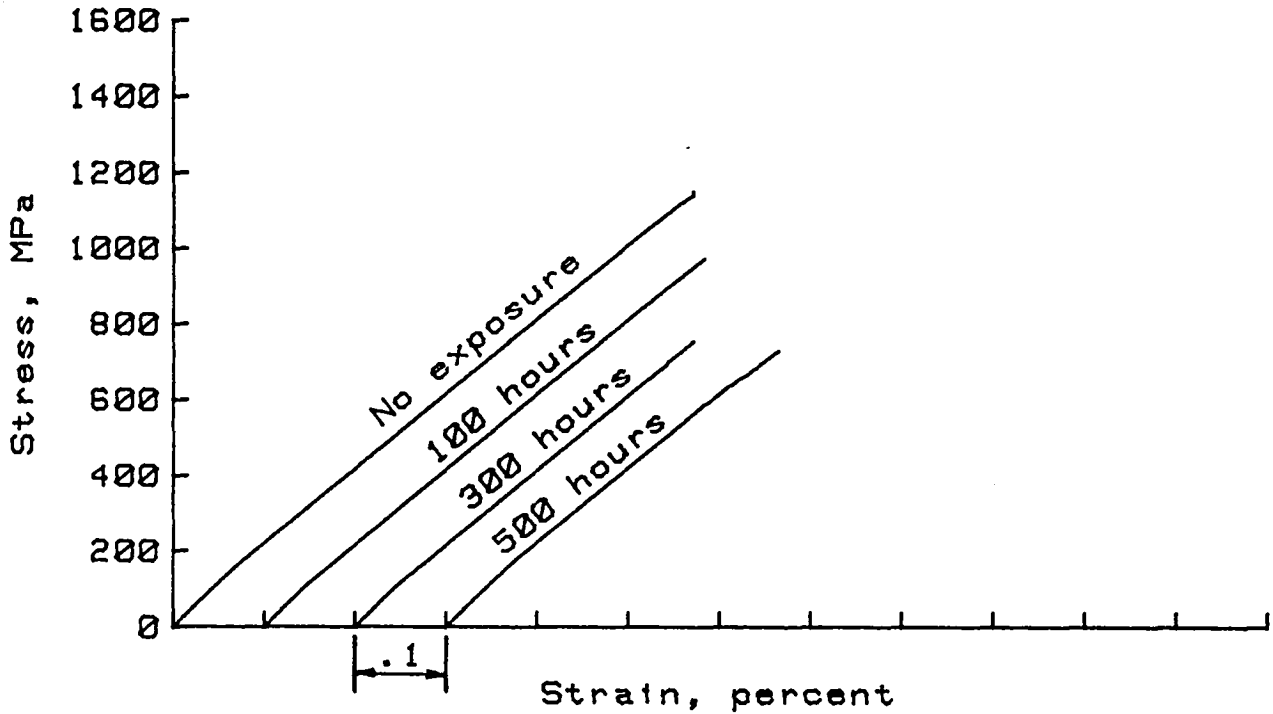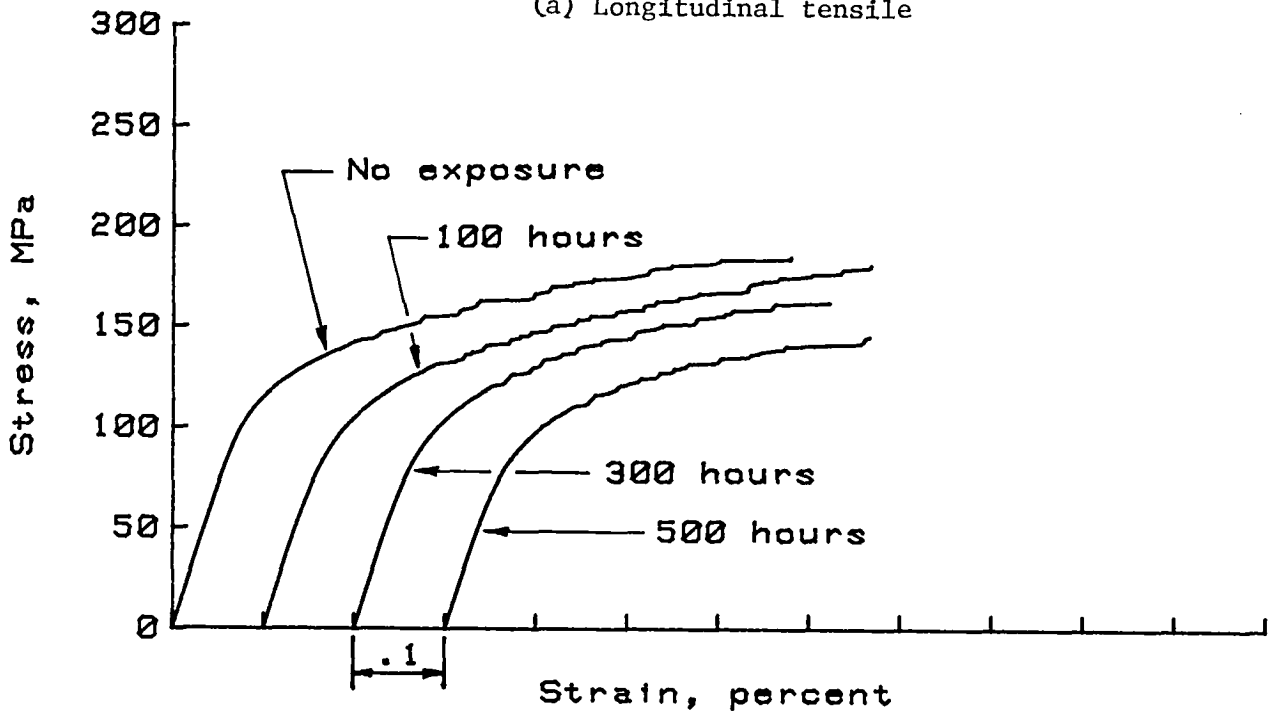
Figure D-4.- Typical room temperature stress-strain curves for B/5052 Al composite material exposed at 730 K.
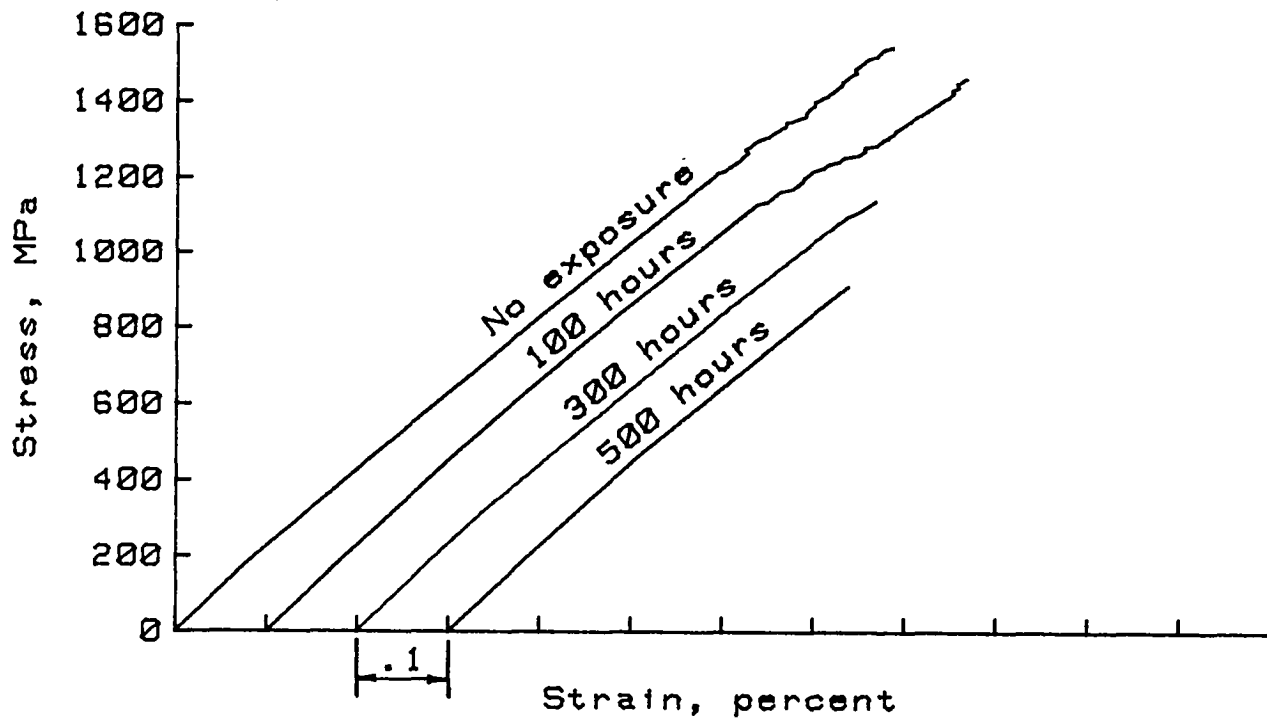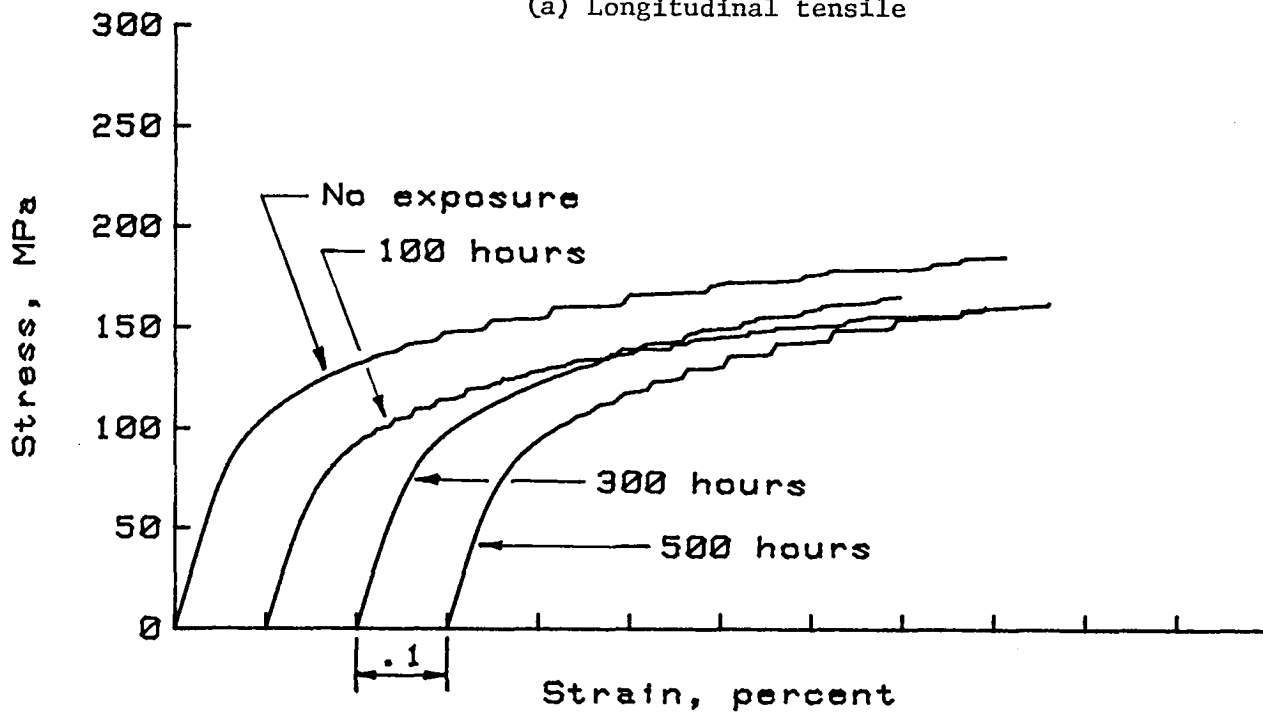
Figure D-5.- Typical room temperature stress-strain curves for B/6061 Al composite material exposed at 730 K.
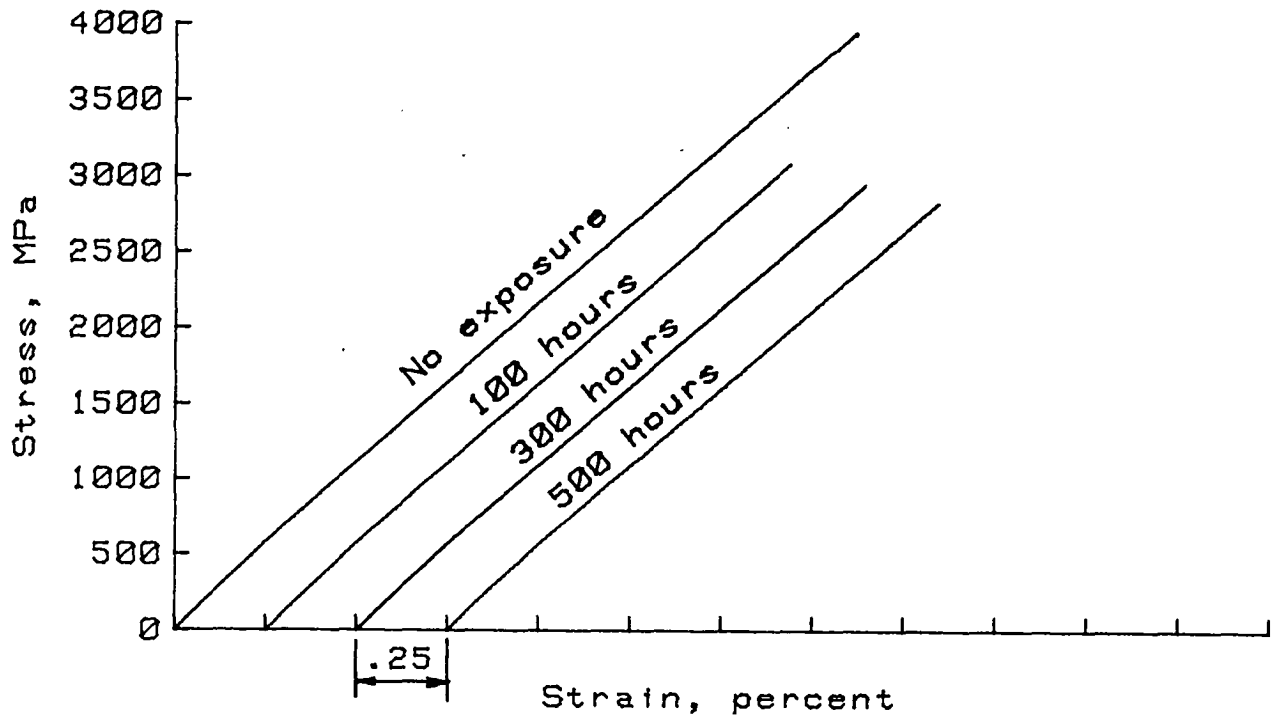
(c) Longitudinal compression
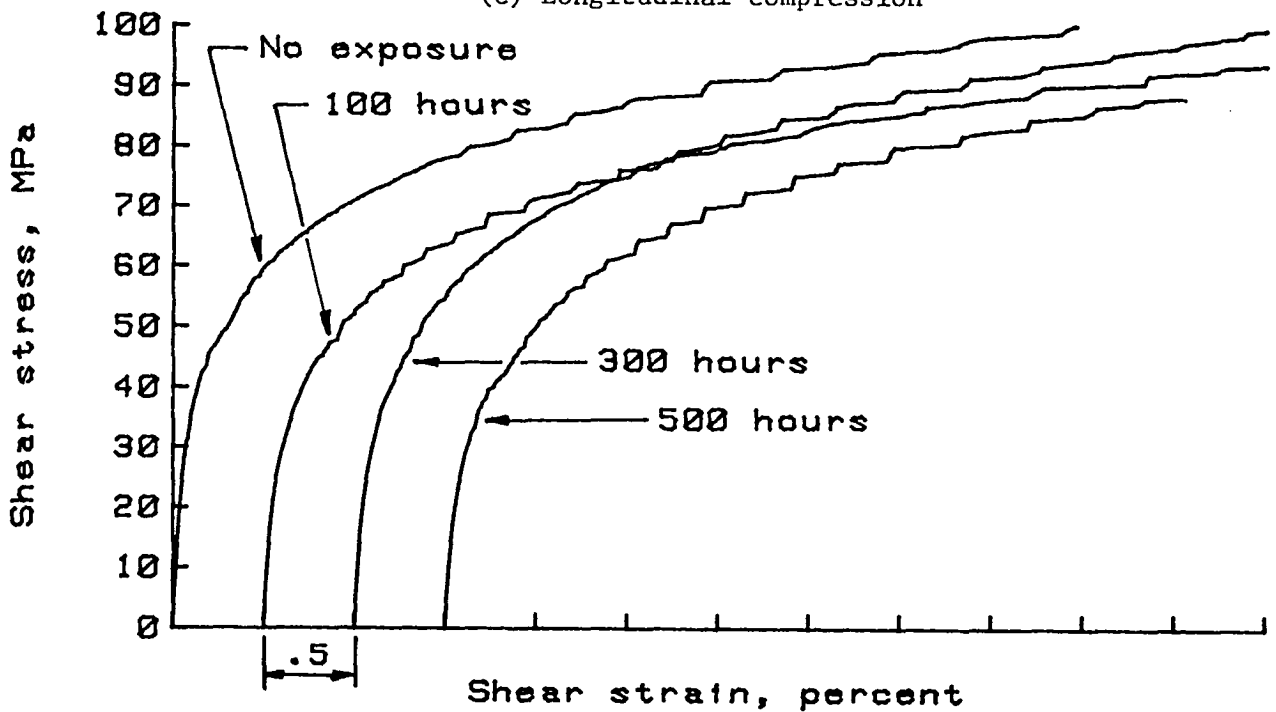
(d) In-plane shear

Figure D-5.— Concluded.

(a) Longitudinal tensile

(b) Transverse tensile

Figure E-1.– Typical room temperature stress–strain curves for B/1100 Al composite material thermally cycled between 200 K and 590 K.

(c) Longitudinal compression
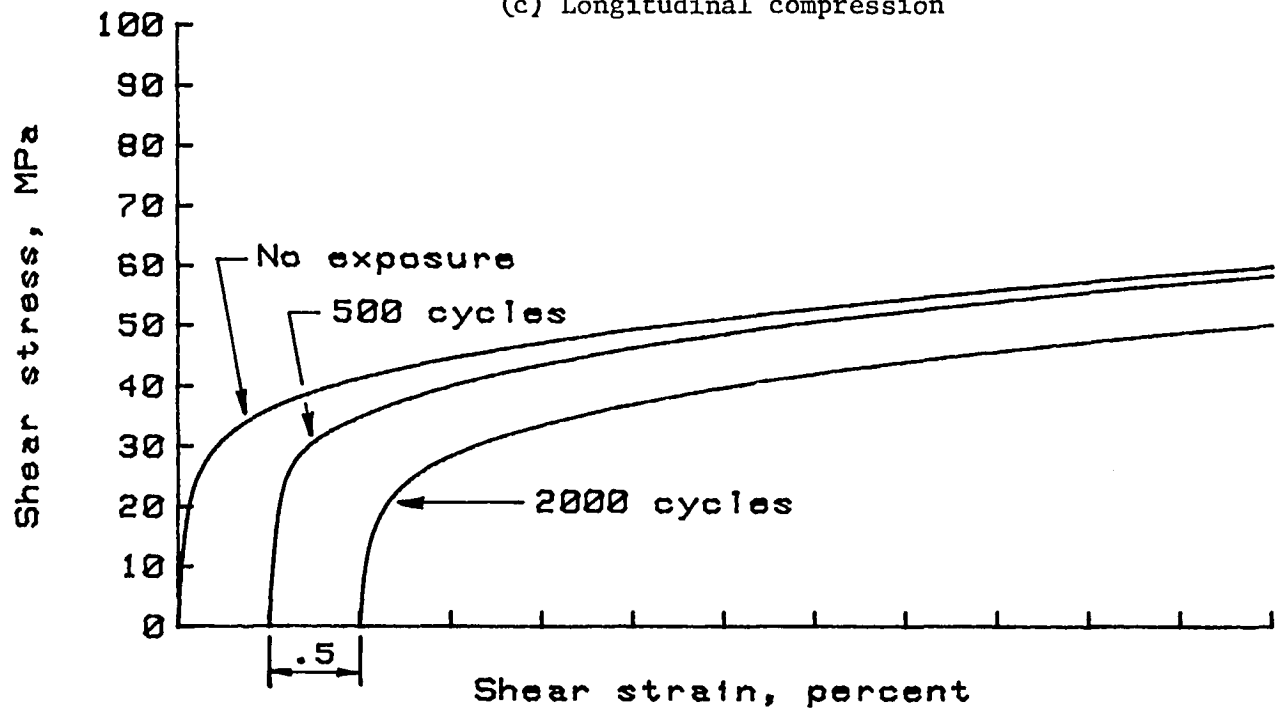
(d) In-plane shear

Figure E-1.- Concluded.

Figure E-2.- Typical room temperature stress-strain curves for B/2024 Al composite material thermally cycled between 200 K and 590 K.

76

(a) Longitudinal tensile

(b) Transverse tensile

Figure E-3.- Typical room temperature stress-strain curves for B/3003 Al composite material thermally cycled between 200 K and 590 K.

(c) Longitudinal compression

(d) In-plane shear

Figure E-3.– Concluded.

(a) Longitudinal tensile

(b) Transverse tensile

Figure E-4.— Typical room temperature stress-strain curves for B/5052 Al composite material thermally cycled between 200 K and 590 K.

(a) Longitudinal tensile
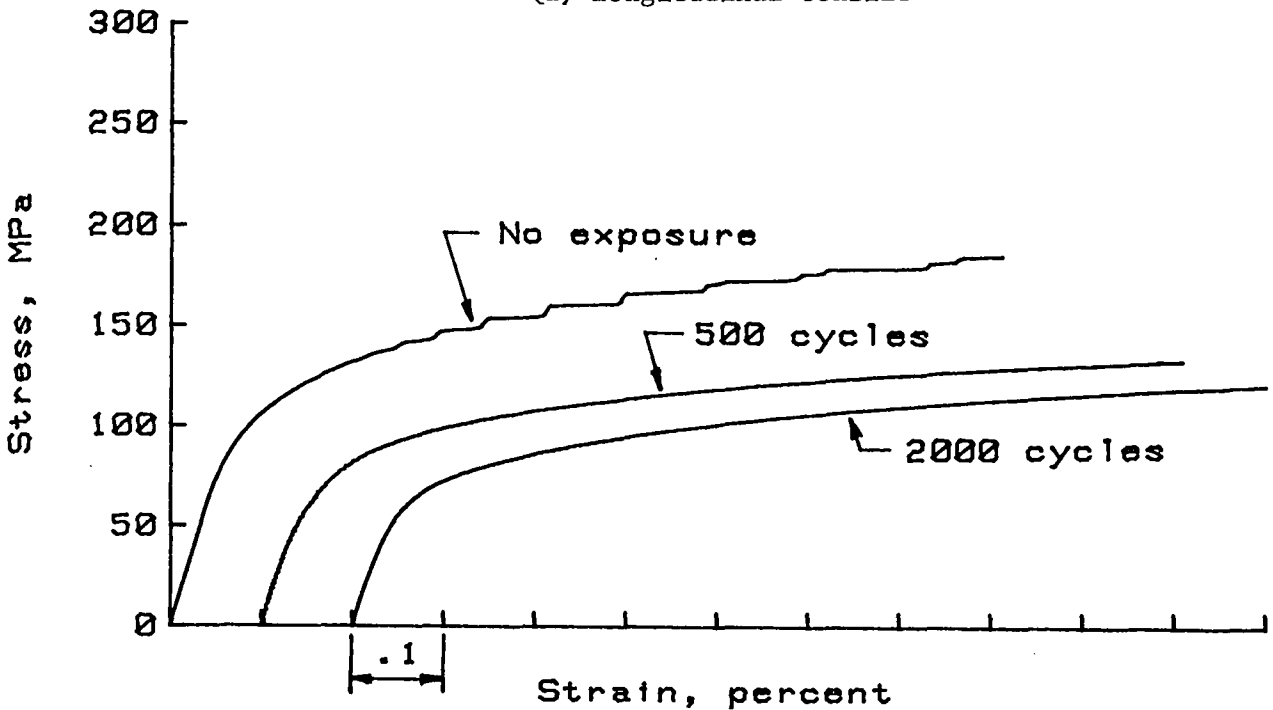
(b) Transverse tensile

Figure E-5.— Typical room temperature stress-strain curves for B/6061 Al composite material thermally cycled between 200 K and 590 K.

(c) Longitudinal compression
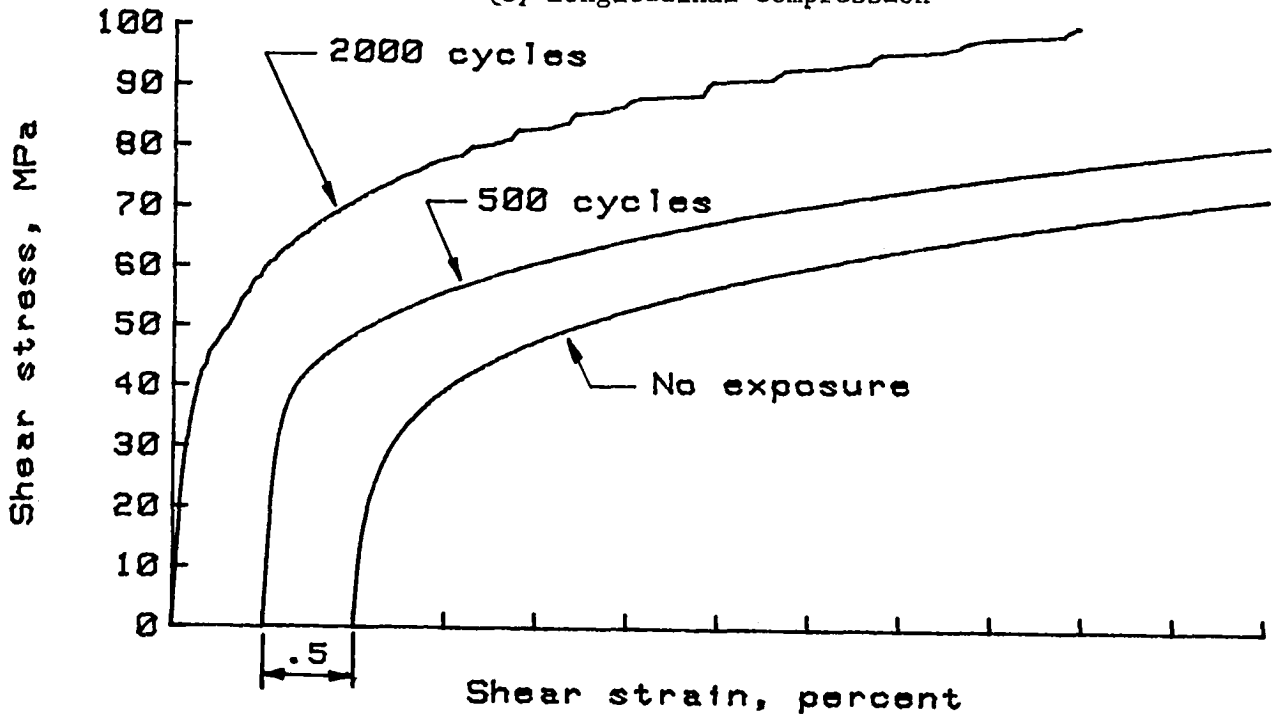
(d) In-plane shear

Figure E-5.– Concluded.

REFERENCES

1. Krukonis, V.: Chemical Vapor Deposition of Boron Filament. Boron and Refractory Borides, V. I. Matkovich ed., Springer-Verlag, 1977, pp. 517-540.

2. Kreider, Kenneth G. and Prewo, K. M.: Boron Reinforced Aluminum. Metallic Matrix Composites, Kenneth G. Kreider, ed., Academic Press, Inc., 1974, pp. 399-471.

3. Toth, I. J.; Brentnall, W. D.; and Menke, G. D.: A Survey of Aluminum Matrix Composites. Composites: State of the Art, J. W. Weeton and E. Scala eds. The Metallurgical Society of AIME, 1974, pp. 139-207.

4. Lynch, C. T. and Kershaw, J. P.: Metal Matrix Composites. CRC Press, 1972.

5. Kerr, J. R. and Haskins, J. F.: Time-Temperature-Stress Capabilities of Composite Materials for Advanced Supersonic Technology Applica- - Phase I (GDC-MAP-80-001, Convair Division of General Dynamics; NASA Contract NAS-1-12308), 1980.

6. Metcalfe, Arthur G. and Klein, Mark J.: Effect of the Interface on Longitudinal Tensile Properties. Interfaces in Metal Matrix Composites, Arthur G. Metcalfe ed., Academic Press, Inc., 1974, pp. 125-168.

7. Olsen, George C. and Tompkins, Stephen S.: Effects of Continuous and Cyclic Thermal Exposure on Boron- and Borsic-Reinforced 6061 Aluminum Composites. NASA TP 1063, Nov. 1977.

8. Olsen, George C. and Tompkins, Stephen S.: Continuous and Cyclic Thermal Exposure Induced Degradation in Boron Reinforced 6061 Aluminum Composites. Failure Modes in Composites IV, J. A. Cornie, and F. W. Crossman, eds., The Metallurgical Society of AIME, 1979, pp. 1-21.

9. Shahinian, P.: Thermal Fatigue of Aluminum-Boron Composites. SAMPE Q., vol. 2, no. 1, Oct. 1970, pp. 28-35.

10. Wright, M. A.: The Effect of Thermal Cycling on the Mechanical Properties of Various Aluminum Alloys Reinforced With Unidirectional Boron Fibers. Metal. Trans., vol. 6A, no. 1, Jan. 1975, pp. 129-134.

11. Van Horn, Kent R.: Aluminum, vol. I Properties, Metallurgy and Phase Diagrams. American Society for Metals, 1968.

12. Clark, Ronald K.; and Lisagor, W. Barry: Effects of Method of Loading and Specimen Configuration on Composite Strength of Graphite/Epoxy Composite Materials. NASA TM-81796, 1980.

13. Popov, E. P.: Mechanics of Materials. Prentice-Hall Inc., 1964.

14. Mondolfo, L. F.: Aluminum Alloys: Structure and Properties. Butterworth and Co., Ltd., 1976.

15. Metterties, Earl L.: The Chemistry of Boron and Its Compounds. John Wiley and Sons, Inc., 1967.

16. Thompson, Raymond: The Chemistry of Metal Borides and Related Compounds. Progress in Boron Chemistry, vol. 2, R. J. Brotherton and H. Steinberg, eds., Pergamon Press, 1970, pp. 173-230.

17. Dardi, Louis E.; and Kreider, Kenneth G.: Thermal Cycling in Boron-Alumin-ium Composites. New Horizons in Materials and Processing, 18th National SAMPE Symposium and Exhibition, Los Angeles, CA, April 3-5, 1973.

18. Moorjani, K.; and Feldman, C.: Amorphous Boron Films. Boron and Refractory Borides, V.I. Matkovich ed., Springer-Verlag, 1977, pp. 581-596.

19. Greenwood, N. N.; Parish, R. V.; and Thornton, P.: Metal Borides: Quarterly Reviews, 20, 1966, pp. 441-464.

20. Hoover, William R.: The Critical Energy Release Rate as a Failure Criterion for B/Al Composites. Failure Modes in Composites III, T. T. Chiao and D. M. Schuster, eds., 105th AIME Annual Meeting, Las Vegas, NV, Feb. 22-26, 1976.

21. Makarenko, G. N.: Borides in the IV b Group. Boron and Refractory Borides, V. I. Matkovich ed., Springer-Verlag, 1977, pp. 310-330.

22. Gurin, V. N.; Korsukova, M. M.: I b and II b Subgroup Borides. Boron and Refractory Borides, V. I. Matkovich, ed., Springer-Verlag, 1977, pp. 293-309.

23. Perry, A. I.; Nicoll, A. R.; Phillips, K. ; and Sahm, P. R.: The Copper-Boron Eutectic-Unidirectionally Solidified. J. Mater. Sc. 8, 1973, pp. 1340-1348.

24. Carlsson, J. O.; Lundstrom, T.: The Solution Hardening of β-Rhombohedral Boron. J. Less-Common Metals, 22, 1970, pp. 317-320.

25. Chaban, N. F.; et al; Met. A. 7, 110300.

TABLE I.– ALUMINUM ALLOY COMPOSITIONS AND ROOM TEMPERATURE STRENGTHS

Alloy – Temper (Classification)	Nominal Composition, Volume Percent	Ultimate Tensile Strength MPa	
		Original Temper	Annealed
1100 – H19 (Non-heat-treatable)	99.0% Al (min.) 1.0% impurities* (max.)	207	76
2024 – T81 (Heat-treatable)	91.9% Al (min.) 4.5% Cu 0.6% Mn 1.5% Mg 1.5% impurities* (max.)	448	186
3003 – H19 (Non-heat-treatable)	97.0% Al (min.) 1.2% Mn 1.8% impurities* (max.)	248	110
5052 – H19 (Non-heat-treatable)	96.4% Al (min.) 0.1% Cu 0.1% Mn 2.5% Mg 1.0% impurities* (max.)	331	193
6061 – T81 (Heat-treatable)	96.4% Al (min.) 0.6% Si 0.3% Cu 1.0% Mg 0.2% Cr 1.5% impurities* (max.)	379	124

* Impurities normally are Fe and Si with traces of Ti, Cr, Mn, Cu, and Zn

TABLE II.- COMPOSITE DIFFUSION BONDING PARAMETERS

Composite System	Temperature, K	Pressure MPa	Time, min.
B/1100	820 to 840	31	40
B/2024	770 to 780	31	30
B/3003	820 to 840	31	40
B/5052	800 to 810	31	30
B/6061	800 to 805	31	30

TABLE III.- SPECIMEN CONFIGURATION

Test Type	Material Tested	Fiber Orientation	Nominal Specimen Dimensions, mm			
			Length	Width	Thickness	Gage Length
Longi-tudinal Tensile	B/1100 Al B/2024 Al B/3003 Al B/5052 Al B/6061 Al	0°	300	25.0	2.0	100 (1)
	1100 Al 2024 Al 3003 Al 5052 Al 6061 Al	Not Applicable	300	25.0	1.0	100 (1)
Trans-verse Tensile	B/1100 Al B/2024 Al B/3003 Al B/5052 Al B/6061 Al	90°	130	25.0	2.0	50 (1)
Longi-tudinal Compres-sion	B/1100 Al B/3003 Al B/6061 Al	0°	150	12.5	2.0	12
In-Plane Shear	B/1100 Al B/3003 Al B/6061 Al	±45°	150	25.0	2.0	50 (1)

(1) Distance between grips.

TABLE IV.- MECHANICAL PROPERTY TESTS

Test	Fiber Orientation	Test Standard	Properties Reported	Load Rate N/sec.
Composite Longitudinal Tensile	0°	ASTM D-3552	σ_{1t} E_1	110
Composite Transverse Tensile	90°	ASTM D-3552	σ_{tt} E_2	90
Composite Longitudinal Compression	0°	ASTM D-3410 (1,2)	σ_{1c}	75
Composite In-Plane Shear	±45°	ASTM D-3518 (1)	τ_{12} G_{12}	90
Alloy Tensile	Not Applicable	ASTM D-3552 (3)	σ_t	15

(1) Resin matrix composite standard (no metal matrix standard established).
(2) IITRI modification of fixture used.
(3) Tested in the same manner as composites.

σ_{1t} - ultimate longitudinal tensile strength

σ_{tt} - ultimate transverse tensile strength

σ_{1c} - ultimate longitudinal compressive strength

σ_t - ultimate tensile strength (alloy only)

τ_{12} - ultimate in-plane shear stress

E_1 - longitudinal elastic modulus

E_2 - transverse elastic modulus

G - in-plane shear modulus

TABLE V.- B/1100 Al COMPOSITE TENSILE, COMPRESSION, AND SHEAR PROPERTIES

Specimen History	Test Temp. K	Longitudinal Tensile		Transverse Tensile		Ultimate Compression Stress, MPa	Shear	
		Ultimate Stress, MPa	Elastic Modulus, GPa	Ultimate Stress, MPa	Elastic Modulus, GPa		Ultimate Stress, MPa	Elastic Modulus, GPa
As Fabricated	295	1495 1538 1310	231 232 226	67 66 70	138 137 133	2528 2294 1867	141 134 131	51 53 50
	500	1333 1019 1284	227 231 224	51 47 50	--- 112 118	917 1169 1251	125 134 135	49 46 44
	590	1407 1356 1024	189 192 186	26 26 27	106 --- 111	474 539 426	106 111 103	32 --- 35
5000 Hours at 500 K	295	1248 1194 1190	226 222 224	79 57 47	130 124 136	---	---	---
10,000 Hours at 500 K	295	1054 1076 1261	223 222 219	82 61 58	124 137 136	---	---	---
2500 Hours at 590 K	295	1422 1162 1289	231 226 229	91 66 69	127 137 ---	2796 2180 1949	163 129 132	54 56 --
5000 Hours at 590 K	295	1488 1242 1289	232 228 226	64 68 63	133 130 135	2407 1917 2021	130 122 131	55 52 56
7500 Hours at 590 K	295	1331 1120 1374	225 226 218	64 74 63	137 131 135	1529 1638 1724	125 123 126	54 55 54
10,000 Hours at 590 K	295	1334 1251 1379	225 223 218	61 72 52	139 134 133	1274 1469 1454	115 117 125	56 52 53
100 Hours at 730 K	295	1318 1305 1296	--- 222 224	74 76 80	140 141 139	2169 1783 ----	115 113 113	54 53 54
300 Hours at 730 K	295	951 912 968	223 228 231	93 85 92	136 130 132	2029 1832 1982	100 107 96	55 53 53
500 Hours at 730 K	295	613 590 824	230 229 228	87 77 66	130 134 132	2133 1641 2347	105 104 98	54 53 54
500 Cycles 200 K to 590 K	295	1151 1254 1470	233 231 228	71 67 45	132 120 128	2203 2234 2402	137 130 133	54 55 52
2000 Cycles 200 K to 590 K	295	1125 1030 1174	214 215 216	64 62 38	48 127 114	1717 ---- 1776	110 118 127	48 49 48

90

TABLE VI.- B/2024 Al COMPOSITE TENSILE PROPERTIES

Specimen History	Test Temp. K	Longitudinal		Transverse	
		Ultimate Stress, MPa	Elastic Modulus, GPa	Ultimate Stress, MPa	Elastic Modulus, GPa
As Fabricated	295	1537 1440 1592	234 236 233	196 256 251	149 154 153
	500	1534 1439 1454	238 235 233	177 186 179	141 136 138
	590	1464 1194 1389	212 --- 202	85 86 83	119 125 111
5000 Hours at 500 K	295	---- 1331 1369	--- 233 231	156 159 159	161 152 152
10,000 Hours at 500 K	295	1369 1395 1387	218 227 218	173 166 175	151 150 143
2500 Hours at 590 K	295	1292 1272 1322	231 233 240	162 194 195	151 156 151
5000 Hours at 590 K	295	1289 1279 1350	231 236 239	182 182 194	151 149 152
7500 Hours at 590 K	295	1263 1246 1428	226 228 229	186 183 191	152 148 152
10,000 Hours at 590 K	295	1326 1307 1397	231 232 230	179 175 180	146 144 141
100 Hours at 730 K	295	1200 950* 1139	232 234 234	256 228 204	151 155 153
300 Hours at 730 K	295	849 792 748	234 234 234	214 206 186	149 153 153
500 Hours at 730 K	295	637 580 709	231 232 232	177 186 251	149 151 150
500 Cycles 200 K to 590 K	295	1519 1408 1437	230 235 233	196 201 196	137 140 145
2000 Cycles 200 K to 590 K	295	1264 1230 1324	227 234 229	134 138 166	144 142 146

* Out-lying data point dropped in regression analysis.

TABLE VII.- B/3003 Al COMPOSITE TENSILE, COMPRESSION, AND SHEAR PROPERTIES

Specimen History	Test Temp. K	Longitudinal Tensile		Transverse Tensile		Ultimate Compression Stress, MPa	Shear	
		Ultimate Stress, MPa	Elastic Modulus, GPa	Ultimate Stress, MPa	Elastic Modulus, GPa		Ultimate Stress, MPa	Elastic Modulus, GPa
As Fabricated	295	1180 1214 1172	225 223 225	90 74 95	---- 140 146	2519 2154 2899	134 132 142	56 53 55
	500	1149 1221 1149	223 221 228	43 54 55	116 ---- ---	824 928 992	136 129 128	45 52 42
	590	1217 1199 1202	189 177 183	35 37 47	---- 100 96	794 698 864	112 114 108	37 -- 38
5000 Hours at 500 K	295	1057 ---- 1087	218 --- 219	102 78 84	145 --- 147	---	---	---
10,000 Hours at 500 K	295	1154 1101 1106	208 210 220	108 70 87	138 145 141	---	---	---
2500 Hours at 590 K	295	1157 1025 1086	223 219 223	108 74 90	137 146 141	2349 2772 2287	135 147 140	56 57 56
5000 Hours at 590 K	295	1055 1042 1099	225 218 225	66 87 100	139 148 142	2658 3156* 2460	134 120 129	56 58 55
7500 Hours at 590 K	295	1137 1025 1086	220 217 215	74 95 100	145 145 145	2027 1891 1816	124 118 130	58 56 56
10,000 Hours at 590 K	295	1029 1039 1064	213 213 210	79 90 93	137 139 141	1640 1507 ----	111 124 133	58 56 57
100 Hours at 730 K	295	903 953 958	223 225 227	92 92 92	139 145 141	2196 2301 2917	119 118 113	54 55 56
300 Hours at 730 K	295	--- 780 874	--- 226 226	104 99 106	144 135 145	2319 2390 2941	107 115 108	56 54 55
500 Hours at 730 K	295	803 847 766	223 228 223	105 103 83	134 143 135	2834 2504 3107	103 103 101	56 55 55
500 Cycles 200 K to 590 K	295	1219 1201 1222	233 231 231	95 95 68	123 128 124	2344 2669 2352	130 131 123	56 55 56
2000 Cycles 200 K to 590 K	295	1214 1137 1059	225 223 227	82 99 64	124 136 123	---- 1920 1791	114 113 109	51 51 49

* Out-lying data point dropped in regression analysis.

92

TABLE VIII.- B/5052 Al COMPOSITE TENSILE PROPERTIES

Specimen History	Test Temp. K	Longitudinal		Transverse	
		Ultimate Stress, MPa	Elastic Modulus, GPa	Ultimate Stress, MPa	Elastic Modulus, GPa
As Fabricated	295	1197 1148 1130	230 230 230	189 185 169	146 145 145
	500	1178 1174 1100	228 227 230	115 132 ---	108 114 ---
	590	1316 1299 1217	199 194 200	66 66 61	--- 102 92
5000 Hours at 500 K	295	1134 1151 1168	230 228 233	140 131 150	151 148 150
10,000 Hours at 500 K	295	1119 1128 1183	233 230 229	155 155 169	147 146 144
2500 Hours at 590 K	295	1121 1094 1131	236 235 236	162 143 165	146 139 ---
5000 Hours at 590 K	295	1072 1114 1117	236 235 239	191 160 151	143 143 139
7500 Hours at 590 K	295	1043 1074 1092	231 231 229	163 160 164	145 142 138
10,000 Hours at 590 K	295	1046 1082 1138	233 234 226	158 159 133	139 137 137
100 Hours at 730 K	295	978 961 970	230 232 232	181 190 138	144 145 147
300 Hours at 730 K	295	763 735 752	231 231 230	180 162 147	141 149 146
500 Hours at 730 K	295	727 761 711	230 233 230	178 132 145	140 144 139
500 Cycles 200 K to 590 K	295	1074 1133 1146	228 231 234	165 121 111	--- 134 137
2000 Cycles 200 K to 590 K	295	1115 1137 1137	231 232 232	112 59 81	136 119 113

TABLE IX.- B/6061 Al COMPOSITE TENSILE, COMPRESSION, AND SHEAR PROPERTIES

Specimen History	Test Temp. K	Longitudinal Tensile		Transverse Tensile		Ultimate Compression Stress, MPa	Shear	
		Ultimate Stress, MPa	Elastic Modulus, GPa	Ultimate Stress, MPa	Elastic Modulus, GPa		Ultimate Stress, MPa	Elastic Modulus, GPa
As Fabricated	295	1685 1653 1557	235 233 232	--- 182 185	--- 151 153	2960 3726 3934	211 179 214	61 54 57
	500	1657 1518 1612	234 233 232	121 118 118	123 131 125	1555 1389 1191	189 202 216	49 48 48
°	590	1423 1402 1393	210 207 ----	65 63 56	121 --- 118	818 1080 762	155 155 156	--- 42 42
5000 Hours at 500 K	295	1388 1392 1418	233 233 232	137 144 144	150 148 153	---	---	---
10,000 Hours at 500 K	295	1319 1346 1382	228 234 233	126 140 136	151 153 156	---	---	---
2500 Hours at 590 K	295	1277 1440 1494	233 228 227	135 141 133	144 151 155	3356 3096 2741	154 171 147	56 57 56
5000 Hours at 590 K	295	1490 1429 1406	236 236 239	139 138 133	145 153 145	3467 2831 2440	145 193 200	59 56 57
7500 Hours at 590 K	295	1295 1396 1509	224 229 223	136 141 129	152 153 146	2346 2297 2482	159 218 218	58 58 58
10,000 Hours at 590 K	295	1417 1520 1545	224 228 221	131 139 128	147 151 151	2081 2250 2240	217 208 229	59 59 57
100 Hours at 730 K	295	1591 1474 1430	229 232 234	161 165 160	145 141 147	2679 3379 3072	205 196 173	57 56 60
300 Hours at 730 K	295	1178 1111 1138	234 231 233	165 164 168	150 144 146	3006 2950 2771	152 138 151	57 59 58
500 Hours at 730 K	295	911 907 889	230 227 229	162 160 169	144 142 145	3582 3397 3002	119 132 108	58 56 57
500 Cycles 200 K to 590 K	295	1585 1507 1671	233 234 235	132 127 138	152 136 139	3453 2890 2808	219 218 213	57 58 56
2000 Cycles 200 K to 590 K	295	1539 1567 1545	233 233 232	125 119 126	136 136 134	2291 2028 2193	196 206 153	54 52 53

94

TABLE X.- TENSILE STRENGTHS OF DIFFUSION BONDED ALUMINUM ALLOYS

Specimen History	Test Temp. K	Ultimate Tensile Stress, MPa				
		1100	2024	3003	5052	6061
As Fabricated	295	75 65 70	377 365 362	113 112 112	219 225 208	249 255 255
	500	34 33 35	202 189 190	56 57 46	121 128 125	166 176 185
	590	21 22 18	65 67 66	31 31 30	55 54 52	65 60 ---
5000 Hours at 500 K	295	73 72 70	200 195 193	109 110 110	188 189 189	146 145 146
10,000 Hours at 500 K	295	71 72 71	193 191 191	110 111 109	194 189 189	128 129 128
2500 Hours at 590 K	295	67 71 70	188 188 185	105 105 105	183 184 184	113 113 113
5000 Hours at 590 K	295	68 70 69	182 183 184	106 105 106	184 183 183	112 113 114
7500 Hours at 590 K	295	71 70 72	182 182 182	107 107 106	183 183 184	113 113 114
10,000 Hours at 590 K	295	69 71 69	175 174 175	108 106 106	182 183 186	114 115 116
100 Hours at 730 K	295	72 69 68	357 357 357	108 110 108	189 185 187	146 155 147
300 Hours at 730 K	295	73 72 68	368 377 368	108 109 106	189 186 191	161 159 162
500 Hours at 730 K	295	69 75 67	365 366 364	107 107 106	187 187 189	159 164 161
500 Cycles 200 K to 590 K	295	72 70	208 213	108 108	186 188	122 129
2000 Cycles 200 K to 590 K	295	69 72	195 196	111 110	192 192	122 122

NOTE: The mean room temperature elastic modulus of all the alloys was 7.29 GPa.

TABLE XI.- MECHANICAL PROPERTIES OF AS-FABRICATED UNIDIRECTIONAL B/Al
COMPOSITES AT ROOM TEMPERATURE

MECHANICAL PROPERTY	Composite System				
	B/1100 Al	B/2024 Al	B/3003 Al	B/5052 Al	B/6061 Al
Longitudinal Tensile Strength, σ_{1t}, MPa	1448 (-11%)	1523 (-7%)	1189 (-27%)	1158 (-29%)	1632
Longitudinal Elastic Modulus, E_1, GPa	230 (-1%)	234 (0%)	225 (-3%)	230 (-1%)	233
Transverse Tensile Strength, σ_{tt}, MPa	68 (-63%)	234 (+27%)	86 (-53%)	181 (-2%)	184
Transverse Elastic Modulus, E_2, GPa	136 (-11%)	152 (0%)	143 (-6%)	145 (-5%)	152
Longitudinal Compressive Strength, σ_{1c} MPa	2230 (-37%)	----	2524 (-29%)	----	3540
In-plane Shear Stress, τ, GPa	135 (-33%)	----	136 (-32%)	----	201
In-plane Shear Elastic Modulus, G_{12}, MPa	51 (-11%)	----	54 (-5%)	----	57

Quantity in parentheses indicates percentage difference
when compared with B/6061 Al property.

96

TABLE XII.- B/AL COMPOSITE PROPERTY DEGRADATION AFTER 10 000 HOURS
EXPOSURE AT 500 K AND 590 K

B/Al Composite System	Mechanical Property Degradation			
	Transverse Tensile Strength	Longitudinal Tensile Strength	Longitudinal Compression Strength	In-Plane Shear Strength
B/1100 Al	None	22% (Occurred at 500 K worse condition may exist)	38%	12%
B2024/Al	15% (all due to matrix annealing)	14% (includes 6% attributed to matrix annealing)	----	----
B/3003 Al	None	10%	38%	10%
B/5052 Al	10% (all due to matrix annealing)	8% (includes 1% attributed to matrix annealing)	----	----
B/6061 Al	28% (all due to matrix annealing)	17% (occurred at 500 K worse condition may exist) (includes 4% attributed to matrix annealing)	38%	22% (all due to matrix annealing)
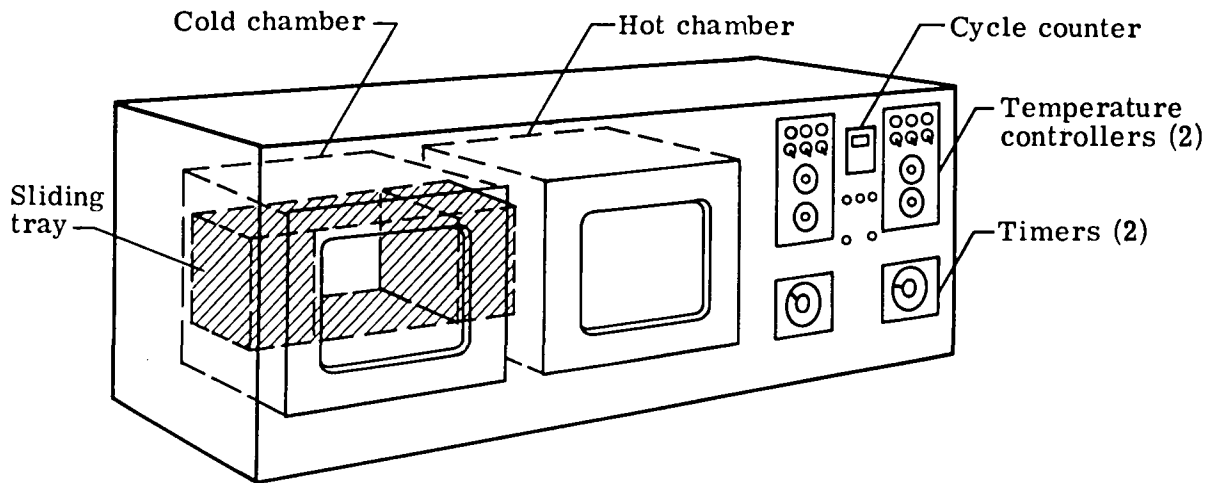
(a) Thermal cycling apparatus.
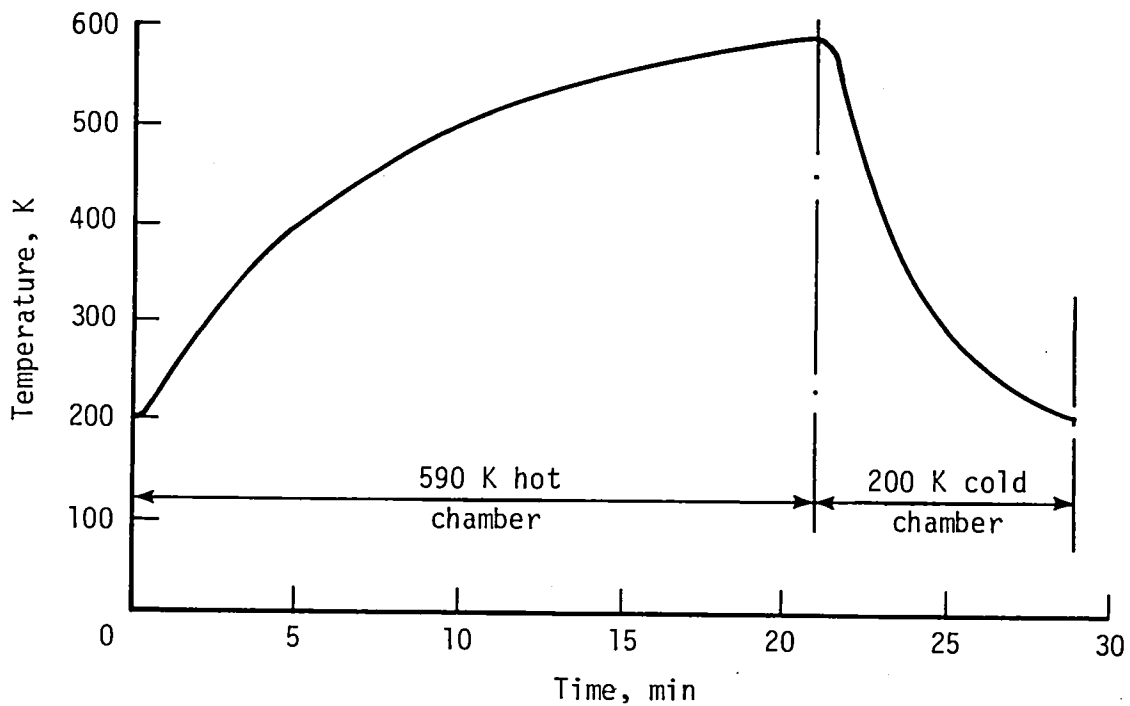
(b) Typical specimen temperature history for one cycle.

Figure 1.- Thermal cycling exposure.

Test Fixture Key

Fiber breaks on mandrel no.	Strength range of 203-μm diam. boron fiber, GPa
1	Less than 1.80
2	1.80 to 2.00
3	2.00 to 2.20
4	2.20 to 2.40
5	2.40 to 2.60
6	2.60 to 2.80
7	2.80 to 3.00
8	3.00 to 3.20
9	3.20 to 3.40
10	3.40 to 3.60
11	3.60 to 3.80
12	3.80 to 4.00
13	4.00 to 4.27
14	4.27 to 4.65
15	4.65 to 5.12
16	5.12 to 5.67
Fiber does not break	Greater than 5.67

16 Mandrels graduated in size from 45 mm. to 14.3 mm.
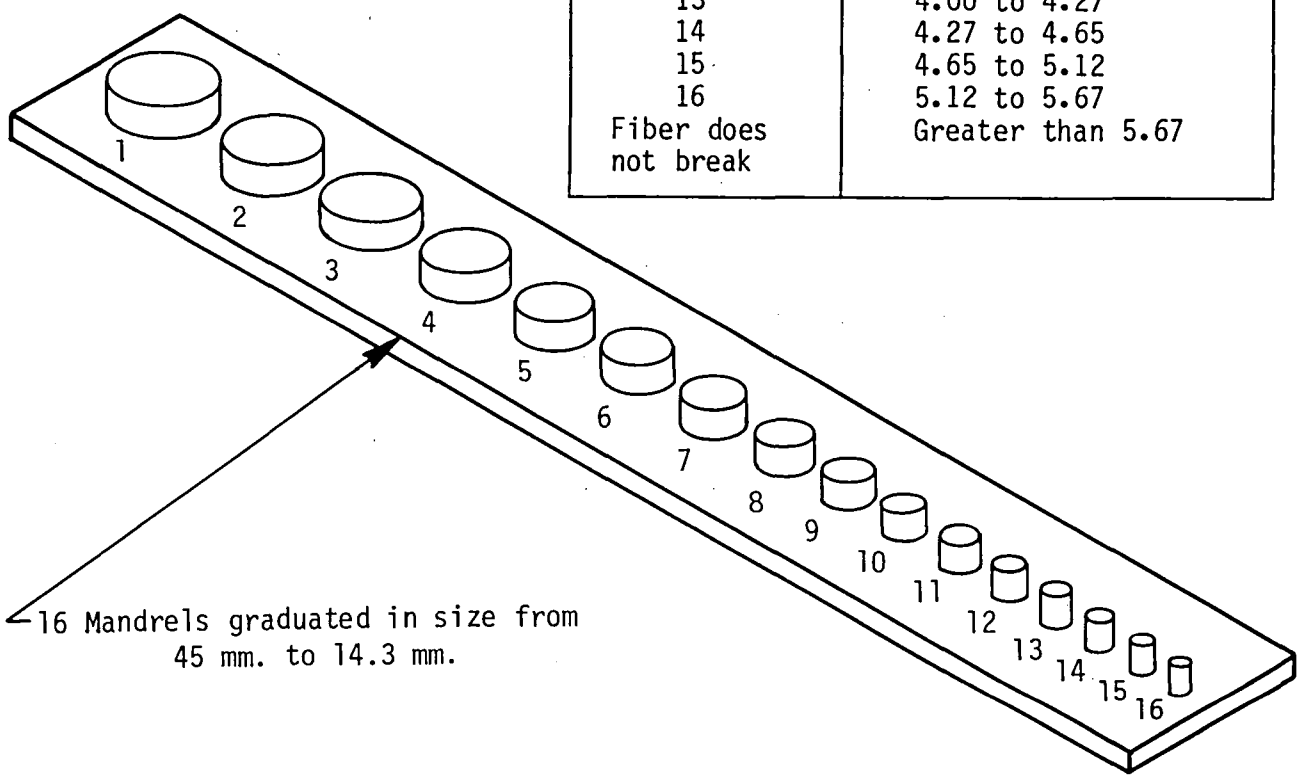
Figure 2.- Schematic of fiber bend-test fixture.
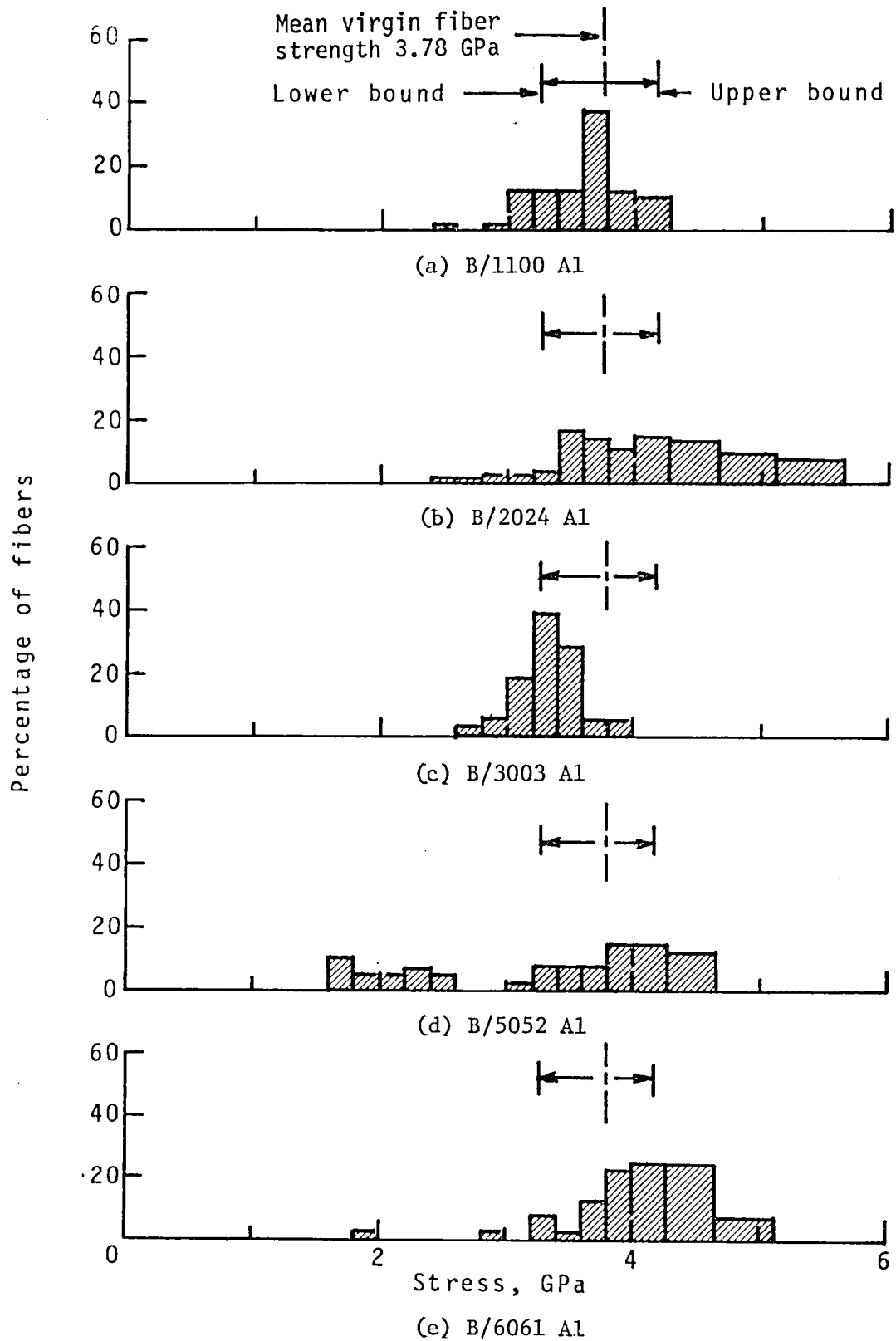
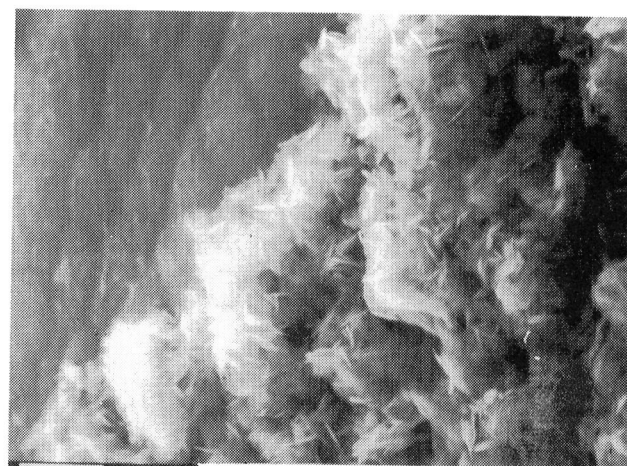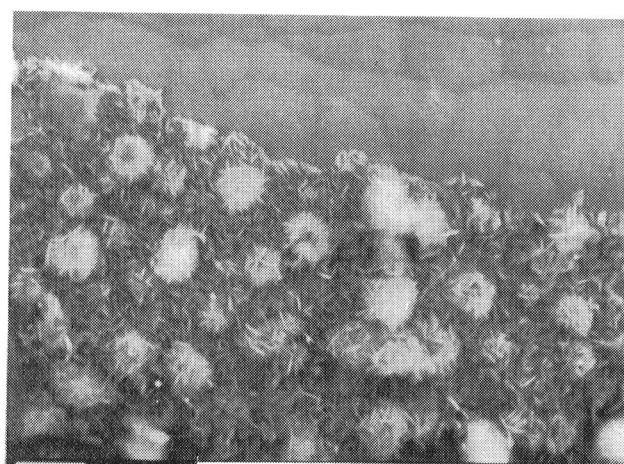Figure 3.— Fiber strength distributions for as-fabricated composites.
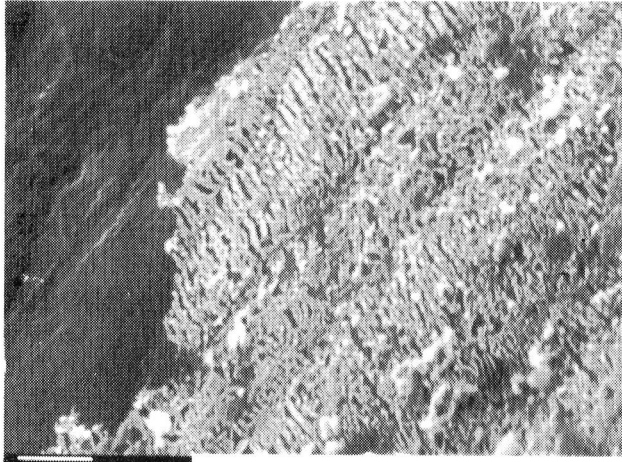
(a) B/1100 Al
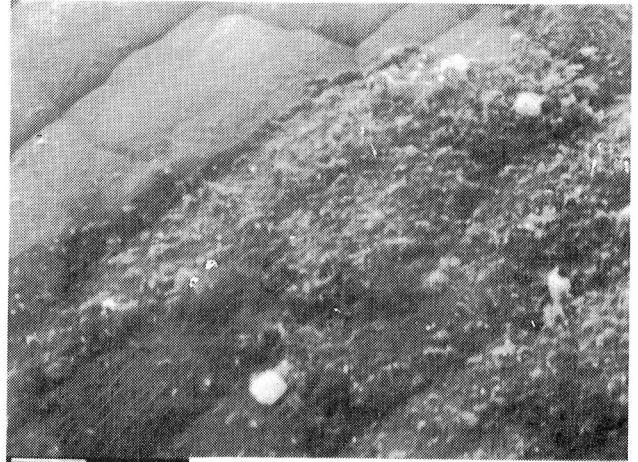
(b) B/2024 Al
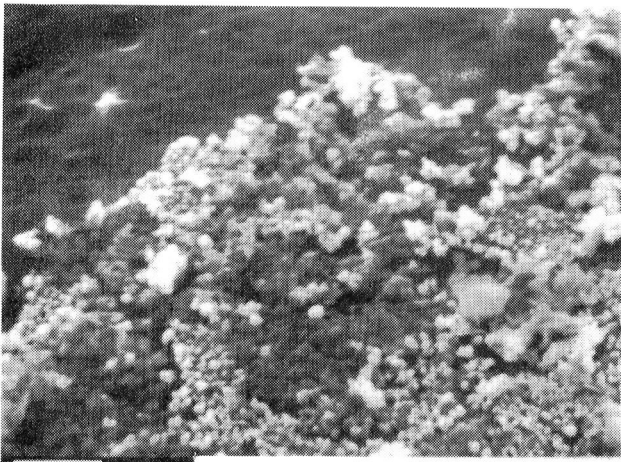
(c) B/3003 Al
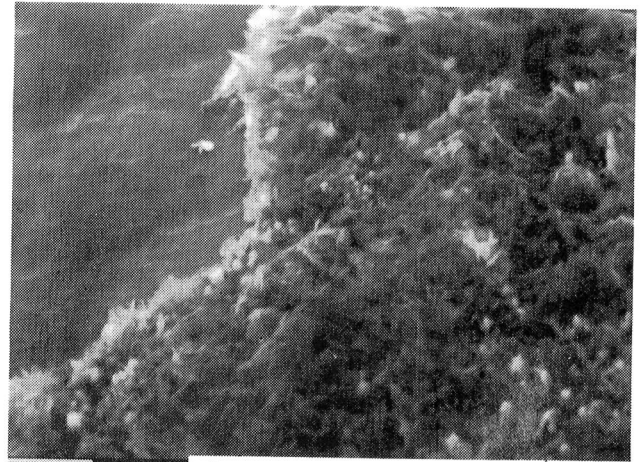
(d) B/5052 Al
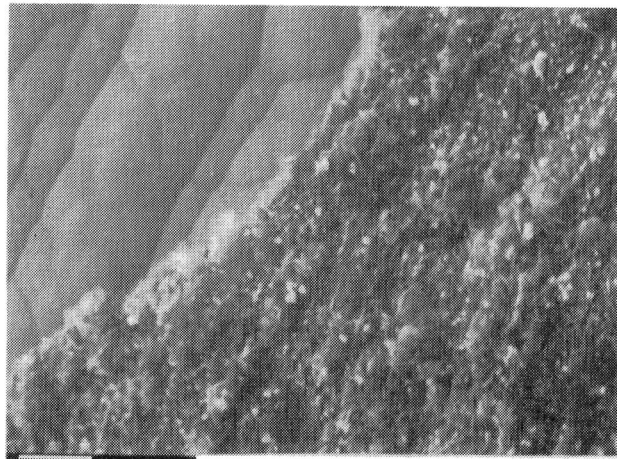
(e) B/6061 Al

Figure 4.- Reaction layers on fibers removed from as-fabricated composite specimens.
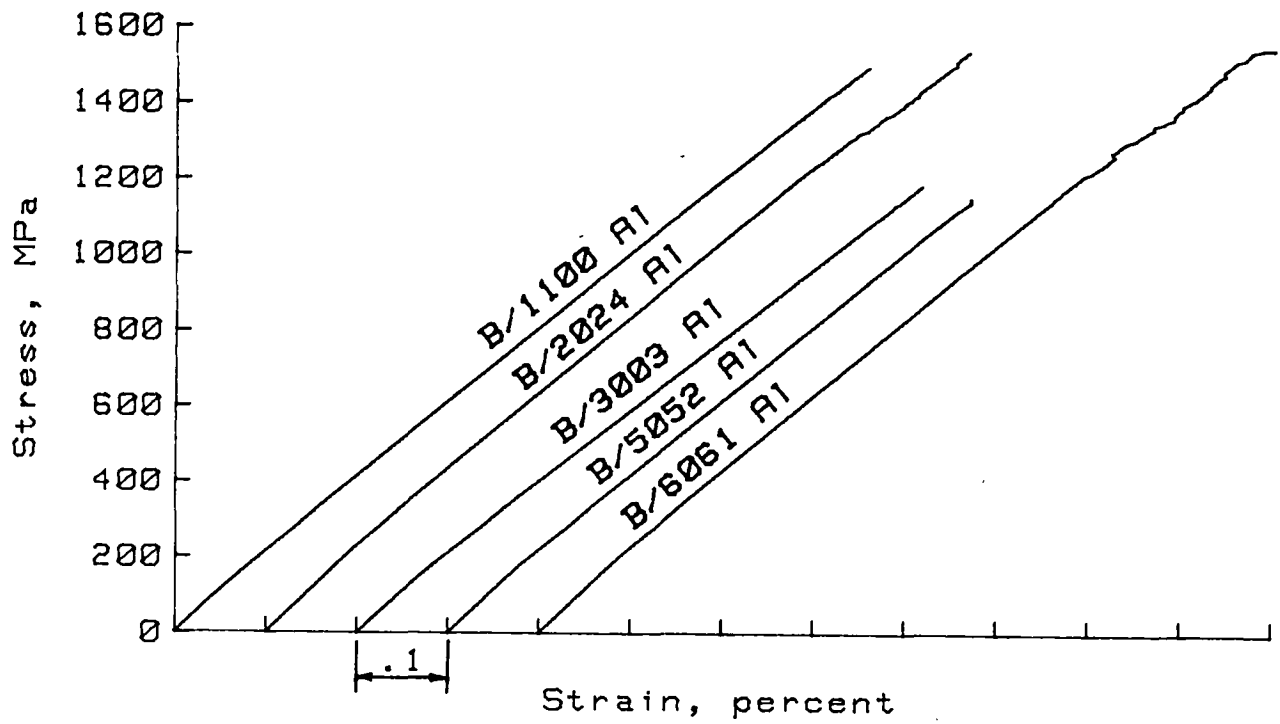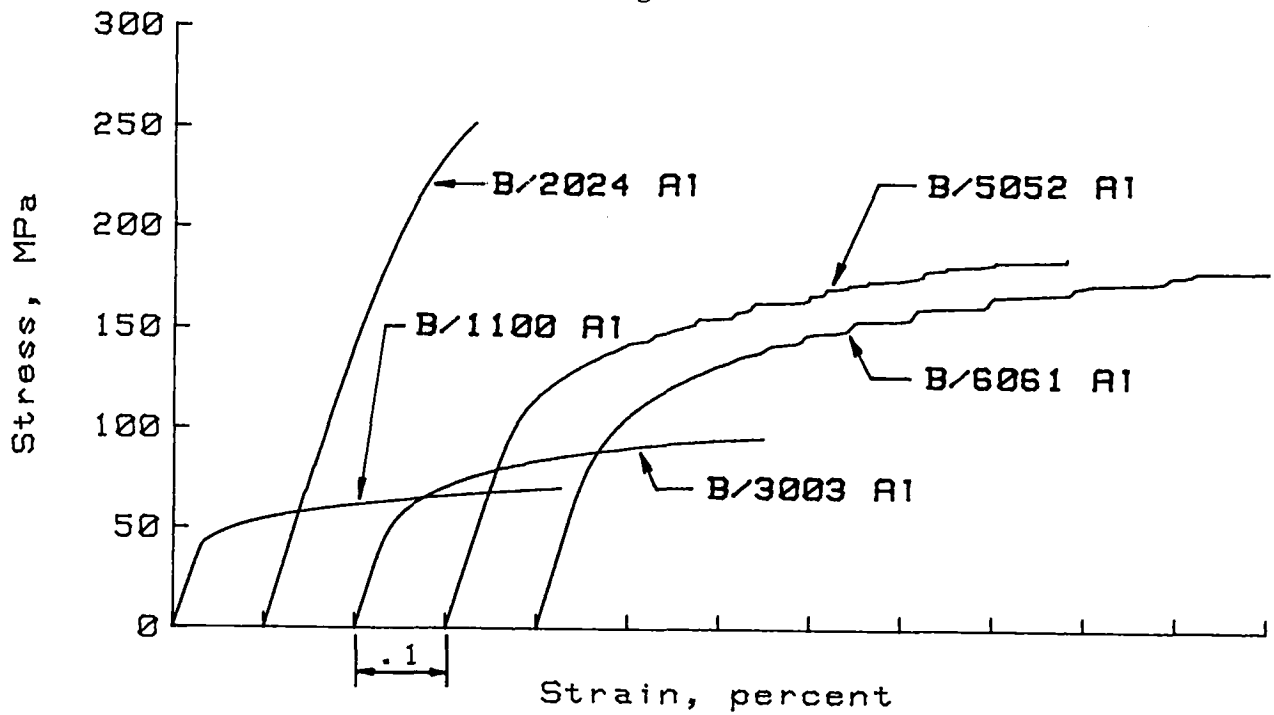
Figure 5.– Typical room temperature stress-strain curves for as-fabricated B/Al composites.
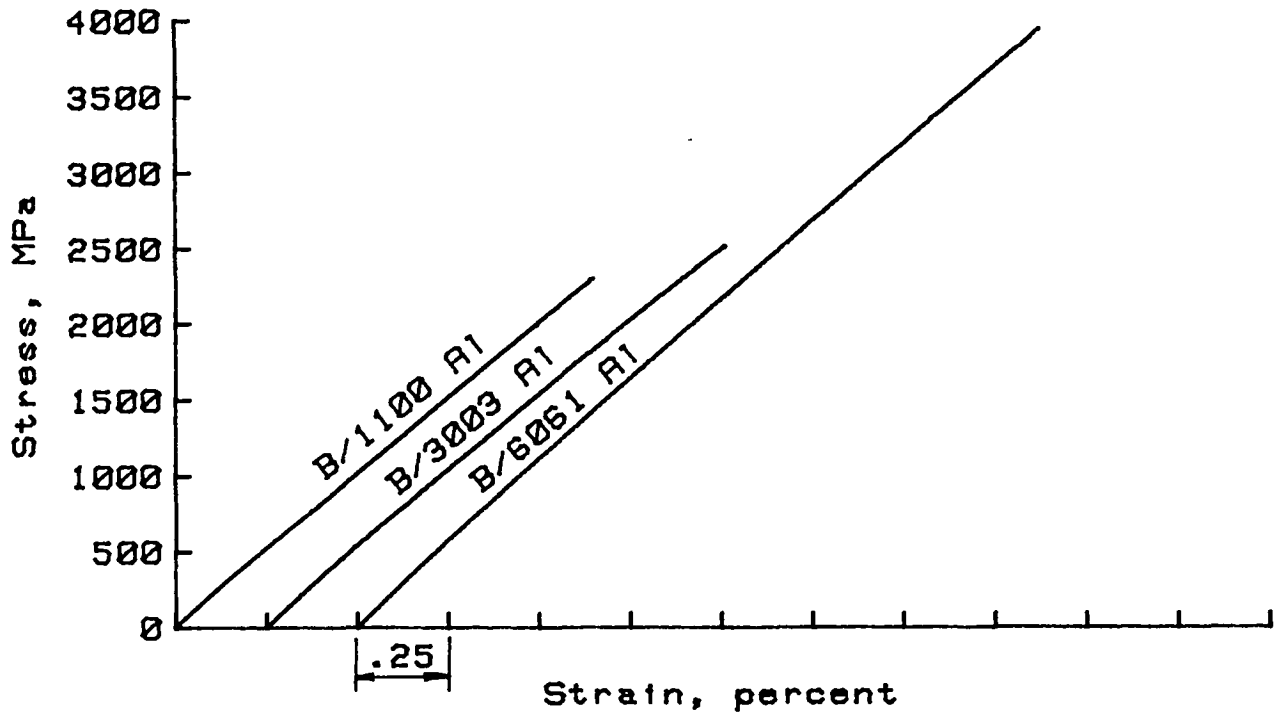
(c) Longitudinal compression
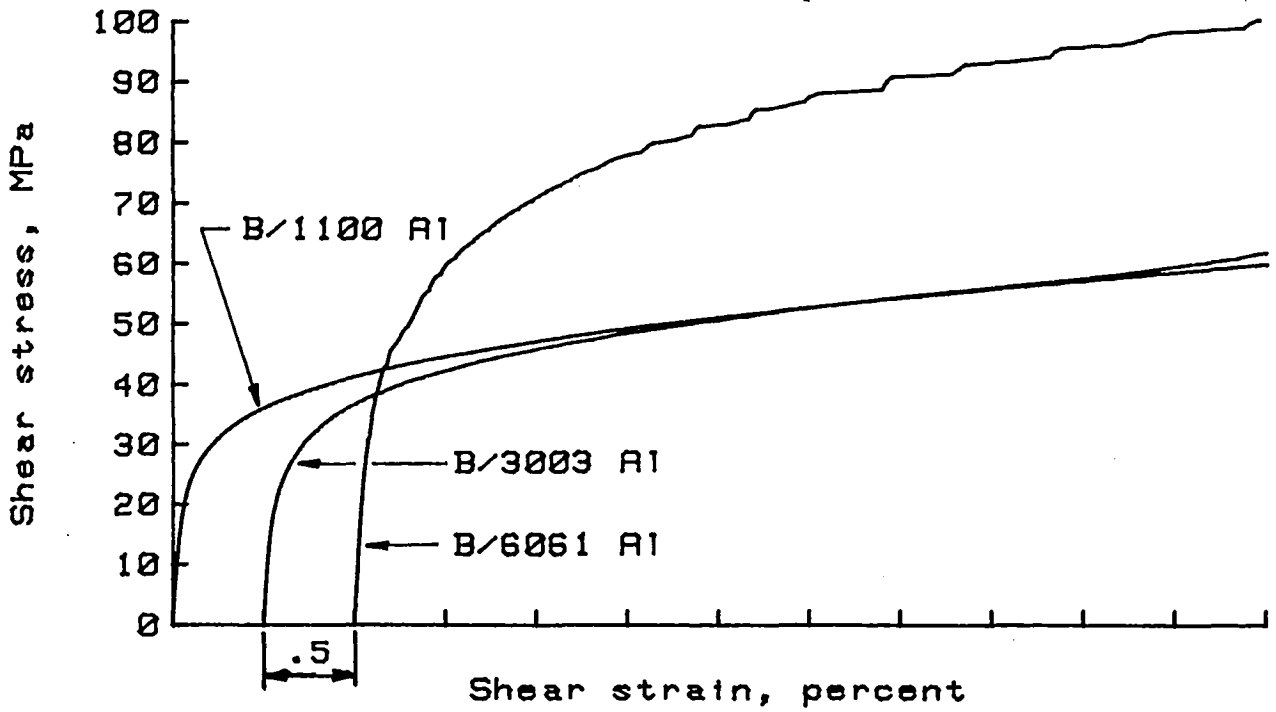
(d) In-plane shear

Figure 5.- Concluded.

(a) B/1100 Al

(b) B/2024 Al

(c) B/3003 Al
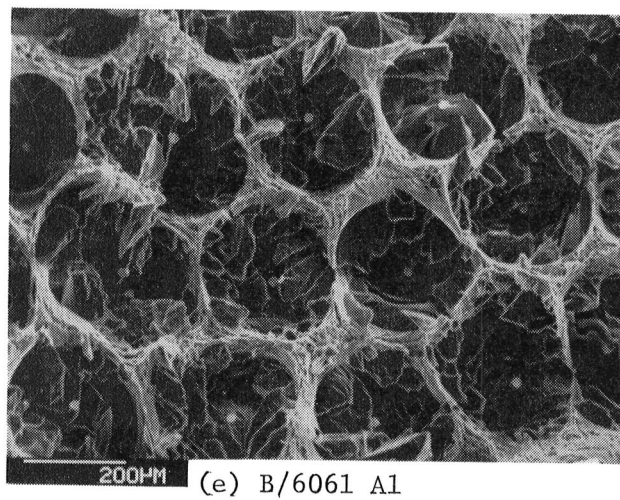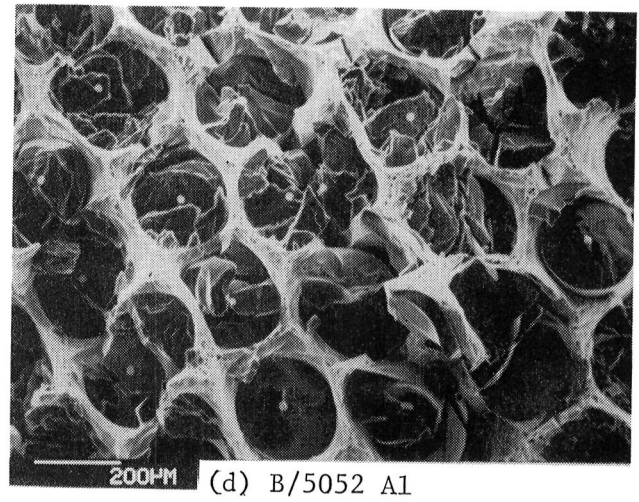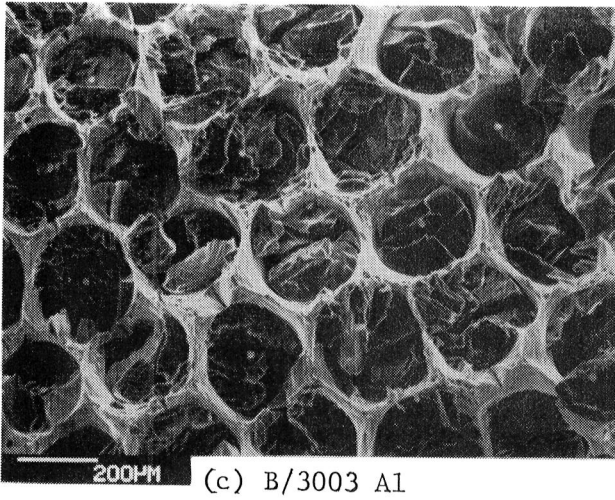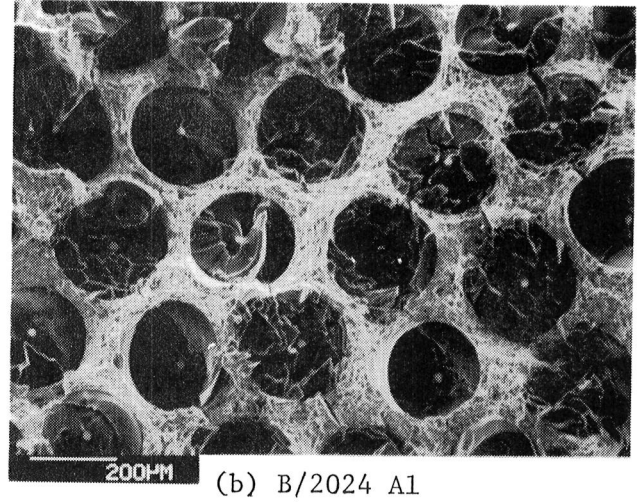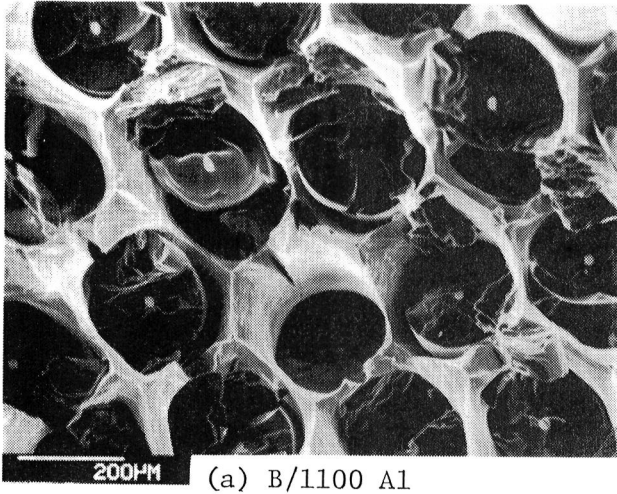
(d) B/5052 Al

(e) B/6061 Al

Figure 6.- Longitudinal fracture surfaces of as-fabricated specimens.
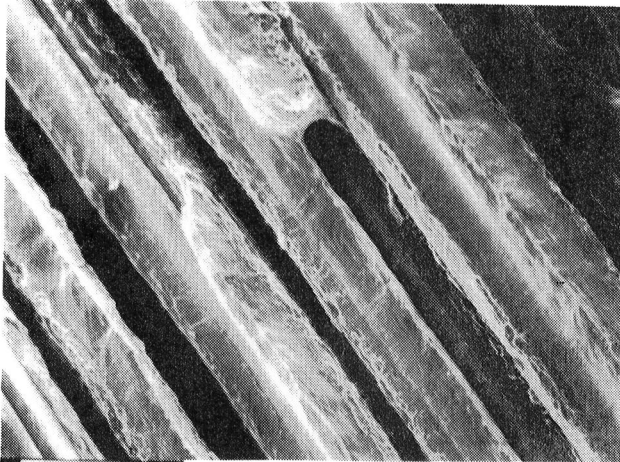
(a) B/1100 Al
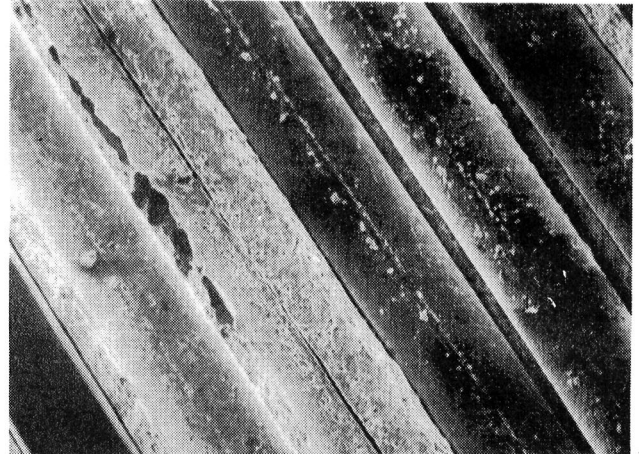
(b) B/2024 Al
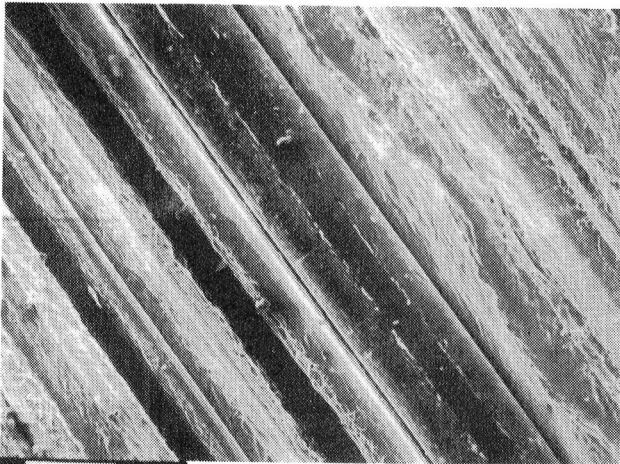
(c) B/3003 Al
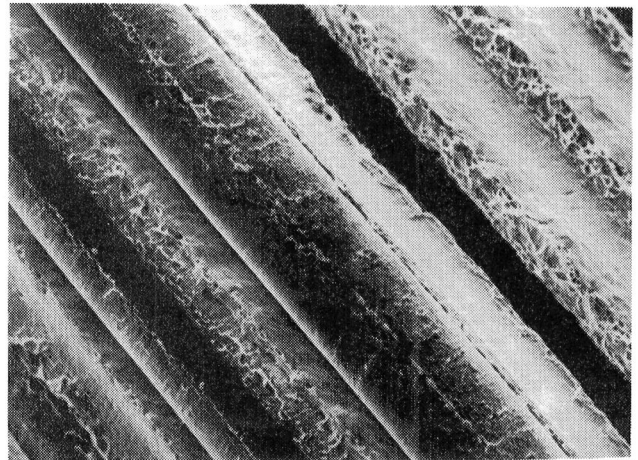
(d) B/5052 Al
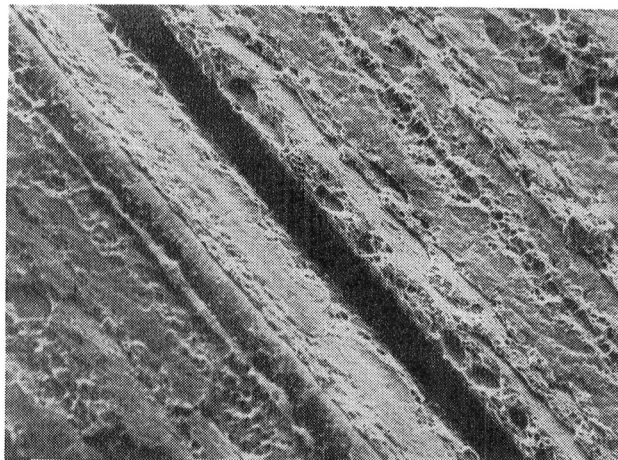
(e) B/6061 Al

Figure 7.- Transverse fracture surfaces of as-fabricated specimens.

105
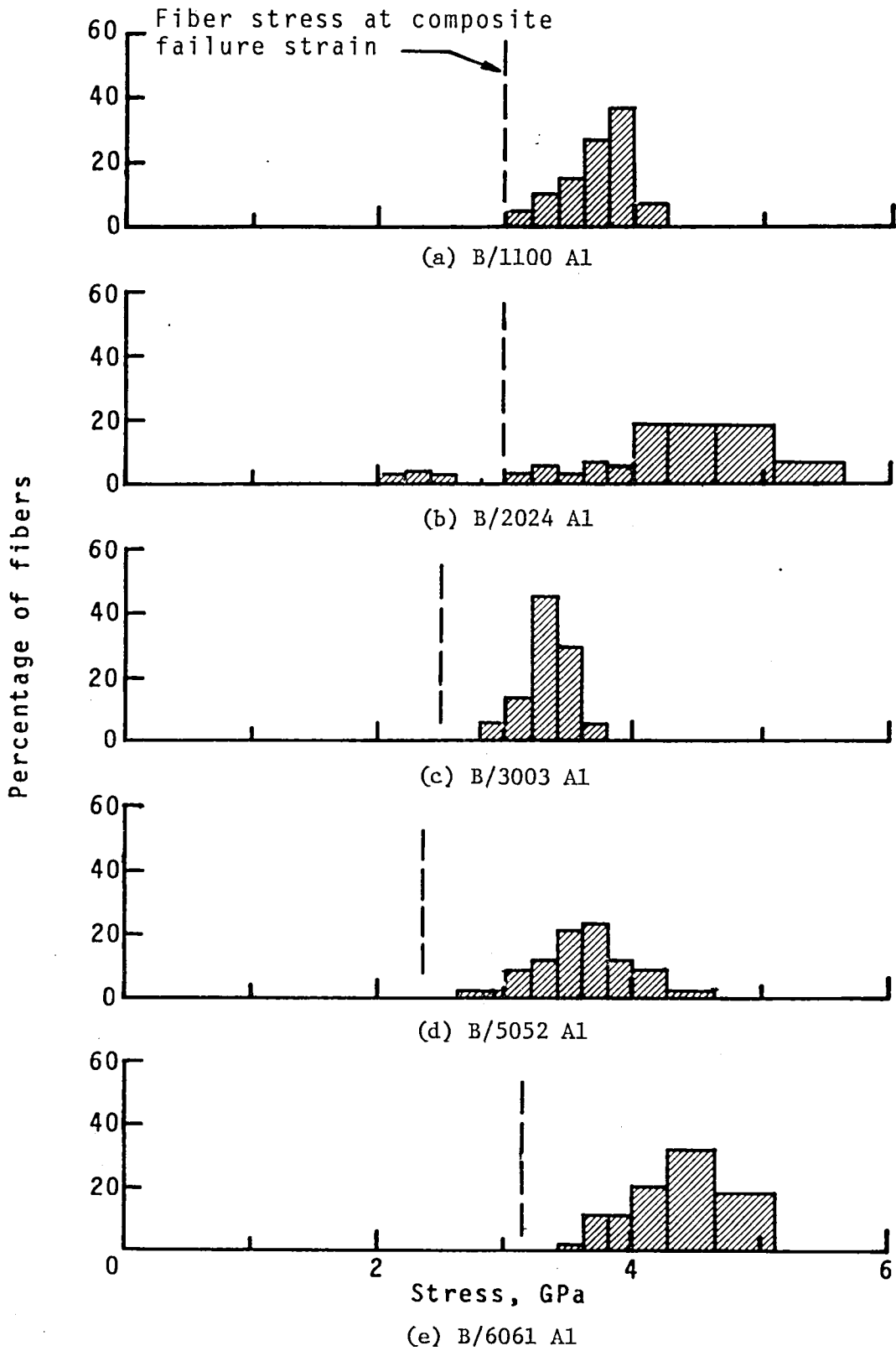
Figure 8.— Residual fiber strength distribution for as-fabricated composites after tensile testing.

(a) Matrix alloy tensile strength

(b) Composite transverse tensile strength

1100 Al and B/1100 Al
2024 Al and B/2024 Al
3003 Al and B/3003 Al
5052 Al and B/5052 Al
6061 Al and B/6061 Al

(c) Composite longitudinal tensile strength
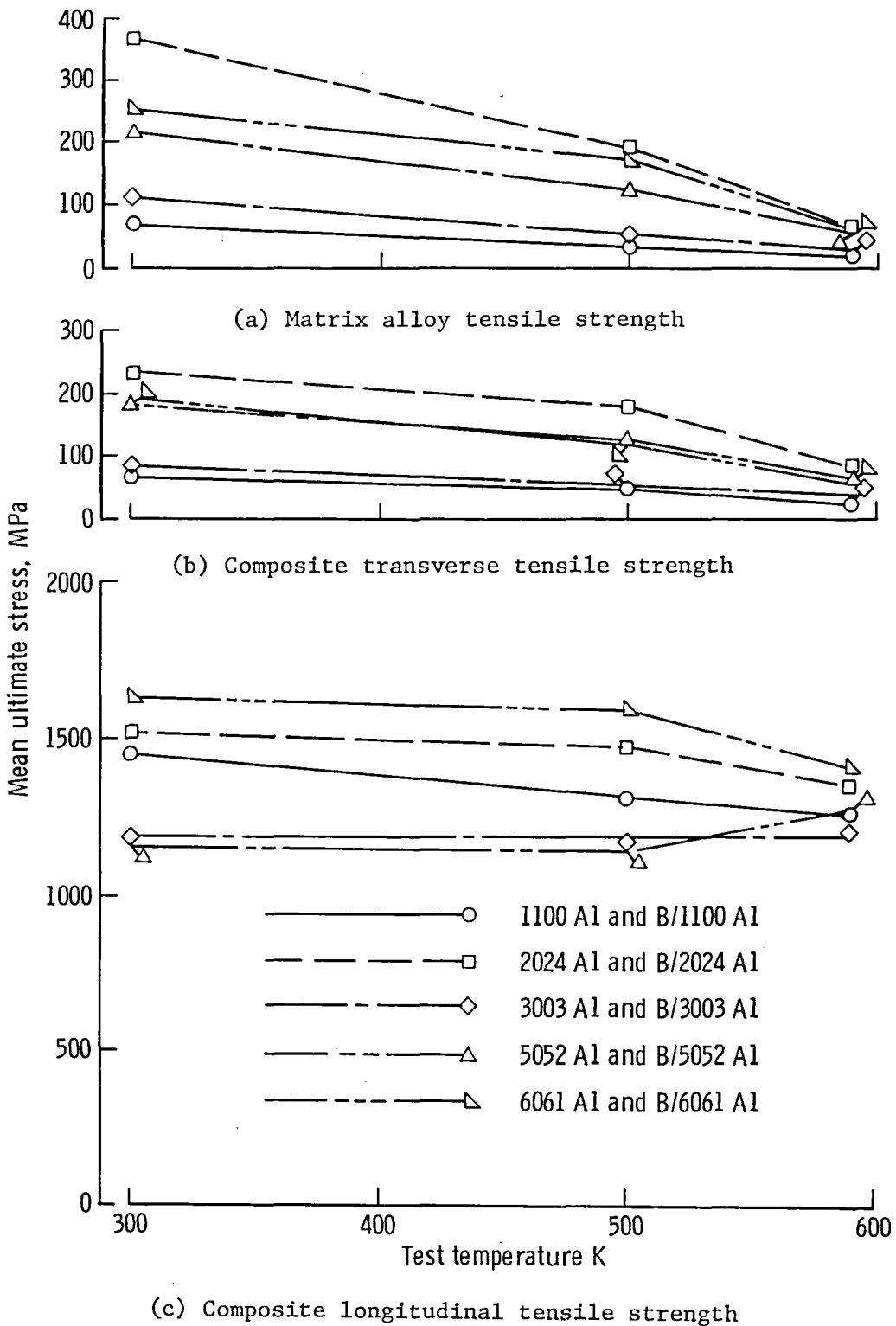
Figure 9.- Effect of elevated test temperature on the mean ultimate strengths of B/Al composites.
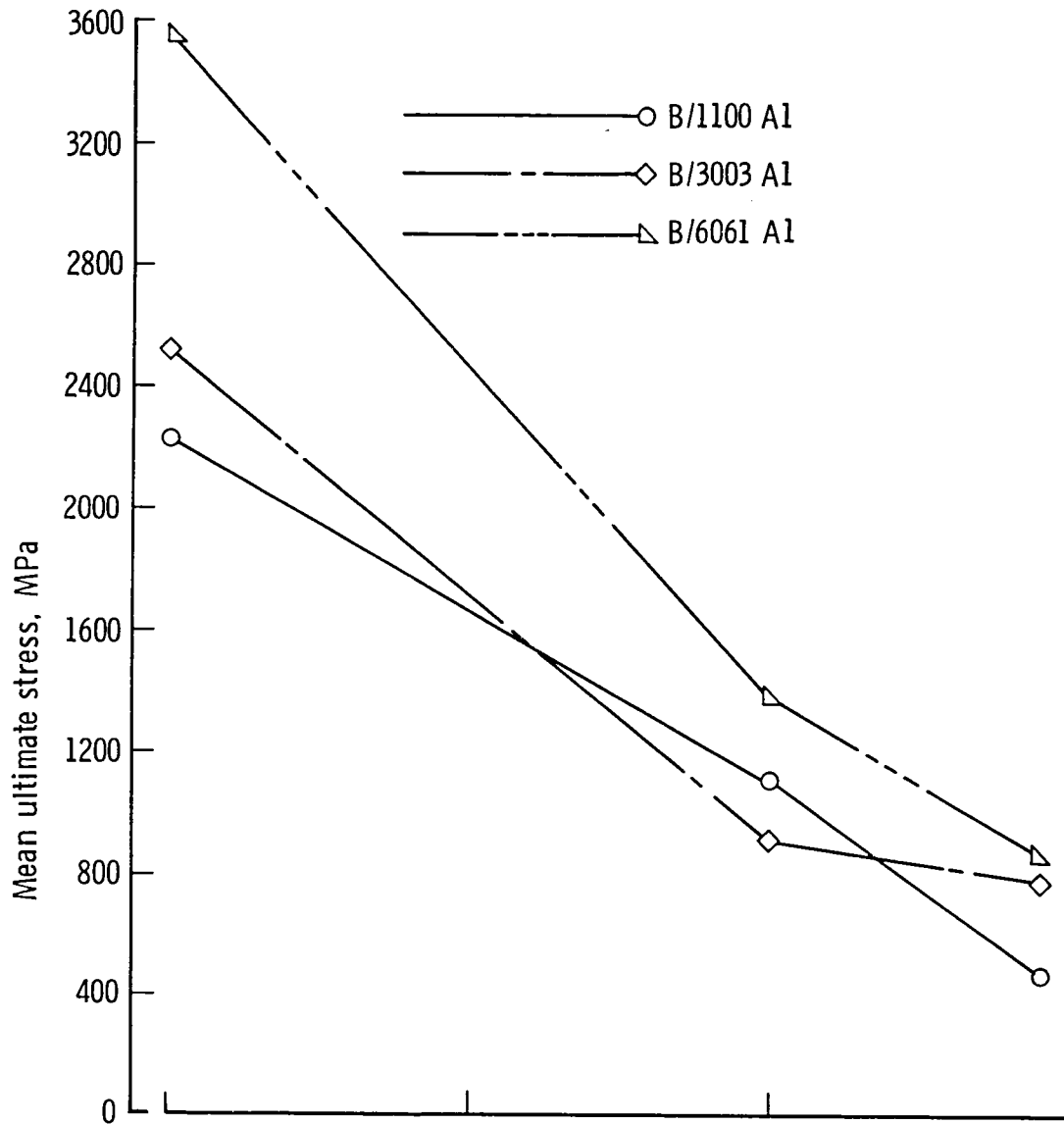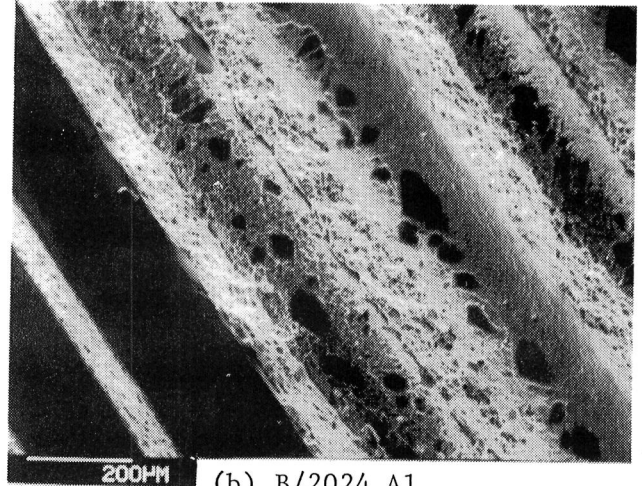
(d) Composite longitudinal compression strength
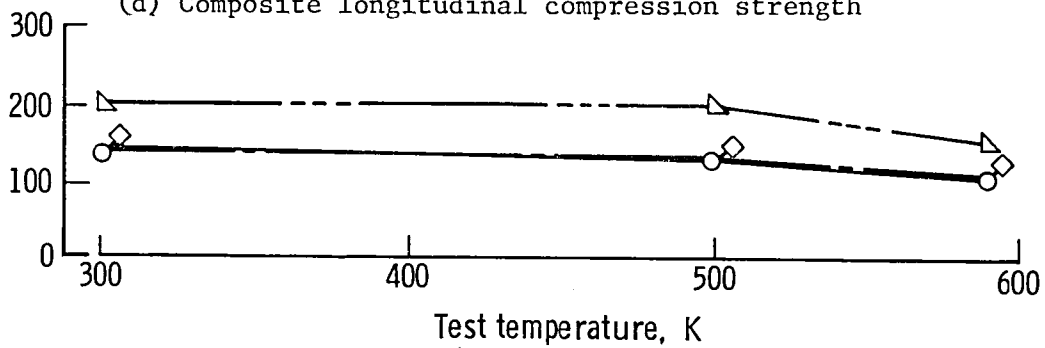
(e) Composite in-plane shear strength

Figure 9.- Concluded.

(a) Matrix alloy tensile strength

(b) Composite longitudinal tensile strength

——○ 1100 Al and B/1100 Al

— — —□ 2024 Al and B/2024 Al

——◇ 3003 Al and B/3003 Al

——△ 5052 Al and B/5052 Al

——◁ 6061 Al and B/6061 Al

(c) Composite longitudinal tensile strength
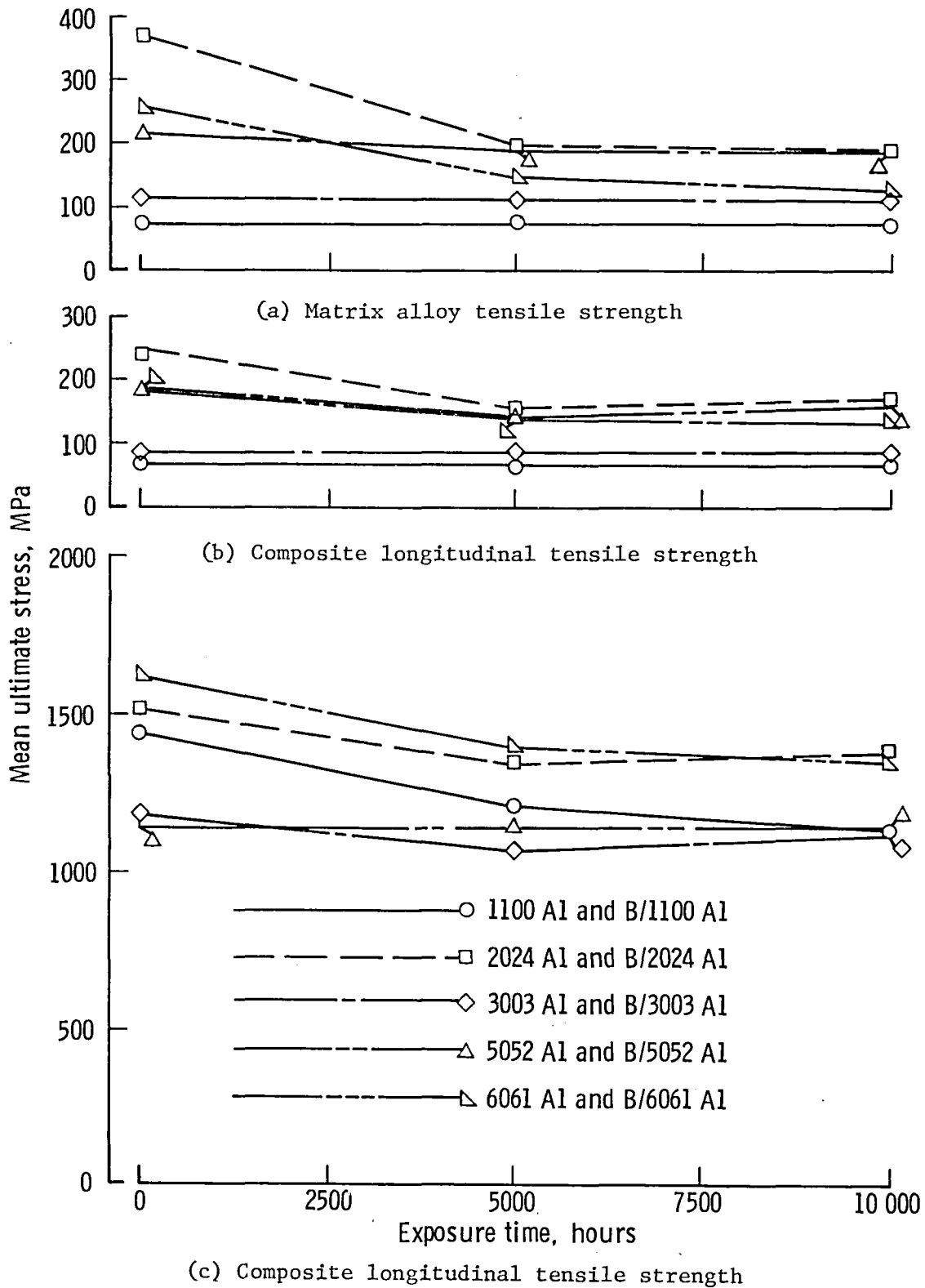
Figure 10.– Effect of isothermal exposure at 500 K on the ultimate stress of B/Al composites and their matrix alloys.
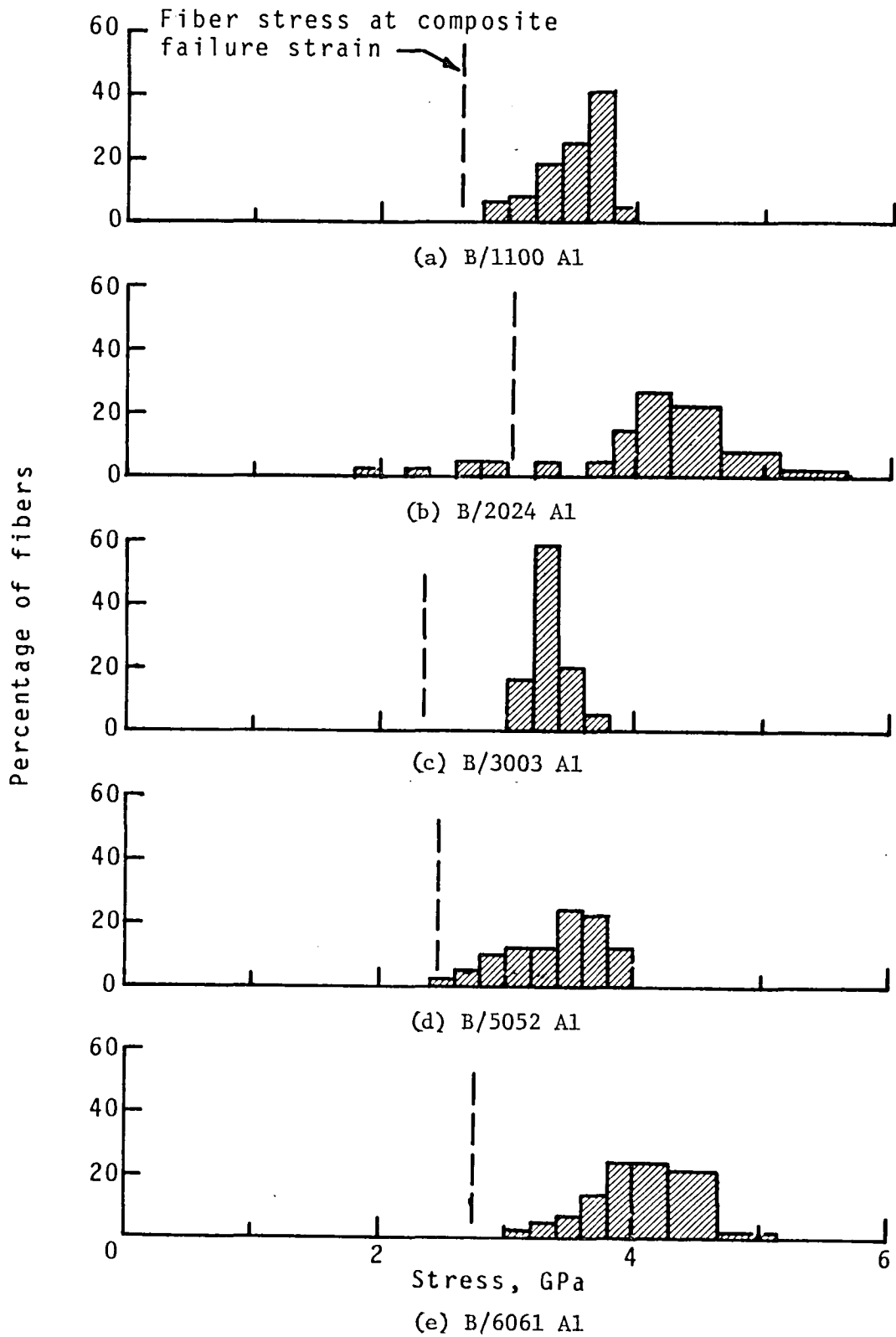
Figure 11.- Residual fiber strength distributions for composites after 10 000 hours exposure at 500 K and tensile testing.
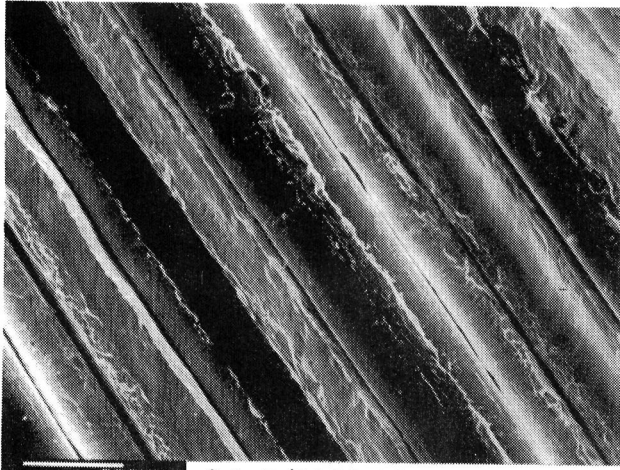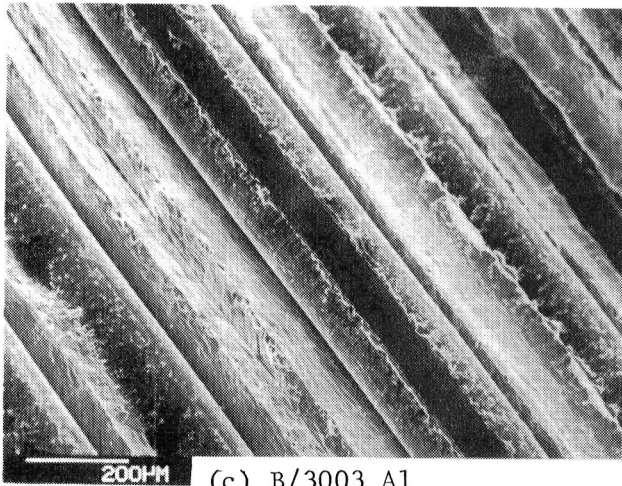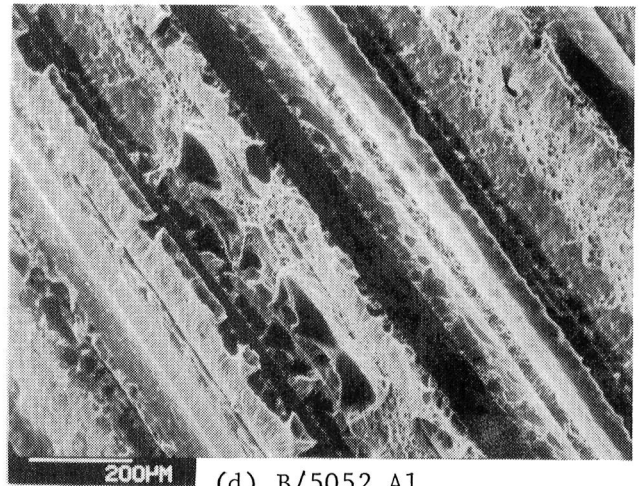
(a) B/1100 Al
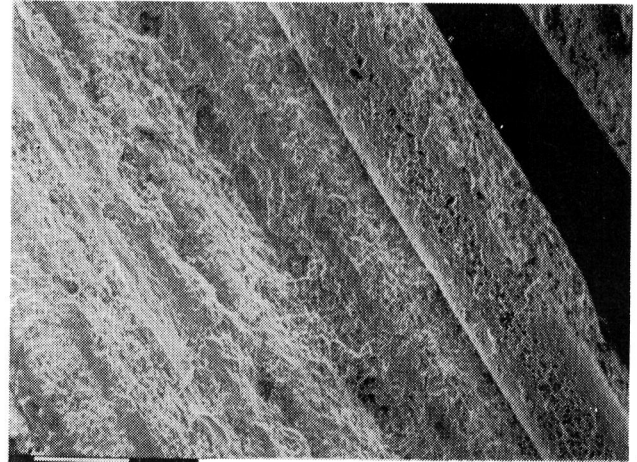
(b) B/2024 Al
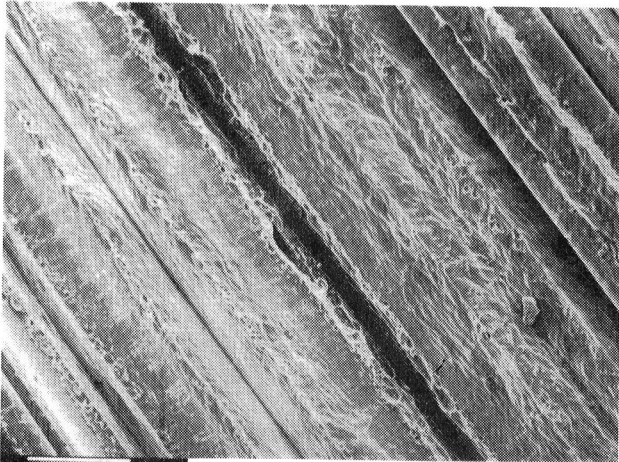
(c) B/3003 Al
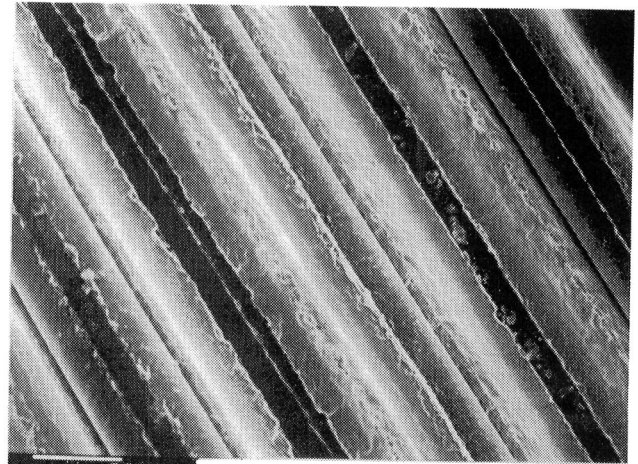
(d) B/5052 Al
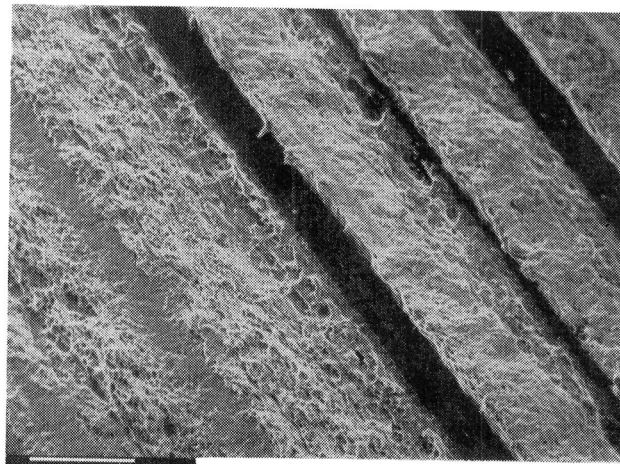
(e) B/6061 Al

Figure 12.- Transverse fracture surfaces of specimens isothermally exposed for 10 000 hours at 500 K.

111

(a) Matrix alloy tensile strength

(b) Composite transverse tensile strength

1100 Al or B/1100 Al
2024 Al or B/2024 Al
3003 Al or B/3003 Al
5052 Al or B/5052 Al
6061 Al or B/6061 Al

(c) Composite longitudinal tensile strength
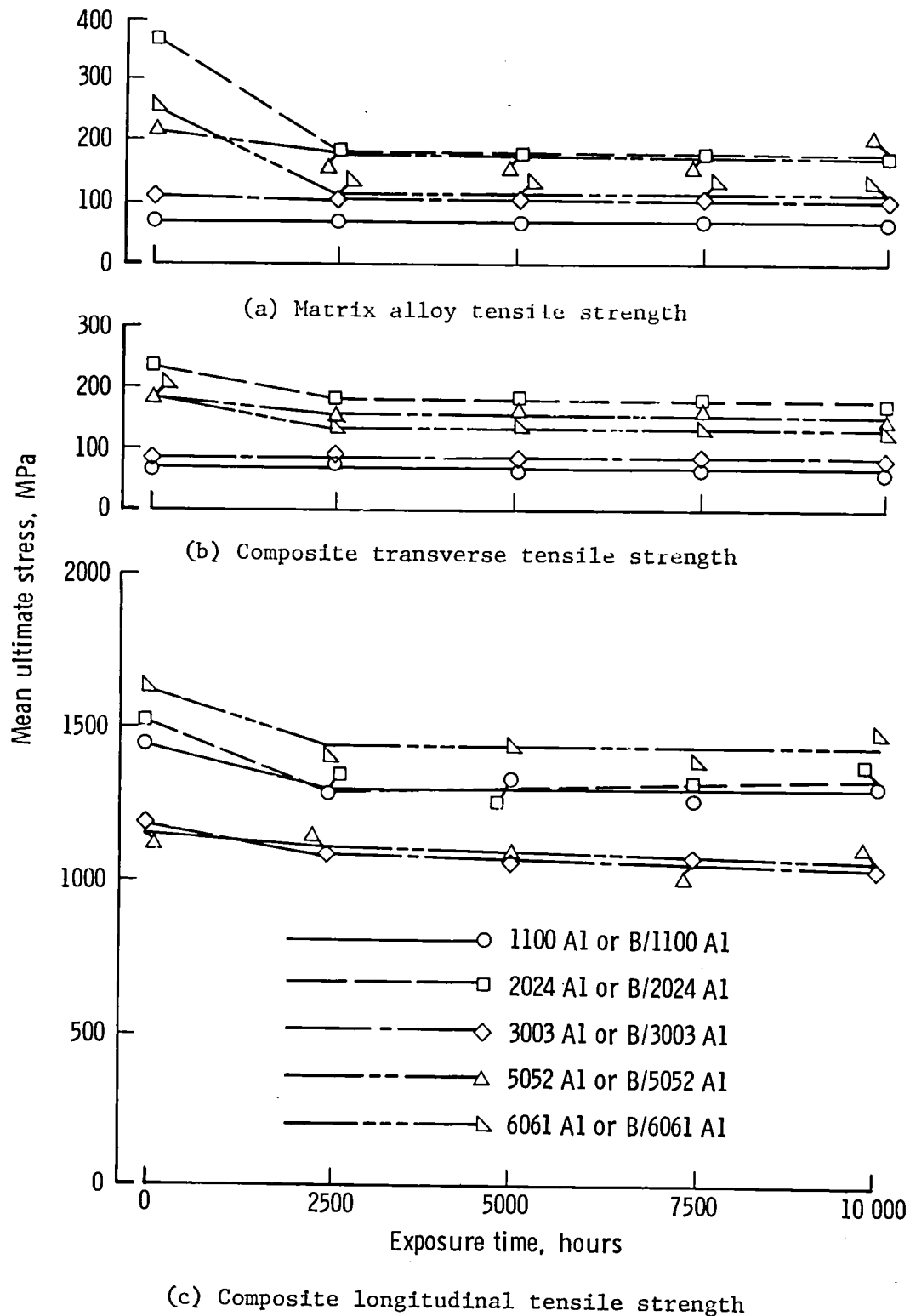
Figure 13.— Effect of isothermal exposure at 590 K on the ultimate stress of B/Al composites and their matrix alloys.
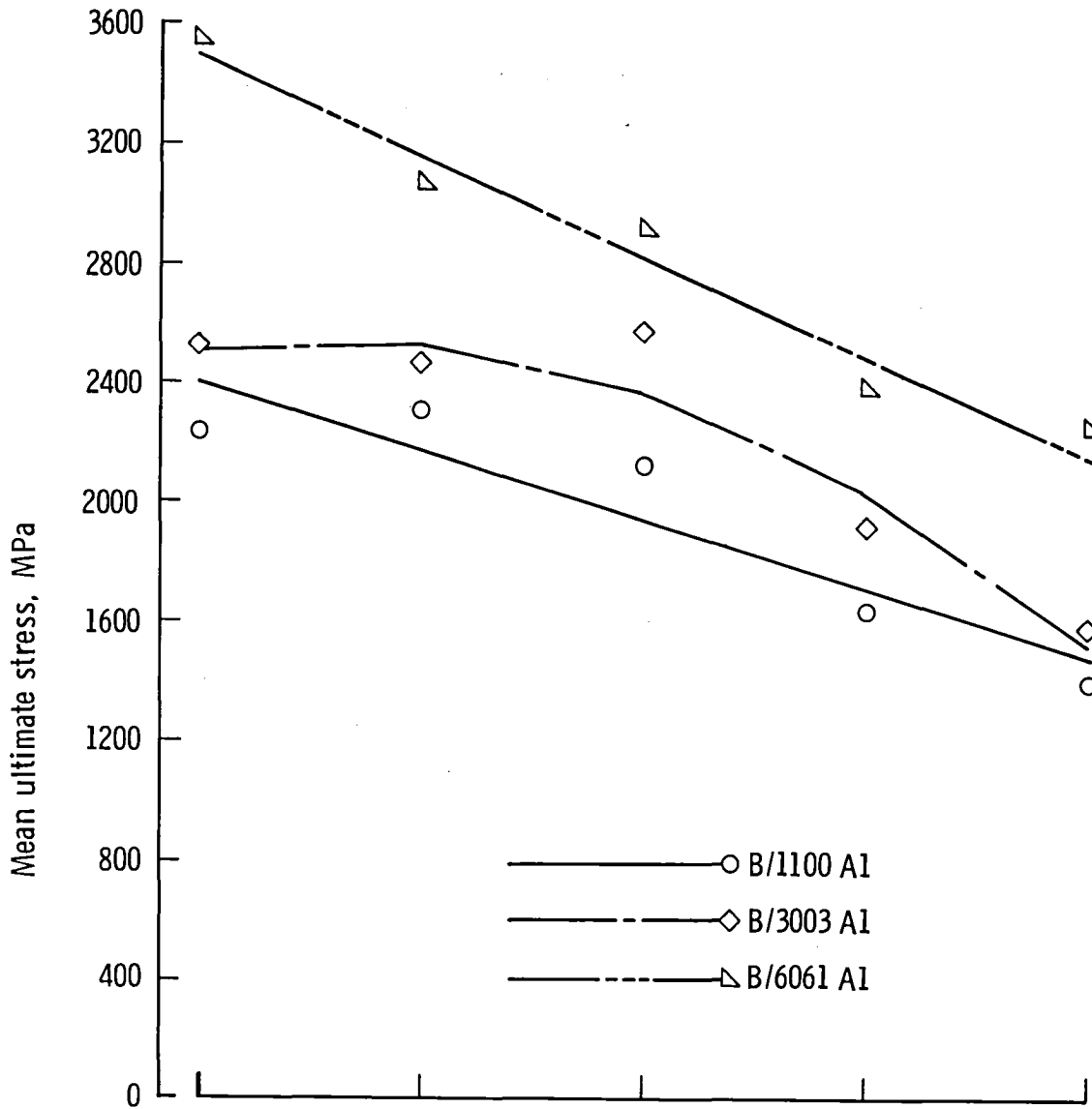
(d) Composite longitudinal compression strength
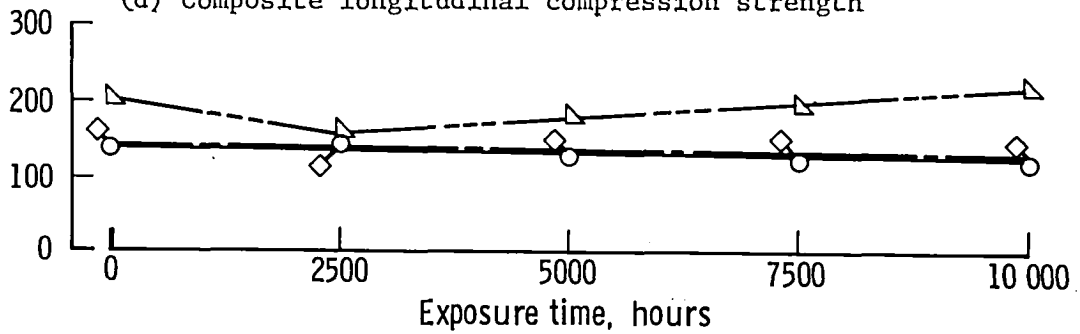
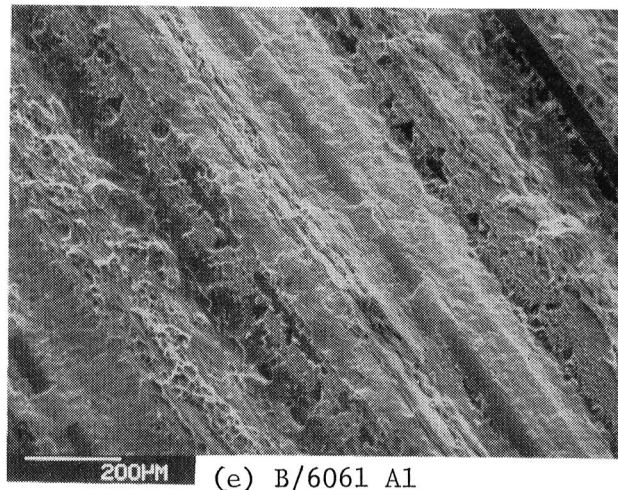(e) Composite in-plane shear strength

Figure 13.- Concluded.
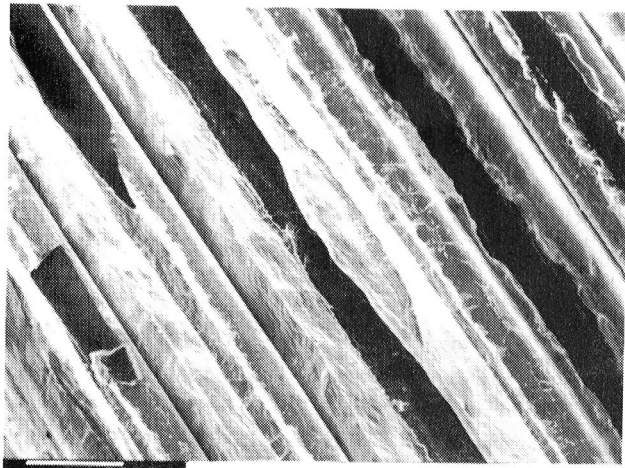
(a) B/1100 Al
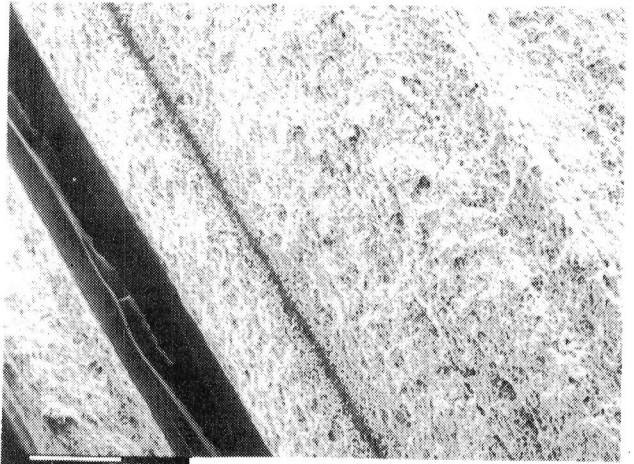
(b) B/2024 Al
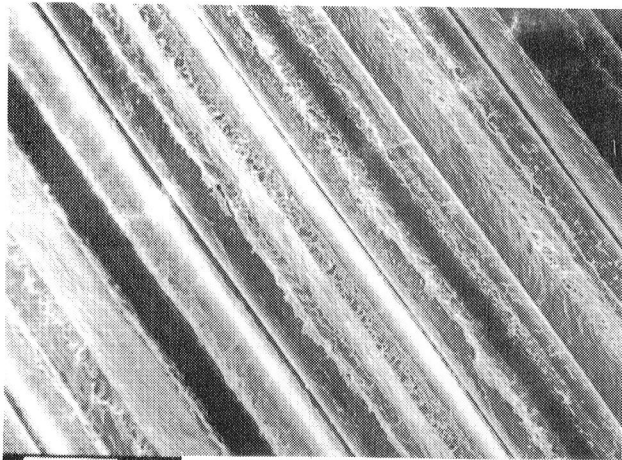
(c) B/3003 Al
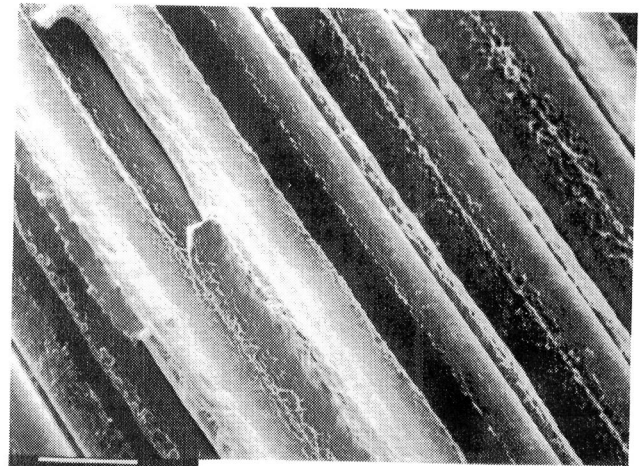
(d) B/5052 Al
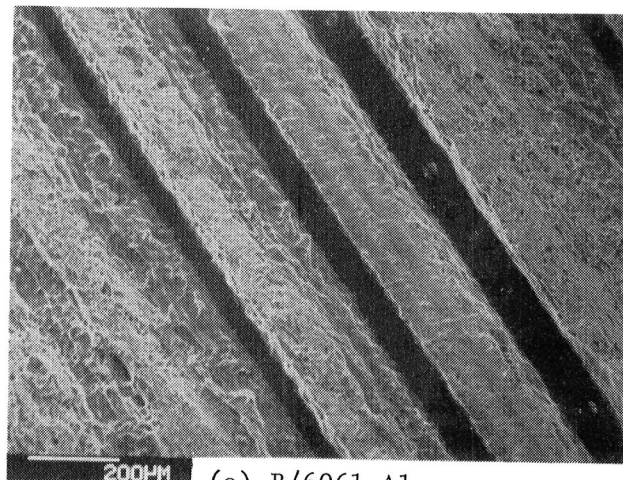
(e) B/6061 Al

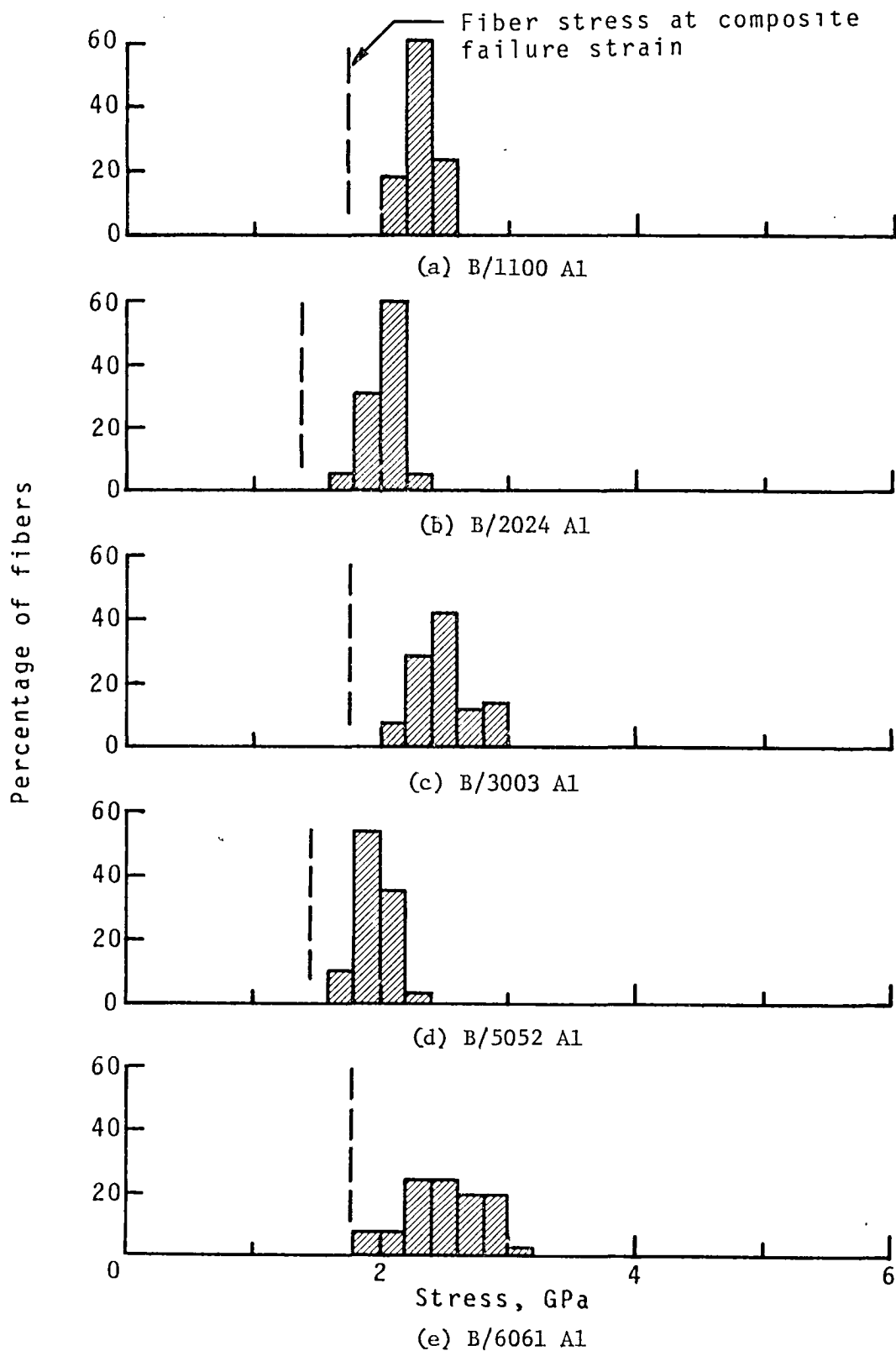Figure 14.- Transverse fracture surfaces of specimens isothermally exposed for 10 000 hours at 590 K.
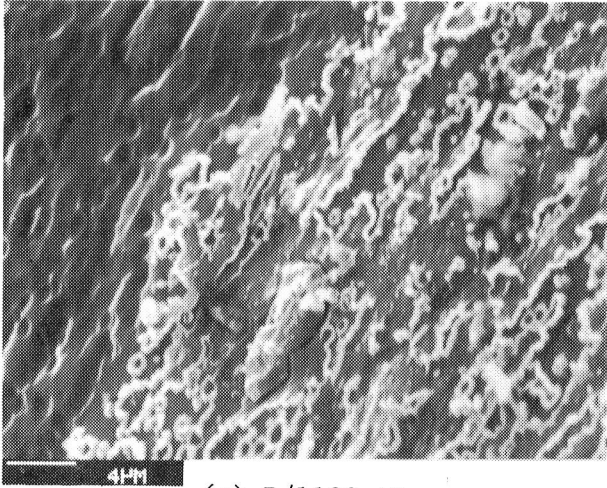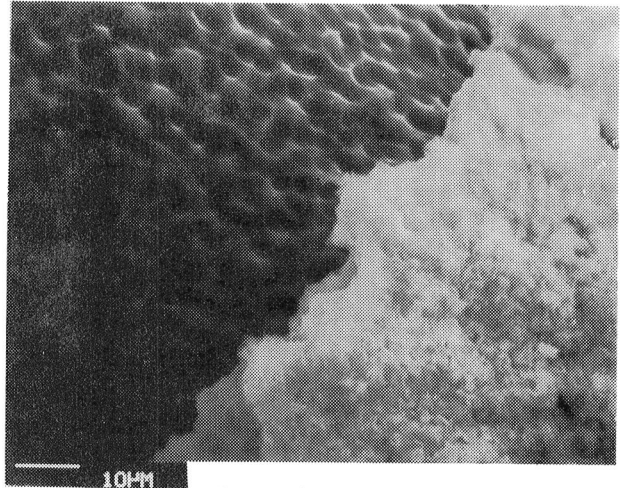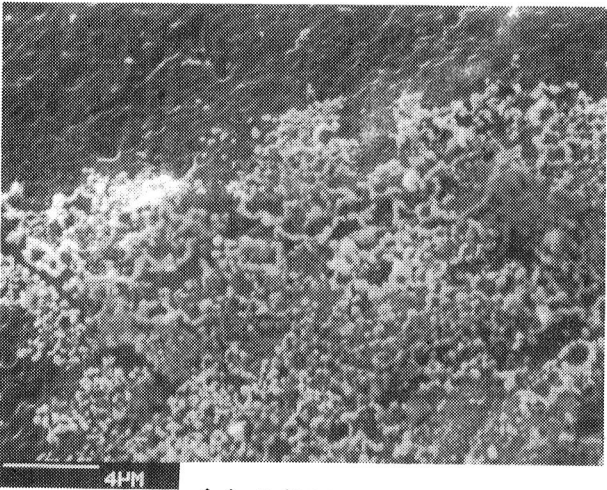
114
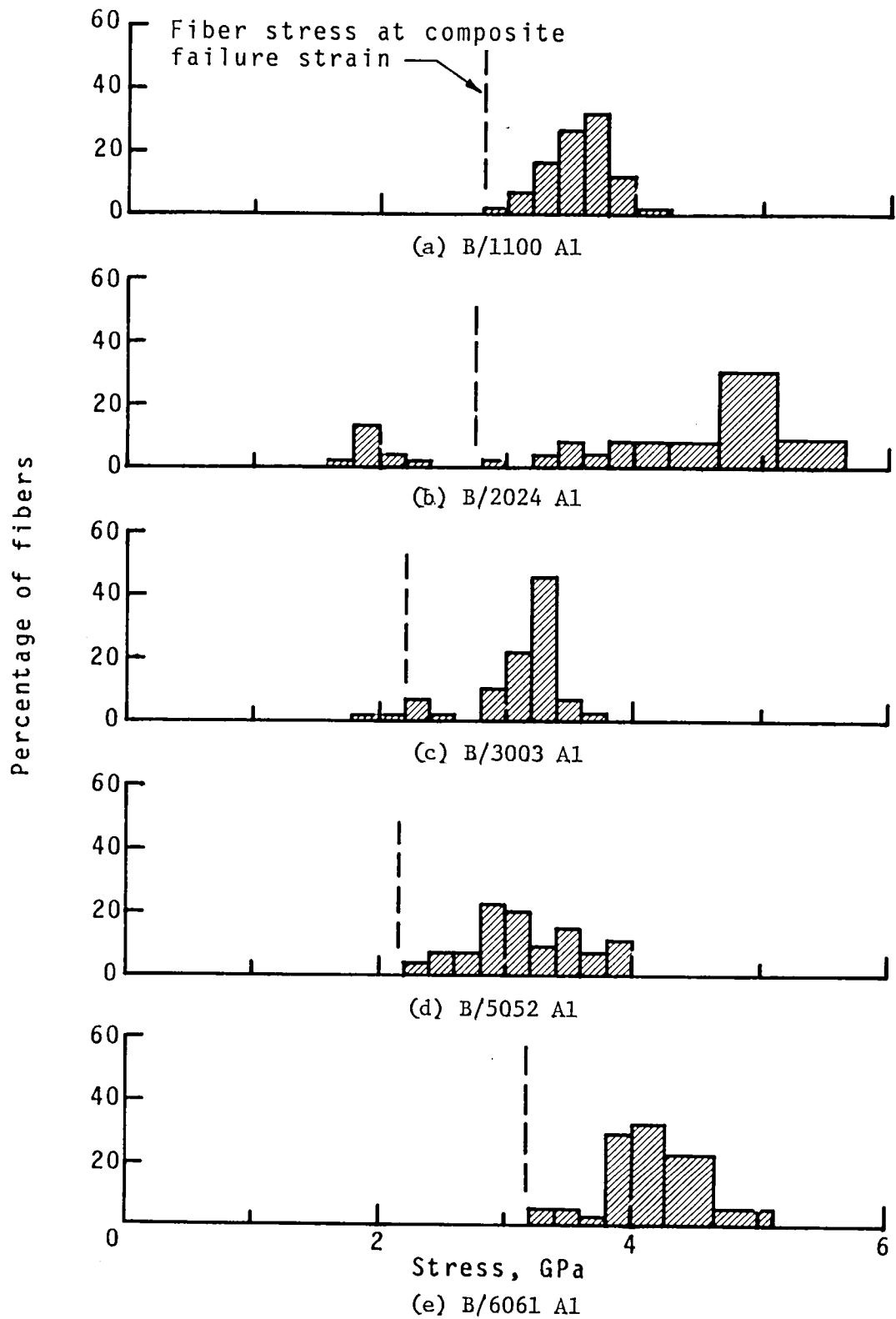
Figure 15.— Residual fiber strength distributions for composites after 10 000 hours exposure at 590 K and tensile testing.
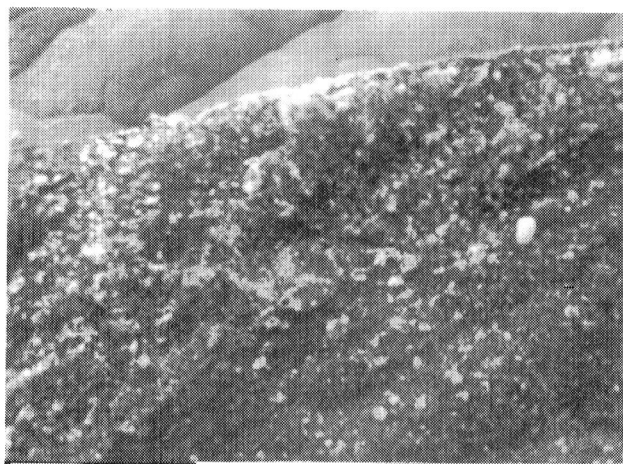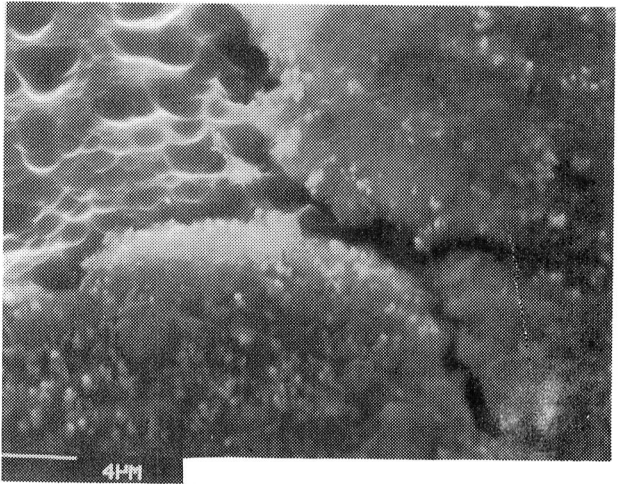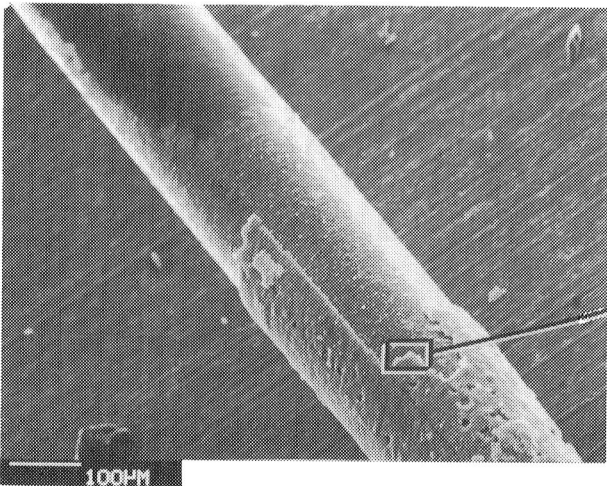
(a) B/1100 Al

(b) B/2024 Al
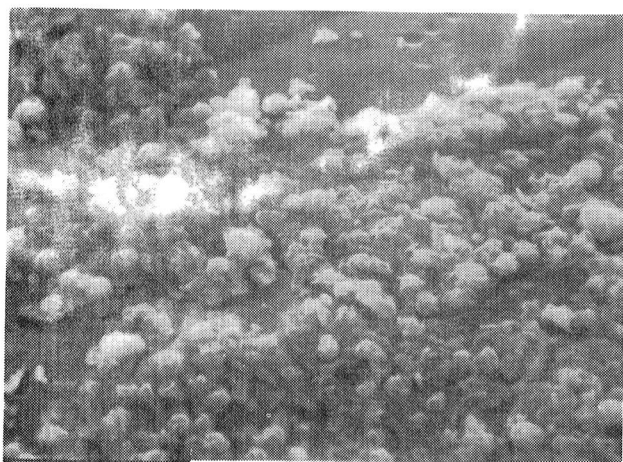
(c) B/3003 Al

(d) B/5052 Al

(e) B/6061 Al

Figure 16.– Reaction layers on fibers removed from composite specimens after
10 000 hours exposure at 590 K.
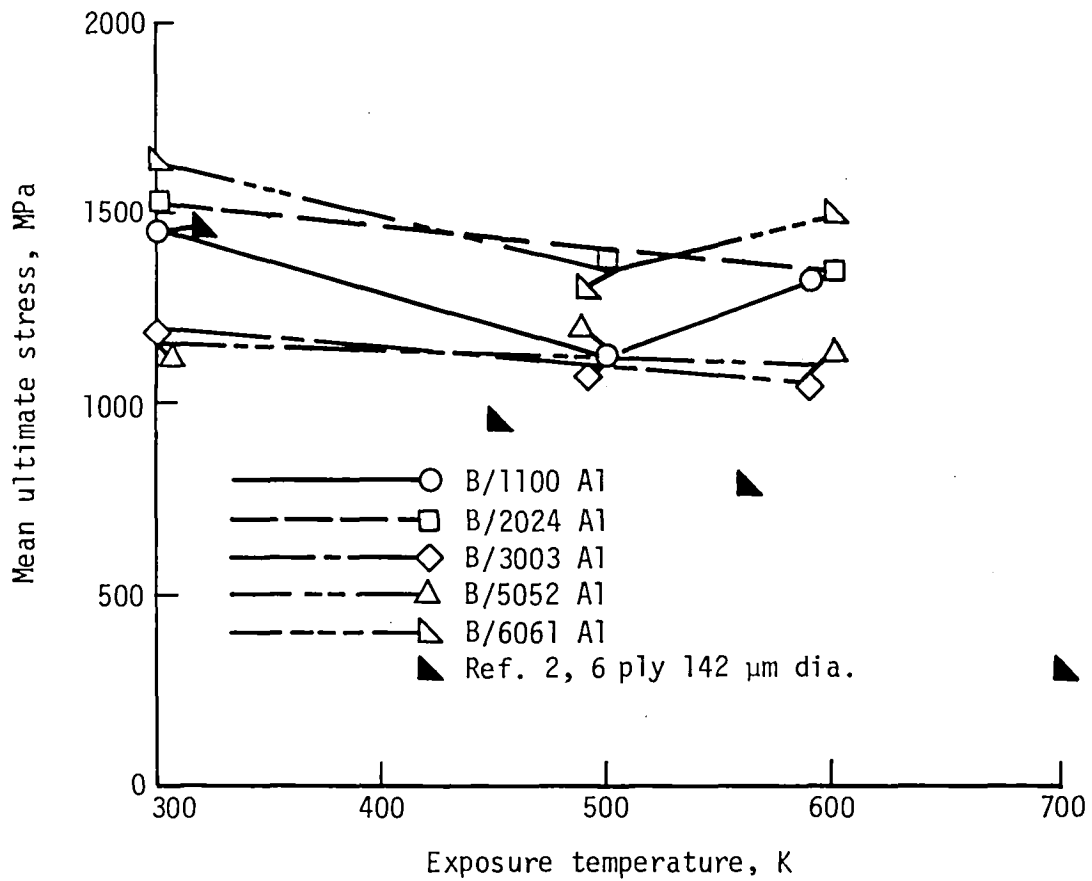
Figure 17.- Longitudinal tensile strength as a function of 10 000 hours exposure at elevated temperature.

(a) Matrix alloy tensile strength

(b) Composite transverse tensile strength

Legend:
- 1100 Al or B/1100 Al
- 2024 Al or B/2024 Al
- 3003 Al or B/3003 Al
- 5052 Al or B/5052 Al
- 6061 Al or B/6061 Al

Mean ultimate stress, MPa

Exposure time, hours

(c) Composite longitudinal tensile strength
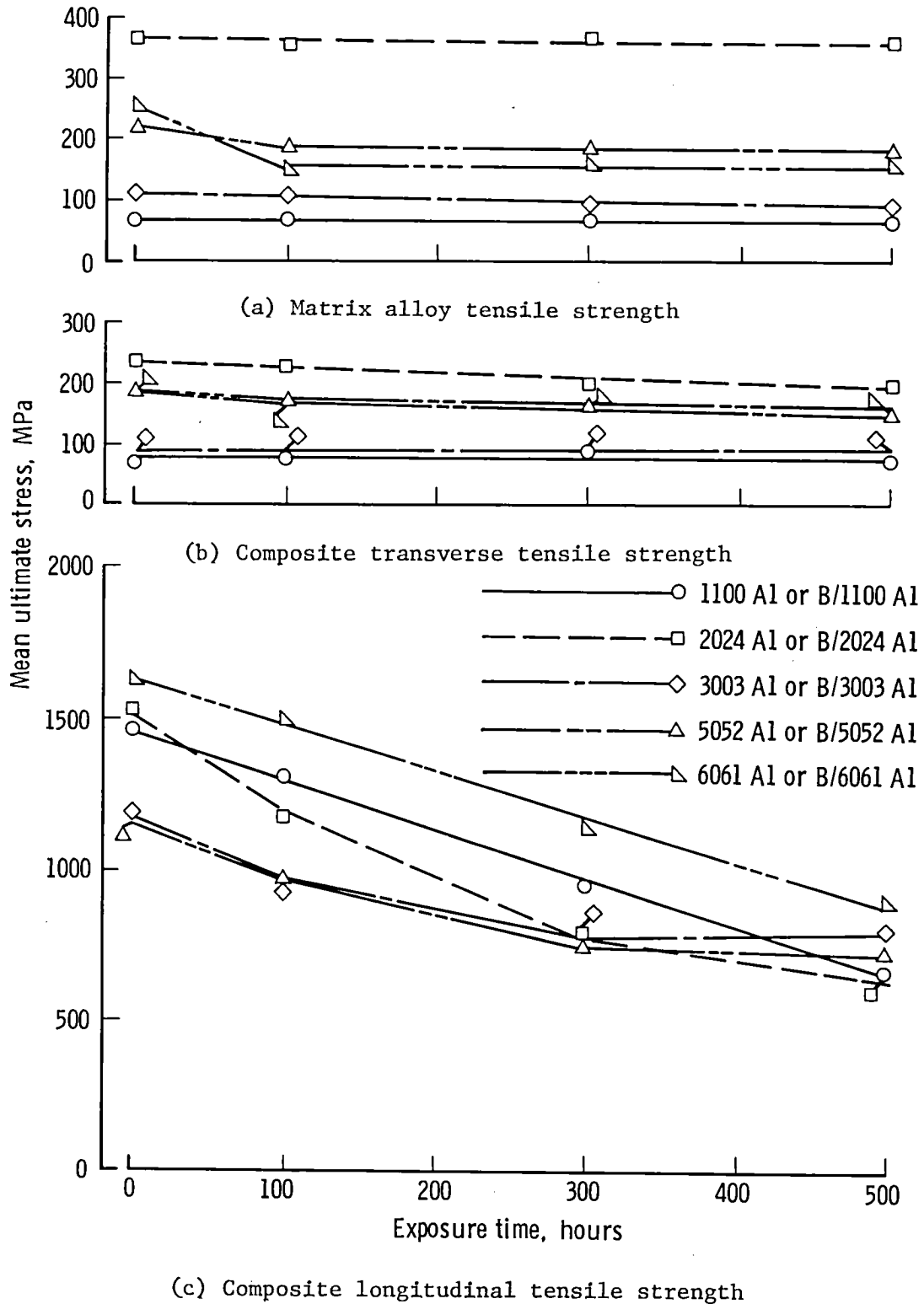
Figure 18.— Effect of isothermal exposure at 730 K on the ultimate stress of B/Al composites and their matrix alloys.
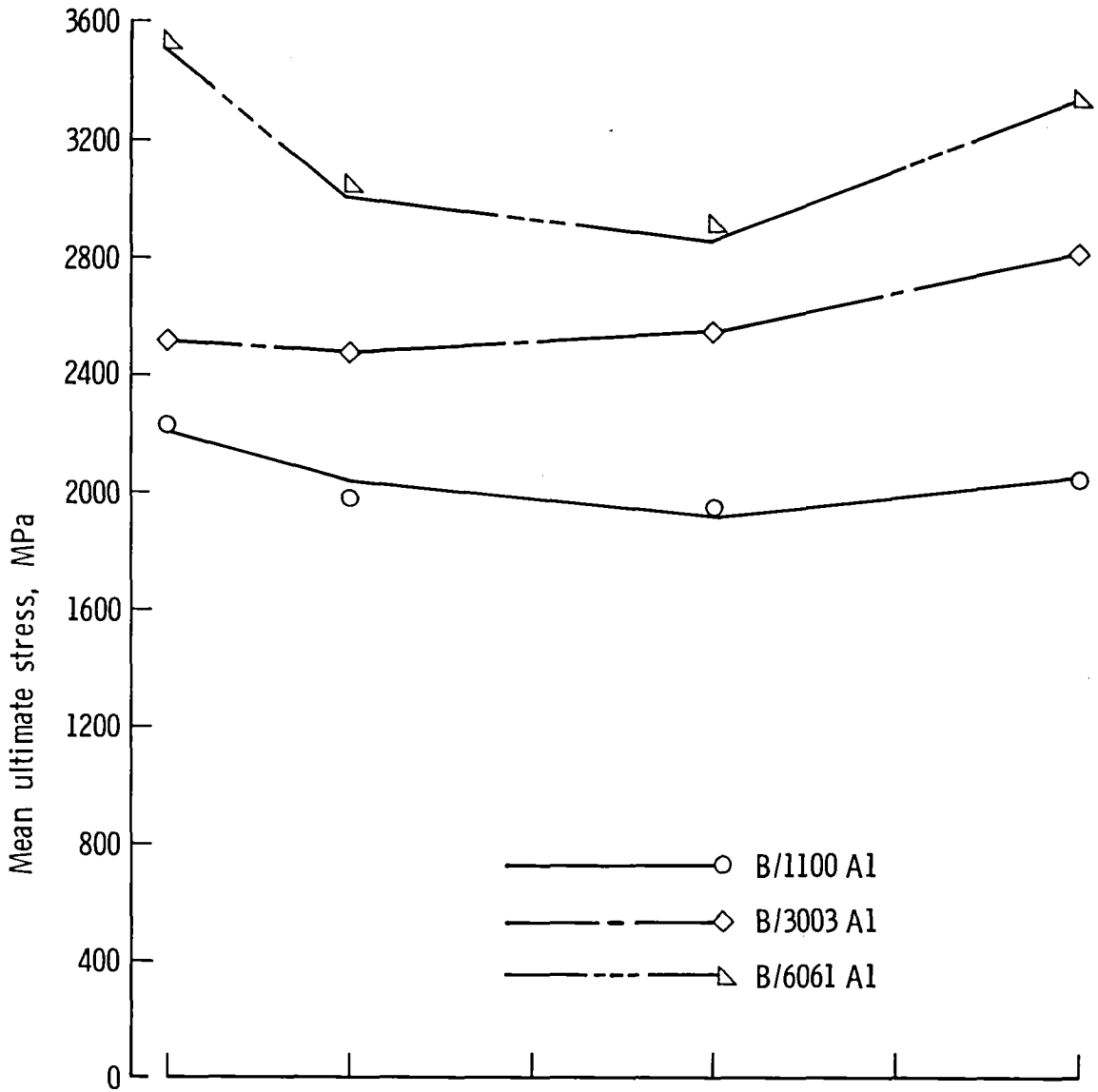
(d) Composite longitudinal compression strength
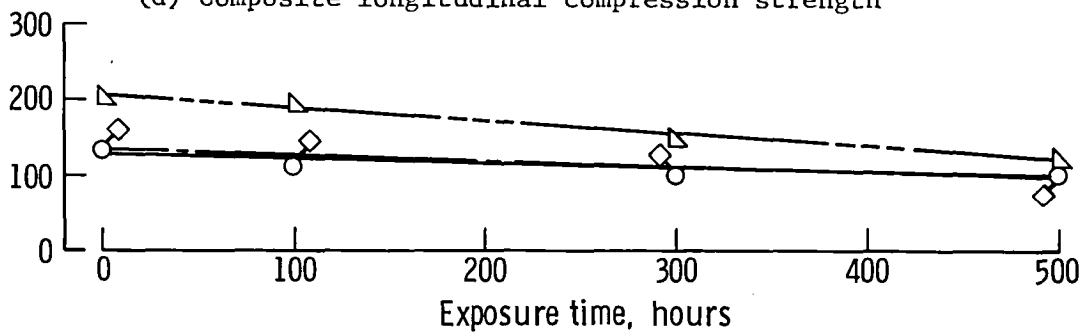
(e) Composite in-plane shear strength

Figure 18.- Concluded.
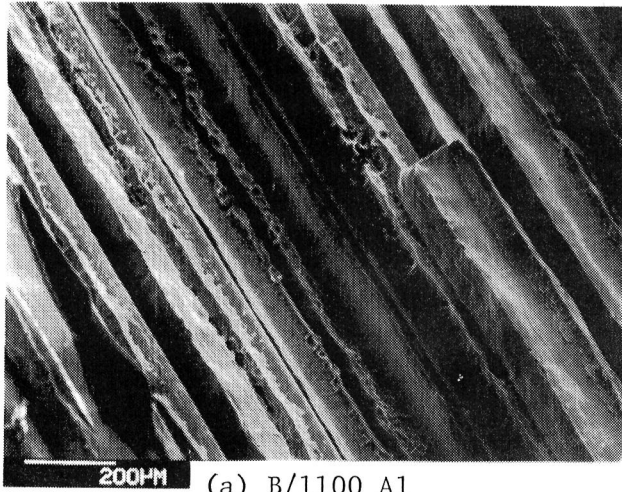
(a) B/1100 Al   (b) B/2024 Al

(c) B/3003 Al   (d) B/5052 Al

(e) B/6061 Al

Figure 19.— Transverse fracture surfaces of specimens isothermally exposed for 500 hours at 730 K.

Figure 20.— Residual fiber strength distributions for composites after 500 hours exposure at 730 K and tensile testing.

(a) B/1100 Al

(b) B/2024 Al

(c) B/3003 Al

(d) B/5052 Al

(e) B/6061 Al

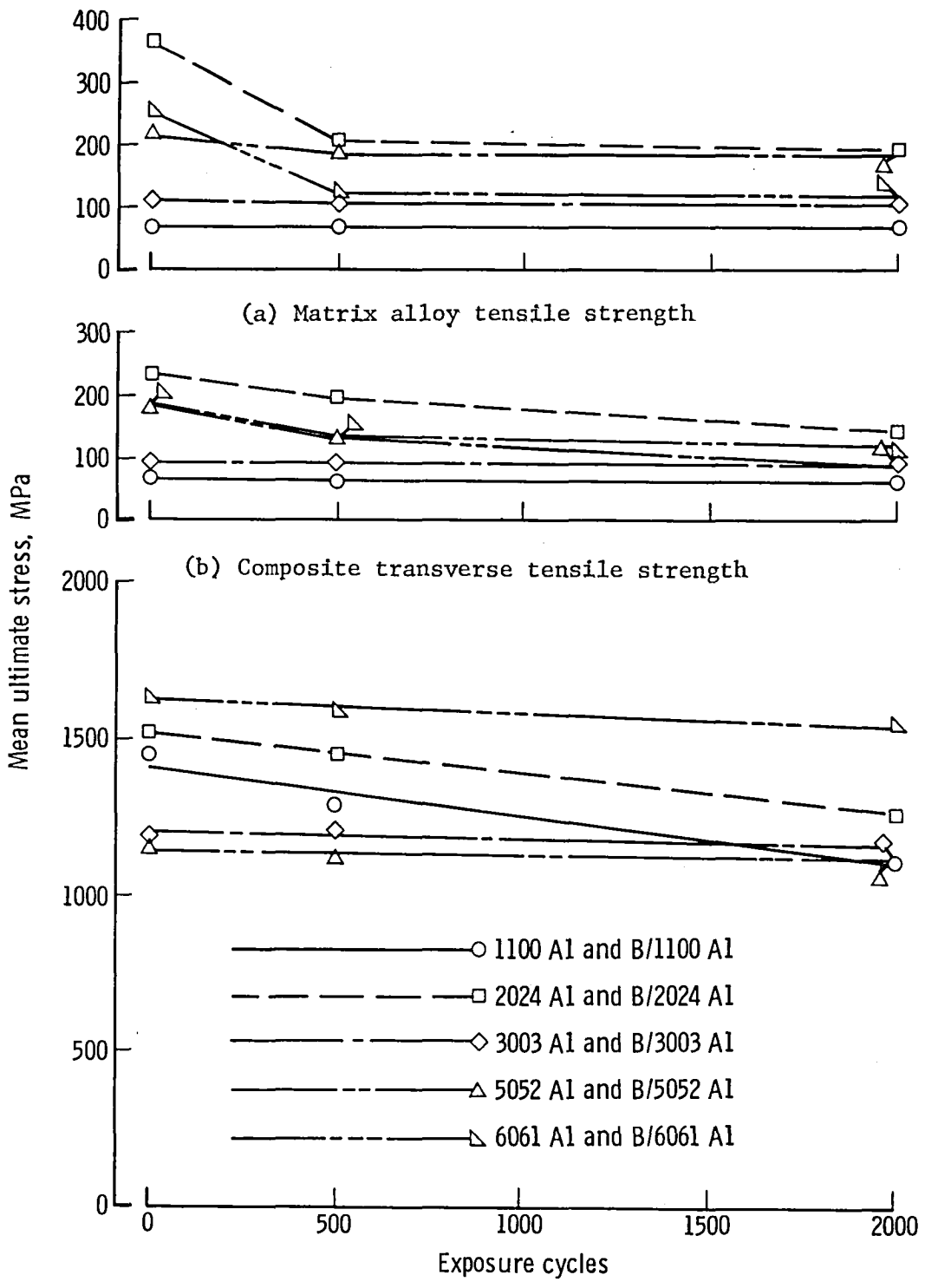Figure 21.- Reaction layers on fibers removed from composite specimens after 500 hours exposure at 730 K.
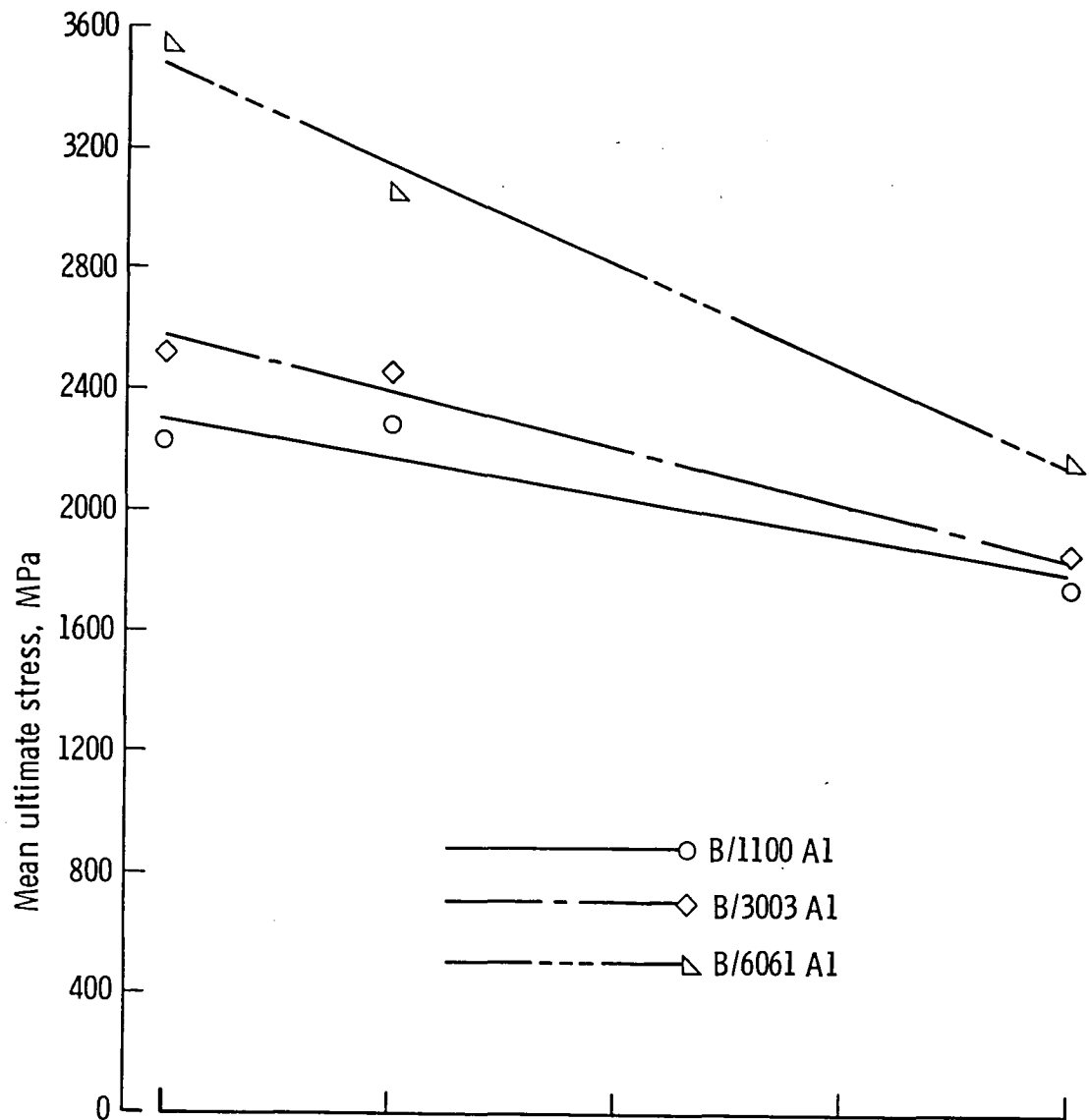
122

(a) Matrix alloy tensile strength

(b) Composite transverse tensile strength

1100 Al and B/1100 Al
2024 Al and B/2024 Al
3003 Al and B/3003 Al
5052 Al and B/5052 Al
6061 Al and B/6061 Al

(c) Composite longitudinal tensile strength

Figure 22.- Effect of thermal cycling between 200 K and 590 K on the ultimate tensile strength of B/Al composites and their matrix alloys.

123

(d) Composite longitudinal compression strength
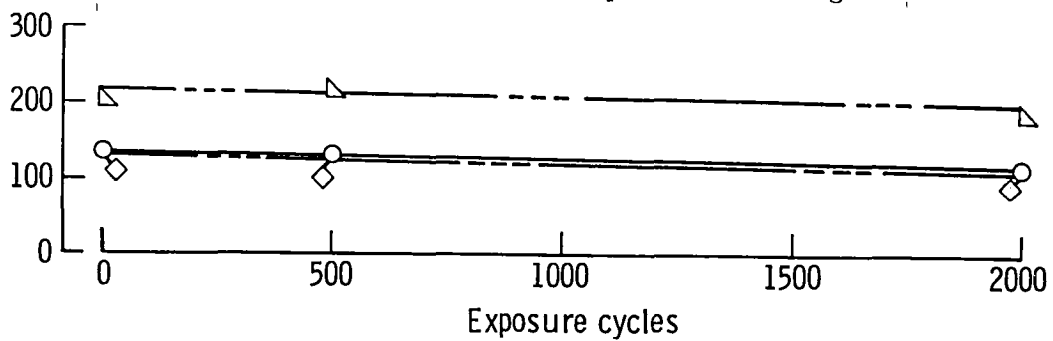
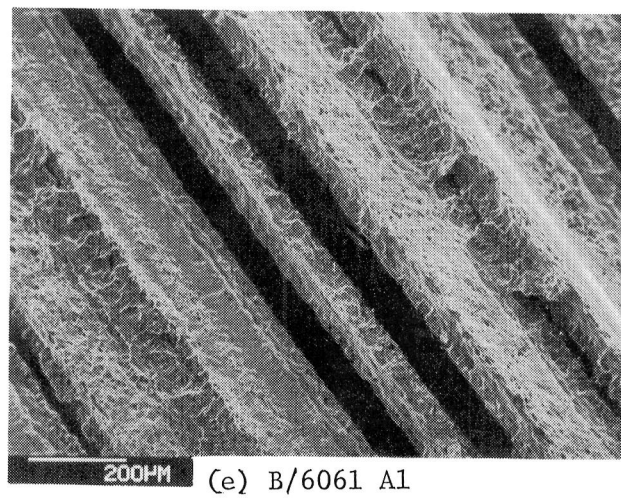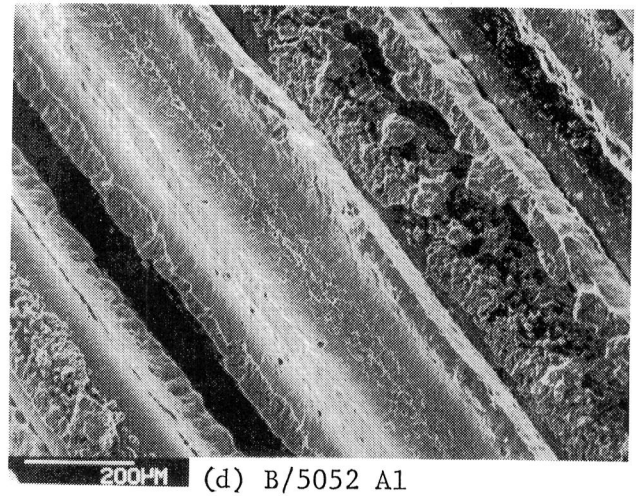(e) Composite in-plane shear strength
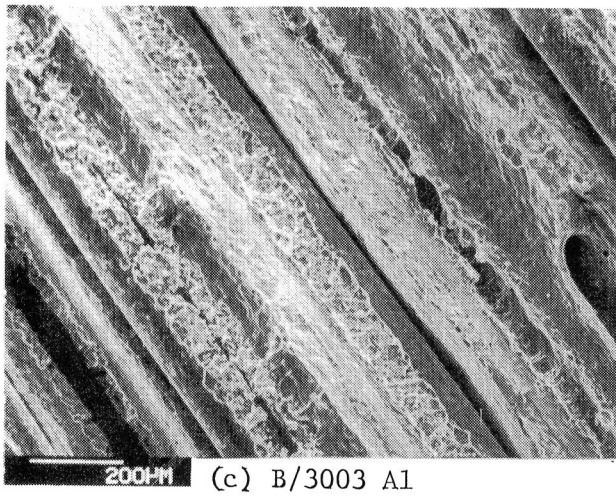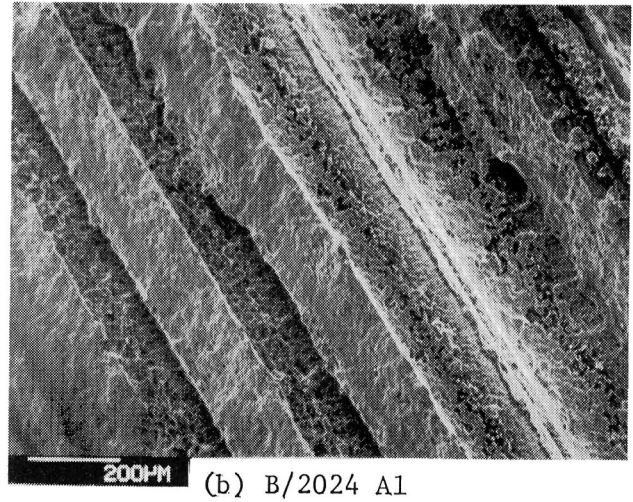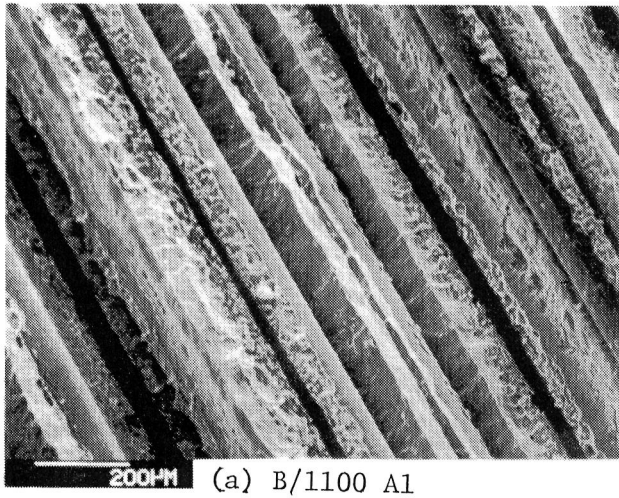
Figure 22.- Concluded.

124

Figure 23.– Transverse fracture surfaces of specimens thermally cycled 2000 times between 200 K and 590 K.
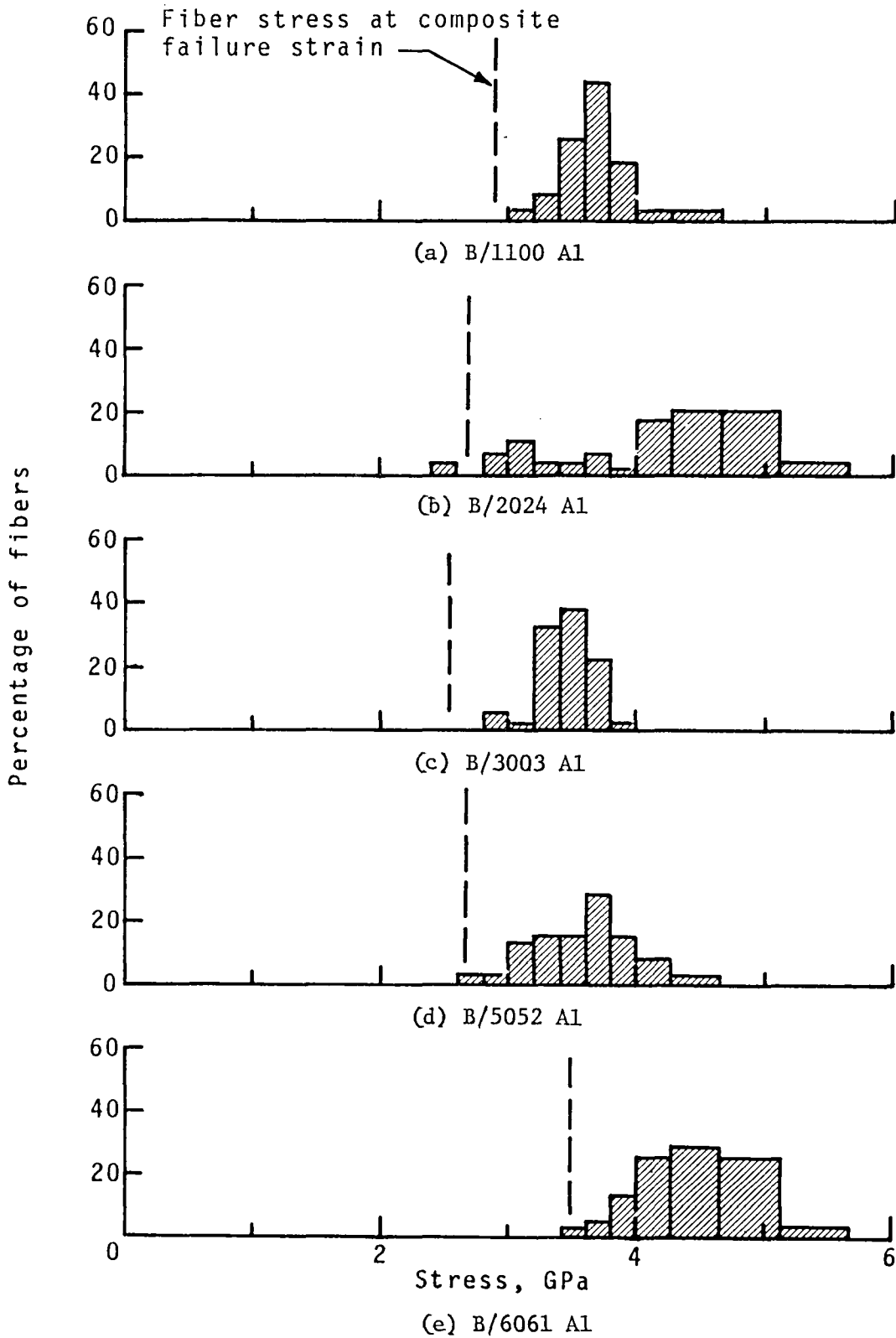
125

Figure 24.— Residual fiber strength distributions for composites after 2000 thermal cycles between 200 K and 590 K.

1. Report No. NASA TP	2. Government Accession No.	3. Recipient's Catalog No.
4. Title and Subtitle FIVE BORON/ALUMINUM COMPOSITES: LONG-TERM THERMAL DEGRADATION AND ALLOYING CONSTITUENT EFFECTS		5. Report Date
		6. Performing Organization Code
7. Author(s) George C. Olsen		8. Performing Organization Report No.
9. Performing Organization Name and Address NASA Langley Research Center Hampton, VA 23665		10. Work Unit No.
		11. Contract or Grant No.
12. Sponsoring Agency Name and Address National Aeronautics and Space Administration Washington, DC 20546		13. Type of Report and Period Covered Technical Paper
		14. Sponsoring Agency Code

15. Supplementary Notes

16. Abstract

The effects of thermal exposures on the properties of five boron-aluminum composite systems were experimentally investigated. Composite specimens were fabricated with 49 volume percent boron fibers (203 μm diameter) in aluminum alloy matrices 1100 Al, 2024 Al, 3003 Al, 5052 Al, and 6061 Al. In addition specimens of matrix alloy only were identically fabricated. The specimens were tested as-fabricated and after thermal exposures of up to 10 000 hours at 500 K and 590 K, up to 500 hours at 730 K, and up to 2000 thermal cycles between 200 K and 590 K. Composite longitudinal and transverse tensile strengths, longitudinal compression strength, and in-plane shear strength were determined in each condition by mechanical testing. None of the systems was severely degraded by the long-term exposure at 590 K. The best performing system was B/2024 Al with no transverse tensile strength degradation due to interaction and less than 10 percent longitudinal tensile strength degradation due to interaction.

The effects of the matrix alloying constituents on the degradation mechanisms of each of these systems were experimentally investigated. Composite specimens and individual fibers were metallurgically analyzed using a scanning electron microscope and an electron microprobe to determine failure characteristics, chemical element distribution, and reaction layer morphology. Alloying constituents were found to effect the degradation mechanisms as follows: iron causes low temperature degradation unless manganese is present as a stabilizer; magnesium, iron, and manganese increase degradation; and copper strengthens fibers.

17. Key Words (Suggested by Author(s)) Metal matrix composite Boron/Aluminum Thermal degradation Thermal fatigue	18. Distribution Statement Unclassified – Unlimited Subject Category 24	
19. Security Classif. (of this report) Unclassified	20. Security Classif. (of this page) Unclassified	21. No. of Pages	22. Price